Clean Routes to Sustainable Polymers

Joachim Christopher Lentz

Thesis submitted to the University of Nottingham for the Degree of Doctor of Philosophy.

August 2023

Declaration

All work presented in this Thesis is the original work of the author, apart from results referenced to other sources. It has not been submitted as part of any other degree or professional qualification.

Acknowledgements

I would firstly like to acknowledge my supervisors Steve Howdle, Vincenzo Taresco, Paul Hunt, Amy Goddard, Daniel Keddie, Francesca Paradisi, and Ben Cale. Their guidance and support has been invaluable throughout the project.

This PhD has been made possible by generously donated economic support. For that, I express my gratitude towards the Biotechnology and Biological Sciences Research Council, Croda International, G.M. & J.C. Lentz, as well as the Mary-Anne Gyllenstierna and Bertil Weitz Foundation.

For their ability to keep the School of Chemistry functioning, I would like to thank all technical and operational staff. Kevin Butler, Shazad Aslam, Lola Ogunyemi, Ben Pointer-Gleadhill, Jim Fyfe, Eric Delea, Richard Wilson, David Litchfield, Mark Guyler, amongst many others.

A great thank you goes to all my family, friends, colleagues, coaches, and teammates for their continued encouragement and good spirits.

Lastly, I must thank Alice Rubini for her compassion, sensibility, and (endless) patience.

Tusen Tack.

Abstract

The first experimental chapter of this thesis, Chapter 2, reports on the use of Novozym 435 as a catalyst for the synthesis of acrylamide initiated aliphatic polyesters by enzymatic ring-opening polymerisation. *N*-Hydroxyethyl acrylamide was utilised as a functional initiator to overcome transesterification issues associated with the use of acrylates in combination with Novozym 435. Two lactones, ε-caprolactone and δ-valerolactone, were used as model monomers. Novozym 435 was shown to be highly reusable under the reaction conditions employed. Incomplete initiator conversion was observed during kinetics experiments, and computational docking studies were used to gain a deeper understanding of enzyme binding interactions during the reaction. Amphiphilic copolymers were prepared using free-radical copolymerisation with PEGMA, and produced materials were tested against three cell lines for cytotoxicity. To increase the greenness of the process, 2-methyl tetrahydrofuran was utilised as a biobased solvent throughout.

In the following chapter, Chapter 3, biobased polyglycerol (PG) was explored as a building block to synthesise polyol polyesters for application as rheological modifiers. Polyglycerols underwent polycondensation with dimethyl succinate (DMS) in the presence of catalytic potassium carbonate to form hydrophilic polyesters. Of the polyglycerol lengths tested, PG4 was the most suitable due to its lower viscosity and lack of discolouration after reaction. The reaction achieved quantitative DMS conversion at mild temperatures (60-100 °C). Discolouration became more noticeable at elevated temperatures (140-180 °C). A selection of catalysts was screened, and K_2CO_3 was found to be the most suitable transesterification catalyst. Post-polymerisation functionalisation using succinic and maleic anhydrides was also explored. Increasing DMS loading resulted in cross-linked polymeric materials of varying swelling capability in aqueous media. This was highly promising for rheological modification of aqueous media.

Evaluation of lightly cross-linked PG4-based polyesters as rheological modifiers for aqueous media was conducted in Chapter 4. PG4 polymerised with 1.25 equivalents of DMS yielded the highest performing viscosity enhancer, but it faced issues relating to rapid degradation in aqueous formulation. However, materials prepared with PG4 and 1.5 equivalents of DMS (PG4-1.5DMS) showed good rheological modification at loadings above 10 wt.% and exhibited greater stability in aqueous formulation. Increasing DMS loading beyond this point was detrimental to rheological modification performance. These formulations also displayed excellent electrolyte tolerance, maintaining thickening performance with minimal decrease

in viscosity upon addition of NaCl or $MgSO_4$. Good thickening performance was maintained in a pH range relevant for personal care applications. Oscillatory rheology showed the aqueous formulations exhibit viscoelasticity, with excellent structural recovery after multiple cycles of high shear strain. In addition, PG4-1.5DMS also exhibited significant water swellability, absorbing nearly 20 times its own mass of water. Degradation testing of aqueous formulations revealed PG4-1.5DMS undergoes hydrolysis, leading to acidification and reduced viscosity.

To enhance PG4-1.5DMS performance, the gel fraction of the thickener was increased. This was achieved by freeze-drying following swelling in excess water. This process significantly improved rheological modification performance, achieving viscosity enhancements at a loading of only 2.5 wt.%. In aqueous formulation, the freeze-dried material maintained viscoelastic behaviour, exhibited excellent structural recovery, and demonstrated significantly increased swellability, absorbing nearly 50 times its own mass of water.

Anionic polymerisation to synthesise linear polyglycerols of higher molar mass was investigated in Chapter 5. This was done to investigate the possibility of enhancing the rheological modifier by increasing the chain length of the hydrophilic segment. Anionic polymerisation of ethoxy ethyl glycidyl ether was employed for this purpose. Molar masses of up to 20.7 $kg \cdot mol^{-1}$ were achieved. The reactions generally reached high conversions. To remove unreacted monomer, supercritical extraction with CO_2 was employed as an environmentally friendly method. After extraction, linPG was obtained through deprotection using the heterogeneous acidic catalyst, Amberlyst 15.

In Chapter 6, the same polyglycerols explored in Chapters 3 and 4 were investigated for their applicability as the basis of a photoactive resin for Additive Manufacturing. Volumetric printing has revolutionized Additive Manufacturing, offering an efficient approach whilst circumventing traditional layer-by-layer methodology. Polyglycerol-6 was acrylated using a scalable one-pot process. Successful volumetric printing of high-resolution models (smallest feature size 300 µm) was achieved, and reusability of the resin was demonstrated. Fluorescein was incorporated into the resin to show the ability to print objects embedded with a drug-like molecule. Micelles of 10,12-pentacosadiynoic acid were introduced to the resin and used to print thermoresponsive structures. This bio-based, biocompatible, scalable resin signifies a significant advancement towards environmentally sustainable resins in volumetric printing, fostering a more sustainable future with exciting applications.

Table of Abbreviations

AM	Additive Manufacturing
AIBN	Azobisisobutyronitrile
ASE	Alkali Swellable (or Soluble) Emulsion
AST	Alkali Swellable Thickener
AV	Acid Value
BM	Basal Culture Media
CAL	Computed Axial Lithography
CaLB	*Candida antarctica* Lipase B
CL	ε-Caprolactone
Đ	Dispersity
DAPI	4',6-Diamino-2-phenylindole
DBU	1,8-Diazabicyclo(5.4.0)undec-7-ene
DCM	Dichloromethane
DCTB	Trans-2-[3-(4-*tert*-butylphenyl)-2-methyl-2-propenylidene]malononitrile
DEPT	Distortionless Enhancement by Polarization Transfer
DI	Deionised
DLS	Dynamic Light Scattering
DMAP	4-Dimethylaminopyridine
DMEM	Dulbecco's Modified Eagle Medium
DMS	Dimethyl Succinate
DMSO	Dimethyl Sulfoxide
DP	Degree of Polymerisation
DRI	Differential Refractometer

DSC	Differential Scanning Calorimetry
EEGE	Ethoxyethyl glycidyl ether
eROP	Enzymatic Ring-Opening Polymerisation
FBS	Foetal Bovine Serum
FRP	Free-Radical Polymerisation
G'	Storage Modulus
G''	Loss Modulus
G*	Complex Modulus
GBSA	Generalized Born Surface Area
GC	Gas Chromatography
GPC	Gel Permeation Chromatography
HEAA	*N*-Hydroxyethyl acrylamide
HEMA	Hydroxyethyl methacrylate
HEMAM	*N*-Hydroxyethyl methacrylamide
HPLC	High-Performance Liquid Chromatography
HSQC	Heteronuclear Single Quantum Coherence
ISO	International Organisation for Standardisation
LAP	Lithium phenyl-2,4,6-trimethylbenzoylphosphinate
LDH	Lactate Dehydrogenase
LED	Light-emitting diode
LinPG	Linear Polyglycerol
LVE	Linear Viscoelastic Region
MA	Maleic Anhydride
MALDI-TOF MS	Matrix Assisted Laser Desorption/Ionisation Time-of-Flight Mass Spectrometry

MD	Molecular Dynamics
M_n	Number Average Molar Mass
M_w	Mass Average Molar Mass
MS	Mass Spectroscopy
η	Viscosity
N435	Novozym 435
NMR	Nuclear Magnetic Resonance
NP	Nanoparticle
OHV	Hydroxyl Value
PAA	Polyacrylic acid
PCDA	10,12-pentacosadiynoic acid
PCL	Polycaprolactone
pEEGE	Poly(ethoxyethyl glycidyl ether)
PEG	Polyethylene glycol
PEGMA	Polyethylene glycol methacrylate
PET	Polyethylene terephthalate
PG	Polyglycerol
PG4	Polyglycerol-4
PG6	Polyglycerol-6
PG10	Polyglycerol-10
PLA	Polylactic acid
PMMA	Polymethyl methacrylate
*p*TsOH	*Para*-Toluenesulfonic acid
PVL	Polyvalerolactone

R^2	Coefficient of Determination
RFP	Red Fluorescent Protein
ROP	Ring-Opening Polymerisation
RPM	Rotations Per Minute
SA	Succinic Anhydride
SAP	Saponification Value
SCF	Supercritical Fluid
$scCO_2$	Supercritical Carbon Dioxide
SEM	Scanning Electron Microscopy
τ	Shear Stress
τ_F	Flow Point
T_g	Glass Transition Temperature
T_m	Melting Temperature
TBD	Triazabicyclodecene
t-BuOK	Potassium *tert*-butoxide
THF	Tetrahydrofuran
TX	Triton X-100
UV	Ultraviolet
VAM	Volumetric Additive Manufacturing
VL	δ-Valerolactone

Table of Contents

Chapter 1. General Introduction

This thesis investigates the use of renewable feedstocks and green synthetic methodology for the synthesis of polymers with application primarily in personal care. This project has been sponsored by Croda, a Yorkshire-headquartered specialty chemicals company. Their commercial interests are in the development and manufacture of polymeric ingredients for personal care, crop care, home care, and biomedical applications. As part of Croda's sustainability targets, more than 75% of organic raw materials must be bio-based by 2030. As a result, the chemical feedstocks used in this thesis have been, or have the potential to be, biobased. In addition, the development of degradable materials to avoid bioaccumulation of their products is of vital importance to Croda's strategy.

Etymologically, the word polymer derives from the Greek "*polus*" and *"meros"*, meaning "many" and "part", respectively.[1] The modern IUPAC definition defines a polymer as a substance composed of macromolecules. A macromolecule is in turn defined as "a molecule of high relative molecular mass, the structure of which essentially comprises the multiple repetition of units derived, actually or conceptually, from molecules of low relative molecular mass".[2] In essence, polymers are the outcome of when multiple smaller molecules are coupled together to form larger molecules.

Naturally occurring polymers, such as cellulose, have been used by humankind since prehistorical times for the manufacture of textiles and papyrus.[3] The macromolecular structure of polymers was first recognised by Staudinger in 1920, for which he was awarded a Nobel Prize in 1953.[4,5] With the advent of the petrochemical industry and development of commodity polymers, the use of synthetic polymers has skyrocketed over the previous century. Commodity polymers are ubiquitous in daily life, and are found in packaging, clothing, personal care products, amongst countless other applications. The most commonplace route for polymer synthesis is petrochemical, and it is estimated that 7% of all oil is utilised for polymer production.[6]

Petrochemically-sourced polymers, such as polyethylene terephthalate, polyethylene, and polypropylene are extremely persistent in the environment.[7] Due to their lack of degradability and large commercial volumes, environmental accumulation of polymer waste has become increasingly problematic.[8] Waste plastic has become omnipresent on our planet. Plastic pollution has been found from the depths of the Mariana Trench, to the Arctic, and even in clouds above Mount Fuji.[9–11] The formation of microplastics is well-documented, although their health effects are still poorly understood.[12] These microscopic particles are capable of penetrating into human bodies, entering the lungs, bloodstream, and even placentas.[12] To prevent the further accumulation of plastic pollution, new polymers need to be developed. It is essential that these new materials are biobased to prevent reliance on fossil fuels, and biodegradable to prevent accumulation in the environment.

This thesis focuses on the development of biobased and biodegradable polymeric materials to meet the challenges of the present – without compromising the needs of the future.

Introduction to Chapter 2. Functional Enzymatic Ring-Opening Polymerisation

Chapter 2 focuses on the implementation of enzymatic catalysis to form linear aliphatic polyesters containing reactive head groups. These materials were targeted for their potential application as dispersants or nanoparticle formers.

Monomer Selection

δ-Valerolactone (VL) and ε-caprolactone (CL) were selected as the monomers to be investigated. These lactones can be produced industrially from biobased sources, and their polymers are known to be degradable.[13] VL can be produced from furfural, which in turn is produced by the acid treatment of biomass derived pentosan (Figure 1).[14–16]

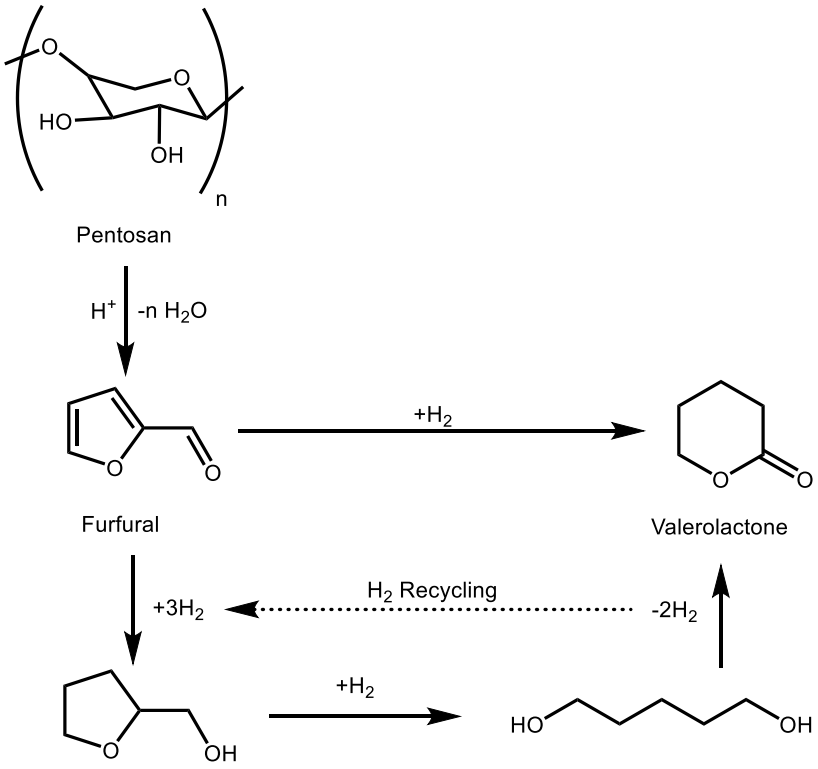

Figure 1 Pathway towards δ-valerolactone from pentosan via furfural. The pathway proceeds via acid treatment of pentosan to form furfural,[15] followed by hydrogenation of furfural to tetrahydrofurfuryl alcohol, subsequent hydrogenation to 1,5-pentanediol, and dehydrogenation to δ-valerolactone.[16]

The traditional synthetic route to caprolactone involves the oxidation of petrochemically sourced cyclohexane.[17] Developments have however been made towards the production of biobased caprolactone. In 2021, Lanxess reported that BP will start supplying biobased cyclohexanone for the manufacture of caprolactam at their plant in Antwerp.[18] Production of cyclohexanone using a non-naturally occurring microbial organism has also been patented.[19] Cyclohexanone can in turn be catalytically oxidised using peracetic acid in a Baeyer-Villiger oxidation.[20,21] Renewable cyclohexanone would slot into the existing infrastructure smoothly, allowing continued utilisation of high-investment manufacturing plants.[22]

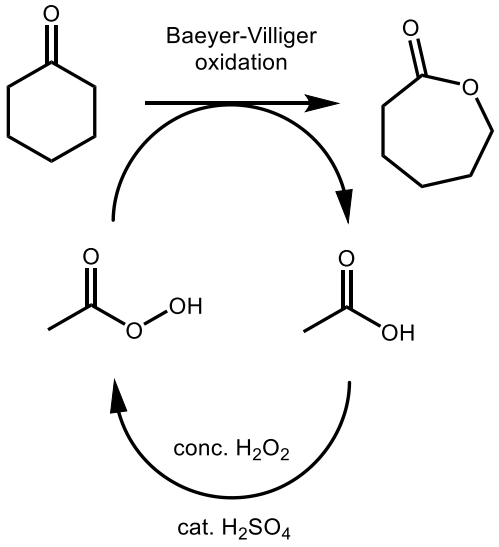

Figure 2 Industrial methodology of converting cyclohexanone to ε-caprolactone by Baeyer-Villiger Oxidation.[17,20,21]

Sustainably manufacturing CL can also be accomplished using fructose as a starting feedstock.[23] Acidic treatment of fructose yields 5-hydroxymethylfurfural, which can be reduced to 1,6-hexanediol and subsequently lactonized to yield CL (Figure 3).[24] Economic analysis of corn stover valorisation to CL has shown that the renewable pathway can be economically competitive with conventional hydrocarbon-centred methods, as long as major by-products are utilised.[24]

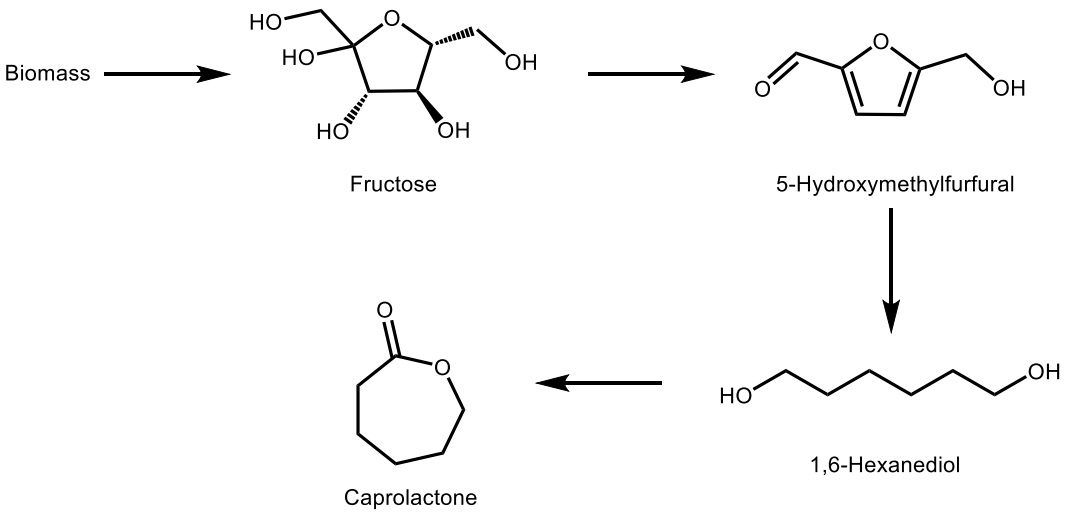

Figure 3 Renewable pathway to ε-caprolactone starting from biomass via 5-hydroxymethylfurfural and 1,6-hexanediol.[23]

Functionality in Ring-Opening Polymerisation

A limitation of aliphatic polyesters is their lack of functionisable chemical handles. One approach to introduce various functionalities is through the initiator method (Figure 4). A wide variety of initiators have been explored in the literature. Initiators containing a free-radical polymerisable functional group, such as a methacrylate group, allows for the synthesis of macro-monomers suitable for further radical (co-)polymerisation.[25] Incorporation of a PEG chain imbues the produced polymer with amphiphilicity and self-assembling properties.[26] Chain-transfer agents allow for more complex polymeric architectures to be accessed.[27] Dyes facilitate the characterisation of cellular delivery of the produced polymers.[28] For a molecule to be suitable as a ROP initiator, it should possess a nucleophilic group (typically a hydroxyl) and be stable under reaction conditions.

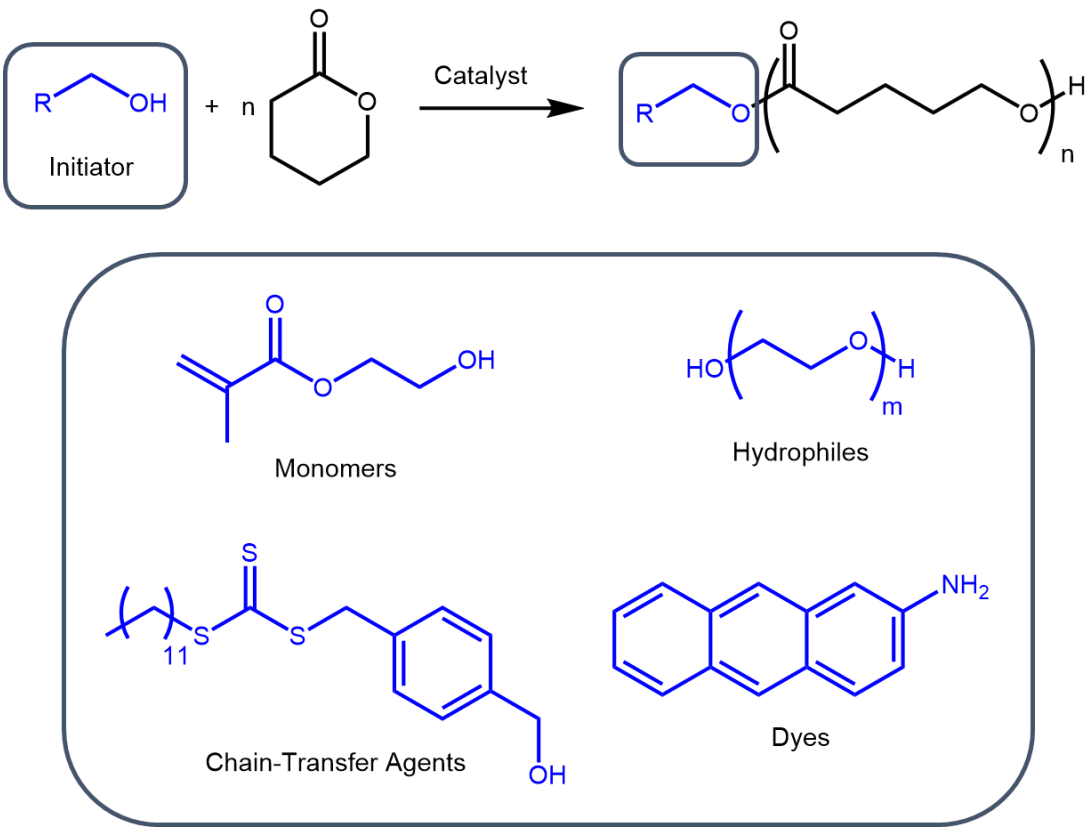

Figure 4 Schematic of the initiator method in ring-opening polymerisation of valerolactone, with some examples of suitable initiators shown.

In Chapter 2, aliphatic polyesters with a radically polymerisable initiator group were targeted. Initiation with such an initiator allows for further tuning of the final material properties through incorporation of various species through radical co-polymerisation. An advantage of this approach is that a wide variety of commercially available monomers can be utilised. To enable formulation of the produced materials into nanoparticles installation of hydrophilicity is investigated in Chapter 2 by co-polymerisation with PEGMA.

Catalyst Considerations

Catalyst choice is significant in designing a ring-opening polymerisation process. The "usual suspects" of catalysts utilised in the literature are tin-based organometallics,[29] organic bases,[30] and lipases (Figure 5).[31]

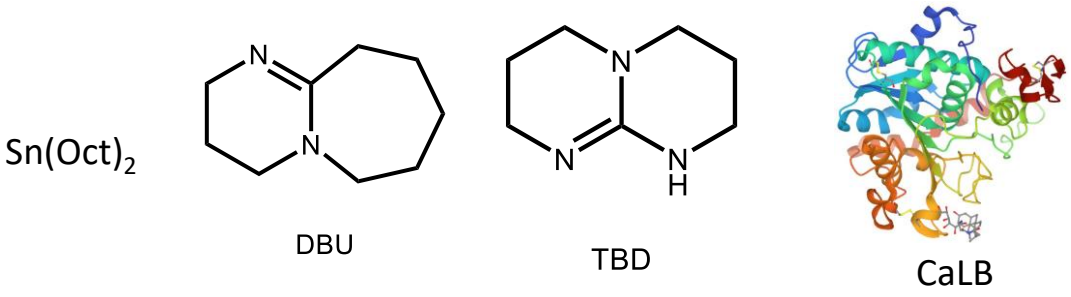

Figure 5 A selection of catalysts typically employed for ring-opening of lactones.

One of the most well-investigated catalysts for ring-opening of lactones is tin(II) bis(2-ethylhexanoate), more widely known as stannous octanoate or $Sn(Oct)_2$.[29] Stannous octanoate is typically utilised at high reaction temperatures (140-180 °C).[32] Consequently, thermally labile monomers and initiators are unsuitable as undesired degradation processes become significant. A further consideration with tin-based systems is their inherent toxicity.[33] Furthermore, tin residues are challenging to remove from the produced polymeric material.[34,35] These characteristics pose significant limitations to tin-based catalysts.[32]

Organocatalytic approaches to ring-opening have gained traction as metal-free alternatives to $Sn(Oct)_2$.[30] The first report of living organocatalytic ROP was reported in 2001, where lactide was polymerised using catalytic 4-dimethylaminopyridine (DMAP) as a catalyst in the presence of alcoholic initiating species.[36] Since then, a broad range of organocatalysts have been developed and explored.[30] Of relevance to Chapter 2 is the use of bicyclic organic guanidine-based organic bases, such as 1,8-diazabicyclo[5.4.0]undec-7-ene (DBU) and triazabicyclodecene (TBD).

DBU is a highly active catalyst for the polymerisation of lactide, yielding quantitative conversions after short reaction times (1 h) at ambient temperature.[37] The exceptional reactivity facilitates straightforward polylactide (PLA) synthesis. It is also known that DBU does not display catalytic activity towards CL and VL at ambient temperatures.[37,38] Addition of co-catalysts, such as thioureas, can also be used to facilitate DBU catalysed ROP.[37] The orthogonality of DBU and Novozym 435 in CL and lactide systems has been used to chain-

extend poly(caprolactone) with polylactide (Figure 6).[26] The selectivity of DBU can thus be exploited to generate block-copolymers in co-catalytic systems.

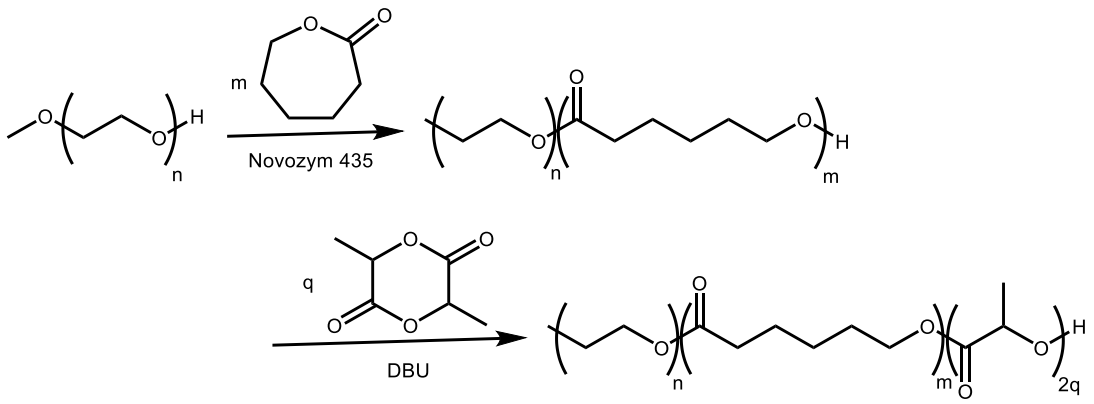

Figure 6 Formation of tri-block PEG-PCL-PLA polymers is enabled by enzymatic catalysis followed by organocatalytic chain extension with lactide.[26]

TBD is capable of facilitating polymerisation of lactide, as well as ε-caprolactone and δ-valerolactone at ambient temperatures.[37] The pK_a of TBD is almost 2 units higher than that of DBU (26.03 and 24.34 respectively, in acetonitrile).[39] It has been hypothesised that an increased pK_a is associated with greater catalytic activity.[37] The catalytic activity of TBD is more water sensitive than that of DBU, due to full protonation and ionic cluster formation lowering reactivity.[40] Solubility issues of TBD in organic solvents has also been reported.[41] Furthermore, TBD is problematic for use in conjunction with labile initiators such as hydroxyethyl methacrylate (HEMA) due to adverse side-reactions taking place.[25]

The homogeneous nature of DBU, TBD, and $Sn(Oct)_2$ also limits their recyclability. Extraction from the reaction mixture requires significant solvent usage and neutralisation steps, producing waste solvent in the process.[42] Attempts to recycle TBD in the depolymerisation of polyethylene terephthalate (PET) resulted in significantly increased reaction times due to catalyst deactivation and incomplete recovery.[43] Immobilised formulations of TBD and DBU are available to facilitate catalyst recycling, although are generally less reactive than their unbound counterparts.[44,45]

Enzymatic Catalysis for Ring-Opening Polymerisation

Lipases have shown themselves to be excellent catalysts for polyester synthesis and provide an alternative to more traditional chemocatalytic approaches.[31] Enzymatic catalysts are highly selective, metal-free, and operate in mild conditions.[46,47] *Candida antarctica* Lipase B (CaLB) is a well-established catalyst in polymer synthesis.[48] An immobilised formulation of

CaLB has been commercialised by Novozymes as Novozym 435 (N435). The experiments in Chapter 2 utilise N435 to access the benefits of enzymatic catalysis whilst maintaining industrial applicability by utilising a commercially available catalyst.

In nature, lipases catalyse hydrolysis of fatty acid triglycerides (Figure 7). In anhydrous media they can also catalyse the reverse reaction. The position of the equilibrium is governed by the same principles in both enzymatic and chemical catalysis. As such, excess water will facilitate complete hydrolysis, whilst an absence of water will drive the equilibrium towards esterification. Utilisation of difunctional carboxylic acids has allowed for the synthesis of polyesters by polycondensation using lipase catalysis.[47] Lipases have also been shown to be capable of catalysing ROP of several different lactones.[49]

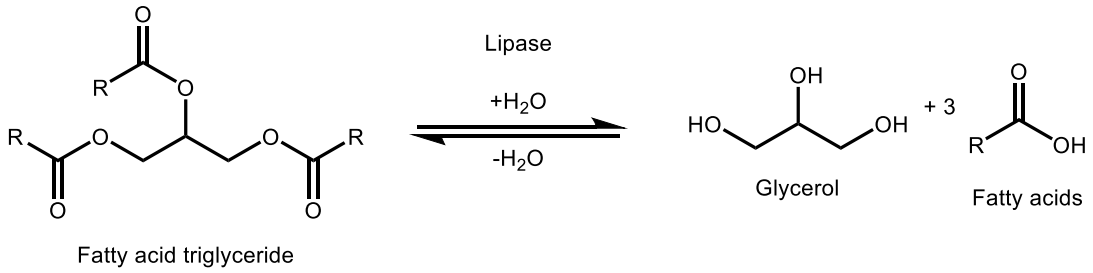

Figure 7 Natural reactivity of lipases is the hydrolysis of fatty acid triglycerides. The position of the chemical equilibrium can be shifted in accordance with Le Chatelier's Principle.

Serine-lipases, such as CaLB, function using a catalytic triad in their active sites (Figure 8).[50] Consisting of aspartic acid, histidine, and serine the catalytic triad motif functions by enhancing the nucleophilicity of the serine pendant hydroxyl group.[31] Orientation of the basic histidine nitrogen towards the hydroxyl proton weakens the oxygen-hydrogen bond. The aspartic acid residue is essential to maintain the correct orientation of the histidine. Without hydrogen bonding from the aspartate residue, the imidazole would not be fixed in position, leading to a dramatic loss of activity.[51] The aspartate residue locks the histidine in the correct orientation to maximise interaction between the nitrogen lone pair and hydroxyl proton. Whereas hydroxyl groups and imidazole rings have large differences in pK_a (approximately 16 and 7 respectively)[52], the enzyme-mediated orientation to maximise orbital overlap allows this to be overcome in a gentle manner. Electron movement can be pushed from the aspartic acid residue, leading to a proton-shuttling effect across the catalytic triad. It has been found that acids exhibiting a pK_a below 4.8 cause irreversible deactivation of CaLB.[53] It is hypothesised that the observed deactivation is a result of the

aspartate residue being protonated, and therefore unable to fulfil its role in the catalytic triad. Other reasons for this deactivation could be that the presence of strong acid leads to the disruption of key structural hydrogen bonds, leading to unfolding and irreversible deactivation.[53]

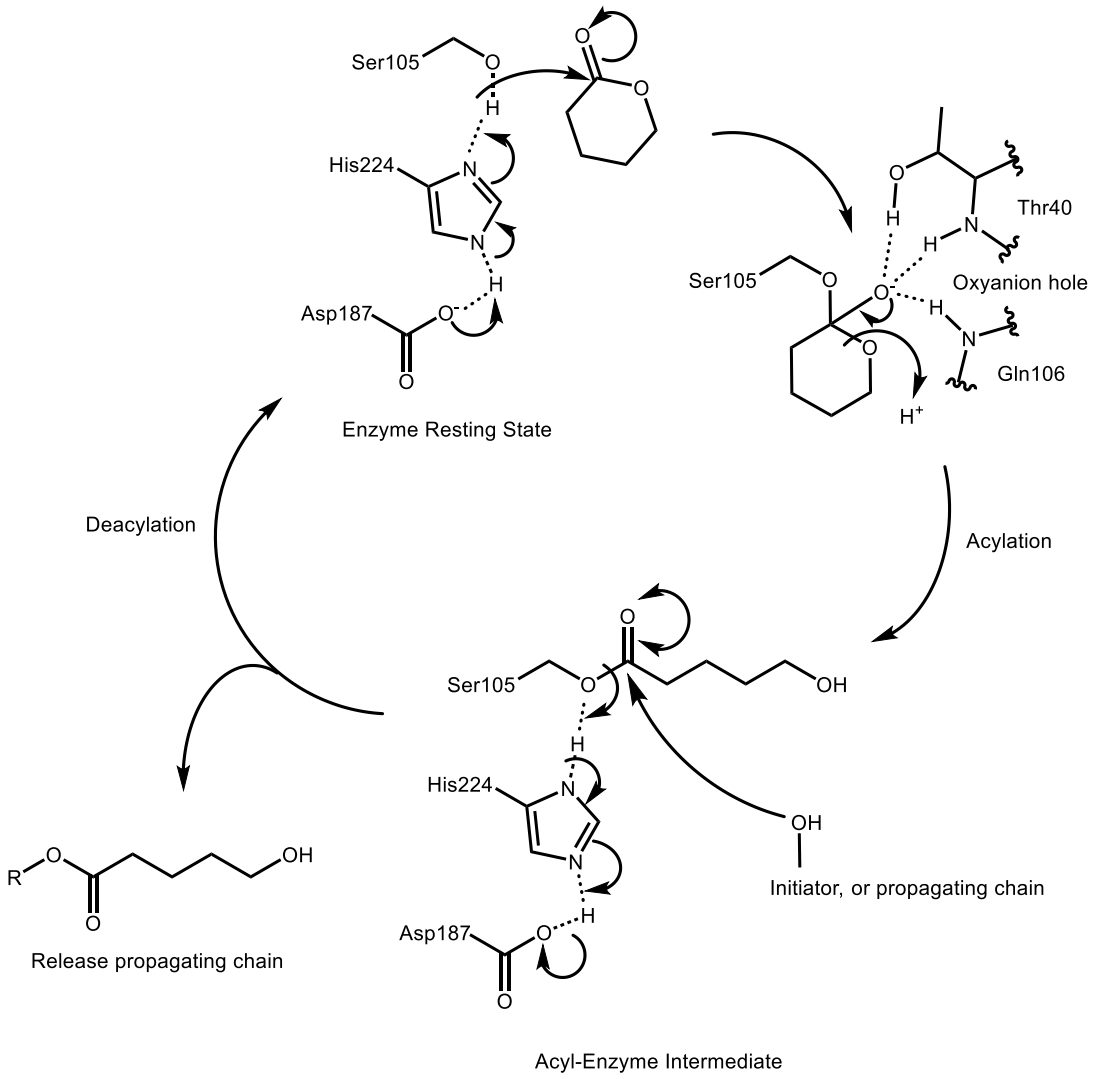

Figure 8 Mechanism of serine-lipase ring-opening polymerisation of δ-valerolactone.

Serine-lipases also act to stabilise the charged tetrahedral intermediate and activate the carbonyl bond (Figure 8). This stabilisation is achieved by use of the 'oxyanion hole', where hydrogen bond donors are oriented to stabilise the accumulating negative charge.[54] In CaLB threonine and glutamine residues are used to stabilise the oxyanion using their backbone amide protons, and the side-chain hydroxyl proton of threonine. Oxyanion stabilisation is the major factor for lowering the energy of the transition state.[55] Mutation to replace threonine with valine or alanine generates mutants with an activity three orders of magnitude lower

than that of the wild-type enzyme, due to an increase in activation energy by 15-19 kJ·mol^{-1}.[55] The combination of activated serine hydroxyl, and the effective stabilisation of the ionic intermediate allows for the high catalytic activity of these enzymes.

The active centre of CaLB has a large hydrophobic pocket above the catalytic triad, and a medium-sized pocket underneath. It is believed that the acyl component of the monomer lies in the larger pocket, whilst the nucleophile that releases the growing chain from the active site enters through the medium pocket.[31] Featuring a large active site, CaLB has shown itself to be active to a large variety of substrates allowing for facile synthetic use without extensive genetic modification. The robustness and large substrate scope have led to CaLB being one of the most popular lipases for use in polymerisation.[56]

Release of the growing polymer from the acyl enzyme intermediate occurs through a nucleophilic attack. The nature of the nucleophile can vary greatly, and in ROP allows for the introduction of a controlled end-group by addition of a desired initiator.[46] Multiple initiating species have been explored in the literature to generate a broad range of polymer architectures.[46,57–59] Utilising the initiator method enables installation of functional handles on the polymer chains themselves in a one-pot system. Limiting moisture content is of importance to avoid production of water-initiated polymer chains lacking the desired functionality of the desired initiator.[57]

Enzyme Immobilisation

Immobilisation of enzymes onto supporting structures facilitates product purification and catalyst recovery.[60–63] Improving enzyme performance leads to higher product output per unit of enzyme, and directly determines the economic cost associated with the enzymatic catalyst.[61] Immobilisation enables the use of flow systems,[64] and can improve enzyme characteristics such as: activity, stability, selectivity, recyclability, chemical resistance, and purity.[56,61,63,65,66]

In N435, CaLB is physically adsorbed to Lewatit VP OC 1600 macroporous acrylic resin.[56] The resin is composed of methacrylic esters and divinyl benzene cross-linker to form a porous polymeric support. The hydrophobic nature of the resin is particularly well suited for lipase immobilisation.[56] N435 is formulated using interfacial activation, which aims to selectively immobilise monomeric open forms of CaLB (Figure 9).[56]

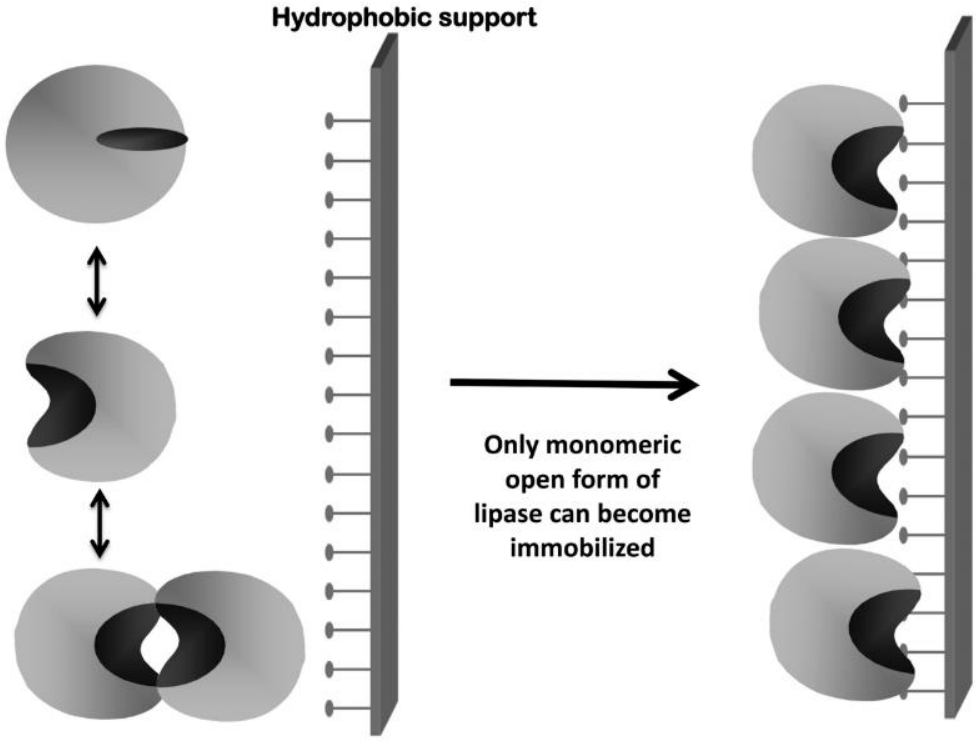

Figure 9 Interfacial activation and adsorption of CaLB to form Novozym 435. Interfacial activation prevents immobilisation of closed and dimeric enzymes. Reproduced with permission from Ortiz et al.[56]

Decreases in reactivity of the immobilised enzyme can be induced by factors such as: removal of essential water, extreme pH, support degradation, enzyme leaching into the reaction media, and excessive temperatures.[61] Leaching is the process by which immobilised enzymes are released from the support structure (Figure 10).[67] In the event of significant leaching, the support structure will eventually be completely devoid of active catalyst and lose reactivity. Leaching is promoted by factors such as high temperatures, organic solvents, and detergents.[56] A drawback of physically adsorbing, rather than covalently linking, the enzyme to the supporting structure is that leaching may be more prevalent during use, lowering the activity of the immobilised formulation with extended use.[61]

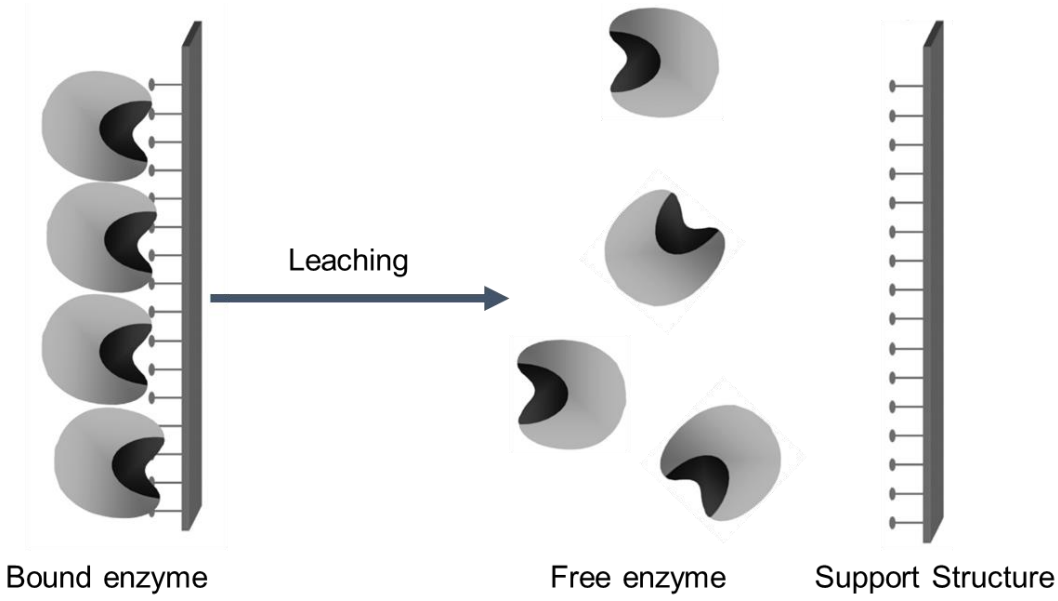

Figure 10 Leaching of bound enzyme from the support structure. Figure adapted from Ortiz et al.[56]

It is a known issue with N435 that stirring can lead to mechanical degradation of the enzyme support, resulting in a finely powdered support.[53,62] The increase in surface area can lead to a perceived hyperactivation as diffusion limitations are lessened.[68] On an industrial scale, the finely powdered support can clog filters leading to the reactor and require the enzyme to be replaced prematurely. To maintain support stability, appropriate stirring techniques need to be used. On an academic scale simply lowering the stirrer frequency can be sufficient to prevent support degradation. More scalable alternatives involve using flow systems,[64,69,70] vortex reactors,[65] trapping the immobilised enzyme in a fine mesh cage,[71] and reactive extrusion.[72]

Enzyme immobilisation provides a very versatile approach to make biocatalysis more accessible. There are undoubtedly considerations that need accounting for during their use, maintaining integrity of the support structure can be achieved by utilising appropriate agitation techniques and compatible solvent. Enzyme leaching can be minimised by avoiding detergent-like molecules and overly harsh reaction conditions. Taking the limitations into account allows for very powerful catalytic activity with facile purification procedures to be harnessed in straightforward conventional glassware at low temperatures. The benefits of utilising an immobilised enzyme often outweigh the limitations, as complications regarding whole-cell catalysis are avoided, and issues such as free-enzyme instability are circumvented.

Summarising Remarks and Next Steps

The aim of Chapter 2 is to combine the initiator method with enzymatic catalysis of lactones to produce aliphatic polyesters with reactive end-groups. These aims were largely achieved, as these types of species were successfully synthesised. Computational docking studies were also used to gain further insight into the enzymatic behaviour during ROP. These findings were published in *Polymer Chemistry* (Royal Society of Chemistry).[73]

At this stage of the project, it was decided to shift experimental focus. Whilst the aliphatic polyester component of these polymers is degradable, the radically polymerised acrylate backbone is most likely not. Croda's sustainability goals target fully degradable material, and resultingly materials containing acrylate backbones were deemed to be outside of their commercial interest. An alternative area that Croda has an interest in, is the development of sustainable and degradable alternatives to current hydrophilic polymers. To achieve complete biodegradability and expand the scope of the project, the decision was made to target hydrophilic polyesters for use in aqueous rheology modification instead.

Introduction to Chapter 3. Synthesis of Sustainable Aqueous Rheology Modifiers

Chapter 3 explores the utilisation of biobased polyglycerols as hydrophilic building blocks for the synthesis of hydrophilic polyesters. Rheology modifiers are a core component of Croda's portfolio and are widely used by their customers to achieve desired physical characteristics in their products. Biobased and (bio)degradable synthetic rheology modifiers are perceived to be a gap in the market and a valuable business opportunity that aligns with sustainability targets.

Polymeric Rheology Modifiers

Rheology is the science of how materials flow and deform.[74] Of concern to rheologists is how materials behave whilst they are subjected to applied forces. Rheological properties of materials play crucial roles in numerous applications, ranging from cosmetics and pharmaceuticals to foods and adhesives.[74–77] To achieve the desired performance characteristics, systems such as paints, drilling fluids, lubricants, and personal care products will require specific rheological properties.[78–82] In the formulation of a skin cream for example, the cream should have a rheological profile that facilitates application whilst also having an appropriate viscosity to prevent dripping or sagging once it has been applied.[78]

Rheological modification refers to the process of altering the viscosity and flow behaviours of solutions or suspensions. Whilst rheological modification is possible in a variety of media, this chapter will focus specifically on aqueous systems. The addition of rheological modifiers can be used to modify viscosity, yield stress, stability, thixotropy, and shear-thinning characteristics of the system.[78,81,83] To achieve the desired rheological properties addition of a rheological modifier is often crucial to the formulation.[74–78,80,82]

Many different types of rheology modifiers can be employed to modify the rheological behaviour of aqueous systems. These range from synthetic polymeric species, natural polymers like cellulose, to inorganic materials such as clays.[78] Factors such as pH, compatibility with other components, temperature, and environmental effects all impact the selection process of the viscosity modifier.[84] Modifiers can be classified into different categories based on their mechanism of action. Broadly speaking, synthetic rheological modifiers can be separated into associative and non-associative mechanisms.[84]

Associative thickeners function in micellar systems (Figure 11). By forming bridges between micelles, a network of micelles that will disrupt the flow of the system and increase viscosity is formed.[81] Associative thickeners typically consist of hydrophilic polymers end-capped with hydrophobic moieties. The hydrophobic segments will associate with the inside of the micelles, whereas the hydrophilic chain will remain outside, enabling the other chain-ends to find other micelles to form the bridging structures. Commercially, PEG chains are predominantly used as the polymeric hydrophilic segment.[84] Typical hydrophobic segments consist of linear alkyl chains and can be fatty acid derived. In the case of short hydrophilic linking segments intramolecular attractions between the hydrophobic groups is favoured due to their proximity, leading to micelle formation over network formation. As such, longer hydrophilic linking segments are preferred, since intermolecular interactions become more prevalent as the hydrophobic groups are further apart. These intermolecular attractions lead to network formation and accompanying viscosity modification.[81,85]

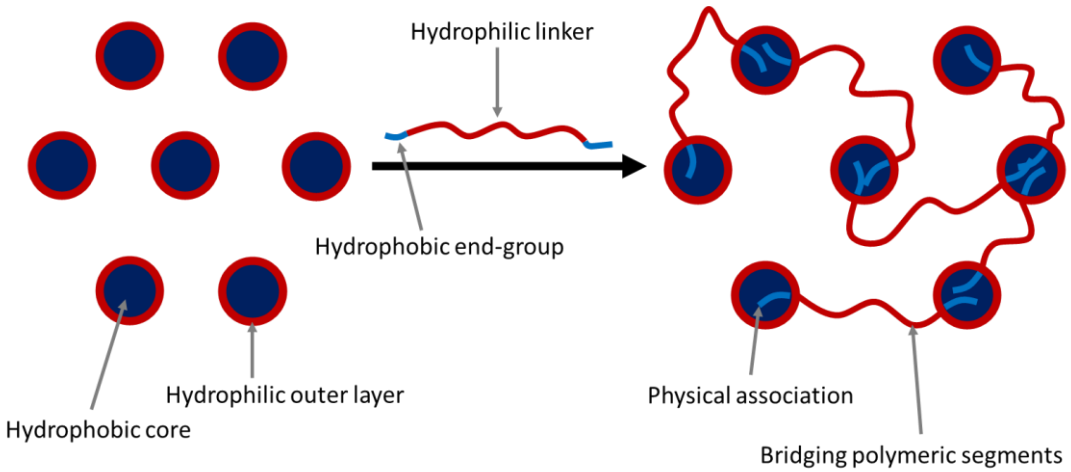

Figure 11 A schematic representation of the mode of action of an associative thickener. Left: a solution of micelles. Right: following the addition of an associative rheology modifier polymeric bridging segments are formed between the micelles through association of the hydrophobic end groups of the thickener with the micelle cores.

The widespread use of PEG has led to increases in the formation of PEG antibodies and PEG allergies becoming more prevalent.[86,87] Skin sensitisation, redness, and itching has been reported especially in individuals with sensitive skin.[88] Furthermore, high molar mass PEG chains are not biodegradable and lead to issues regarding bioaccumulation and end-of-life concerns.[89] From a commercial perspective, personal care brands are diverting from PEG due to negative publicity surrounding dioxane impurities and customer demand.[89] The synthesis

of PEG is also problematic as it requires large quantities of ethylene oxide – a highly flammable gas prone to forming explosive mixtures.[89] Besides the hazards of ethylene oxide, it is also predominantly produced from petrochemical sources.[90] In short, replacements for PEG are in high demand due to concerns with safety, immune response, and their petrochemically sourced nature.

Non-associative thickeners, unlike their associative counterparts, do not rely on a micellar system to achieve viscosity enhancement.[91] A well-known example of a non-associative thickener is high molar mass polyacrylic acid (PAA) (Figure 12). PAA is part of a class of viscosity modifier referred to as alkali-swellable or alkali-soluble thickeners (AST, collectively).[91,92] ASTs can consist of either linear polymer chains, or a small fraction (usually less than 1%) of cross-linker can be added to improve performance.[92] It has been demonstrated that slight cross-linking leads to significant performance increases.[93] Introduction of cross-linking prevents solubility, and allows for the formation of highly swollen microgel particles.[92] On the other hand, too tightly cross-linking the polymers leads to swelling being restricted and a decrease in thickening performance.[92]

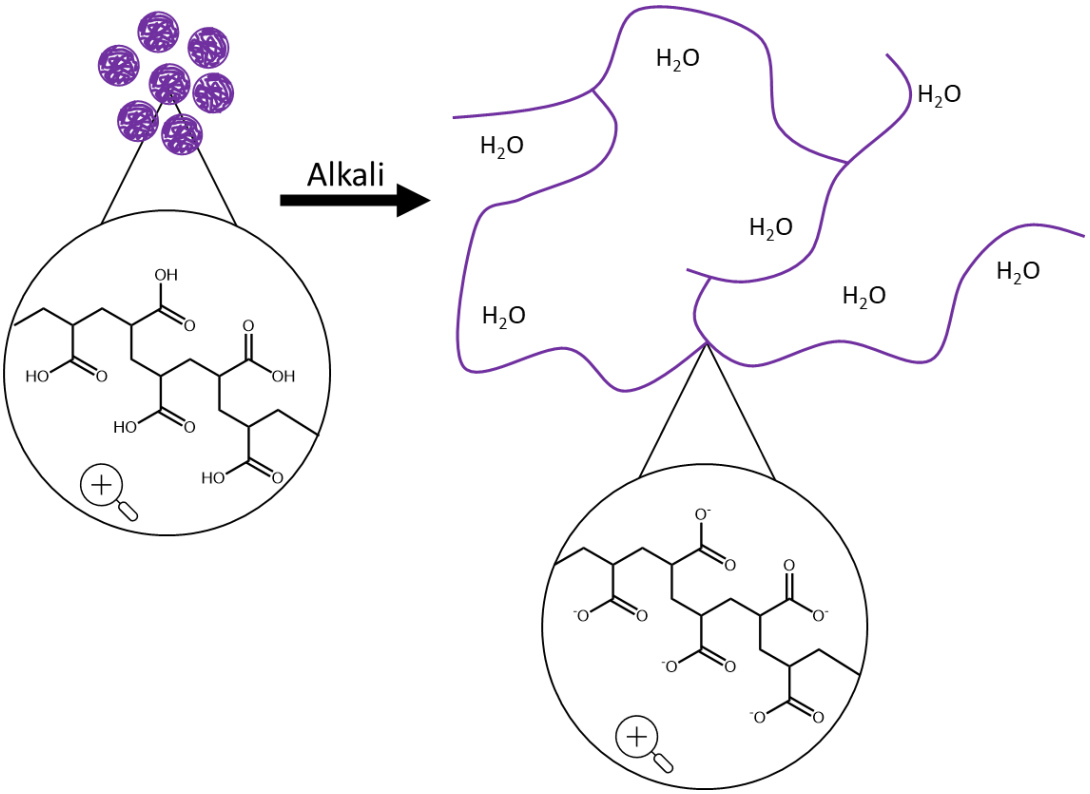

Figure 12 A schematic representation of the mode of action of a non-associative thickener. Left: tightly coiled polymer chains of protonated PAA. Right: following addition of alkali electrostatic repulsion forms an anionic network that traps water and increases viscosity.

Before any pH modification occurs, the chains of PAA are tightly coiled and lack rheological modifying properties.[93] To activate the ASE thickener, alkali (such as NaOH) is added, resulting in the deprotonation of PAA.[92,93] This process leads to the formation of an anionic framework (Figure 12). Electrostatic repulsion between negatively charged carboxylate groups results in the straightening and separation of the polymer chains.[91] The repulsion between the chains leads to significant swelling, and the volume between the chains fills with water molecules that hydrogen bond to the pendant carboxylate groups.[92]

At high concentrations, the AST absorbs all available water in the system, causing a substantial increase in viscosity due to severe limitations on water flow.[92] However, the limit of swelling can be reached by adding an excess of water, resulting in unbound water being present in the system and leading to a reduction in viscosity. It is worth noting that AST-type thickeners can also incorporate hydrophobic moieties, offering a combination of associative and non-associative thickening mechanisms.[92,94]

Commercially available non-associative thickeners suffer from several issues that warrant attention. While they demonstrate high effectiveness in increasing viscosity at low loadings (typically around 1 wt.%), their performance is greatly compromised in the presence of electrolytes.[92–95] When salts are added to a formulation, the anionic network of these thickeners collapses, as the introduced ions shield the electrostatic repulsions fundamental to the thickening behaviour.[91–94,96] This sensitivity to electrolytes can be highly limiting in many applications where the addition of electrolytes is desirable. Moreover, the chemistry of the materials used in these thickeners poses additional restrictions. PAA, particularly at the molar masses employed for rheological modification, is non-biodegradable due to its all-carbon backbone.[96–98] Consequently, PAA exhibits environmental persistence, which is undesirable from ecological standpoint.[96–98] Additionally, PAA synthesis requires the use of acrylic acid, a typically petroleum derived and potentially toxic molecule.[99,100] Mishandling of acrylic acid also carries the risk of runaway polymerisation.[101] These challenges highlight the need for improvements in the development of non-associative aqueous rheology modifiers, aiming to overcome electrolyte sensitivity whilst also addressing safety risks and environmental concerns with the materials used.

Considering these limitations, degradable, biobased, and environmentally friendly synthetic aqueous rheology modifier is needed. Building on existing technologies, Chapter 3 aims to explore alternative solutions that align more closely with the Principles of Green

Chemistry.[102,103] Several key properties are considered when selecting molecular building blocks for synthesising effective rheological modifiers. An ideal building block will be biobased, non-hazardous, readily available, and exhibit hydrophilicity as they are intended for use in aqueous media.

Biobased and Degradable Hydrophilic Polymers

Current synthetic aqueous rheology modifiers utilise hydrophilic polymers of high molar mass.[85,91] To develop a more sustainable alternative to PEG and PAA based technologies, it follows that new hydrophilic polymers have to be developed.

To facilitate degradation the backbone of the materials should be susceptible to bond breakage in naturally occurring environments. Sunlight, air, and water are some naturally occurring reagents that can facilitate polymer degradation.[104,105] As the final materials are intended for use in aqueous media, incorporating susceptibility to hydrolysis could be a suitable method to facilitate degradability. There exists a large variety of functional groups predisposed to both hydrolysis as well as polymerisation.[106] In Chapter 3, esters were selected as a suitable backbone functionality to incorporate hydrolytic sensitivity.

Specifically, polyol polyesters were deemed to be interesting candidates as biobased and degradable hydrophilic polymers. The hydroxyl groups along the polymer backbone of these polymers contribute to hydrophilicity, whilst the ester backbone linkages provide sites for end-of-life degradation. In addition, many suitable polyol building blocks, such as sugars and glycerol, are naturally occurring in large quantities (Figure 13).[107]

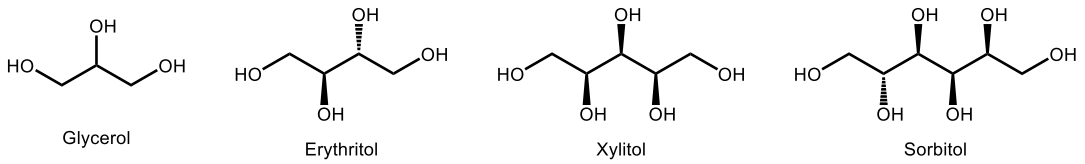

Figure 13 A selection of naturally occurring polyols suitable for polyesterification.

Upon polycondensation of a polyol building block with a dicarboxylic acid or diester polyesters are formed (Figure 14). The polyols shown feature two primary alcohols, and between one and four secondary alcohols (Figure 13). To maintain linearity of the produced polymer it is imperative that the primary hydroxyl groups are selectively esterified, with the secondary hydroxyl groups remaining unreacted and granting hydrophilicity to the final polymer. Thankfully, tuning reaction conditions and catalyst selection allows for preferential condensation of the primary hydroxyl groups to be achieved.

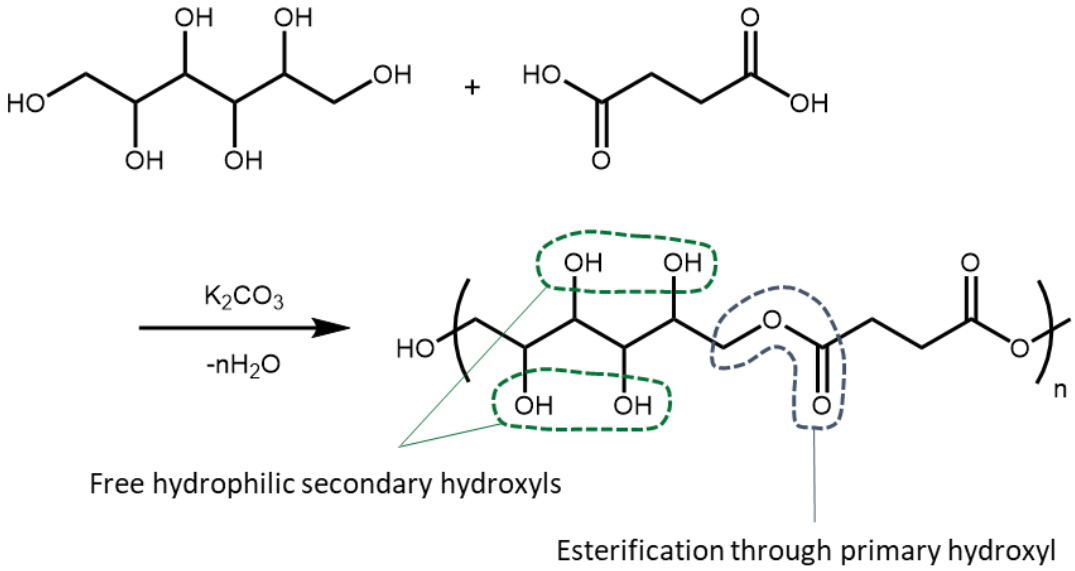

Figure 14 Reaction scheme of potassium carbonate catalysed polycondensation between sorbitol and succinic acid to form a linear polyol polyester.[109] *Stereochemistry omitted for simplicity.*

In the Howdle Group, glycerol and sorbitol have been investigated in recent years for the purpose of polyol polyester synthesis (Figure 14).[108,109] Enzymatic and potassium carbonate catalysed polycondensation was found to give primarily linear polyesters. Other efforts in the literature have utilised scandium triflate to preferentially form linear polyesters.[110–112]

Oligomeric polyglycerol (PG) was identified as an alternative polyol building block for the synthesis of polyol polyesters (Figure 15). PGs are available in a variety of chain lengths and are industrially produced through the direct polymerisation of glycerol at elevated temperatures in the presence of alkali catalysts.[113,114] Glycerol is an underutilised waste stream from the biodiesel and soap industries.[113] The wide availability and economic viability makes the valorisation of glycerol a promising prospect.[113,114]

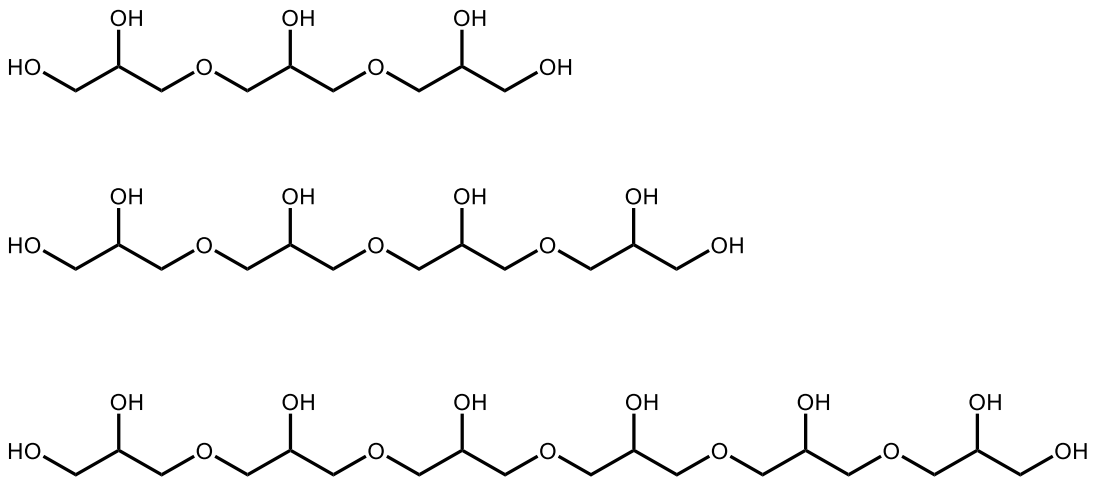

Figure 15 A selection of glycerol oligomers.

To form a fully biobased polyester, the polyol building block needs to be polymerised with a biobased dicarboxylic acid. Recently, economical, and sustainably sourced dicarboxylic acids have become more widely available. Aliphatic dicarboxylic acids of various chain lengths (e.g., C3, C4, C6) can be synthesised using fermentation methods.[115–117] Longer chain dicarboxylic acids (e.g., C9) can be accessed using ozonolysis of oleic acid.[118] Succinic acid has been identified as a sustainable platform chemical, and several industrial actors have developed chemical plants to produce this diacid from sustainable sources.[119]

Typical of aliphatic dicarboxylic acids are their high melting points, generally exceeding 100 °C (Table 1).[120] These high melting points complicate material handling as they cannot readily be pumped across an industrial plant. Furthermore, to obtain a homogeneous polymerisation mixture, without resorting to solvent usage, high temperatures are required. Utilisation of high reaction temperatures increases the prevalence of side reactions, thermal degradation, and is overall more energy intensive.[121]

A method to improve the usability of aliphatic dicarboxylic acids is to utilise their short chain diesters (e.g., dimethyl or diethyl esters) rather than the dicarboxylic acids themselves. The diesters have significantly lower melting points and are usually liquids at ambient temperatures (Table 1). Owing to their liquid state, the diesters are easier to handle on industrial scales as metered pumps can be utilised. The lowered melting point, and increased volatility of the condensate produced, also enables reactions to be performed at milder temperatures, lessening the energy intensity of the process.

Trivial Name	Carbon Chain Length	Diacid T_m (°C)	Dimethyl Ester T_m (°C)
Malonic acid	3	135	-62
Succinic acid	4	190	18
Glutaric acid	5	98	-37
Adipic acid	6	150	10
Azelaic acid	9	110	18

Table 1 Melting points of a selection of aliphatic dicarboxylic acids and their respective dimethyl esters.[120]

A drawback of utilising diesters rather than the dicarboxylic acids arises from atom economy. In the case of dimethyl esters, methanol will be produced during polycondensation. Methanol has a greater molar mass than water, resulting in a lowered atom economy of the process. Produced methanol can however be collected and recycled.

Summarising Remarks and Next Steps

In Chapter 3, polyol polyesters are synthesised for the purpose of rheological modification of aqueous media. Following promising water absorbing properties of a lightly cross-linked polyol polyester these were selected for more extensive testing. The evaluation of these materials as aqueous rheology modifiers is described in Chapter 4.

Introduction to Chapter 4. Evaluation of Sustainable Aqueous Rheology Modifiers

Chapter 4 delves into the application testing of the materials synthesised in Chapter 3. The lightly cross-linked polyol polyesters were evaluated primarily on their ability to modify the rheological properties in aqueous solution.

Rheology has been used extensively throughout this chapter to analyse thickened aqueous solutions. In personal care applications, the texture of the product is paramount to consumer satisfaction, these are influenced by rheological properties such as yield stress, viscosity, thixotropy, as well as storage and loss moduli.[122–125] Personal care products are subjected to a wide range of rheological environments during storage, dispensing, and application. As such, rheological studies are a useful method to investigate the behaviour of formulations.[125]

Rheology

Modern rheometers are sophisticated instruments used to study the flow and deformation behaviour of complex fluids, soft materials, and viscoelastic substances. In this work, an Anton Paar MCR 102 rheometer with parallel plates has been employed to characterise the polyol polyesters in aqueous solution (Figure 16).

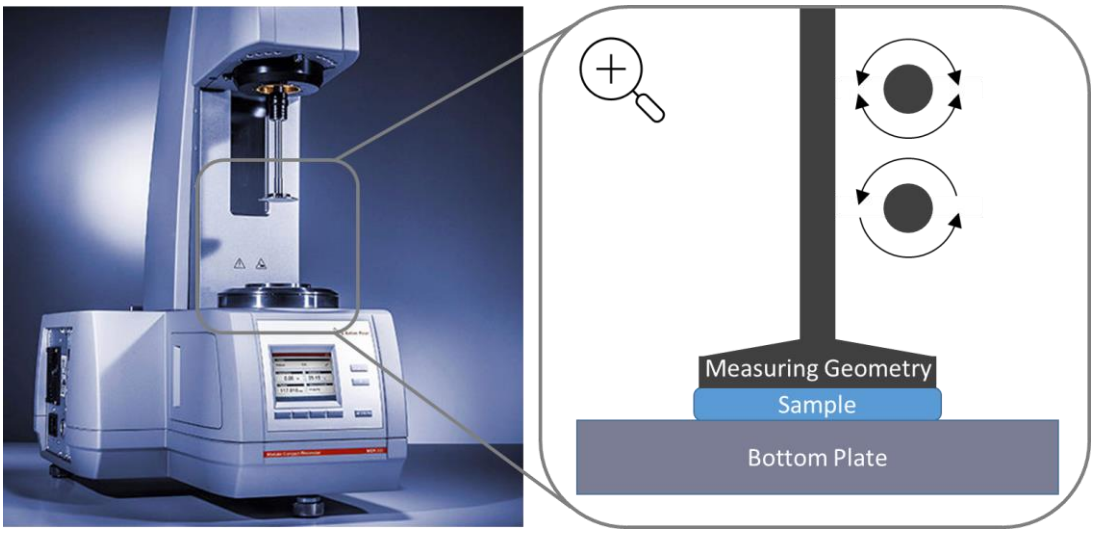

Figure 16 Image of the rheometer model used (left), and a schematic of correct sample loading in a parallel plate measuring geometry (right).

Rotational Rheology

Rheometers can operate in both rotational and oscillating modes.[126] These modes indicate the manner in which the measuring geometry moves relative to the sample. Rotational rheology is used to determine viscosity of the sample in different environments, simulating processes highly relevant for personal care products such as: spraying, pumping, or spreading. Varying the shear rate applied provides valuable insight into the flowability of the material and provides insight into its applicability as a personal care formulation.

The two-plates model is used to define relevant rheological parameters (Figure 17). In this model, the sample is placed between two parallel surfaces. The upper plate can be moved parallel to the lower stationary plate, applying shear to the sample. In the case of a rheometer, the upper plate is part of the measuring geometry and the bottom plate is usually fixed in position. The rheometer simultaneously records the rotational velocity of the upper plate, and the torque applied through its motor.[126]

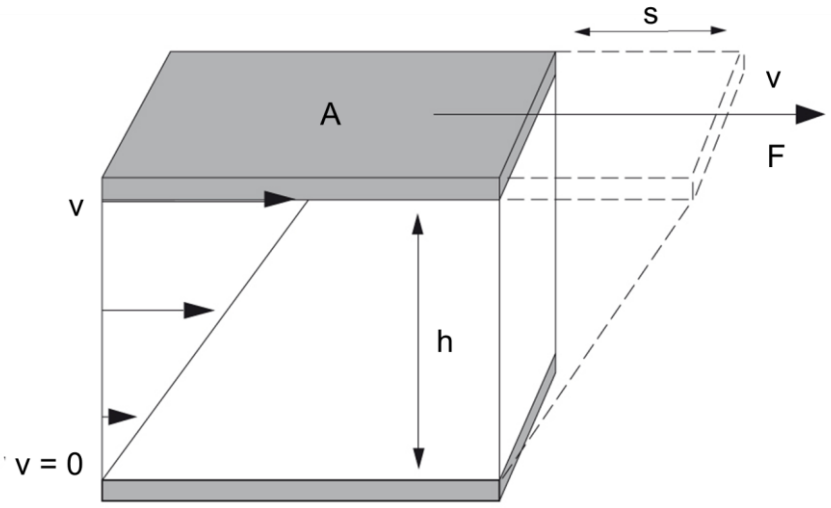

Figure 17 A schematic of the two-plates model used to define rheological parameters. Adapted from Mezger.[126] With shear area A, shear gap h, shear force F, deflection path s, and velocity v.

From the two-plates model, shear stress and shear rate can be defined, enabling the viscosity of the sample to be calculated (Equation 1).

$$Viscosity\ (Pa\ s) = \frac{Shear\ Stress\ (Pa)}{Shear\ Rate\ (s^{-1})}$$

Equation 1 Newton's Law.[126]

Shear stress is the ratio of shear force to shear area (Equation 2). The shear area determined by the physical dimensions of the measuring geometry, and shear force is determined *via* the torque applied by the rheometer motor.[126]

$$Shear\ Stress\ (Pa) = \frac{Shear\ Force\ (N)}{Shear\ Area\ (m^2)}$$

Equation 2 Calculation of shear stress.[126]

Shear rate is the ratio of velocity to shear gap (Equation 3). Velocity is set through the rotational speed of the measuring geometry, and shear gap is set through the instrument (a 1 mm shear gap is used in this thesis).

$$Shear\ Rate\ (s^{-1}) = \frac{Velocity\ (ms^{-1})}{Shear\ Gap\ (m)}$$

Equation 3 Calculation of shear rate.[126]

There are instrumental limitations that need to be considered when performing rotational rheological measurements. These are prevalent at the extreme ends of the measuring capabilities. In the case of low viscosity fluids, measurements at low shear rates can be inaccurate, as the torque applied by the rheometer can drop below the sensitivity of the instrument. To measure low viscosity samples more accurately, shear rate should be increased, as a larger, and more readily measurable, torque is needed to achieve higher shear rates. Conversely, highly viscous samples are often unsuitable for measurements at high shear rates. At a high viscosity the torque required from the rheometer motor can be insufficient to achieve a high shear rate. In addition, the centrifugal force generated by the rotating measurement geometry tends to eject highly viscous samples from the shear gap at increased shear rates.

Sample Viscosity	Shear Rate	Limitations
Low	Low	Torque below measurement threshold
High	High	Instrument motor insufficiently powerful
		Ejection of sample from measuring gap

Table 2 Instrumental limitations to consider during rotational rheometry.

Oscillatory Rheology

Personal care products often display a mixture of viscous (liquid-like) and elastic (solid-like) behaviour depending on the shear applied to them. This is known as viscoelastic behaviour. For example, hand creams can often retain their shape at rest, whilst also being spreadable when sheared. Oscillatory rheology can be used to probe the behaviour of viscoelastic materials and provide insight into properties such as the storage modulus, loss modulus, and flow point of the investigated substance.[126]

The key parameters in oscillatory experiments are shear strain and shear stress. Shear strain is the ratio between deflection path and shear gap and be expressed as a unitless number or a percentage (Equation 4).

$$Shear\ Strain\ (\%) = \frac{Deflection\ Path\ (m)}{Shear\ Gap\ (m)} \times 100$$

Equation 4 Calculation of shear strain in oscillatory rheology.[126]

Shear stress is a measurement of force applied to the sample per unit area (Equation 5).

$$Shear\ Stress\ (Pa) = \frac{Shear\ Force\ (N)}{Shear\ Area\ (m^2)}$$

Equation 5 Calculation of shear stress in oscillatory rheology.[126]

Shear stress and strain provide a comprehensive picture of the deformation of the sample. In terms of personal care products, increasing shear strain mimics the act of spreading a product. Shear stress is the amount of force required to spread the product. The oscillatory experiments in this thesis are performed using pre-set shear strain, that is, shear strain is predetermined by the rheometer through the deflection angle of the oscillations, and shear stress is determined through the torque input required to achieve said deflection angle.[126] This was done to achieve consistent sample deformation to mimic spreading of a personal care product.

In a typical experiment, the rheometer oscillates the measuring geometry around its equilibrium position (Figure 18). This applies a shear strain with a sinusoidal profile, deforming the sample.[126]

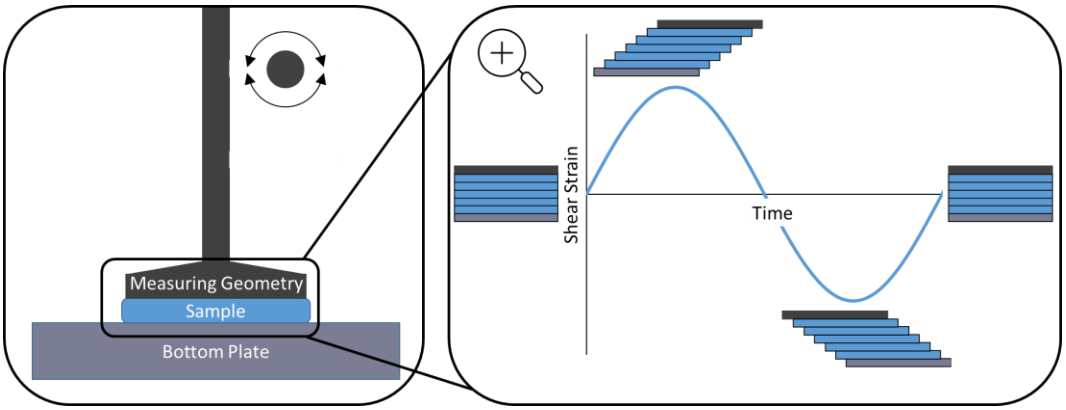

Figure 18 Schematic of a sample loaded between parallel plates with an applied sinusoidal oscillatory shear profile.

To achieve the desired shear strain and deform the sample, the rheometer must apply torque. From this torque, shear stress acting on the sample can be determined. The maxima of shear stress and shear strain are achieved at certain angular displacements. The time difference in angular displacement between these maxima is known as the phase shift (δ). A completely elastic sample will have a phase shift of 0°, as shear stress increases with shear strain, without any delay (Figure 19A). On the other hand, a perfectly viscous sample will exhibit its maximum shear stress when the rate of change of shear strain is greatest, as this is when the highest flow rate is achieved. As a result, the phase shift of a perfectly viscous sample will be 90° (Figure 19B). A viscoelastic sample will be in-between these two extremes, exhibiting a mixture of solid-like and liquid-like behaviour (Figure 19C).[126]

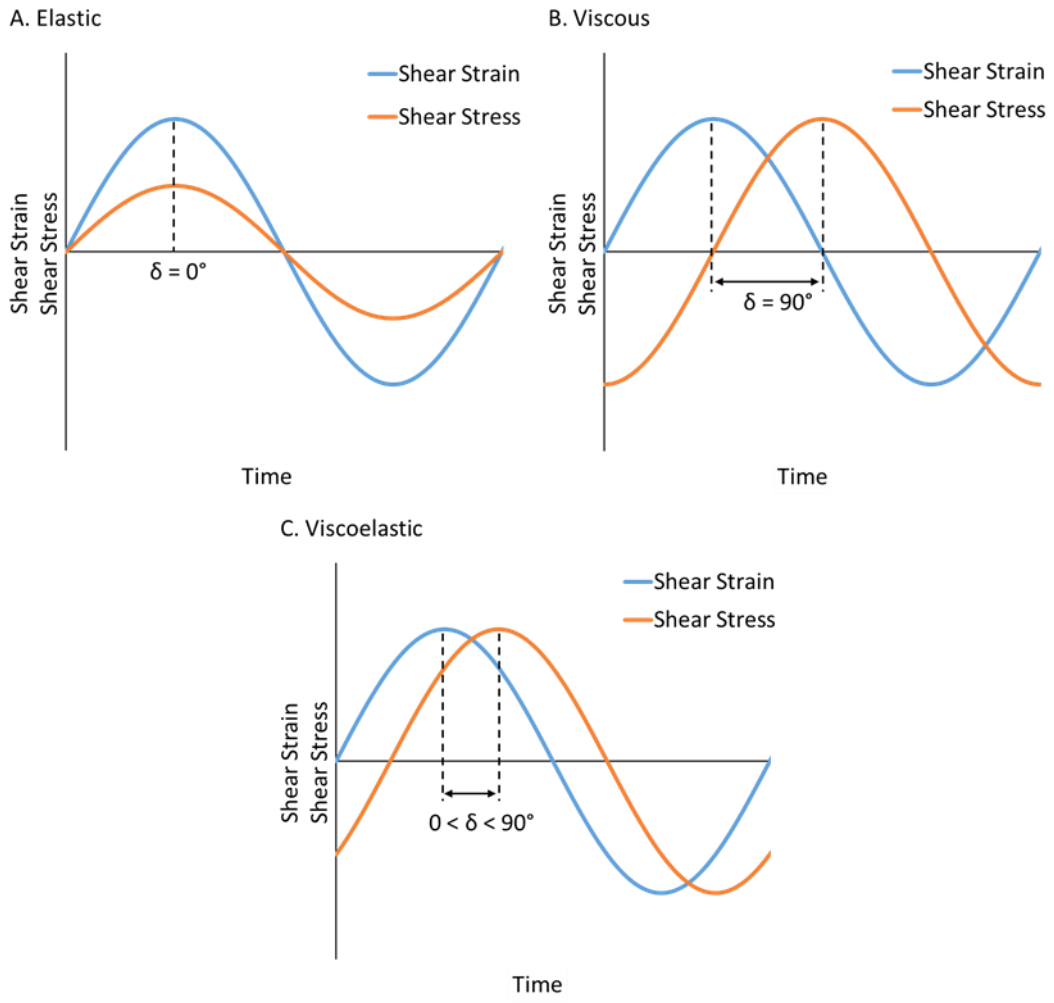

Figure 19 The phase shift between shear strain and shear stress varies depending on the nature of the material. A: Fully elastic behaviour. B: Fully viscous behaviour. C: Viscoelastic behaviour.

From the maxima of strain and stress, the complex modulus (G*) can be determined. The complex modulus is a quantitative measure of resistance to deformation or material stiffness.

$$Complex\ Modulus\ (Pa) = \frac{Shear\ Stress\ (Pa)}{Shear\ Strain\ (unitless)}$$

Equation 6 Calculation of complex modulus from the maxima in shear stress and shear strain.[126]

The complex modulus is composed of both a storage and a loss component. The storage modulus gives information about the amount of structure in the material, or how much energy is stored in the elastic structure of the material. The loss modulus gives information about the viscous "unstructured" portion of the sample, or how much energy is dissipated

by the sample. The phase shift between shear strain and shear stress allows the storage modulus (G') and loss modulus (G'') to be separated from the complex modulus. This can be represented geometrically (Figure 20).[126]

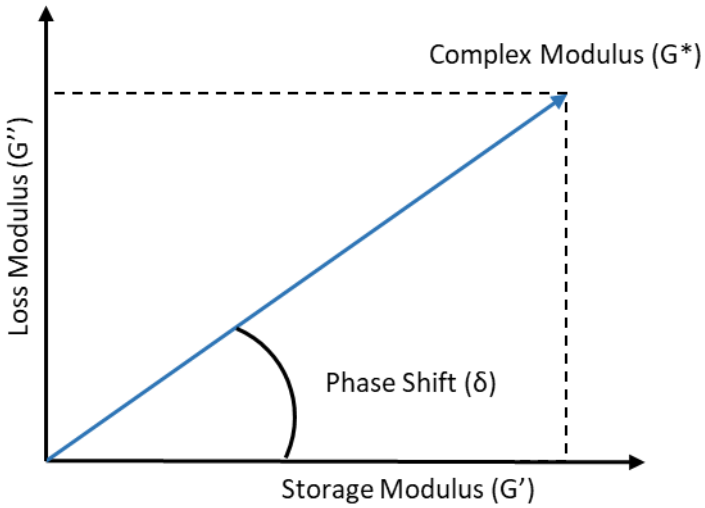

$$G' = G^* \sin\delta$$

$$G'' = G^* \cos\delta$$

$$G^* = \sqrt{(G')^2+(G'')^2}$$

$$\tan\delta = \frac{G''}{G'}$$

Figure 20 Geometric relationship between the complex, storage, and loss modulus, and relevant equations.

The viscoelasticity desired depends on the area of application of the personal care product, for example, certain products should display elasticity at rest whilst being spreadable at higher shear (hand cream is a typical example). For these products storage modulus should exceed loss modulus at low shear, with the opposite being true at high shear. The crossover point between storage and loss modulus is known as the flow point and gives an indication of the force required to spread the viscoelastic material.

Summarising Remarks and Next Steps

The results shown in Chapter 4 showcases the effectiveness of lightly cross-linked PG-based polyesters as rheological modifiers. Significant thickening effects were achieved at loadings as low as 2.5 wt.%. Studies investigating the swelling in aqueous media and degradation were also conducted, providing a complete overview of the characteristics displayed by the rheological modifier.

To further enhance the performance of the rheological modifier, alternative synthetic methodology to polycondensation was explored. This was done with the aim of increasing the molar mass, which is usually very high for rheology modifiers, and increasing the control over branching in the system, which is difficult to precisely control during polycondensation.

Introduction to Chapter 5. Anionic Polymerisation for Linear Polyglycerols

Chapter 5 evaluates the potential of anionic polymerisation for the synthesis of linear, high molar mass, hydrophilic polymers for potential application as rheology modifiers.

In anionic polymerisation, the propagating chain contains a negatively charged species.[127] Double-bond containing monomers such as styrene, butadiene, and acrylates can be polymerised using this technique. Other monomers include cyclic species such as epoxides, lactones, and lactams, which undergo anionic ring-opening polymerisation (Figure 21).[127–131]

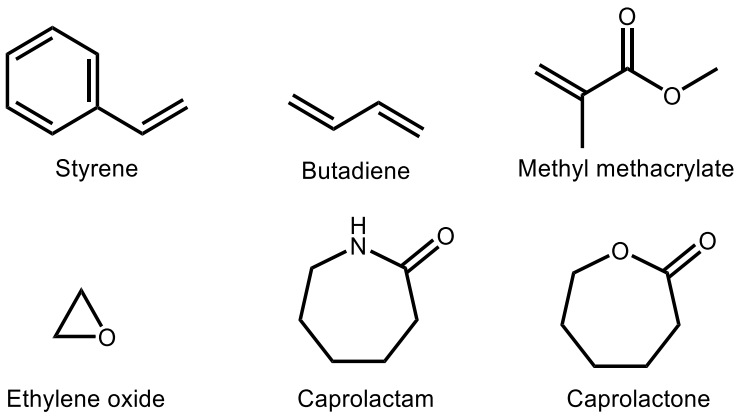

Figure 21 A selection of monomers suitable for anionic (ring opening) polymerisation.

In contrast with polycondensation, anionic polymerisation allows for polymers to be synthesised with high molar mass and low dispersity.[127] This is a result of the living nature of anionic polymerisation, as termination and chain transfer processes are prevented under appropriate reaction conditions.[132] Anionic polymerisation is extremely moisture sensitive, as the negatively charged propagating chain ends are easily quenched.[133]

For rheological modification of aqueous media, a hydrophilic polymer is required. Anionic ring-opening polymerisation of protected glycidol species is commonly used in the literature to synthesise linear polyglycerol.[134] Owing to its free hydroxyl group linear polyglycerol is hydrophilic, and could be suitable for use in aqueous systems. Protecting groups are required to prevent the formation of hyperbranched systems, as is the case for the direct polymerisation of glycidol.[135] A variety of protected glycidols have been reported in the literature for the synthesis of linPG (Figure 22).[136]

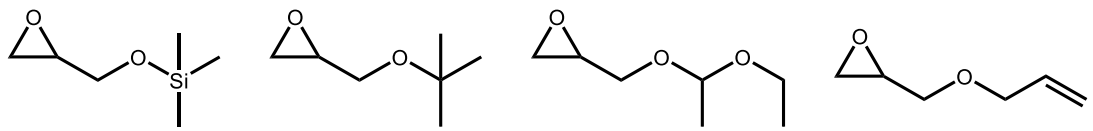

Figure 22 Structures of protected glycidol structures. Left to right: trimethylsilyl glycidyl ether, tert*-butyl glycidyl ether, ethoxyethyl glycidyl ether, and allyl glycidyl ether.*

Summarising Remarks

Chapter 5 briefly explores anionic polymerisation for the purpose of synthesising linear polyglycerol. Whilst anionic polymerisation unlocks the synthesis of higher molar mass polymers with greater control than polycondensation approach of Chapter 3, it is at a cost of the green credentials of the process. The chemicals employed are significantly more hazardous, wasteful protecting groups are essential, and degradability of the final polymer cannot be taken for granted. So, whilst being promising in terms of the eventual performance, this approach does feature severe limitations.

Introduction to Chapter 6. Project Vole

Chapter 6, the final experimental chapter, applies biobased polyglycerols as the basis for the synthesis of a photoactive resin for volumetric additive manufacturing (VAM). During work exploring biobased oligomeric polyglycerols in Chapter 3, the suitability of these materials as the framework of a photocurable resin became apparent.

Additive manufacturing (AM) technologies have gained popularity of producing end-use parts with multiple components and materials.[137] These parts find use in several fields, ranging from personalised medical devices,[138] microfluidics,[139] optics,[140] and aerospace components.[141] Current AM methodologies build three-dimensional components by means of repeatedly performing one- or two-dimensional operations, to achieve three-dimensionality by a layer-by-layer approach.[142,143] However, this stepwise approach features multiple limitations, including compromised surface quality, reduced throughput, increased postprocessing requirements, restricted geometric capabilities, and potential for mechanical performance anisotropy.[142,143] Considering these constraints, an AM technique which simultaneously fabricates all points within any three-dimensional geometry is needed.

Employing volumetric part formation this all-at-once approach is enabled.[143–145] VAM opens new possibilities for integrating multiple components, broadens material options, and reduces build time, increasing throughput.[143–145] Volumetric printing operates based on computed axial lithography (CAL).[143] Using CAL, the three-dimensional build is deconstructed into a series of two-dimensional projections which are projected into a rotating vial containing photoactive resin (Figure 23). The overall superposition of projections from multiple angles produces a three-dimensional energy dose sufficient to polymerise the photoactive resin in the desired geometry.[143] Resin outside of the targeted geometry will receive a lower dose of light, and remain uncured.

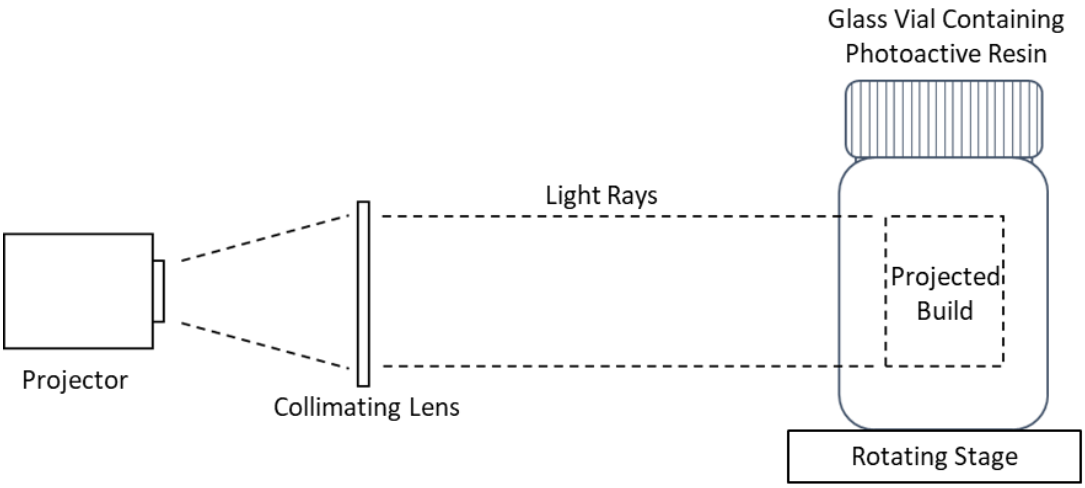

Figure 23 Schematic illustration of a volumetric printer.

Forming the build in a concerted manner, within the surrounding resin, allows for supporting structures seen in other AM techniques to be avoided.[144] Supporting structures generate waste and require post-processing to be removed, and are therefore ideally avoided.[142] In VAM, the uncured resin itself acts as the supporting structure, stabilising overhanging features.[146]

To be suitable for use in VAM, the photoactive resin needs to fulfil a selection of criteria. The resin should be viscous to avoid gravitational sedimentation of the printing part during manufacture.[147] A suitable resin must also be optically transparent to allow the projection to enter the resin volume without strong attenuation or light scattering.[146] In addition, the resin needs to be photoactive for it to be cured upon exposure to light.[145]

Currently, photoactive resins employed for VAM remain of limited abundance, with the majority being of petrochemical origin. Resins previously used in the literature include bisphenol A methacrylate,[147] poly(ethylene glycol) diacrylate,[143,148] and dipentaerythritol pentaacrylate based materials.[149] A limited number of resins made from renewable feedstocks have been utilised for VAM, including gelatin-methacrylate,[150] polycaprolactone-based,[151] and silk.[152] These materials are challenged by issues related to scalability, batch-to-batch variations, and environmentally unsound synthetic procedures. It follows that there is substantial need for a renewably sourced resin that can be produced using scalable, robust, and environmentally sound synthetic methodologies.

Oligomeric polyglycerols were identified to be highly promising for VAM. These polyglycerols are viscous, transparent, commercially available, and renewable. Polyglycerols only require

installation of curable groups, such as acrylates, and mixing with an appropriate photoinitiator to be useful as VAM resins. Thanks to their abundance of hydroxyl groups, polyglycerols are readily functionalised by esterification, which is utilised in Chapter 6 to install acrylate functionality.

Chapter 2. Functional Enzymatic Ring-Opening Polymerisation

2.1 Aims & Objectives

Aliphatic polyesters containing reactive end-groups have been used for the formulation of nanoparticles for drug-delivery applications. Unfortunately, the synthesis of these materials usually requires the use of toxic catalysts that are difficult to recycle.

This chapter investigates the use of Novozym 435, a commercially available immobilized lipase, to produce aliphatic polyesters with reactive end-groups for the synthesis of polymeric nanoparticles.

2.2 Abstract

Enzymatic ring-opening polymerisation (eROP) using *N*-hydroxyethyl acrylamide (HEAA) as a functional initiator was explored using ε-caprolactone and δ-valerolactone as model monomers. In literature, the susceptibility of acrylates to nucleophilic attack in the presence of lipases limits their employability in eROP. Species such as HEMA undergo self-transesterification, leading to a loss of control over the enzymatic reaction. It was found that, under the reaction conditions employed, HEAA does not undergo self-reaction in the presence of Lipase B from *Candida antarctica*. Unexpectedly, HEAA consistently reached a significantly lower conversion than that seen for the lactone monomers. Computational docking studies showed that the initiator has a lower binding affinity to the enzyme active site than an initiated polymer chain, leading to initiation proceeding at a slower rate than propagation, resulting in incomplete initiator conversion. Organocatalytic chain extension with lactide was performed to demonstrate hydroxyl end-group fidelity. Radical copolymerisation of HEAA initiated polycaprolactones with poly(ethylene glycol) methacrylate (PEGMA) was performed to produce a small set of amphiphilic copolymers. These amphiphilic polymers were self-assembled into nanoparticles displaying low cytotoxicity in 2D *in vitro* experiments. To adhere to the Principles of Green Chemistry more closely, the biobased solvent 2-methyl tetrahydrofuran (2-MeTHF) was utilised as an alternative to more commonplace petrochemical solvents.

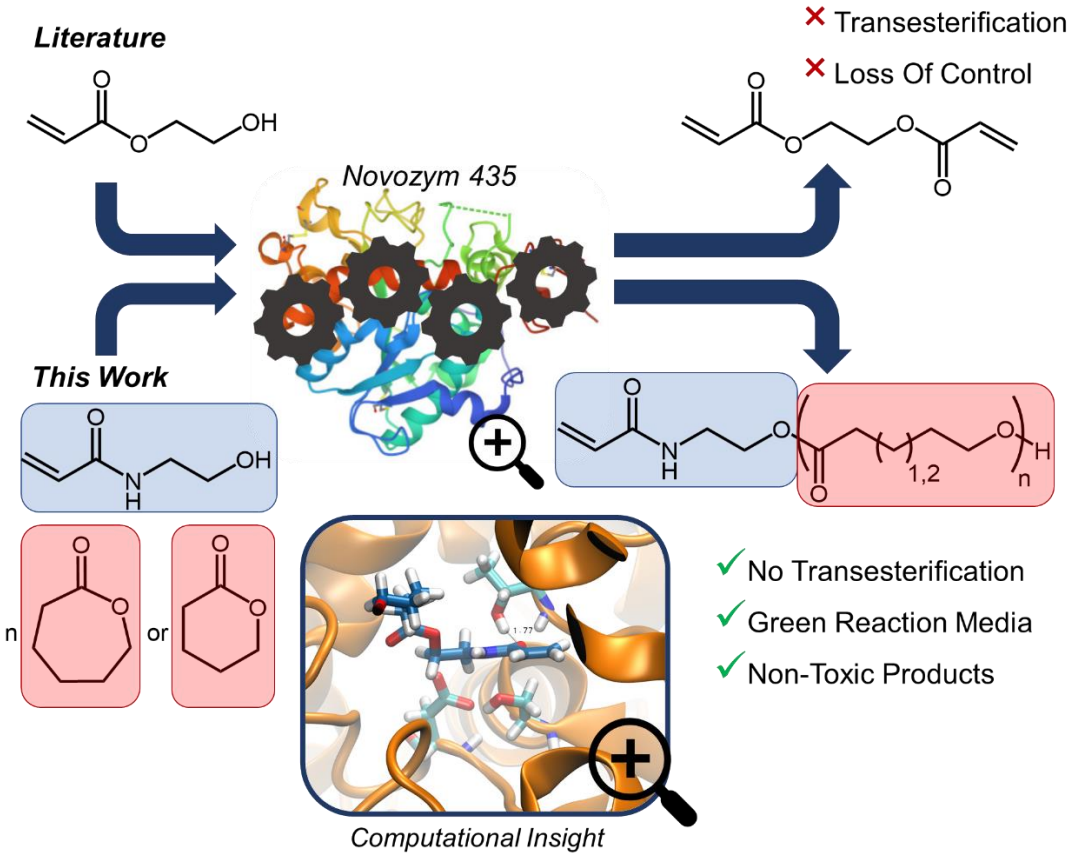

Figure 24 Graphical abstract of this chapter.

2.3 Introduction

Aliphatic polyesters have garnered research interest for their biodegradability, low cost of production, and biocompatibility.[25] These factors are particularly interesting for pharmaceutical applications.[153] Unfortunately, aliphatic polyesters such as polycaprolactone (PCL), polylactic acid (PLA), and polyvalerolactone (PVL) have very limited chemical functionality. Installing terminal and side-chain groups can increase the applicability of these materials.[31] Introduction of a radically polymerisable functional group, such as an acrylate or acrylamide, allows for further reactions to occur, and more demanding applications to be accessed.[25,26,154,155] Polymerisation of the installed functional group yields hybrid materials containing both polyester as well as polyacrylate/polyacrylamide components (Figure 25).

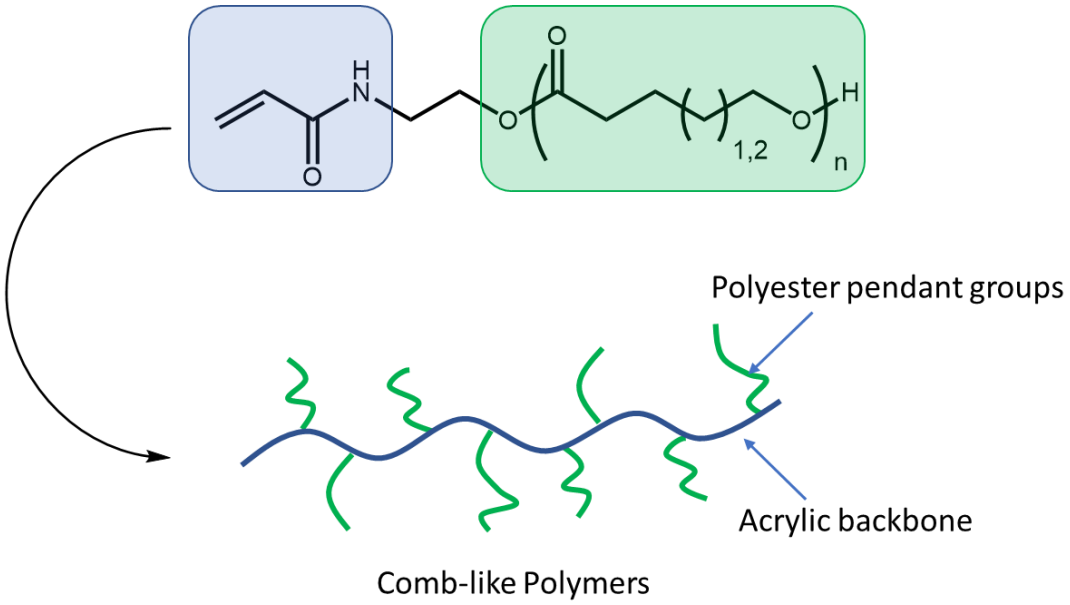

Figure 25 Installing a radically polymerisable end-group on aliphatic polyesters unlocks comb-like architectures through radical co-polymerisation.

Utilising the initiator method in ROP enables straightforward installation of desired functionality.[57] HEMA has been explored in the literature as an example of a functional initiator, since it contains a methacrylate group suitable for further polymerisation steps following initial ROP. HEMA has been explored for ROP using enzymatic,[154,155] metal-based,[156] and organocatalytic[38,157] methodologies. In the case of HEMA, several limitations are encountered. Most notable is the lability of the acrylic ester bond, which is susceptible to nucleophilic attack.[154,157] Utilisation of lipase or strongly basic catalysis results in transesterification reactions and loss of control over the reaction.[25] Tin-based catalysis can be employed, although this approach requires elevated temperatures.[31,153] Furthermore, tin catalysts have been shown to exhibit significant toxicity towards mouse fibroblasts and human endothelial cell fibroblasts.[33] In addition, tin catalysts are challenging to separate from the final product.[49,158]

Enabling the use of enzymatic catalysis to synthesise hybrid materials would be highly desirable. Lipases are highly selective, metal-free, and non-hazardous – in stark contrast with many chemical catalysts.[49,159] N435 was chosen as an ideal candidate for this work. N435 is commercially available, has a broad substrate scope, and is readily recycled.[160–162] The heterogeneous nature of the catalyst is a distinct advantage in comparison to tin-based or organic catalysts. N435 is easily recovered by filtration, unlike homogeneous catalysts that require wasteful liquid-liquid extraction and purification in order to be recycled.[43] On an

industrial scale, extraction of the catalyst using liquid-liquid extraction introduces an additional non-negligible waste stream – increasing the cost of the overall system and in contradiction to the Principles of Green Chemistry.[102] Heterogeneous catalysts, such as N435, are much more straightforward to remove and reuse.[163]

A well-established problem with N435 in functional eROP is the transesterification of ester containing initiators.[154,155] The lipase is unable to distinguish between the ester bonds of the monomer and initiator, leading to indiscriminate reactivity and loss of control over the reaction. The catalytic cycle of HEMA transesterification, forms ethylene glycol and ethylene glycol dimethacrylate (Figure 26).

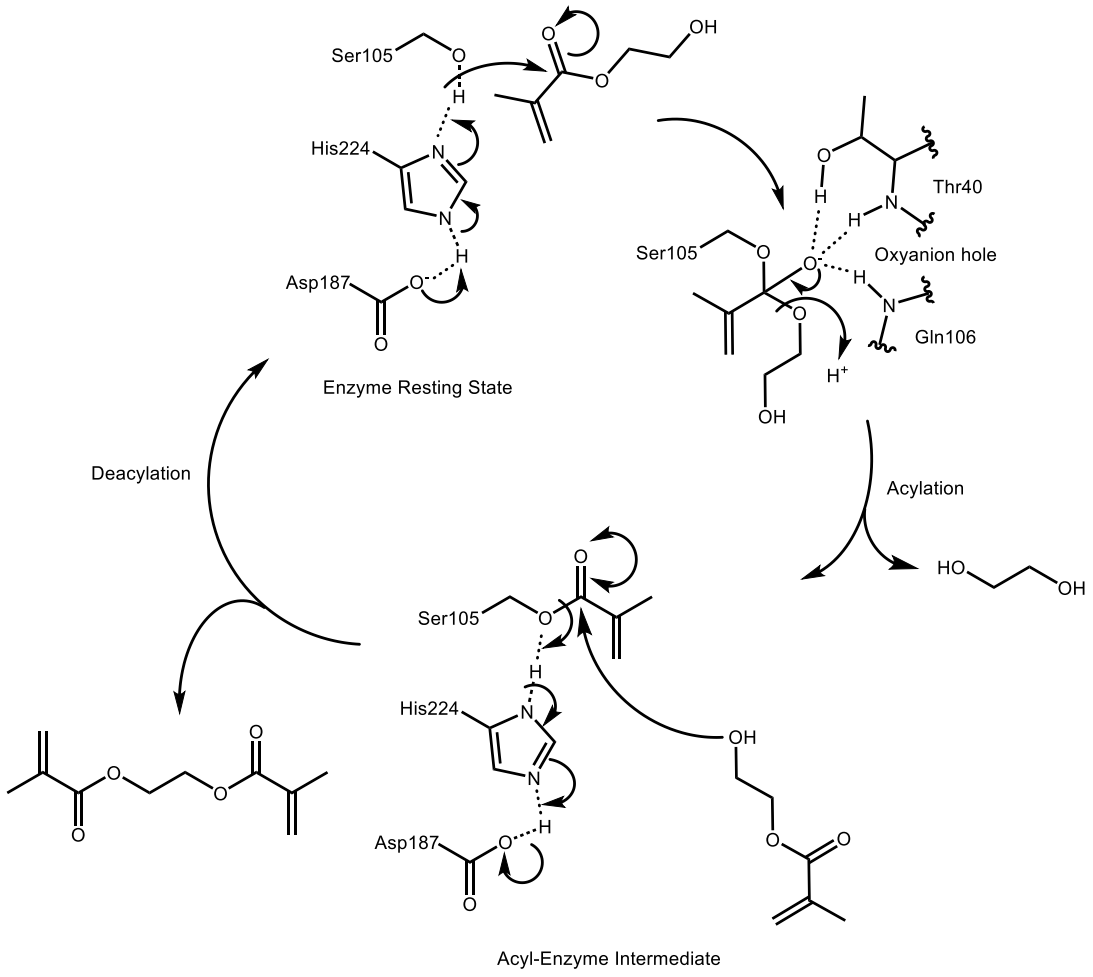

Figure 26 Transesterification of HEMA with CaLB yields ethylene glycol and ethylene glycol dimethacrylate.

Ethylene glycol contains two hydroxyl groups, and can act to initiate eROP, producing chains terminated by hydroxyl group on either side. Due to the presence of two methacrylate groups, ethylene glycol dimethacrylate acts as a cross-linking agent in radical polymerisation. As a result, utilising HEMA in eROP will yield a mixture of products. Therefore, an alternative initiating species that is stable in the presence of N435 is required to synthesise aliphatic polyesters with well-defined end-groups by eROP.

To achieve eROP in a controlled manner alternative approaches must be considered. In this work HEAA was explored as an alternative to HEMA. It was hypothesised that serine-based lipases, like CaLB, would be unable to catalyse amidolysis under the conditions employed owing to the enhanced stability of the amide bond relative to an ester bond.[31] HEAA was deemed to be an ideal candidate, featuring an analogous structure to HEMA, commercially available, and inexpensive. HEAA has been utilised widely, with application in thermosetting paints, coatings, sealants, and personal care products.[164] Poly(HEAA) possesses strong anti-fouling properties,[165] and has been investigated for protein separation[166] and drug delivery systems.[167,168]

The precedent of poly(HEAA) in drug delivery systems encouraged the exploration of HEAA as an eROP initiator to produce materials for nanoparticle formulation. Introduction of hydrophilic co-monomers through radical co-polymerisation can be used to tune the self-assembling properties of the produced materials. A hydrophilic component is needed to stabilise the hydrophobic component of the NPs in aqueous media. The presence of a degradable aliphatic polyester should facilitate eventual excretion of the NPs, avoiding bioaccumulation.[169]

The eROP reactions were performed in 2-MeTHF. 2-MeTHF is a bio-based solvent, produced from enzymatic and chemical treatment of biomass.[170,171] 2-MeTHF features similar solubility parameters to petrochemical solvents like THF and DCM.[26] Additionally, 2-MeTHF possesses an elevated boiling point (80 °C) and lower critical solution temperature with water in comparison to THF.[26,172] The decrease in water solvation is highly desirable for eROP to limit hydrolytically initiated polymer chains. From an economical standpoint, the cost of 2-MeTHF is comparable to non-renewable solvents on the lab scale.[26] Previous work in the Howdle Group has demonstrated the suitability of 2-MeTHF for the combination of eROP and radical techniques.[26]

This chapter describes the use of HEAA as a functional eROP initiator to produce aliphatic polyesters containing acrylamide end-groups. HEAA initiated eROP was studied in-depth

using ^{1}H-NMR spectroscopy, from which incomplete initiator conversion was observed. Computational docking studies were utilised to gain insight into the substrate specificity exhibited by N435 which impacted the course of the reactions investigated. Chain extensions using lactide and radical (co-)polymerisation were performed to demonstrate viability of the polymer end-groups. Amphiphilic co-polymers of HEAA-PCL and PEGMA were assembled into polymeric NPs by nanoprecipitation. Cytotoxicity tests were carried out to assess suitability of the materials for biomedical applications.

2.4 Results and Discussion

2.4.1 *N*-Hydroxyethyl Acrylamide Stability in The Presence of Novozym 435

To lay the groundwork for further experiments, the stability of HEAA had to be assessed in the presence of N435 under suitable reaction conditions. Owing to the structural similarity between HEMA and HEAA, it was imperative that self-reaction was ruled out for the hydroxyl containing acrylamide (Figure 27).

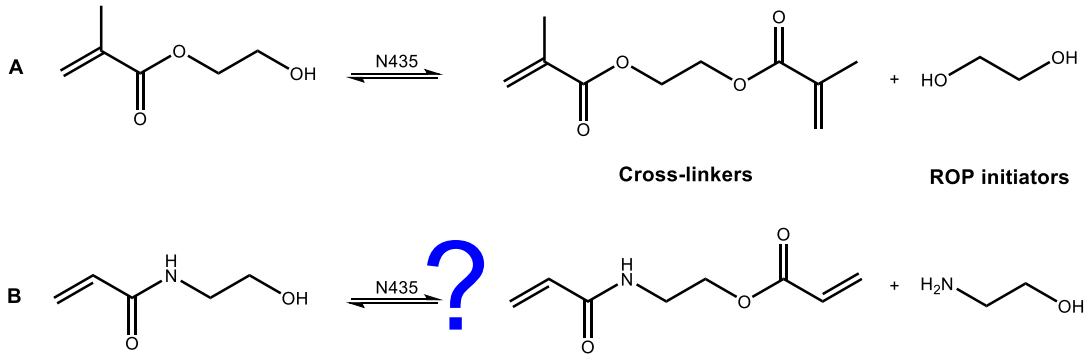

Figure 27 A: HEMA transesterification catalysed by N435 forms ethylene glycol dimethacrylate and ethylene glycol, a radical cross-linker and a bifunctional eROP initiator, respectively. B: HEAA is hypothesised not to undergo analogous reactions in the presence of N435 due to the increased stability of the amide bond.

The transesterification of HEMA in the presence of N435 is well-documented in the literature.[154,155] As such, HEMA was used as a positive control. Progress of transesterification can be readily monitored using ^{1}H-NMR spectroscopy thanks to the appearance of peaks corresponding to ethylene glycol, and ethylene glycol dimethacrylate. Specifically, the vinyl peaks (Appendix Figure 1) allow for straightforward calculation of the extent of transesterification (Equation 7).

$$Transesterification\ of\ HEMA\ (\%) = \frac{\int 6.11\ ppm}{\int 6.13\ ppm + \int 6.11\ ppm} \times 100$$

Equation 7 Transesterification of HEMA (%) was calculated by ^{1}H-NMR analysis at 6.13 and 6.11 ppm. The signal at 6.11 ppm corresponds to the transesterified species, and the peak at 6.13 ppm corresponds to HEMA (Appendix Figure 1).

In contrast to HEMA (Appendix Figure 1), HEAA does not show any self-reaction under reaction conditions. The stability of HEAA was assessed by ^{1}H-NMR spectroscopy (Figure 28), in which no signals corresponding to ethanolamine (triplets at 3.58 and 2.81 ppm, Appendix Figure 2) can be observed. The vinyl region of the spectra also remained unchanged during

the experiment, further demonstrating stability of HEAA in these conditions (65 °C, 10 wt.% N435).

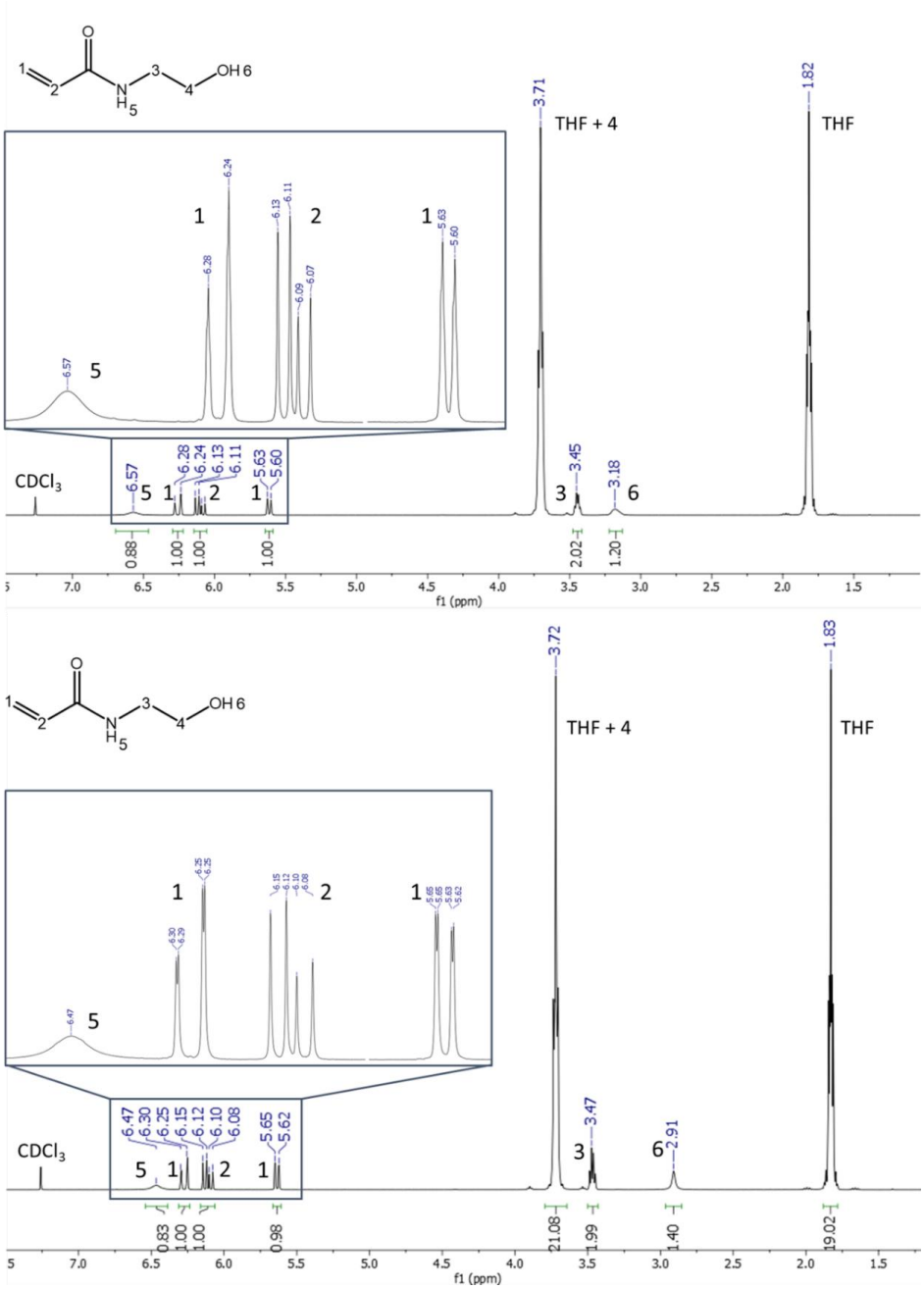

Figure 28 ^{1}H-NMR spectra of HEAA and THF in $CDCl_3$ before (top) and after 20 h at 65 °C with 20 wt.% N435 (bottom). Note that no change has taken place before and after subjecting HEAA to reaction conditions. In the lower spectrum the geminal splitting in the peaks labelled 1 can be resolved to see a doublet of doublets. Note that the peaks corresponding to the protons of 4 are hidden underneath a THF signal.

Various N435 loadings were screened (5, 10, and 20 wt.%). Transesterification of HEMA increased up to 41% after 20 hours with 20 wt.% N435, whilst no self-reaction of HEAA was observed for any of the tested catalyst loadings.

N435 loading (wt.%)[a]	HEMA Transesterification (%)[b]	HEAA Self-reaction (%)[b]
5	25	Not detectable
10	29	Not detectable
20	41	Not detectable

Table 3 Extent of transesterification of HEMA and self-reaction of HEAA with various N435 loadings. HEMA is included as a positive control since it is known to react with itself under these conditions. [a] Wt.% with respect to initiator [b] Determined by ^{1}H-NMR spectroscopy.

The extra stability of HEAA over HEMA can be explained by the greater stability of amides towards nucleophilic attack. The lower electronegativity of nitrogen compared to oxygen leads to a greater contribution of the delocalised resonance form to the overall resonance hybrid. This ensures the carbonyl oxygen holds a greater partial negative charge, thus decreasing the susceptibility of the carbonyl carbon towards nucleophilic attack. CaLB promotes (trans-)esterification through an initial nucleophilic attack by an activated serine residue (Figure 26). This acylation step forms the acyl-enzyme intermediate.[54,55] It was hypothesised that formation of the acyl-enzyme intermediate by nucleophilic attack is hindered due to the increased partial negative charge delocalised onto the acrylamide oxygen, lowering overall electrophilicity of the carbonyl bond (Figure 29).[173,174] Slowing, or preventing entirely, the formation of an undesired HEAA acyl-enzyme intermediate is fundamental to reigning in the reactivity of CaLB and achieve differentiation between initiator and lactone monomer.

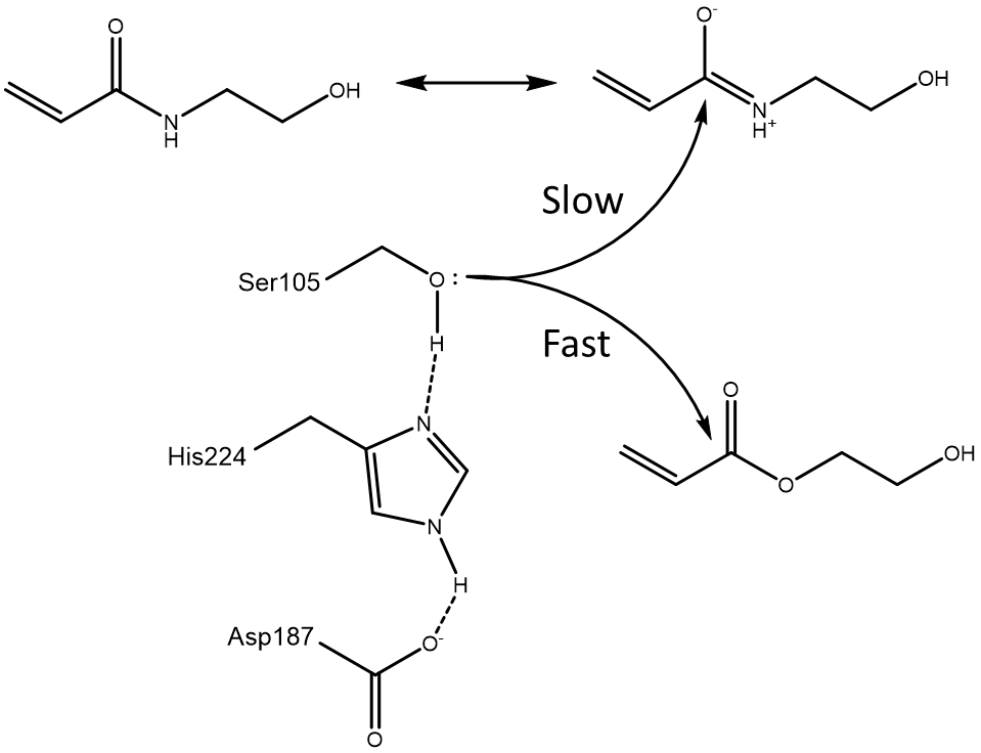

Figure 29 Delocalisation of the nitrogen lone pair in HEAA stabilises the carbonyl bond toward nucleophilic attack by the activated serine residue in CaLB.

It should however be noted that HEAA, in contrast to HEMA, is associated with Hazard Statement H373 – "may cause organ damage through prolonged or repeated exposure". This statement is applicable to HEAA as a monomer, however, once polymerised this is not applicable. Poly(HEAA) has been utilized in a variety of applications, and demonstrates low cytotoxicity. In this chapter, cytotoxicity measurements are performed on produced materials, and minimal *in vitro* cytotoxicity demonstrated.

The control experiments indicated that HEAA would not decompose or undergo other undesirable transformations and looked promising as a functional eROP initiator. These promising results in terms of initiator stability encouraged the investigation of eROP using some model monomers.

Functional eROP using HEAA as an initiator was performed using VL and CL. These monomers were determined to be optimal model-monomers for this investigation thanks to the abundance of literature precedent on their enzymatic polymerisation.[46] These monomers can be produced from renewable feedstocks, and the aliphatic polyesters produced from their ring-opening polymerisation are documented to be biodegradable, biocompatible, and suitable for a variety of applications.[23,24,175,176]

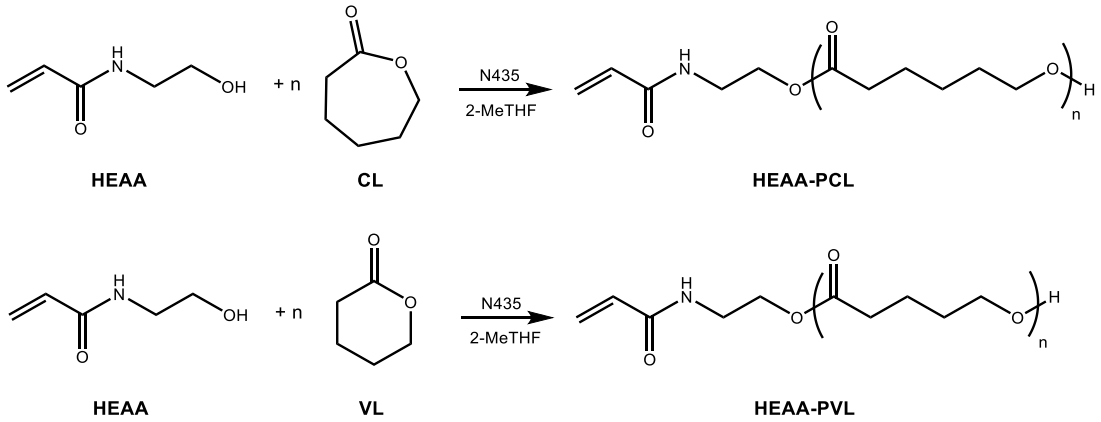

Figure 30 Investigated eROP reactions using HEAA as an initiator, and CL or VL as monomers. n=5 to 40 units.

Reactions were performed in 2-MeTHF to abide by the Principles of Green Chemistry. Experimentally it was found that 2-MeTHF displayed very similar characteristics to THF, and as such the transition to a biobased solvent was seamless.

2.4.2 Lactone Conversion during Enzymatic Ring-Opening Polymerisation

Reaction kinetics of HEAA initiated eROP were investigated by analysing reaction aliquots using ^{1}H-NMR spectroscopy (Figure 32). These spectra allowed conversion of monomer into polymer to be plotted against time and for further insights into the course of reaction to be gained.

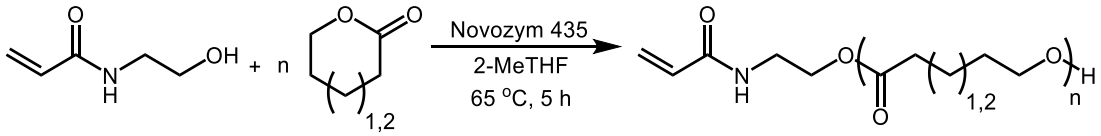

Figure 31 Reaction scheme of HEAA initiated eROP.

The conversion of CL and VL appear to follow pseudo first-order kinetics, with VL conversion approaching 85-90% at equilibrium (Figure 32) and CL tending towards quantitative conversion (Figure 33). Lower conversion at equilibrium for VL can be explained by its lower ring-strain energy in comparison with CL.[177] It follows that a lower ring-strain disfavours ring-opening polymerisation – which is primarily driven thermodynamically by release of ring-strain. Resultingly the equilibrium state of VL to PVL will contain more VL, due to the lower driving force of polymerisation in comparison to CL. Published research has also shown that VL exhibits a lower rate of polymerisation than CL in CaLB catalysed eROP.[178]

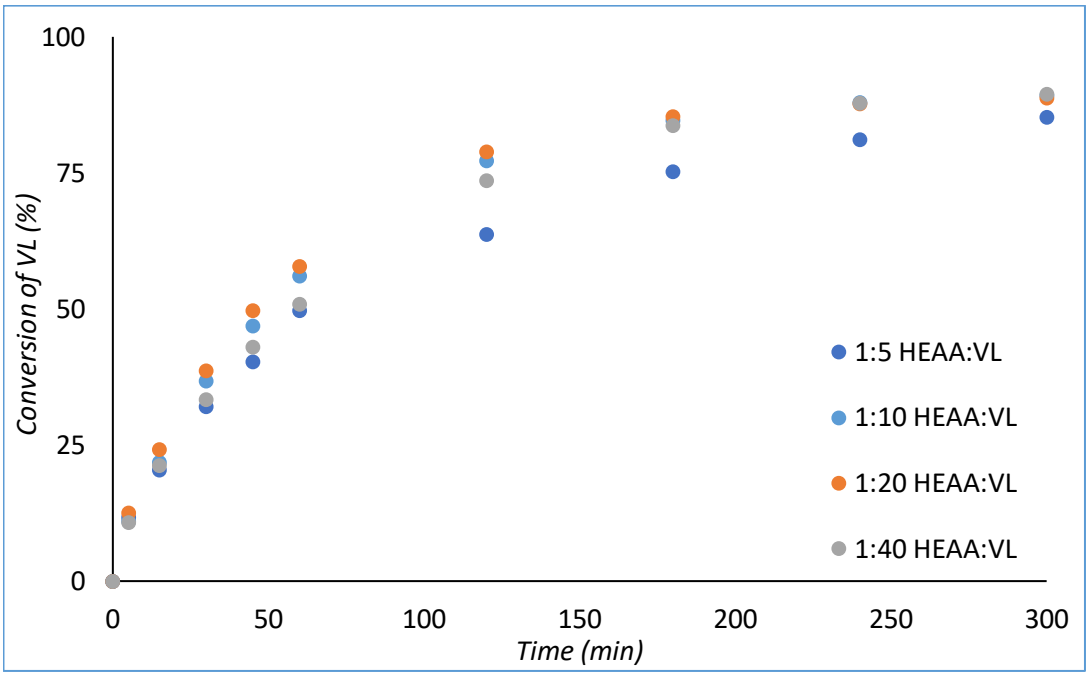

Figure 32 Conversion of VL in HEAA initiated eROP plotted against time.

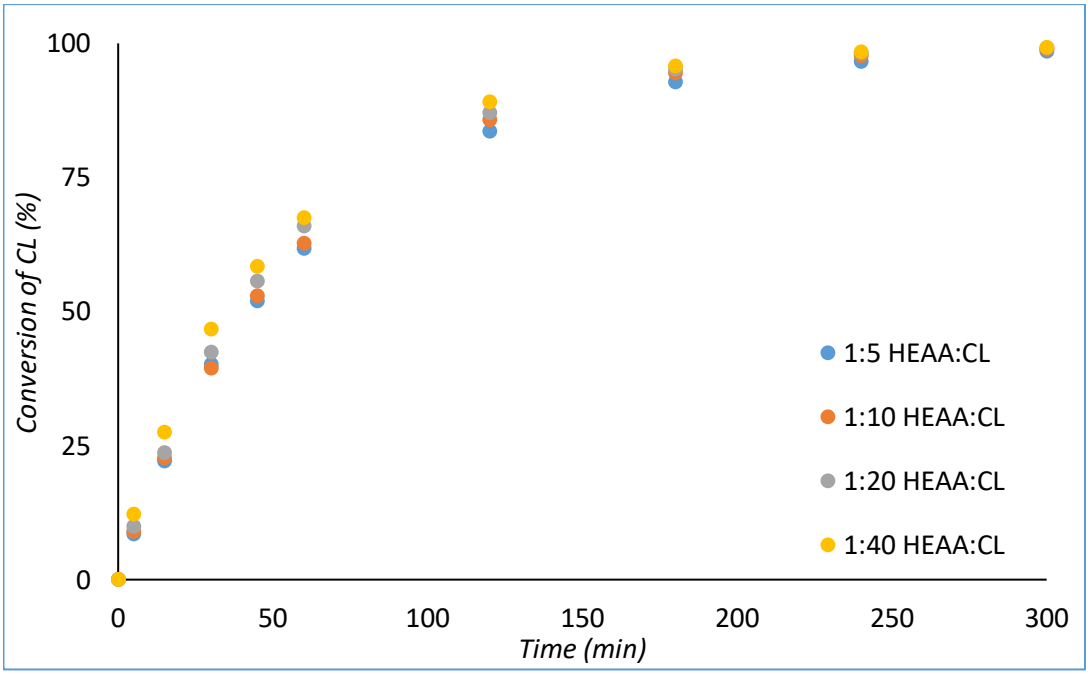

Figure 33 Conversion of CL in HEAA initiated eROP plotted against time.

A variety of chain lengths were targeted during synthesis by altering the ratio of initiator to monomer in the reaction (1:5, 1:10, 1:20, and 1:40). It was found that variations in stoichiometry between initiator and monomer did not significantly impact the kinetics of monomer conversion and, monomer conversions obtained after five hours of reaction time

were comparable for all ratios investigated (Figure 32, Figure 33). Tabulated data can be found in Appendix Table 1 and Appendix Table 2.

Pseudo First-Order Kinetics

Adherence to pseudo first-order kinetics was assessed through plotting the natural logarithm of CL or VL consumption against time.[179] An internal standard was needed to determine the relative quantity of monomer present in the reaction at a given datapoint. HEAA was chosen as internal standard. Specifically, the acrylamide signal at 6.31-6.24 ppm in the ^{1}H-NMR spectrum was used as internal standard. As discussed *vide infra,* splitting in the HEAA signals is observed. This was counteracted by integrating over both HEAA signals during analysis. It was assumed that no HEAA was lost over the course of the reaction, and that HEAA was only converted into HEAA-initiated polymer.

$$[M] = \frac{0.5 \int Lactone}{\int HEAA\ internal\ standard}$$

Equation 8 Calculation of the ratio between monomer and internal standard. A factor of 0.5 is included to correct for the presence of two protons in the signals for the lactones (CH_2-O-) relative to the single proton of HEAA. [M_0] corresponds to [M] at time zero.

The obtained values were subsequently plotted graphically for further analysis. The resulting first-order plots show rate of reaction is proportional to the concentration of monomer. CL follows pseudo first-order kinetics throughout the reaction, whereas VL deviates as equilibrium is reached. Subsequently the data points for VL at 240 and 300 minutes were excluded, as nonconformity is a result of equilibrium being obtained. Over the first 180 minutes of reaction VL demonstrates pseudo first-order kinetics, with R^2 values exceeding 0.95. (Figure 34) VL was found to have lower kinetic constants than CL, as expected due to its lower ring-strain and known slower reactivity in eROP.[178]

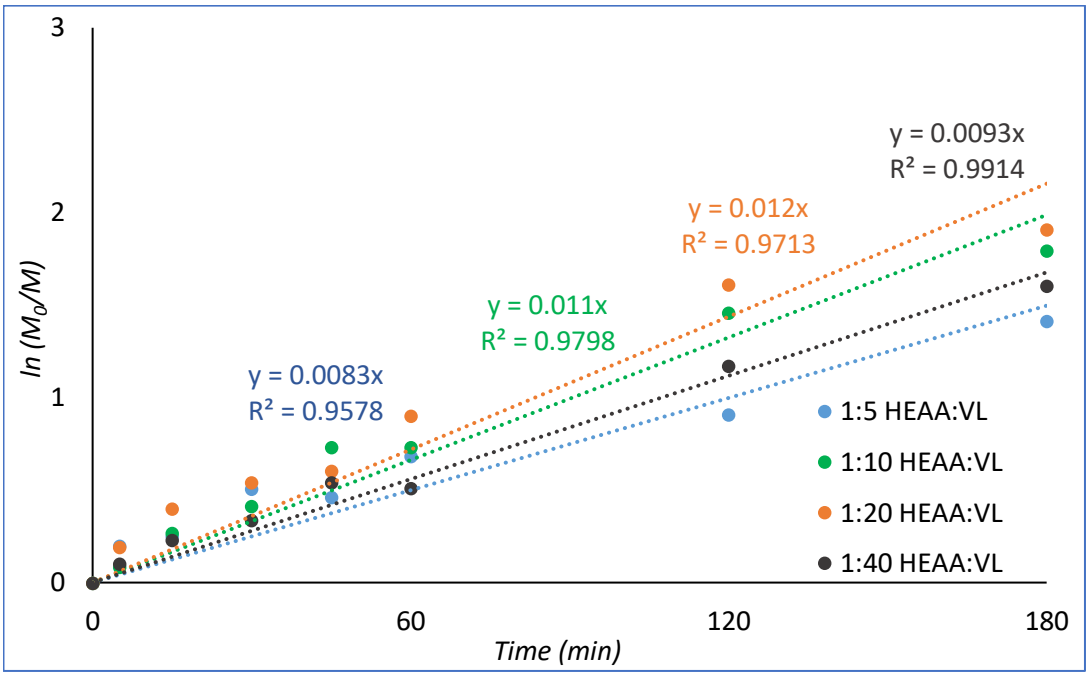

Figure 34 First-order plot of PVL formation. HEAA was used as an internal standard.

CL reveals a stricter adherence than VL to first-order kinetics, demonstrated by R^2 values above 0.99 (Figure 35). No data points had to be excluded as monomer conversion does not stagnate to the same extent as VL. Polymerisation of CL has greater kinetic constants than the polymerisation of VL, owing to its higher ring-strain.

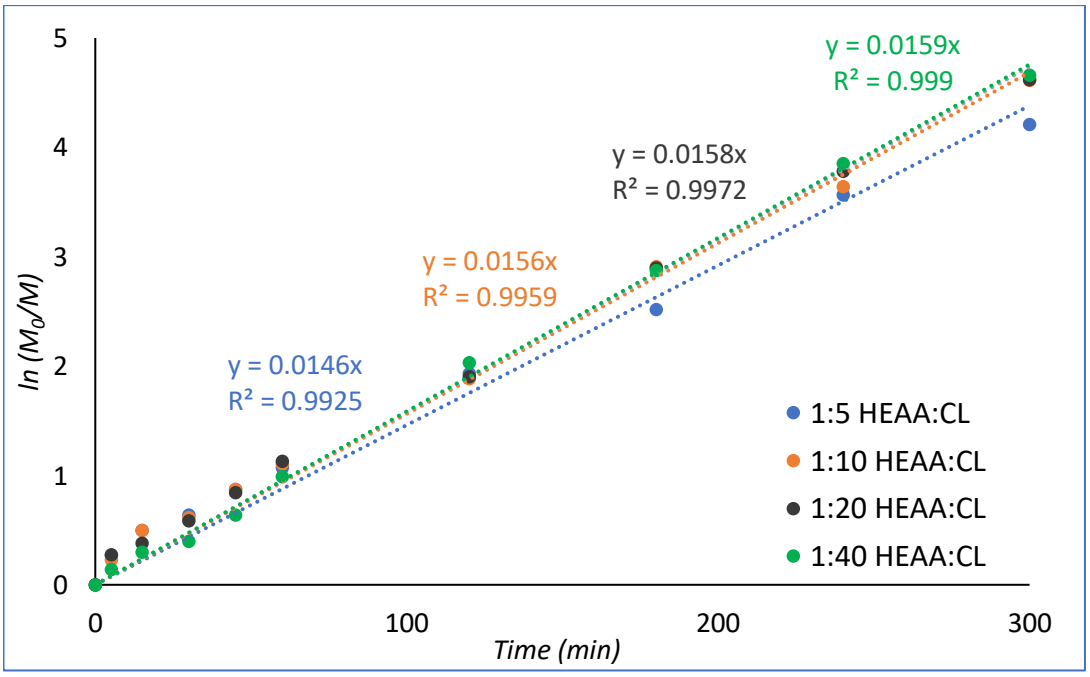

Figure 35 First-order plot of PCL formation. HEAA was used as an internal standard.

Reaction Monitoring using GPC

HEAA initiated eROP of CL (1:20 I:M) was monitored by GPC in addition to ^{1}H-NMR spectroscopy. Polymer growth and formation of oligomeric materials can be observed in the chromatograms (Figure 36). Unimodality is observed in the primary polymer peak, indicating formation of a single species. From the overlaid GPC traces an increase in retention time is observed indicative of polymer growth. The formation of a single polymeric species demonstrates that the reaction is controlled, and that undesired secondary initiation processes which could lead to bimodality are controlled. A small increase in dispersity is observed over the course of reaction, although remains low ($Đ$=1.28 at 30 minutes, and $Đ$=1.51 at 300 minutes). This small increase in dispersity could be a result of transesterification processes taking place during reaction.

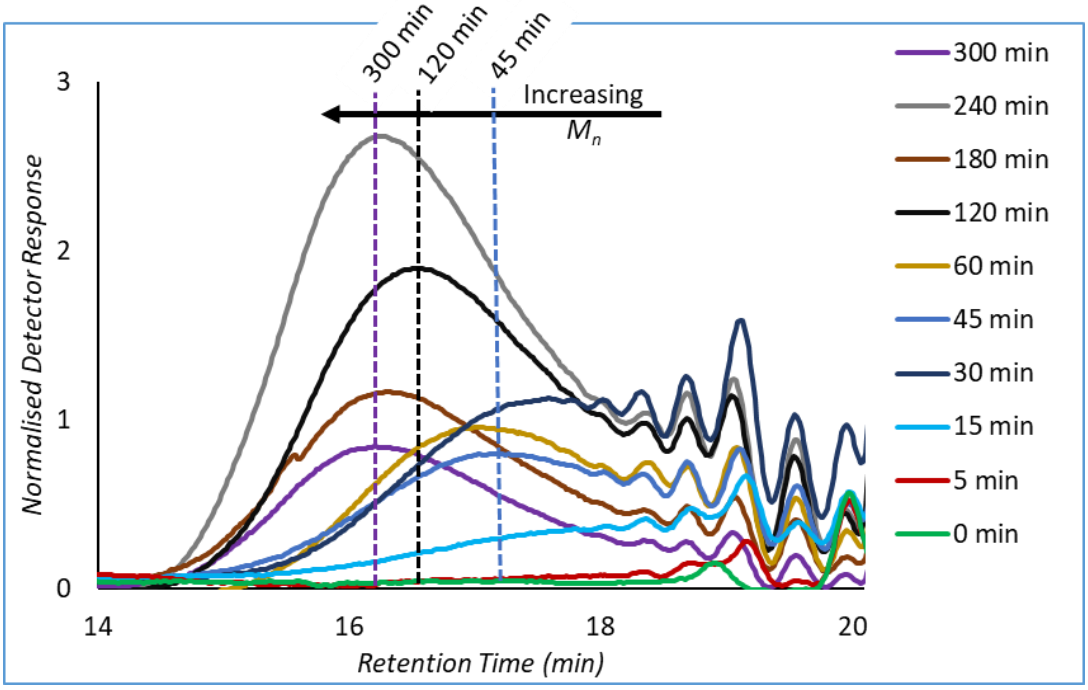

Figure 36 GPC chromatograms of HEAA initiated CL during eROP.

The molar masses predicted by ^{1}H-NMR spectroscopy and GPC are in good agreement (Figure 37). If HEAA conversion is not considered the molar mass is severely underestimated. The underestimation of molar mass is a result of assuming complete initiator conversion, whereas experimentally only partial initiator conversion was observed. An increase in initiating species lowers the number of lactone units available per chain and results in this underestimation. As such, partial HEAA conversion should be considered when estimating molecular mass from ^{1}H-NMR spectra (Equation 9 and Equation 10).

$$DP\ of\ (HEAA - Polylactone) = \frac{Poly(lactone)\ units}{Reacted\ HEAA\ units} = \frac{Lactone_0 \times \frac{Lactone\ conversion}{100}}{\frac{HEAA\ conversion}{100}}$$

Equation 9 Degree of polymerisation of HEAA-Polylactone can be calculated from the ratio of reacted monomer to reacted initiator using ^{1}H-NMR spectroscopy. $Lactone_0$ is the ratio of monomer to initiator at time zero.

$$MW\ of\ HEAA - Poly(lactone) = MW\ of\ HEAA + (DP\ of\ HEAA - poly(lactone)\ \times MW\ of\ Lactone)$$

Equation 10 Molecular mass of HEAA-Poly(lactone) can be estimated from the degree of polymerisation and molecular weights of initiator and monomer, following from Equation 9.

Discrepancies in molar mass obtained from GPC and ^{1}H-NMR spectroscopy can arise due to a variety of factors. The columns used during GPC have a lower limit of calibration, in this case approximately 540 g·mol^{-1}. There is no lower limit of calibration using ^{1}H-NMR spectroscopy, meaning that oligomers below this threshold are considered – unlike in GPC. This leads to an overestimation of molecular weight by GPC when a significant fraction of analysed polymer chains are below the lower limit of calibration. The instrument used for GPC analysis is calibrated using PMMA standards (540 to 1 020 000 g·mol^{-1}), which have different hydrodynamic volume to PCL, leading to further deviations from the expected value.

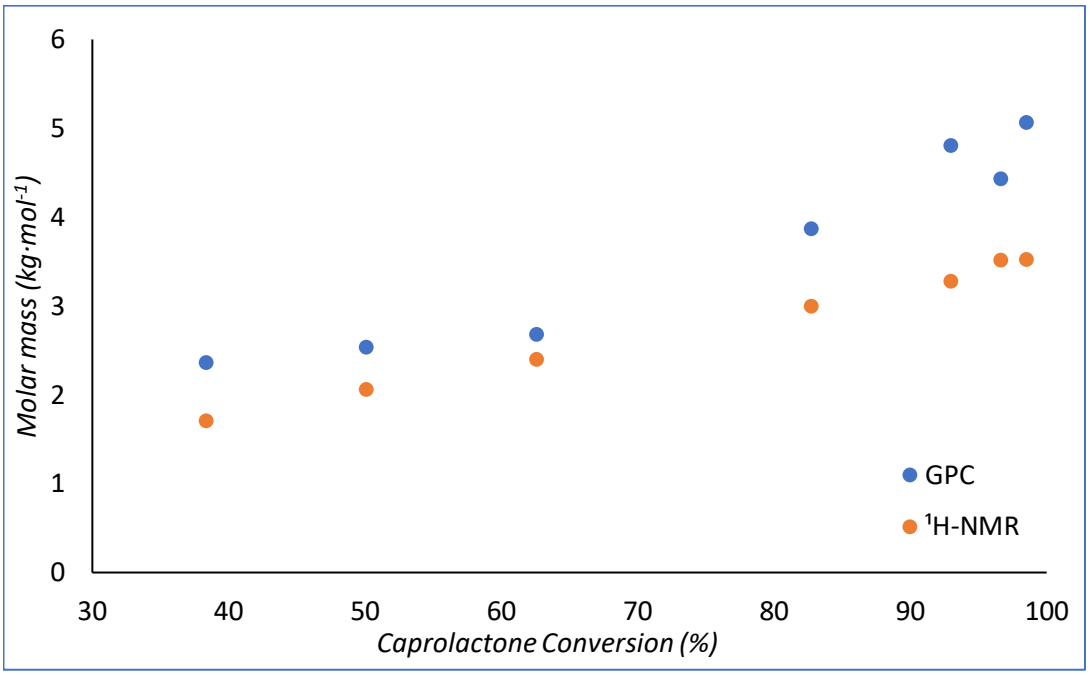

Figure 37 Molecular mass (M_n) determined by GPC and ^{1}H-NMR spectroscopy plotted against caprolactone conversion.

End-Group Fidelity and MALDI-TOF MS

To maintain control over the polymerisation process, it is imperative undesirable initiating species are kept to a minimum. This is especially significant when the initiator is intended to be utilized for further modification after polymerisation, as is the case for HEAA initiated eROP. The primary source of undesired initiation in the ROP of lactone monomers is usually residual moisture. Preventative measures were taken to limit moisture content, such as storing reagents over molecular sieves, and drying glassware prior to use. Nevertheless, enzymes often rely on a small quantity of water to maintain their structure and activity. As such complete exclusion of water could not be guaranteed, and it follows that the presence of water-initiated polymer chains cannot be entirely excluded.

From the GPC chromatograms *vide supra* the unimodality of the primary species forming is indicative of a single initiating species. Matrix Assisted Laser Desorption/Ionisation Time-of-Flight (MALDI-TOF) mass spectrometry was employed to gain deeper insight into the distribution of polymer species present, and to provide insight to the extent of water-initiated chains present in the final product. From the mass spectrum obtained of a sample of HEAA-PCL a single distribution is observed, with separate signals corresponding to species with Na^+ and K^+ counterions (m/z difference of 16) (Figure 38). The distance between signals is 114 m/z, correlating excellently with an addition of a single monomer unit of CL. Unfortunately, exact nature of the end-group could not be accurately quantified from the mass spectrum alone. Mass determined by ^{1}H-NMR analysis (1797 g·mol^{-1}) and by MALDI-TOF MS (most intense peak = 2105 m/z) are in close agreement, and combination of the two analytical techniques strongly suggests that the material is the desired HEAA-PCL.

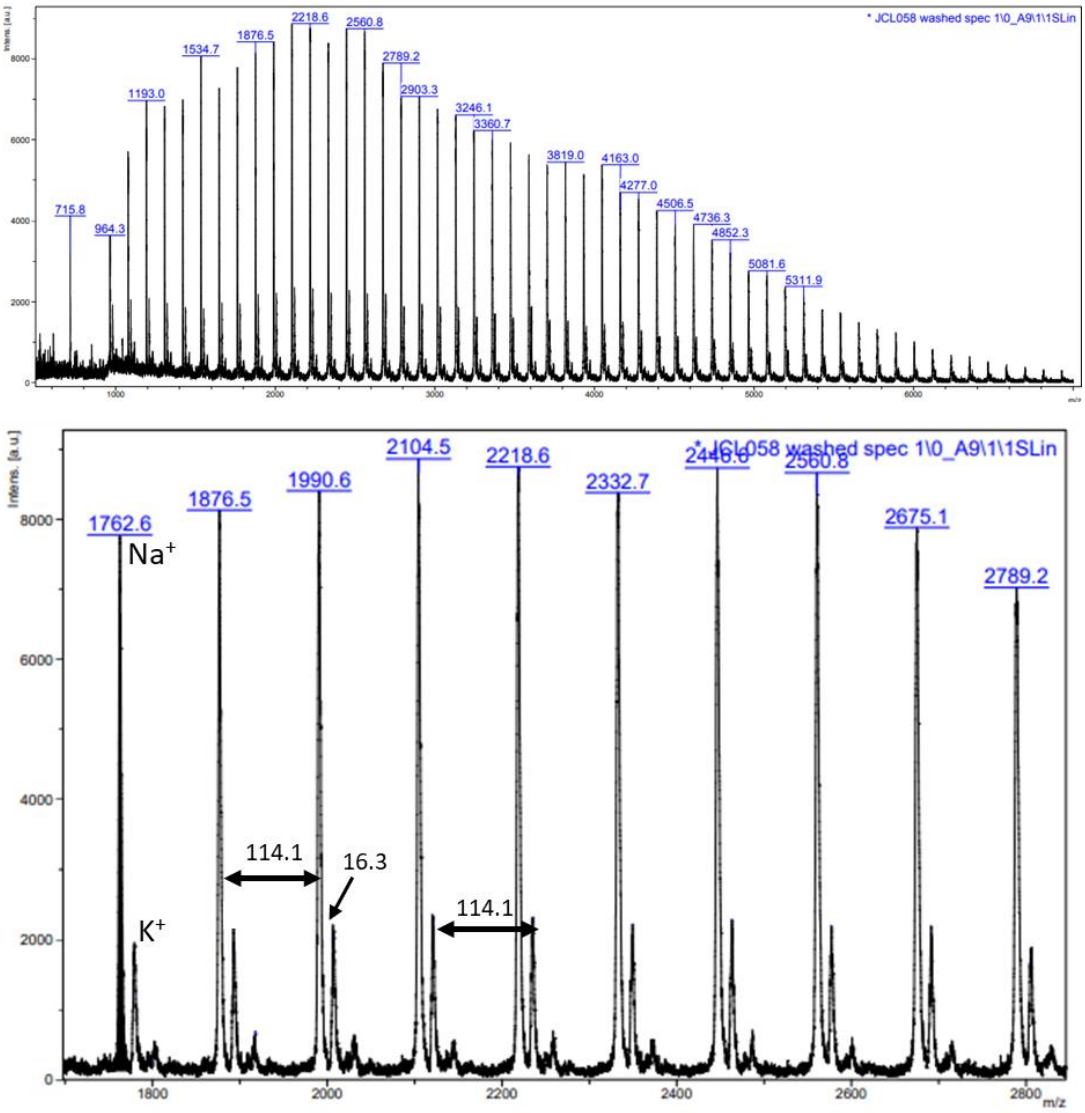

Figure 38 MALDI-TOF mass spectrum of HEAA-PCL. An increase of 114.1 m/z between peaks corresponds to a singular caprolactone unit. Species with Na^+ and K^+ counterions are observed with a difference of 16.3 m/z. Average M_n by GPC of the sample analysed is 1797 g·mol^{-1}.

Turnover Frequency of Novozym 435

Turnover frequency for these reactions was calculated using literature methodology.[180] Conversion data was utilised to calculate the moles of monomer converted, and this number was divided by time and mass of N435, following Equation 11 to yield the turnover frequency. (Equation 11)

$$Turnover\ Frequency = \frac{Lactone\ Loading\ (\mu mol)\ \times \frac{Lactone\ Conversion}{100}}{Time\ (min)\ \times\ Catalyst\ Loading\ (g)}$$

Equation 11 Calculation of turnover frequency in µmol min^{-1} g^{-1} from conversion data. Lactone loading refers to the number of moles of lactone present at time zero.

These turnover frequencies give an indication of the catalytic efficiency of the immobilised enzyme as well as providing insight into the suitability of the chosen substrates. Turnover frequencies are significantly higher in the initial stages of reaction when monomer concentration is highest (Table 4). As monomer is converted to polymer, the turnover frequency decreases with monomer concentration. Over the course of a reaction this could misleadingly suggest that the catalyst is losing activity. Thanks to the recyclability study, enzyme deactivation within this timescale was firmly ruled out.

Time (min)	Turnover Frequency (µmol min^{-1} g^{-1})[a]							
	1:5 HEAA:CL	1:10 HEAA:CL	1:20 HEAA:CL	1:40 HEAA:CL	1:5 HEAA:VL	1:10 HEAA:VL	1:20 HEAA:VL	1:40 HEAA:VL
0	0	0	0	0	0	0	0	0
5	1487	1570	1744	2147	2339	2216	2510	2147
15	1296	1332	1386	1610	1361	1456	1610	1417
30	1173	1154	1240	1368	1070	1225	1289	1112
45	1013	1033	1085	1138	895	1041	1103	955
60	903	917	964	986	827	934	962	848
120	611	627	636	651	531	643	657	613
180	452	460	464	467	418	470	474	464
240	353	357	359	360	338	366	365	366
300	288	289	290	290	284	297	296	298

Table 4 Turnover Frequency of lactone monomers as determined during HEAA initiated eROP. [a] Determined by ^{1}H-NMR spectroscopy.

Recyclability of Novozym 435

A recyclability study was conducted to demonstrate the stability of N435 in the reaction conditions employed. Enzyme stability is equally imperative from both economic and environmental perspectives. Waste minimisation is central to the Principles of Green Chemistry, and simple reuse of immobilized enzymes takes significant strides towards this goal. Industrially, economic viability of the process is fundamental. Being able to use the same catalyst multiple times without loss of activity provides a significant reduction in cost. Facile recycling of the enzymatic catalyst can tilt the argument of cost in its favour, hopefully leading to more widespread implementation of enzymatic catalysis as an alternative to chemocatalysis.

In this recyclability study, three experiments were run in parallel, and the average conversions are plotted (Figure 39, tabulated in Appendix Table 5). Following a reaction cycle, the N435 beads were removed from the reaction mixture and rinsed with 2-MeTHF. The rinsed beads were subsequently placed in a heated solution of fresh solvent and reagents and allowed to undergo another reaction cycle. N435 retained its catalytic activity for all ten reaction cycles investigated. From the average conversions obtained after 5 hours a decrease of 1.6% was detected in the conversion of CL, although it can be argued this is within the margin of error for ^{1}H-NMR spectroscopy. Recyclability studies in the literature have also noted the remarkable stability of N435.[181]

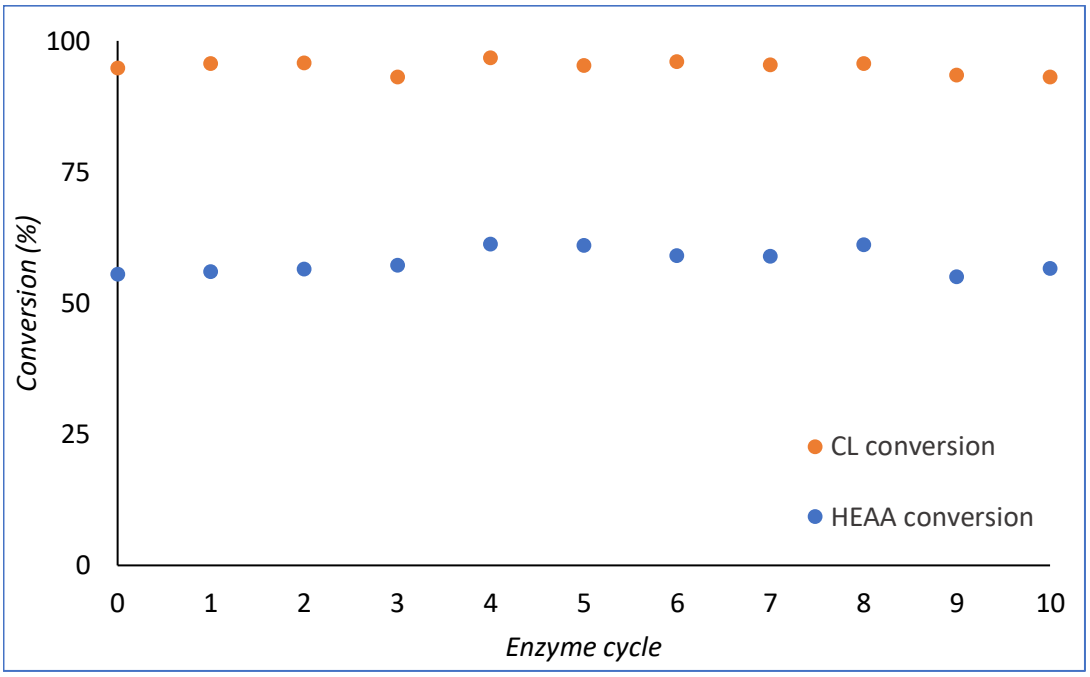

Figure 39 Conversion of CL and HEAA after 5 h of reaction (65 °C, 2-MeTHF, 10 wt.% N435) while recycling the immobilised enzyme. Experiments were performed in triplicate, see Appendix Table 5 for tabulated data.

This data shows that enzyme leaching is kept to a minimum, and that the enzyme remains attached to the support structure. N435 demonstrates excellent reproducibility with consistent conversions obtained for both HEAA and CL.

It is known that mechanical grinding can lead to support degradation.[53] To investigate the physical stability of N435 under the conditions employed SEM images were taken before and after the recyclability study (Figure 40). From these images the overall shape and structure of the immobilised enzyme appears unchanged after ten reaction cycles. Some scratches appear to have formed on the recycled beads, although these appear to be superficial. In the unused sample of N435 some of the polymer beads appear to be crushed, which could be a result of physical handling of the material during production or transportation.

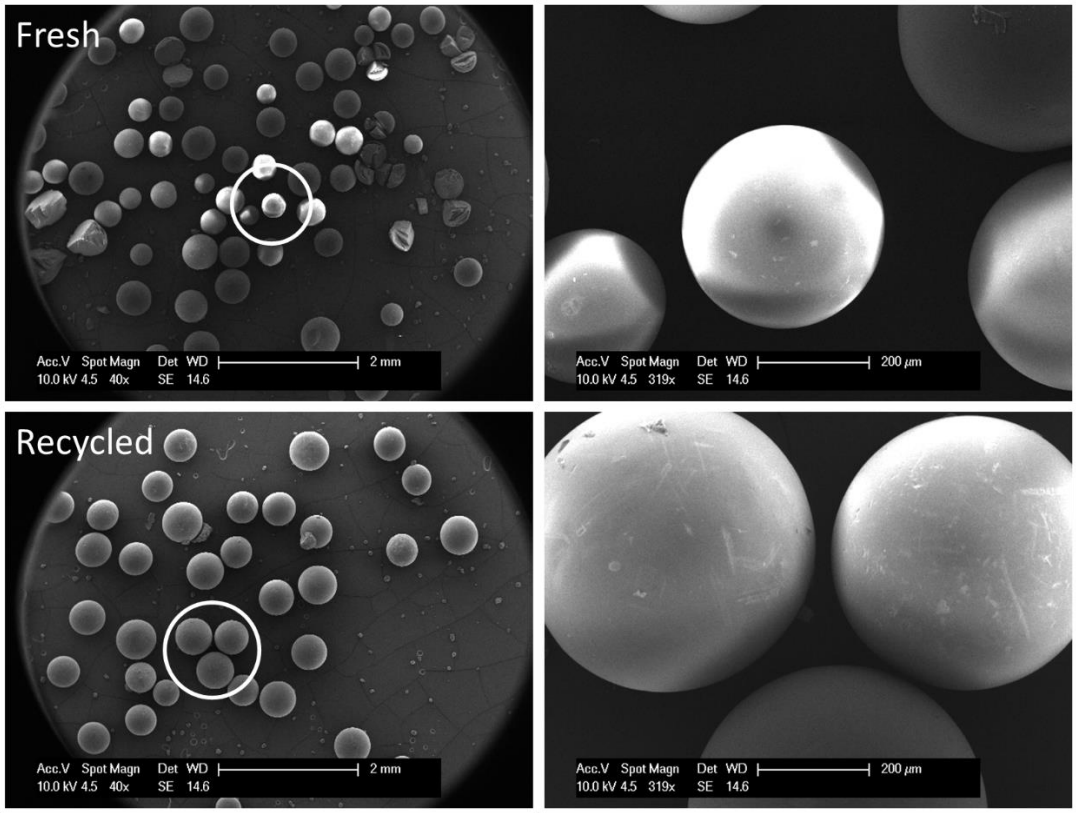

Figure 40 SEM Images of fresh Novozym 435 (40x magnification top left, 319x magnification top right), and after ten reaction cycles (40x magnification bottom right, 319x magnification bottom right). The white overlaid circles indicate the area of the SEM image that has been zoomed in upon further.

From the data showcased it can be ascertained that N435 is a potent catalyst suited for recycling up to (and likely beyond) ten times without loss of catalytic activity in the reaction conditions explored. This maintained activity of the catalyst showcases the suitability of 2-MeTHF as a reaction solvent for enzymatic transformations.

Control Experiments

Control experiments were performed to assess the extent of hydrolytic background initiation present in the reaction. In one control experiment the catalyst was excluded from the reaction mixture (reaction vessel containing only HEAA, CL, and 2-MeTHF), in a separate experiment the initiator (HEAA) was removed (reaction vessel containing only CL, 2-MeTHF, and N435). No conversion of CL into PCL could be detected in the catalyst-free reaction. Polymerisation was however observed in the "initiator-free" reaction which did not contain any HEAA. The observed background polymerisation is likely due to residual moisture bound to the enzymatic catalyst, which has been reported previously.[182] Polymerisation proceeded significantly slower upon removal of HEAA, the resulting polymers also feature a significantly

larger dispersity (*Đ*=1.88 after 5 h, Appendix Table 6). Polymer could only be detected after 2 hours of reaction by GPC (Figure 41), in contrast to reactions with HEAA present in which polymer can be detected after 30 minutes (Figure 36). Whilst these secondary undesired initiation mechanisms could not be entirely prevented, the decreased dispersity and increased rate of reaction can be attributed to the presence of the desirable initiator species during HEAA initiated eROP.

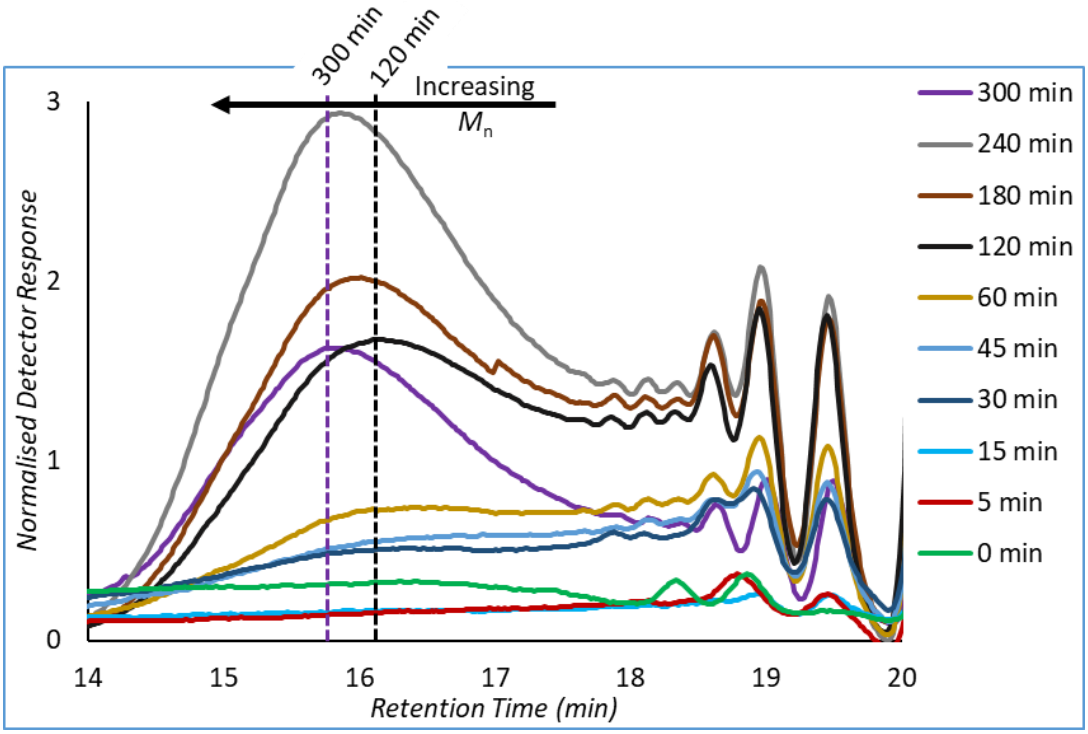

Figure 41 GPC traces during reaction progression of N435 with CL in 2-MeTHF. N435 catalysed eROP of CL without addition of an explicit initiating species such as HEAA.

Conversion of CL during the control experiment without HEAA was plotted against time (Figure 42). In comparison with the HEAA initiated eROP of CL (1:20 I:M) it can be seen that the HEAA-less control proceeds significantly slower, especially in the initial stages of reaction. The conversion at 60 minutes for the initiated reaction is 66%, whereas for the initiator free reaction only 36% conversion has been reached (Appendix Table 6).

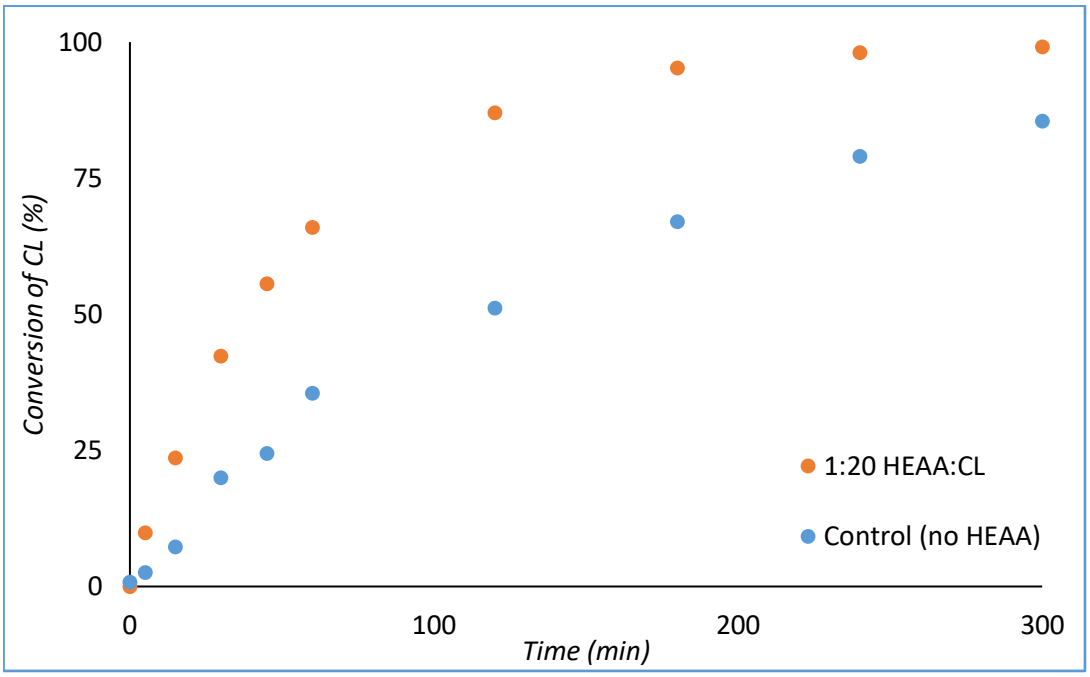

Figure 42 Conversion over time for eROP of CL with and without presence of HEAA as an initiating species. Presence of HEAA substantially increases rate of polymerisation.

The improved rate of reaction and lowered dispersity can be attributed to the addition of HEAA as an explicit initiating species. Unfortunately, background initiation processes could not be fully controlled. Thankfully, analysis by GPC, ^{1}H-NMR and MALDI indicate that these background processes are relatively minimal when an initiator species is added.

Summary Lactone Conversion

In summary, VL and CL reach high conversion in the reaction conditions utilised. HEAA was used as an internal standard for ^{1}H-NMR analysis to monitor monomer consumption against time. First-order plots revealed that the eROP of both VL and CL proceed following pseudo first-order reaction kinetics with respect to the lactones. It was also observed that reaction kinetics for VL deviate from first order after 120 minutes due to an equilibrium state being reached, as polymerisation is thermodynamically less favourable for VL in comparison to CL. Control experiments were performed, which revealed that polymerisation does not take place in the absence of catalyst but does occur without addition of the desired initiator. There is a degree of uncontrolled background polymerisation occurring due to the presence of initiators other than HEAA. Nonetheless, MALDI-TOF MS in combination with ^{1}H-NMR analysis indicate the presence of a single polymer species being produced. An enzyme recyclability study demonstrated excellent reusability of the N435 catalyst, with minimal loss in activity observed after ten reaction cycles.

2.4.3 *N*-Hydroxyethyl acrylamide Consumption during Enzymatic Ring-Opening Polymerisation

During enzymatic ring-opening the number of signals in the vinyl region of the ^{1}H-NMR spectra were found to double. After only 30 minutes, the presence of a second species is clearly detectable in the eROP of both VL (Figure 43) and CL (Appendix Figure 3). These new slightly shifted signals in the ^{1}H-NMR spectra were hypothesised to be corresponding to the HEAA end-group on a propagating poly(lactone) chain. It can be observed that this splitting persists even after the lactone monomer has been fully converted to polymer, suggesting that both unreacted and reacted HEAA is present.

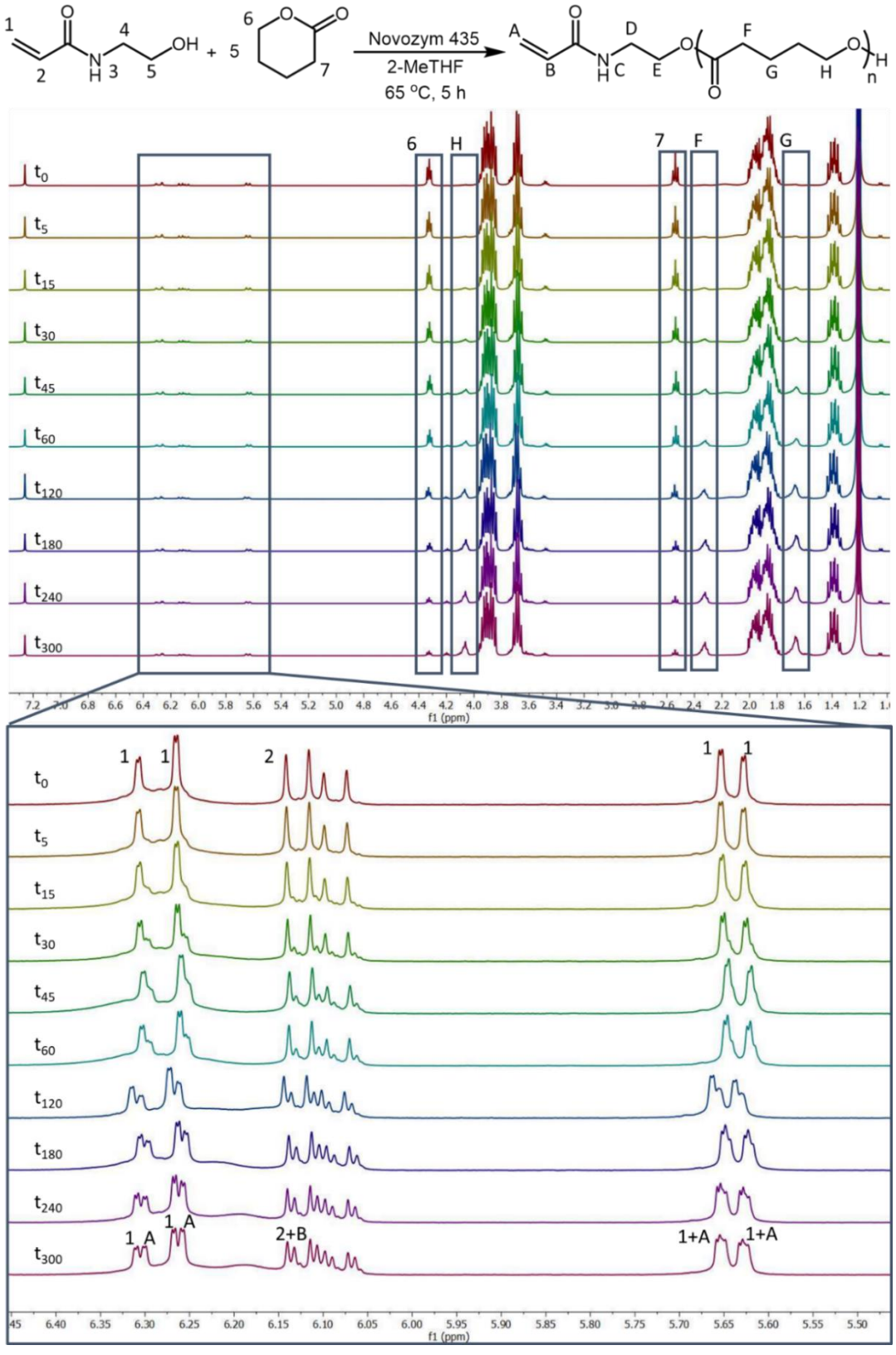

Figure 43 Stack of ^{1}H-NMR spectra used to monitor the kinetics of HEAA initiated eROP of VL (M:I = 5:1). Zoomed in region highlights the formation of two distinct acrylamide species.

The reaction mixture could be purified by precipitation, indicating that the additional ^{1}H-NMR signals are a product of the reaction containing unreacted initiator. Since HEAA has a vastly different solubility profile to HEAA-PCL or HEAA-PVL, precipitation proved a facile method for polymer purification. In addition, purification by precipitation indicates that initiator degradation or self-reaction is not occurring to any measurable extent. This is in stark contrast with HEMA initiated eROP, in which the formed side products possess nearly identical solubility parameters, hindering purification by precipitation.[154,155]

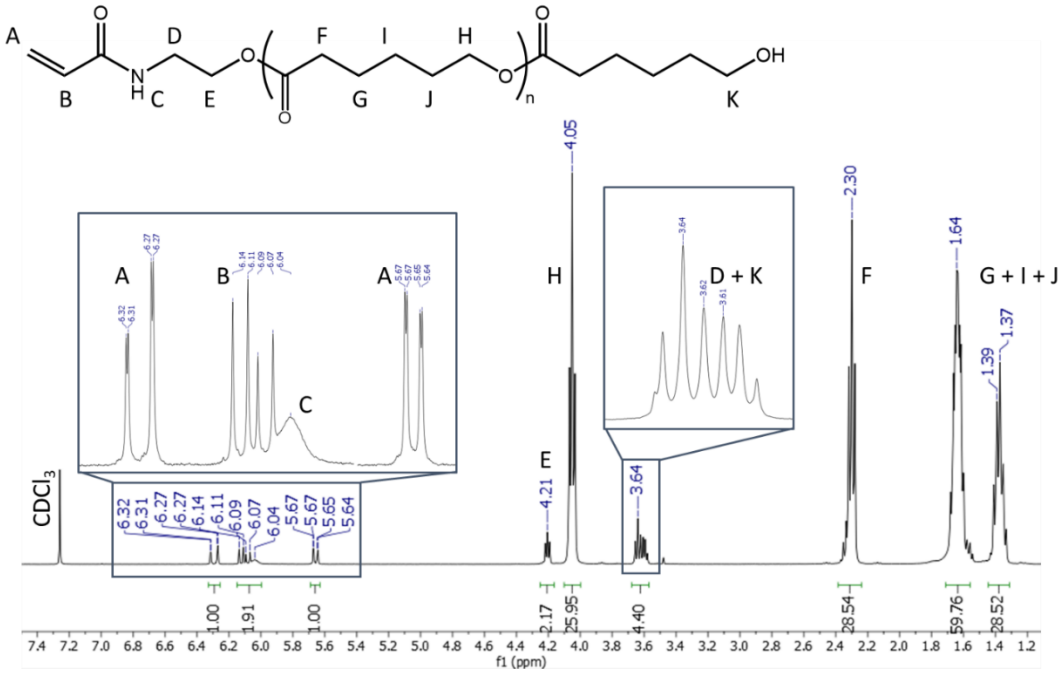

Figure 44 ^{1}H-NMR spectrum of HEAA-PCL after precipitation. Peaks H and A were used to determine DP=13, significantly overshooting the targeted DP=5. The inset between 5.4 and 7.0 ppm highlights the region with the olefinic acrylamide peaks.

The ^{1}H-NMR spectra obtained during kinetic experiments were analysed to ascertain the extent of initiator efficiency. The integrals of the two doublets of doublets between 6.25 and 6.31 ppm were utilised for this purpose (Equation 12**).**

$$Conversion\ of\ HEAA\ (\%) = \frac{\int HEAA - poly(lactone) \times 100}{\int HEAA - poly(lactone) + \int HEAA}$$

$$= \frac{\int 6.29\ ppm \times 100}{\int 6.29\ ppm + \int 6.31\ ppm}$$

Equation 12 Conversion of HEAA can be determined from ^{1}H-NMR integrals. Signal at 6.31 ppm corresponds to HEAA. Signal at 6.29 ppm corresponds to HEAA-poly(lactone).

The calculated HEAA conversions in the HEAA-initiated eROP of VL were plotted against time (Figure 45). HEAA reaches significantly lower conversions than those observed for the lactone monomers employed. Consequently, unreacted HEAA can be found in the reaction mixture, and desired degree of polymerisation is consistently surpassed. The partial initiator conversion has a significant impact on the degree of control exerted over the produced molar mass. HEAA conversion in some cases appears to plateau already after 60 minutes of reaction. These findings are mirrored in the HEAA-initiated eROP of CL (Appendix Figure 4).

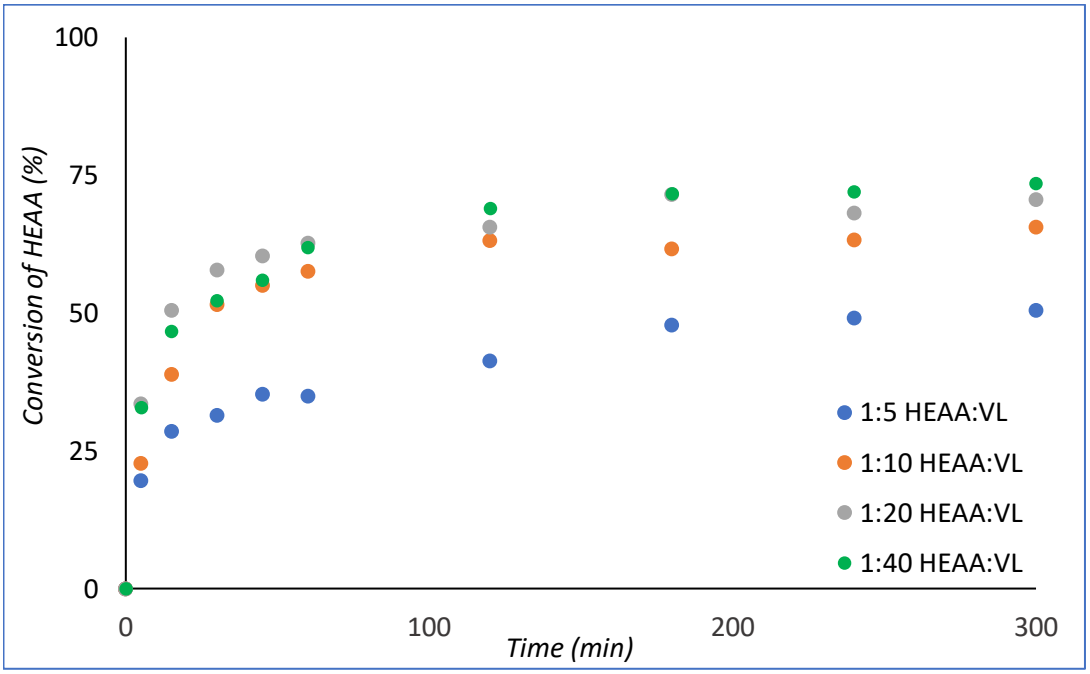

Figure 45 HEAA conversions obtained during eROP of VL in 2-MeTHF with 10 wt.% N435.

Computational Experiments

Computational experiments were conducted in collaboration with Dr. Bruno Falcone Pin of the Prof. Jonathan Hirst group.

This rather unexpected phenomenon of partial initiator conversion appears to be a result of polymer propagation proceeding at a greater rate than polymer initiation. Initiation being slower than propagation implies that propagating polymer chains are better substrates for CaLB. To gain a deeper understanding of this behaviour computational docking experiments were performed. Interactions of HEAA and HEAA-PCL in the active site of CaLB were modelled (Figure 46). Compounds of interest were docked into the active site of the enzyme, and 10 nanosecond molecular dynamics simulations were performed. Interaction energies were obtained using the Generalized Born Surface Area (GBSA) method within the Amber software package.

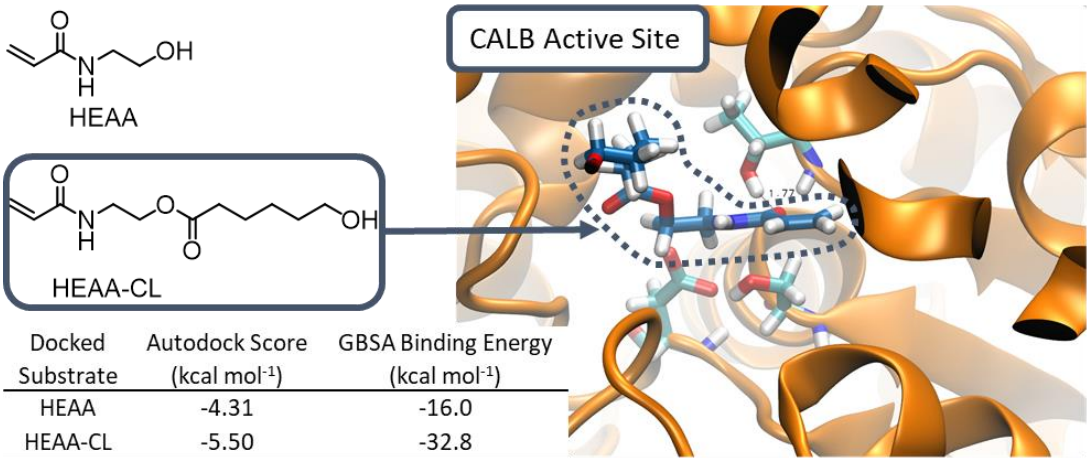

Docked Substrate	Autodock Score (kcal mol^{-1})	GBSA Binding Energy (kcal mol^{-1})
HEAA	-4.31	-16.0
HEAA-CL	-5.50	-32.8

Figure 46 HEAA-CL docked in the active site of CALB (right), Autodock scores (kcal mol^{-1}) and GBSA computed interaction energy (kcal mol^{-1}) for HEAA and HEAA-CL (bottom left). A lower score indicates a higher binding affinity.

The interaction energies computed using GBSA show that HEAA-CL binds more than twice as strongly than HEAA alone. While Autodock scores are more similar, HEAA-CL still displays greater binding affinity to the active site of CaLB than HEAA. Since Autodock and GBSA energies are calculated using different methods the absolute values are not directly comparable. Trends between binding energies obtained using Autodock and GBSA can still be used to gauge relative binding affinity to the enzyme active site.

Mechanistically, chain extension of a propagating poly(lactone) chain using CaLB is achieved by the release of an activated monomer unit from the acyl-enzyme intermediate in the rate-determining step (Figure 8).[178] Release of the activated monomer occurs by means of nucleophilic attack, from either an initiator molecule or a growing polymer chain. Enzymatic rates of reactions are highly dependent on substrate-enzyme binding interactions.[183] As a result of the higher binding affinity of HEAA-CL to CaLB compared to that of HEAA it is expected that propagation will occur faster than initiation (Figure 47). The binding affinities obtained through computational docking provide rationale for the behaviour observed experimentally during eROP.

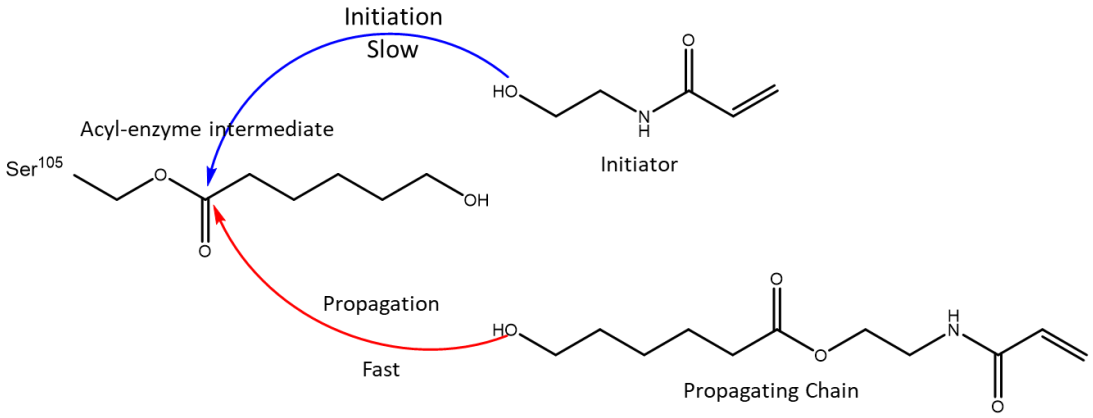

Figure 47 The experimental and computational results both suggest propagation is faster than initiation in liberating the activated caprolactone unit from the acyl-enzyme intermediate.

Enzyme interactions alone do not reveal the whole picture. Initiator conversion increases as longer polymer chains are targeted during synthesis (Figure 45). It is believed that the hydroxyl end-group becomes less accessible as the chain extends due to steric factors, accompanied by a decrease in reactivity (Figure 48).[184,185] This effectively creates a balance between propagation, favoured by increased binding interactions in the enzyme active site; and initiation, favoured by a decrease in propagation due to increasing steric hindrance. As rate of propagation decreases, rate of initiation can compete more effectively leading to a higher initiator conversion. Subsequently, a higher HEAA conversion is obtained when longer poly(lactone) chains are targeted.

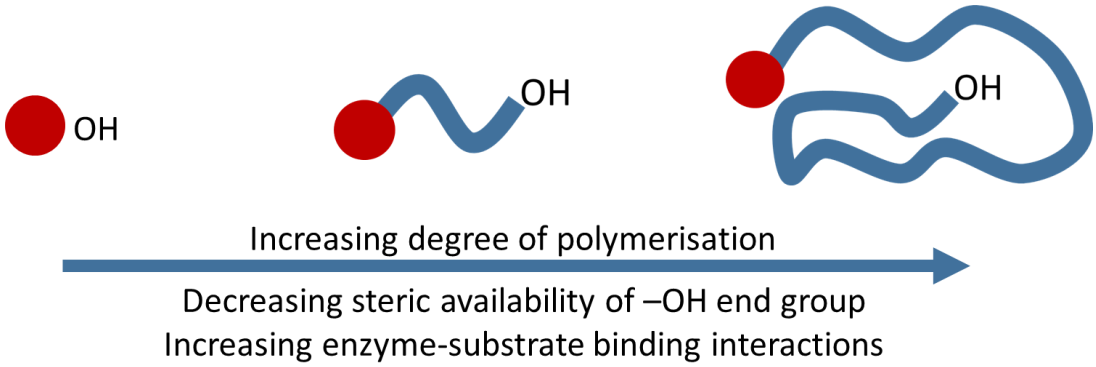

Figure 48 Increasing degree of polymerisation leads to increased steric bulk surrounding the hydroxyl end group of the polymer: suppressing propagation and favouring initiation. On the other hand, increasing degree of polymerisation also creates more favourable enzyme-substrate interactions: promoting propagation and suppressing initiation.

Alternative Initiator Species

For complete initiator conversion to take place, the initiator should react faster than the propagating polymer chains. An alternative initiator with a higher binding affinity to the enzyme active site would in theory also overcome the partial initiator conversion observed. *N*-Hydroxyethyl methacrylamide (HEMAM) was screened as an alternative to HEAA. Originally it was predicted that the increased hydrophobicity could increase the initiator efficiency. It was however found that HEMAM and HEAA have very similar binding affinities for the active site of CaLB, and accordingly behave very similarly in the N435 catalysed eROP of CL. HEMAM reached a conversion of 66.9%, while CL conversion was measured to be 99.7% after 300 minutes. The final initiator conversion is not significantly different from that reached by HEAA at a similar ratio of initiator to monomer.

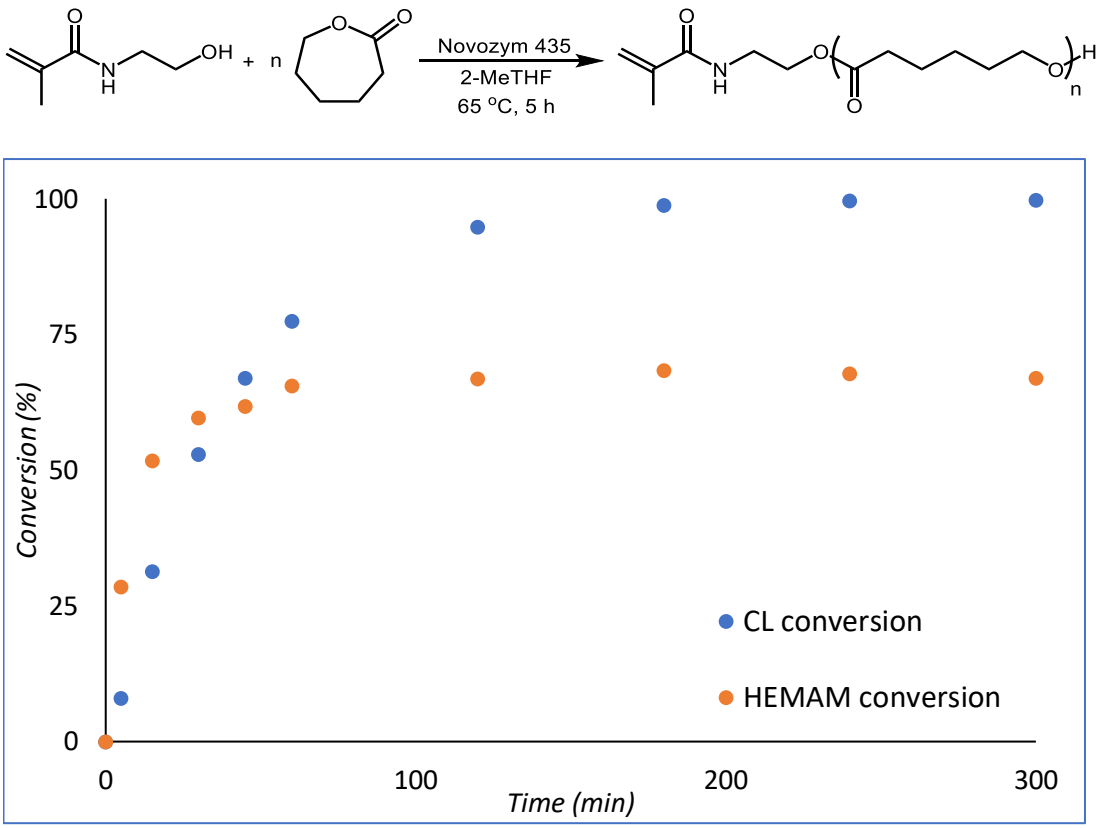

Figure 49 Top: Reaction scheme of HEMAM initiated eROP of CL in 2-MeTHF. Bottom: Conversion of HEMAM and CL in the HEMAM initiated eROP of CL in 2-MeTHF using 10 wt. % N435.

Similar behaviour between HEAA and HEMAM can be rationalised using computational docking techniques. From these docking experiments it can be seen that an initiated chain has a significantly higher affinity to the enzyme active site, leading to increased propagation and suppressed initiation (Table 5).

Docked Substrate	Autodock Score (kcal mol^{-1})	GBSA Binding Energy (kcal mol^{-1})
HEMAM	-4.31	-19.90
HEMAM-CL	-5.58	-31.18

Table 5 Autodock and GBSA results of HEMAM, HEMAM-CL, HEAA, and HEAA-CL in the active site of CaLB. For both initiator species a significant increase in binding affinity is observed once a polymer chain has been initiated.

From these experimental observations it can be ascertained that HEMAM behaves analogously to HEAA in the eROP of CL. The similar docking profiles provide further validation to the effectiveness of computational studies to predict experimental behaviour. Further work in this area could include the computation-guided synthesis of alternative acrylamide species with higher binding affinity for the enzyme active site.

Effect of Enzyme Loading

The effect of enzyme loading on equilibrium conversions of HEAA and CL obtained was investigated. It was found that under the reaction conditions employed catalyst loading did not influence the final conversion of monomer and initiator obtained. In line with previous results, monomer reaches full conversion while initiator does not.

Enzyme loading (wt.%)[a]	CL Conversion(%)[a]			HEAA Conversion (%)[a]		
	1:5 HEAA:CL	1:10 HEAA:CL	1:25 HEAA:CL	1:5 HEAA:CL	1:10 HEAA:CL	1:25 HEAA:CL
0	0	0	0	0	0	0
5	99.2	99.8	99.8	55.7	64.0	70.4
10	99.8	99.8	99.8	55.9	64.4	69.7
20	99.8	99.8	99.8	56.4	59.9	70.9

Table 6 Conversion of CL and HEAA after 17 h in 2-MeTHF at 65 °C, varying loadings of N435. For 0 wt. % N435 no peaks corresponding to HEAA-PCL could be seen. [a] Determined by ^{1}H-NMR spectroscopy.

This data shows that N435 acts as a catalyst and does not alter the position of the equilibrium. It was hypothesised that presence of enzyme-bound moisture could alter the final conversions of HEAA and CL, although from these results the conversions are consistent, and this does not appear to be significant. It can also be observed that without catalyst present no conversion is observed.

Summary Initiator Conversion

To summarise, incomplete initiator conversion was observed during HEAA eROP of CL and VL. ^{1}H-NMR analysis was used to monitor extent of initiator conversion, which was found to plateau rapidly. Computational insight was used to establish that propagation occurs more rapidly than initiation because of initiated polymer chains having significantly greater binding affinity to the enzyme active site than the initiator alone. Greater initiator conversion was obtained when longer polymer chains were targeted, presumably due to increasing steric factors diminishing the availability of the hydroxyl end-group. HEMAM was screened as a more hydrophobic alternative to HEAA and found to display nearly identical behaviour. The surprising behaviour of partial initiator conversion highlights some of the more unexpected aspects of enzymatic catalysis, and that binding interaction of each substrate should be considered to maintain a greater degree of control over the reaction outcome.

2.4.4 Post Enzymatic Ring-Opening Polymerisation Reactions

Quality of the produced degradable hybrid macromonomers was demonstrated by two sets of experiments. The macromonomers were chain extended using organocatalysed ROP of lactide to demonstrate hydroxyl end-group fidelity. Radical polymerisation and copolymerisation was utilized to demonstrate reactivity of the installed acrylamide end-group. FRP is also of industrial importance, and as such demonstrating the ability of these macromonomers to partake is relevant to assess commercial applicability. Radical copolymerisation with hydrophilic monomers also provides a synthetic methodology to incorporate amphiphilic characteristics in the final material. These amphiphilic properties can in turn be utilised to enable polymers to self-assemble in aqueous systems.[186]

Chain Extension using Organocatalysed Ring-Opening Polymerisation of Lactide

Organocatalytic chain extension with *rac*-lactide was employed to demonstrate hydroxyl end-group fidelity of HEAA-PCL produced through HEAA initiated eROP. Use of two distinct catalytic systems showcases an approach to methodically overcome limitations associated with each individual catalyst.[26] In this work, DBU and N435 are employed subsequently to overcome their respective limitations. DBU has been shown to be an excellent catalyst for the ROP of lactide in the presence of functional, acrylate containing, initiators such as HEMA and PEGMA.[187] Since DBU is known to be compatible with acrylate containing moieties it was expected that this catalyst would not be problematic in the presence of an acrylamide such as HEAA.[188] In contrast with N435 however, DBU does not readily catalyse ROP of lactones such as VL and CL. N435 on the other hand, does not readily catalyse the ROP of lactide. As such, synthesis of block copolymers containing both lactide and VL or CL would not be achievable using only one of these catalysts, and as such a combinatory approach is taken. The selectivity of the catalysts enables a sequential approach to synthesise block copolymers. Exploiting the stability of the first block (HEAA-PCL) and the compatibility of DBU with HEAA in 2-MeTHF, sequential catalysis enables the synthesis of targeted block copolymers (Figure 50).

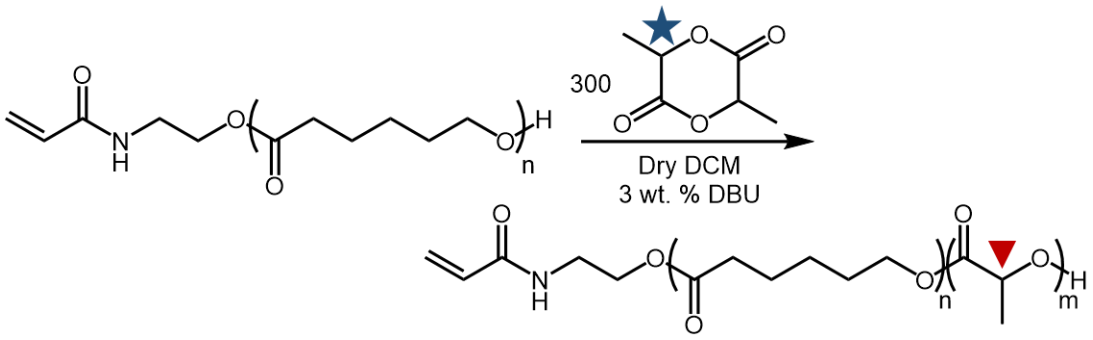

Figure 50 Reaction scheme of HEAA-PCL extension with lactide catalysed by DBU to synthesise HEAA-PCL-PLA block copolymer.

A purified sample of HEAA-PCL was chosen to be chain extended. Purification was necessary to remove unreacted HEAA from the eROP process, in order to prevent unreacted HEAA from initiating lactide chains. Activated 4 Å molecular sieves were used to ensure exclusion of water, as moisture would also lead to undesired hydrolytic initiation of poly(lactide) chains. Presence of unwanted initiating species, such as unreacted HEAA or water, would result in the formation of a bimodal polymer distribution and loss of control over the formed polymer architecture. A bimodal distribution after chain extension could also be indicative of initiator self-reaction during eROP, generating polymers with two end-capping groups unable to initiate further chain extension from the hydroxyl end. Maintaining unimodality following chain extension would demonstrate the absence of undesired initiation processes as well as showcase the HEAA-PCL macromonomers possessing a well-defined hydroxyl end-group.

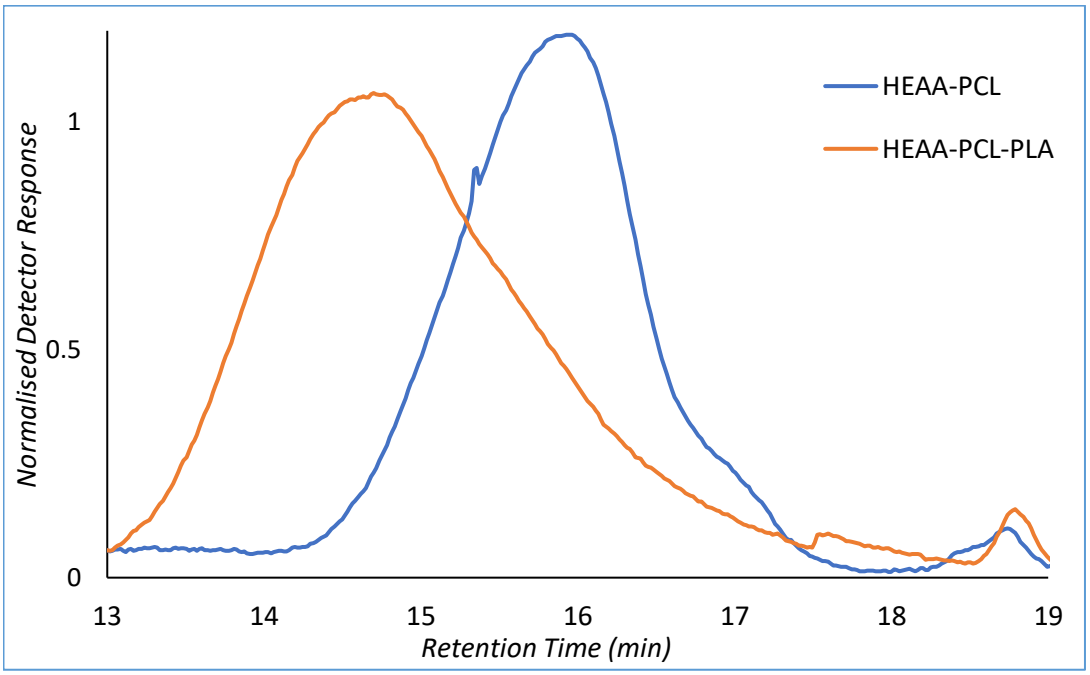

Figure 51 GPC chromatograms of purified HEAA-PCL (M_n 9.45 kg·mol^{-1}, Đ = 1.2) and the same material following extension with PLA (M_n 19.4 kg·mol^{-1}, Đ = 1.2) demonstrating a single polymer peak in both chromatograms.

The results obtained from chain-extension of HEAA-PCL with lactide show a well-defined unimodal distribution is maintained (Figure 51). GPC results show that retention time has decreased after chain extension, whilst dispersity remained unchanged (*Đ* = 1.2, before and after elongation), providing evidence that the polymer was successfully extended. The organocatalytic ROP was also monitored using ^{1}H-NMR spectroscopy to monitor lactide conversion. Conversion was found to be approximately 98% by ^{1}H-NMR analysis (Figure 52, full spectrum Appendix Figure 5). The combination of the shift towards higher molecular weight seen by GPC, and the high conversion is strong evidence for the formation of a HEAA-PCL-PLA block copolymer.

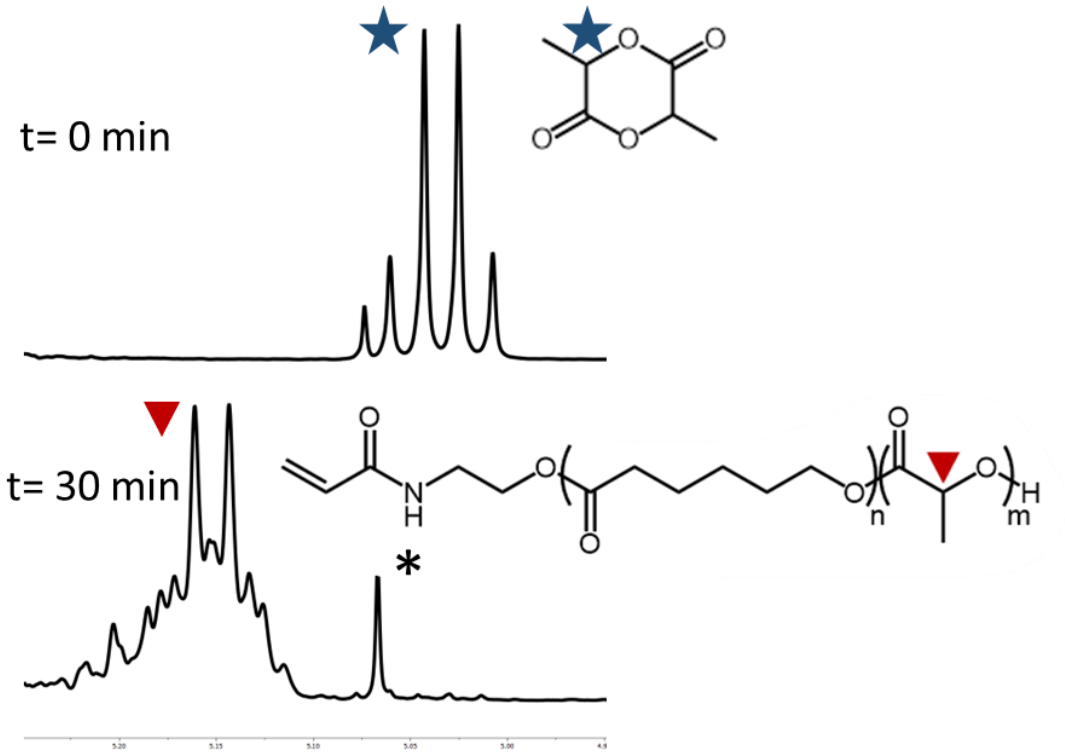

*Figure 52 ^{1}H-NMR spectra of HEAA-PCL chain extension with lactide at time zero and after 30 minutes for the PLA extension of HEAA-PCL in $CDCl_3$. Zoomed in on the region between 5.3 and 4.5 ppm. The signal marked * corresponds to a DCM satellite.*

Introduction of an amorphous PLA block could be used as an avenue for tailoring the properties of the materials produced. Especially rate of biodegradability has been shown to be substantially accelerated by introduction of amorphous regions in crystalline systems, such as PCL.[189] Tuning the rate of biodegradation opens avenues from which to control the eventual release of a drug payload, and expands the toolbox available for nanocarrier formulations.[190] The ability to extend the formed HEAA-PCL from the hydroxyl end demonstrates control over the polymerisation, and that adverse reactions are avoided during macromonomer synthesis.

Synthesis of Hybrid Polymers in 2-MeTHF

Combination of different polymerisation mechanisms, such as FRP and eROP, allows for limitations associated with each to be overcome. From the perspective of eROP, it is challenging to synthesise hydrophilic polymers due to the lack of monomers available. From a radical polymerisation viewpoint, synthesis of hydrophilic materials is facile. Radical polymerisation methodologies are instead limited in their ability to synthesise biodegradable polymers. It follows that if these two techniques could be combined, the resulting materials

could explore chemical space unavailable when only one synthetic methodology is employed.

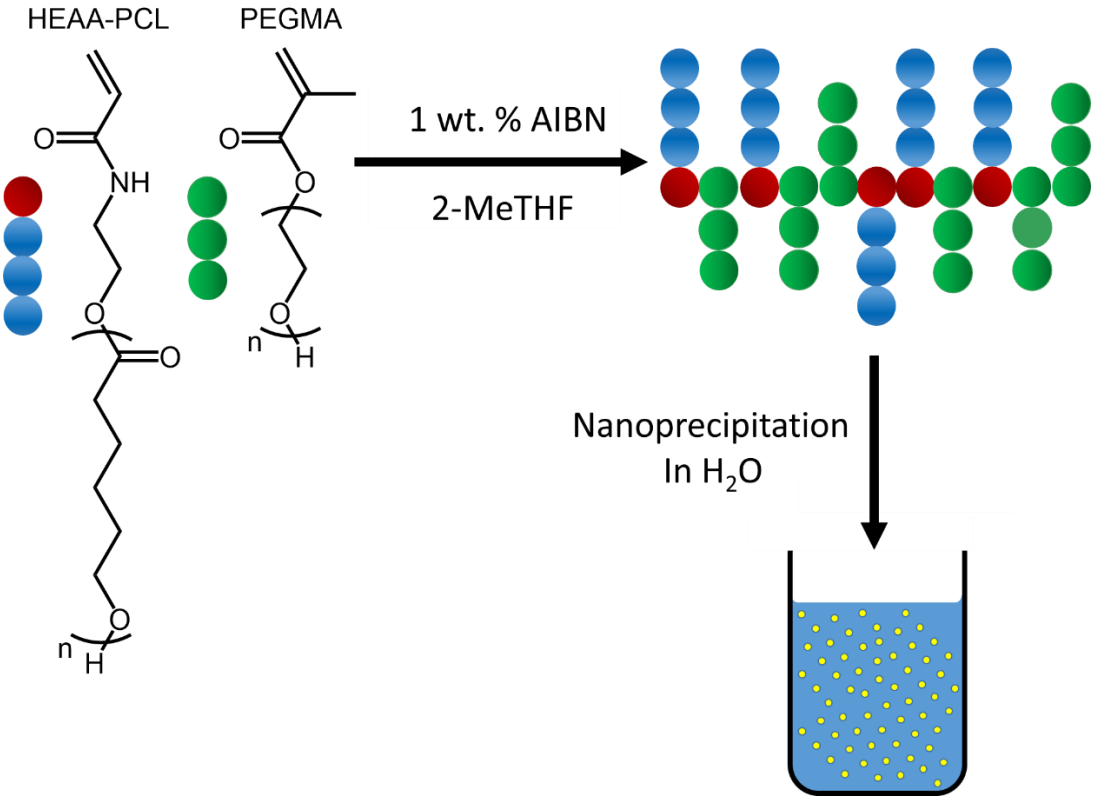

Figure 53 Overall reaction scheme for radical co-polymerisation of HEAA-PCL with PEGMA followed by nanoprecipitation into H_2O.

This work looks to use a combination of eROP and FRP to synthesise amphiphilic polymers capable of self-assembly into biodegradable NPs for potential application in biomedicine (Figure 53). The chosen synthetic strategy exploits the radically polymerisable acrylamide end-group on the enzymatically synthesised HEAA-PCL macromonomers to allow combination with hydrophilic monomers. These radical reactions also act as a method to further demonstrate end-group fidelity of synthesised HEAA-PCL macromonomers. Labile acrylate containing initiators, like HEMA and PEGMA, are well known in this field. As discussed previously, these acrylate containing species are unsuitable for use in lipase catalysed ROP due to issues of selectivity between the initiator and monomers resulting in transesterification reactions taking place.

PEGMA was chosen as the hydrophilic comonomer to be explored in FRP. PEGMA possesses excellent biocompatibility, essential for application in biological systems.[136] In addition, PEGMA has also been shown to be capable of stabilizing nanoparticles in aqueous media. Unfortunately, PEG is not free from drawbacks, and issues have been raised regarding its

widespread use.[86] Nonetheless, due to its excellent properties PEG and PEGMA are still considered the "gold-standard" for hydrophilic polymers and have therefore been used in this chapter.[191] Future work would benefit from the introduction of a biobased, biodegradable, and hypoallergenic radically polymerisable hydrophile.

Significant discrepancies between expected molecular masses and those measured by GPC were observed for the FRP products (Table 7). These effects are likely due to significant chemical differences between synthesised amphiphilic materials and the PMMA standards used for column calibration. These effects have been described in the literature previously and are likely an effect of varying solvated volumes and column-polymer interactions.[28]

Sample	Ratio (HEAA-PCL): Comonomer	Conversion (%)[a]	M_n (kg·mol^{-1}) [b]	M_w (kg·mol^{-1}) [b]	$Đ$ [b]
Poly-(HEAA-PCL)$_{44}$	1:0	99	14.1	21.9	1.6
(HEAA-PCL)$_{44}$-*co*-PEGMA	4:6	99	5.39	9.66	1.8
(HEAA-PCL)$_{44}$-*co*-PEGMA	7:3	94	11.2	15.8	1.4
Poly-(HEAA-PCL)$_{15}$	1:0	99	9.18	13.2	1.4
(HEAA-PCL)$_{15}$-*co*-PEGMA	4:6	98	4.00	5.36	1.3
(HEAA-PCL)$_{15}$-*co*-PEGMA	7:3	99	5.71	8.87	1.6
(HEAA-PCL)$_{10}$-*co*-HEAA	9:1	99	8.90	15.4	1.7

Table 7 Data for FRP (co-)polymerisations using HEAA-PCL macromonomers. [a] Determined by ^{1}H-NMR. [b] Determined by GPC in THF.

The produced materials were tested for their ability to self-assemble into nanoparticles by nanoprecipitation into water. Purified macromonomers, FRP homopolymers, and FRP copolymers were all tested for capability of assembly into nanoparticles (Table 8 and Figure 54). Presence of a hydrophilic moiety was found to be essential for nanoparticle formation. Entirely hydrophobic species, such as purified HEAA-PCL and poly(HEAA-PCL) homopolymers, were incapable of self-assembly and formed only poorly defined aggregates. Upon introduction of hydrophilicity, through PEGMA or HEAA, produced materials were found to be capable of self-assembly.

Entry	Sample	Ratio (HEAA-PCL):comonomer (mass:mass)	Hydrodynamic diameter (nm)	PDI
1	$(HEAA\text{-}PCL)_{44}$-*co*-PEGMA	4:6	104.3 ± 1.2	0.189 ± 0.005
2	$(HEAA\text{-}PCL)_{44}$-*co*-PEGMA	7:3	107.6 ± 1.1	0.213 ± 0.001
3	$(HEAA\text{-}PCL)_{15}$-*co*-PEGMA	4:6	120.2 ± 4.4	0.556 ± 0.039
4	$(HEAA\text{-}PCL)_{15}$-*co*-PEGMA	7:3	141.1 ± 0.8	0.483 ± 0.004
5	$(HEAA\text{-}PCL)_{10}$-*co*-HEAA	9:1	310.8 ± 3.5	0.235 ± 0.005

Table 8 DLS Measurements of polymeric nanoparticles in water (1 mg·mL^{-1}).

Dynamic Light Scattering (DLS) was used to analyse nanoparticles formed. It can be observed that the size distributions are not ideally unimodal for entries 3 and 4. This phenomenon can be attributed to the fact that samples were not filtered before measurement, resulting in some aggregation occurring. This non-ideal particle distribution could also be an effect of compositional drift during free-radical co-polymerisation. Entries 1, 2, and 5 however show unimodal size distributions. This demonstrates that the longer of the two macromonomers tested produces more uniform nanoparticles. Entry 5 is an example of the FRP of an impure macromonomer, still containing unreacted HEAA from the eROP step. The unreacted HEAA can undergo FRP with the macromonomer and imbue the final material with the element of hydrophilicity needed for nanoparticle formation. Purification before (co-)polymerisation could be considered unnecessary, especially for CL containing macromonomers, as any unreacted HEAA will simply be incorporated into the polymer during FRP. The ability to circumvent purification steps is highly desirable from an industrial perspective, where precipitation into large volumes of highly flammable solvents such as methanol or diethyl ether is both impractical, hazardous, and requires additional chemical waste disposal to be taken into consideration. Avoiding extra processing operations and volatile organic solvent usage is also attractive from a Green Chemistry viewpoint for the very same reasons, showing that economic and environmental ideals are often pointing in the same direction.

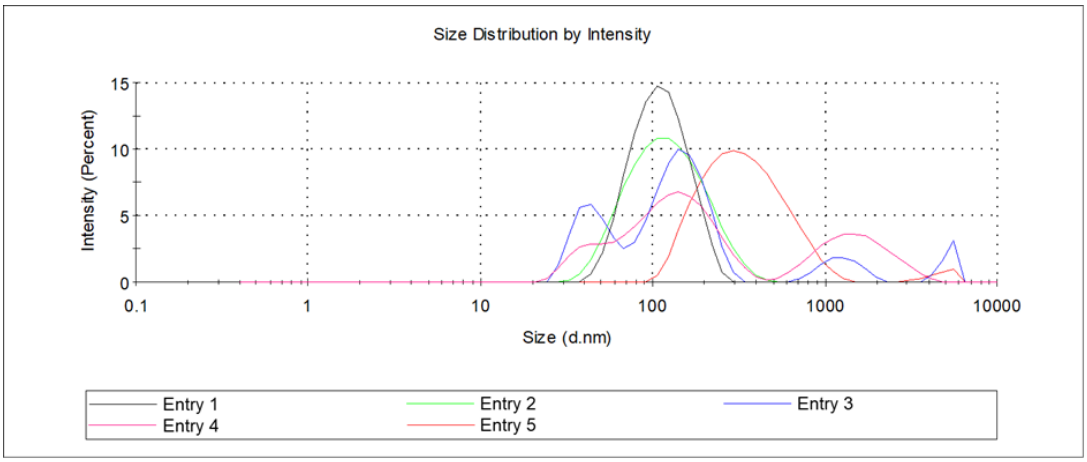

Figure 54 DLS Plots of polymeric nanoparticles in H_2O (concentration 1 mg·mL^{-1}). Entries refer to Table 8.

Cytotoxicity experiments were performed in collaboration with Robert Cavanagh and Cara Moloney.

Cytotoxicity of these materials was tested against several *in vitro* human cell line models. Since these materials could be considered for their potential application in biomaterials, lack of cytotoxicity is essential. Cell lines were chosen to model inhalation, oral, and topical exposure routes. Intestinal epithelial (Caco-2), lung epithelial (A549), and skin epithelial (A431) cell lines were chosen to replicate these various exposure routes. A two-dimensional assay was carried out, where both metabolic activity and lactate dehydrogenase (LDH) release was measured to assess cytotoxicity. Compounds (500 µg·mL^{-1}) were applied to cells in 10% foetal bovine serum containing Dulbecco's Modified Eagle Medium (DMEM) and exposed to cells for 48 hours. DMEM treatment without polymer sample represents the vehicle control, in which the exposed cells are expected to thrive. Triton X-100 (TX) was used at 1% (v/v) as cell death control.

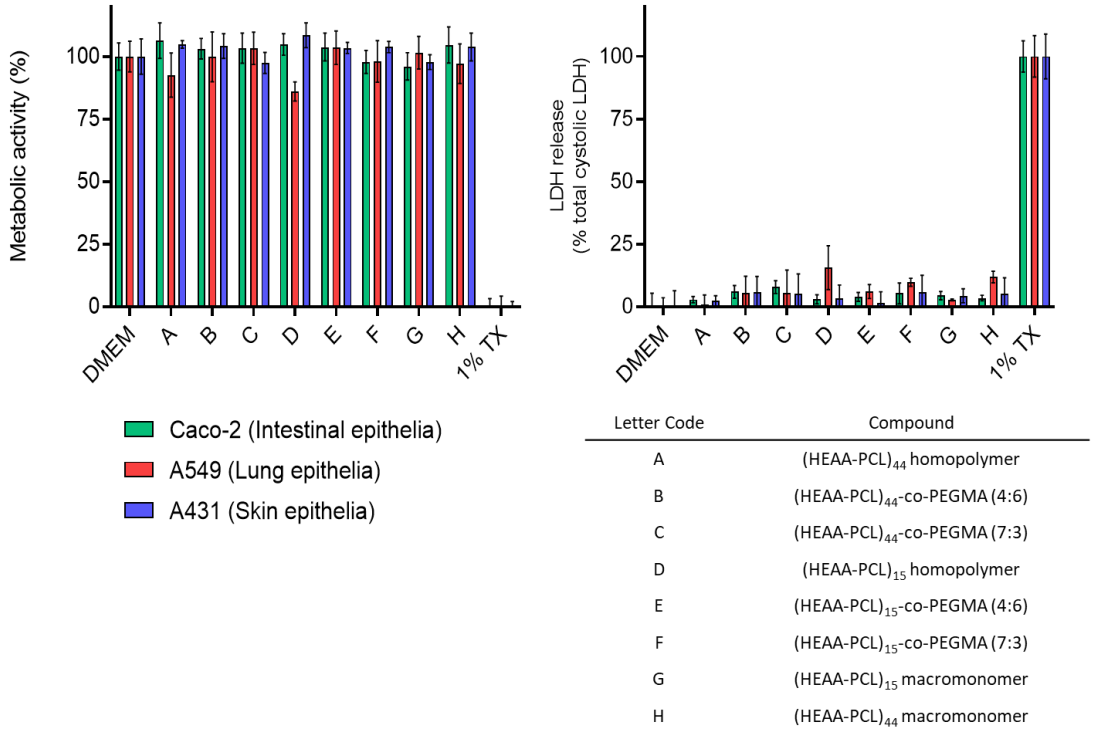

Letter Code	Compound
A	$(HEAA\text{-}PCL)_{44}$ homopolymer
B	$(HEAA\text{-}PCL)_{44}$-co-PEGMA (4:6)
C	$(HEAA\text{-}PCL)_{44}$-co-PEGMA (7:3)
D	$(HEAA\text{-}PCL)_{15}$ homopolymer
E	$(HEAA\text{-}PCL)_{15}$-co-PEGMA (4:6)
F	$(HEAA\text{-}PCL)_{15}$-co-PEGMA (7:3)
G	$(HEAA\text{-}PCL)_{15}$ macromonomer
H	$(HEAA\text{-}PCL)_{44}$ macromonomer

Figure 55 Biocompatibility of compounds on Caco-2 (intestinal), A549 (airway) and A431 (skin) epithelial cells. Cytotoxicity was determined by PrestoBlue metabolic activity and LDH release as an indicator of membrane damage. Compounds (500 µg·mL^{-1}) were applied to cells in 10% FBS containing DMEM and exposed for 48 hours to cells. DMEM treatment represents the vehicle control and TX applied at 1% (v/v) was used as the cell death control. Data are presented as mean ± S.D.

The 2D assays performed demonstrate minimal cytotoxicity of the polymeric materials produced. Metabolic activity is maintained in the cell lines exposed to the synthesised products and DMEM, addition of TX eliminates metabolic activity. The sustained metabolic activity demonstrates that the cells biological processes are uninterrupted by the presence of these materials. LDH release is kept to a minimum when cells are exposed to these materials, indicative that their cell membranes remain intact and minimal necrotic cell death occurred. A slight decrease in metabolic activity and increase in LDH release can be observed for entry D Figure 55, a $(HEAA\text{-}PCL)_{15}$ homopolymer. It should be noted that this is a small change, and entry D cannot be considered cytotoxic as a result.

2.5 Conclusions

This chapter has investigated the use of HEAA as a functional eROP initiator using mild reaction conditions in a biorenewable solvent. Transesterification issues associated with acrylate containing functional initiators, such as HEMA, have been avoided through utilisation of an analogous acrylamide. The stability of HEAA in the presence of N435 facilitated synthesis of desirable aliphatic polyesters with functional end-groups using enzymatic catalysis. Through minimising side reactions exclusively mono-functionalised macromonomers were for the first time prepared using an eROP approach.

Control experiments were performed. It was found that upon exclusion of the enzymatic catalyst no polymerisation occurred. Upon removal of the HEAA initiator, eROP still occurred. Residual water trapped in the enzyme structure is thought to be the cause of this background polymerisation. Reactions without HEAA proceeded more slowly and yielded polymers of greater dispersity than those produced in reactions containing HEAA. Analysis using mass spectroscopy in combination with ^{1}H-NMR spectroscopy was used to ascertain that the produced material was primarily the targeted HEAA initiated poly(lactone), although background reactivity cannot be completely excluded.

Incomplete initiator conversion was detected during kinetic studies of HEAA initiated eROP of VL and CL. The conversion obtained for HEAA was significantly lower than that observed for the respective lactones. Experimental data suggested this was a result of propagation outpacing initiation, resulting in unreacted initiator remaining once full lactone conversion had been achieved. Computational docking approaches were employed to gain further insight, and found that an HEAA initiated chain of CL has a binding affinity twice that of unreacted HEAA. Greater conversions of initiator were observed when longer lactone chains were targeted during synthesis, implying there are counteracting effects present.

N435 was shown to be robust for at least 50 hours of reaction. The stability of N435 is a significant benefit in every regard – whether it be financial, environmental, or practical. Mild reaction conditions facilitate enzyme longevity. In commercial settings long catalyst lifetime is especially beneficial as significant cost reduction is associated with prolonged periods of use. Reactions were carried out in a renewable solvent, 2-MeTHF, to further improve the green credentials of the synthetic pathway. The maintained activity of N435 is indicative of excellent solvent-enzyme compatibility.

Hydroxyl end-group fidelity of a produced HEAA-PCL macromonomer was shown using organocatalytic chain extension using lactide. The maintained unimodality and dispersity

following chain extension, in combination with increased molecular mass observed by GPC demonstrates successful chain extension has taken place. The capability to undergo further chain extension demonstrates hydroxyl end group fidelity and is an overall testament to the control over the reaction during eROP. Sequential use of enzymatic and organocatalytic pathways demonstrates the versatility of this methodology and provides a method to circumvent limitations associated with individual catalysts.

Macromonomeric HEAA-PCL was used in radical homo- and copolymerisation to form a small selection of amphiphilic graft copolymers. This demonstrated the suitability of HEAA-PCL to partake in radical polymerisations after eROP. The amphiphilic materials formed were self-assembled into nanoparticles. Incorporation of a hydrophilic component was essential for successful self-assembly. Purely hydrophobic homopolymers of HEAA-PCL only aggregated into poorly defined aggregates. Furthermore, a one-pot methodology, going from eROP immediately to FRP by removing the heterogeneous N435, also produced a well-defined distribution of nanoparticles. The presence of unreacted HEAA can act as the hydrophilic component of the amphiphile synthesised and stabilise the nanoparticles. Purification by precipitation after eROP could therefore be considered superfluous, as any unreacted HEAA can simply be incorporated into the radical polymerisation product.

To facilitate application in biological environments cytotoxicity measurements were performed. Three human *in vitro* cell-lines (Caco-2, A431, and A459) were used to model various exposure routes. None of the tested materials displayed significant cytotoxicity towards these cell lines at concentrations up to 500 $\mu g \cdot mL^{-1}$. The absence of cytotoxic tendencies is a significant step to take these materials further to more in-depth applications testing.

HEAA has proven an interesting candidate for eROP reactions, opening new avenues for functional aliphatic polyesters to be explored through enzymatic catalysis.

2.6 Further Work

Modification of the CaLB active site would be an interesting method to improve the suitability of hydrophilic initiator species. Replacing amino acid residues near the active site with more hydrophilic amino acids could increase the favourable binding interactions of HEAA. In an ideal scenario, HEAA has a greater binding affinity than HEAA-PCL, as this would allow initiation to occur more rapidly than propagation and result in complete initiator conversion. During genetic modification of the enzyme care must be taken to preserve the structural elements that facilitate catalytic activity. Too drastic alterations could destroy the catalytic activity of the enzyme, and as such care should be taken when undertaking these experiments.

A synthetic approach to the same challenge would be to explore alternative initiator species. These potential initiators could be screened computationally prior to synthesis. In accordance with docking results discussed in this chapter, an extended hydrophobic linker between acrylamide and hydroxyl group would be beneficial to increase the rate of initiation. HEAA-CL itself would also be a promising candidate, however this would be challenging to synthesise without forming polymeric species as well.

These methodologies have not been investigated in this chapter, as a significant advantage of N435 and HEAA are their commercial availabilities. Enzyme modifications might produce more optimised catalysts; however, this must be balanced with the industrial large-scale viability of the process.

Further exploration of radical polymerisation techniques would be beneficial to tune the formation of nanoparticles. Controlled radical polymerisation techniques, such as Reversible Addition Fragmentation Chain Transfer polymerisation, offer the capability to synthesise block copolymers, enabling access to more complex polymeric architectures. Exerting greater control over radical polymerisation would be beneficial to optimise nanoparticle formation.

Alternative monomers could also be explored to install various behaviours in biological environments. One route that could be explored is the introduction of monomers that contain a tertiary amine, such as 2-(dimethylamino)ethyl methacrylate, which will be positively charged at physiological pH. Introduction of charge and alternative monomers can alter the behaviour of the formed nanoparticles and be used to target specific therapeutic targets.

To target therapeutic activity, loading of the nanoparticles with an active pharmaceutical ingredient should be explored. One of the strengths of nanoparticles in drug-delivery is their ability to solubilise hydrophobic molecules in aqueous environments. The suitability of the polymeric systems to solubilise hydrophobic small molecules is often modelled using a hydrophobic dye (such as coumarin-6). The quantity of drug encapsulated can be determined using UV Vis spectroscopy. Similar work can be performed on the HEAA-PCL copolymers synthesised here. Following these studies *in vivo* testing of the nanoparticles would be required to determine their fate in a physiological system.

Formed macromonomers and FRP (co-)polymers should also be tested for degradability. It is known from literature that poly(lactones) such as PCL and PVL can be hydrolytically degraded. The behaviour of FRP copolymers is not as well explored, and further experimental work would be needed to determine their degradative behaviours.

2.7 Materials and Methods

Novozym 435 lipase ([9001-62-1], derived from *C. antarctica* (>5000 U/g) and immobilized on an acrylic macroporous resin, 1 wt.% enzyme w.r.t. support, was kindly donated by Novozymes A/S, Denmark. ε-Caprolactone, δ-valerolactone, PEGMA (300 g·mol^{-1} average M_n) were purchased from Fischer Scientific and stored over molecular sieves. HEAA, and 2-MeTHF, were purchased from Sigma Aldrich and used as received. THF and methanol were purchased from Fisher Scientific UK and used without further purification unless otherwise stated. Water was deionised before use.

2.7.1 Instrumentation

Nuclear Magnetic Resonance Spectroscopy (NMR)

Polymer formation and chemical structure assignment was performed using ^{1}H-NMR spectroscopy. Approximately 4 mg of sample was dissolved in 0.7 mL of DMSO-d_6 or $CDCl_3$ and analysed using a Bruker DPX 400 MHz spectrometer operating at 400 MHz (^{1}H), assigning chemical shifts in parts per million (ppm). Spectra were referenced to residual C*H*Cl$_3$. MestReNova 6.0.2 copyright 2009 (Mestrelab Research S. L.) was used for analysing the spectra.

Gel Permeation Chromatography (GPC)

GPC was performed in THF (HPLC grade, Fisher Scientific) as the eluent at 40 °C using two Agilent PL-gel mixed-D columns in series, an injection loop of 50 µL, with a flow rate of 1 mL·min^{-1}. A differential refractometer (DRI) was used for the detection of samples. Samples were made at a concentration of approximately 2 mg·mL^{-1} in HPLC grade THF and filtered through a 0.22 µm Teflon filter before injection. The system was calibrated using poly(methyl methacrylate) standards with average molecular weight in the range from 540 to 1.02·10^6 g·mol^{-1} and low dispersity (*Đ*).

Dynamic Light Scattering (DLS)

Particle size analyses were performed by DLS utilizing a Zetasizer Nano instrument (Malvern Instruments Ltd) equipped with a 633 nm laser at a fixed angle of 173°. Nanoparticles were prepared at a concentration of 1 mg·mL^{-1} adopting a simple solvent displacement methodology (acetone/DI H_2O ratio 1:5). Samples were equilibrated at 25 °C for 30 seconds prior to measurements. All experiments were performed in duplicate averaging 10 scans per run of the same sample.

Matrix Assisted Laser Desorption Ionisation – Time of Flight Mass Spectroscopy (MALDI-TOF MS)

Polymer formation was assessed on a Bruker Ultraflex III mass spectrometer. *Trans*-2-[3-(4-*tert*-butylphenyl)-2-methyl-2-propenylidene]malononitrile (DCTB) was used as the matrix. Matrix (20 µL, 20 mg·mL^{-1} in acetonitrile) and polymer (10 µL, 10 mg·mL^{-1} in acetonitrile) were mixed, and the mixture (0.5 µL) was spotted onto the MALDI sample plate. PEG was used for calibration. Spectra were recorded at 50 % laser power.

2.7.2 Experimental Procedures

HEAA initiated eROP of CL or VL and Recyclability Study

In a typical procedure CL (1.00 g, 8.76 mmol), HEAA (0.2 to 0.025 mol equiv.), and solvent (2-MeTHF, 7mL, monomer concentration of 0.143 g·mL^{-1}) were combined and stirred until homogeneous. N435 (10 wt.%, 0.10 g) was added, and the reaction was stirred and heated (100 RPM, 65 °C). The mixture was filtered to remove the catalyst, and solvent was removed by rotary evaporation to collect the crude polymeric product. Alternatively, the reaction mixture was precipitated thrice into a cold mixture of methanol and diethyl ether (50:50 v:v) to obtain a polymeric sample free of unreacted initiator.

For the enzyme recyclability study, the same procedure as above was followed, except that the N435 was collected, rinsed (2 mL 2-MeTHF), and re-used with fresh reagents and solvent.

For the control experiments, the same procedure as above was followed, excluding addition of either initiator, monomer, or catalyst.

Lactide Extension of HEAA-PCL

A precipitated sample of HEAA-PCL (M_n 4500 g·mol^{-1} by ^{1}H-NMR analysis) (0.0401 g, 0.00891 mmol), and lactide (0.450 g, 3.12 mmol) were dissolved in dry DCM (6 mL). DBU (3 mol %) was subsequently added. Upon completion, as determined by ^{1}H-NMR spectroscopy, the reaction was precipitated into an ice-cold mixture of diethyl ether and petroleum ether (70:30 v:v, 35 mL). The product was collected by centrifugation (4500 RPM, 10 min) and allowed to dry *in vacuo*.

Computational Docking

Compounds were docked with Autodock version 4.2[192] on the reported crystal structure of CaLB (PDB code: 1LBS). A docking grid with a spacing of 0.375 Å was generated. 500 genetic algorithm runs were performed and the binding mode with lowest energy was selected. Explicit ligand hydrogen atoms were used and Gasteiger charges were added by Autodock.

Molecular Dynamics (MD) simulations were carried out using the graphics processing unit accelerated version of Amber 20.[193] Complexes were built starting from the docking conformation using the tleap module of AmberTools21.[193] The Amber FF19SB force field[194] was used for the protein and GAFF[195,196] with BCC charges for the ligands. A sodium ion was added to neutralize the system and the complex was solvated in an octahedral box of TIP3P[197] water molecules extending 10.0 Å from the protein. Periodic boundary conditions were applied. 1000 cycles of steepest descent minimisation were followed by 1000 cycles of conjugate gradient minimisation. The system was then heated to 300 K for 20 ps using Langevin dynamics with a collision frequency of 2.0 ps^{-1} with no constant pressure scaling, and was then equilibrated for 60 ps at 300 K at constant pressure with isotropic position scaling. The production run consisted of a 10 ns MD simulation at 300 K with no constant pressure scaling and SHAKE[198] for bonds involving hydrogen. Binding energy calculations were performed with the MMPBSA.py package in AmberTools21. 5000 snapshots from the 10 ns MD simulation were evaluated using the Generalized Born solvent model II[199] and a salt concentration of 0.1 M.

FRP General Procedure

Monomers were combined with 2-MeTHF (25 wt. % monomer loading) and allowed to dissolve before cooling (0 °C), and addition of AIBN (1 wt. % w.r.t. total monomer mass). The reaction mixture was degassed using a flow of argon (0.5 h, 0 °C) before being heated (65 °C, 22 h). The polymerisations were halted by exposure to air and precipitation into an excess of ice-cold diethyl ether. The precipitates were cooled (-20 °C) before centrifugation (4500 RPM, 10 min), followed by decantation of the supernatant and drying of the resulting polymers.

One-pot eROP and subsequent FRP

HEAA (0.336 g, 2.92 mmol), CL (1.66 g, 14.6 mmol), and 2-MeTHF (10 mL, 23 wt. % monomer loading) were combined in a vial and stirred until homogenous. N435 (10 wt. % w.r.t. monomer mass, 0.2 g) was added, and the reaction mixture was heated (65 °C, 18 h). N435 was removed by filtration, the remaining solution was cooled (0 °C), AIBN (1 wt. %, 20 mg) was added, and the mixture was degassed using argon (30 min) before sealing and heating (65 °C, 22 h). The polymerisations were halted by exposure to air and precipitation into an excess of ice-cold methanol (35 mL). The precipitates were cooled (-20 °C) before centrifugation (4500 RPM, 10 min), followed by decantation of the supernatant and drying of the resulting polymers.

Nanoparticle Formation

Nanoparticles were prepared by a nanoprecipitation method. Polymers (10 mg) were dissolved in acetone (1 mL). The polymeric solution was then added dropwise to deionised water (10 mL) under constant stirring at 550 RPM. Nanoparticle dispersions were formed through solvent exchange between water and acetone. The final dispersion was then left stirring overnight at room temperature in order to reach complete acetone evaporation, final NPs concentration of 1 $mg \cdot mL^{-1}$. The water level was marked before addition of the polymer solution, and complete solvent evaporation was assumed when the level had returned to the same mark.

Cytotoxicity Evaluation

Caco-2 human colonic cancer epithelial, A549 human lung adenocarcinoma, and A431 human epidermoid carcinoma cells were obtained from the American Type Culture Collection (ATCC; Manassas, Virginia) and used at passages 35-40, 30-35 and 25-30, respectively. Cells were cultured in DMEM (Sigma-Aldrich) supplemented with 10% (v/v) Foetal Bovine Serum (FBS) (Sigma-Aldrich) and 2 mM L-glutamine (Sigma-Aldrich), and at 37°C with 5% CO_2.

The lactate dehydrogenase (LDH) release assay (Sigma Aldrich, TOX7 kit) and PrestoBlue cell viability assay (Thermo Fisher Scientific) were performed to assess cytotoxicity. Cells were seeded at 1.2×10^5 cells per well in 12 well plates and cultured for 24 hours prior to assaying. Polymeric materials were exposed to cells at 500 $\mu g \cdot mL^{-1}$ for 48 hours and applied in 1 mL phenol red free DMEM containing 10 % (v/v) FBS and 2 mM L-glutamine. TX applied at 1 % (v/v) applied in phenol red free medium was used as a cell death (positive) control and a vehicle control containing no polymeric material used as a negative control. Following exposure, sample supernatant was collected from wells for analysis of LDH content. Cells were then washed twice with warm phosphate-buffered saline and 10 % (v/v) PrestoBlue reagent diluted in phenol red free medium applied per well for 60 minutes. The resulting fluorescence was measured at 560/600 nm ($\lambda_{ex}/\lambda_{em}$). Relative metabolic activity was calculated by setting values from the negative control as 100 % and positive control values as 0 % metabolic activity. Assessment of LDH release was performed according to the manufacturer's instructions and involved adding LDH reagent to collected supernatant samples and incubating at room temperature shielded from light for 25 minutes. Absorbance was then measured at 492 nm. Relative LDH release was calculated with the negative control absorbance at 492 nm taken as 0 %, and the positive control, assumed to cause total cell lysis, as 100 %.

Chapter 3. Synthesis of Sustainable Aqueous Rheology Modifiers

3.1 Aims & Objectives

Rheology modifiers for aqueous media are used for a host of applications, including adhesives, paints, and personal care. Unfortunately, commercially available synthetic products are usually petrochemically derived. Regulatory tightening and customer demand are driving research to find biobased and biodegradable alternatives for rheological modification.

This chapter looks at utilising commercially available polyglycerol as a biobased and biodegradable building block to synthesise polyesters for application as aqueous rheology modifiers.

3.2 Abstract

Polycondensation of polyglycerols with dimethyl succinate (DMS) in the presence of catalytic potassium carbonate was explored to synthesise hydrophilic polyesters. Three PG (PG4, PG6, and PG10) species were screened for this purpose. Analysis of the PG starting materials highlights that they consist of a distribution of oligoglycerol species containing various structural isomers. It was found that PG4 was most suited for polyester synthesis owing to its lower viscosity relative to other PGs screened, as well as the lack of discolouration following polymerisation. A temperature screening of the reaction was performed, and it was found that quantitative DMS conversion can be achieved at mild temperatures (60-100 °C). At elevated temperatures (140-180 °C) discolouration became increasingly significant. A small selection of transesterification catalysts was screened, including inorganic bases (NaOH, K_2CO_3), organic base (DBU), and a Lewis acid ($Sc(OTf)_3$). K_2CO_3 was identified as the most suitable, owing to its ability to dissolve in the polymer melt, lack of toxicity, widespread availability, and low cost. Polycondensations in equimolar stoichiometry between PG4 and DMS yielded soluble polymers. Increasing the loading of DMS to 1.5 equivalents relative to PG4 led to the formation of a highly swellable polymeric material. Further increases in DMS loading led to greater cross-linking density, diminishing the ability of the formed material to swell in aqueous media. These absorbent materials are evaluated for their ability to act as rheological modifiers in Chapter 4. Post-polymerisation functionalisation of poly(polyglycerol succinate) was explored using succinic and maleic anhydrides. Temperature control was critical during functionalisation to allow for ring-opening to occur whilst avoiding excessive polycondensation between pendant hydroxyl and carboxyl groups. The hydrophilic polyester is readily functionalised, enabling the installation of pendant carboxylic acid groups. One-pot

polycondensation and functionalisation was feasible for linear species of poly(polyglycerol succinate). For cross-linked species cryo-grinding and supercritical CO_2 were explored as methodologies to overcome mixing constraints and functionalise the polymer matrix. Following decoration of the polymer with pendant carboxylate groups a pH dependency on their behaviour as aqueous rheological modifiers was observed.

3.3 Introduction

Oligomeric polyglycerols (PGs) have been identified as highly promising candidates for the synthesis of aqueous rheology modifiers (Figure 15). The synthesis of PGs can be accomplished using a variety of methods; although the commercially sourced PGs employed in this chapter are made through the direct polycondensation of glycerol.[136,200,201]

Glycerol, a biproduct from the soap and biodiesel industries, is produced on a significant scale, amounting to millions of tonnes per year (Figure 56).[113,114] Currently, there are limited means to take advantage of such enormous quantities of glycerol, making direct oligomerisation to form PGs an effective approach to valorise this waste stream and create higher value products (Figure 57).[201] The utilisation of PGs offers numerous benefits. PGs and their fatty acid esters are commonly employed in the food and personal care industries as emulsifiers and humectants, demonstrating their extensive use in areas where chemical safety is of utmost importance.[202,203] The PGs used in this chapter are fully biobased in addition to being Kosher and Halal. Additionally, the PGs used in this study are readily biodegradable, further affirming their environmental compatibility.[204] With their abundance of hydroxyl groups, PGs exhibit strong hydrophilicity and are readily water soluble.

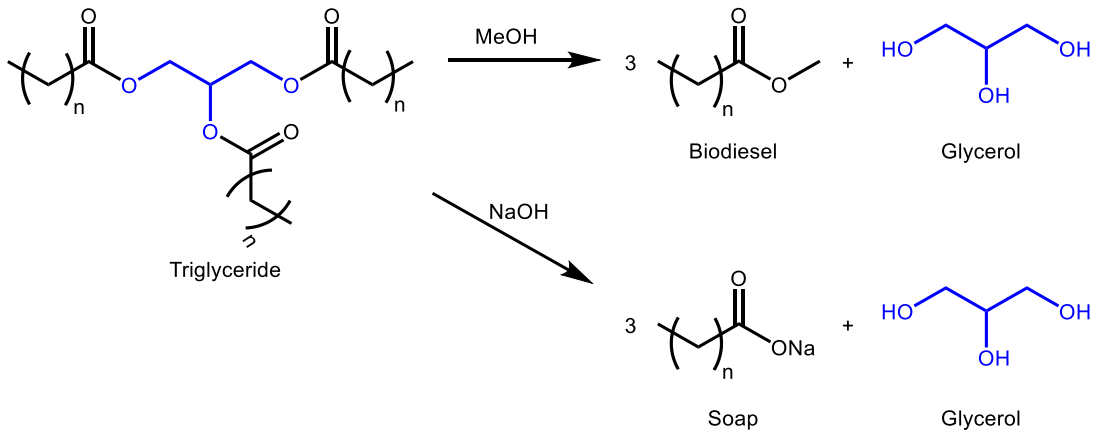

Figure 56 Triglycerides are used as feedstocks for biodiesel (top) and soap (bottom) yielding glycerol as a biproduct.[114]

Glycerol is polymerised industrially using a variety of catalysts and elevated

temperatures.[201,205] Typically, basic catalysts are preferred over acidic catalysts to minimise the formation of cyclic and acyclic side products.[205] The oligomerisation of glycerol can be performed using either homogeneous or heterogeneous catalysis.[206] Barros *et al.* even utilised calcined waste eggshells to catalyse glycerol oligomerisation.[206] Regardless of specific conditions employed, oligomerisation is performed at elevated temperatures (typically around 200 °C) to increase rate of reaction, decrease reaction-mass viscosity, and drive the removal of water.[114,201,206,207]

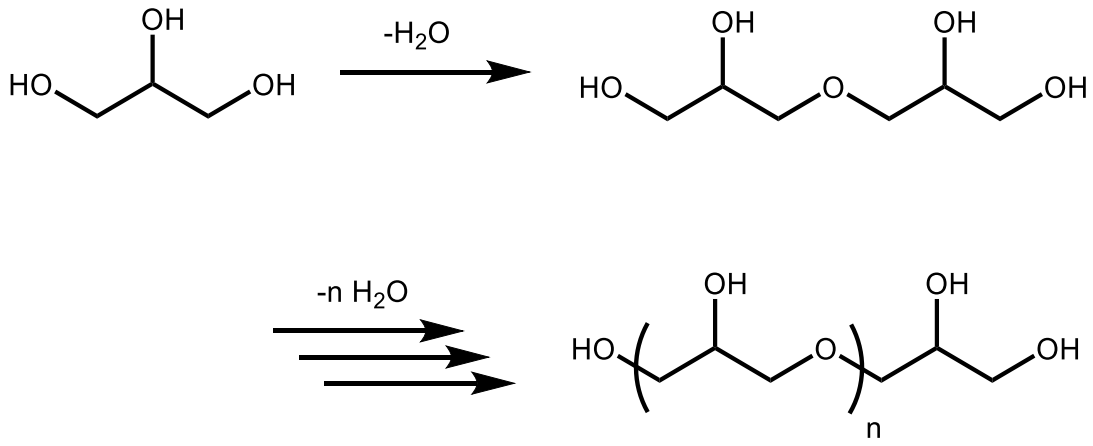

Figure 57 Direct polycondensation of glycerol leads to the formation of PG in a step-growth process. Structures shown are idealised, not showing any branching structures.

To achieve the desired rheological modification, it is necessary to modify the PGs. As supplied, PGs exhibit water solubility without significant thickening effects at reasonable loadings. To produce an associative thickener, the PG should be extended and end-capped with hydrophobic moieties to facilitate the formation of micelle networks.[81] This modification would allow for the PG to link together micelles resulting in the desired thickening effect. To mimic a non-associative viscosity modifier, the PGs need to be significantly extended and lightly cross-linked to produce a swellable system.[92] Furthermore, the PG will have to be decorated with ionic pendant groups to establish inter- and intra-molecular electrostatic repulsions to form an ionic network and enhance performance.[92] This structural arrangement would enable the separation and straightening of PG chains, leading to water being trapped in the polymer structure and increasing the viscosity of the system.[93]

In non-associative as well as associative rheology modifiers, the hydrophilic component is usually a high molar mass polymer.[85,91] Polyesterification serves as one method to increase

the molar mass of a polyol, such as PG, by formation of a polyol polyester.[208] Previous research in the group has successfully utilised sorbitol in combination with succinic acid to form polyesters for surfactant applications.[109] Maintaining linearity in the polymer necessitates careful consideration of the reaction conditions and catalyst selection.[108,109,208] Undesirable excessive reactivity of the polyol can result in the formation of highly cross-linked resins.[209] In the sorbitol-based work, potassium carbonate was utilised as a catalyst as it preferentially catalysed esterification of primary hydroxyl groups.[109] This produced linear hydrophilic polymers with minimal cross-linking. The ester bonds also serve as sites for hydrolytic degradation of the polymer backbone.[210] This presents a promising avenue to address the limited biodegradability observed in current rheological modifiers.

Succinic acid has been widely recognised as a suitable difunctional carboxylic acid for the synthesis of polyesters.[24] It holds significant industrial value due to its wide applicability and the possibility of sustainable production from renewable resources.[121,211,212] Fermentation processes offer a means to produce succinic acid from diverse carbon sources, including crop stalk wastes, corn fibre, and straw, thereby enhancing its sustainability and reducing dependency on fossil feedstocks.[115] Several industrial actors have already initiated large-scale production of biobased succinic acid, further demonstrating its viability as a sustainable platform chemical.[119] Moreover, succinic acid is readily biodegradable, aligning with Green Chemistry principles.[213]

The short carbon chain of succinic acid helps maintain hydrophilicity in the formed polymers by limiting the presence of hydrophobic moieties. As a result, succinic acid has been identified as a promising difunctional monomer for the synthesis of polymers for aqueous rheology modification. In this work, the dimethyl ester of succinic acid, dimethyl succinate (DMS), was utilised instead of succinic acid itself. This choice was made to facilitate lower reaction temperatures during polycondensation owing to the greater volatility of methanol as a condensate.[214] Importantly, DMS is classified as readily biodegradable and is not a hazardous substance.[215]

Through the synthesis of polyol polyesters using PG and DMS, this chapter explores the transformation of PG into a rheologically active material, with potential applicability in personal care applications.

3.4 Results and Discussion

3.4.1 Polyglycerol Analysis

Since glycerol molecules can couple between primary positions (prim-prim), secondary positions (sec-sec), and primary to secondary positions (prim-sec), the possible structural isomers are many (Figure 58).[216] The presence of structural isomers influences the ratio of primary to secondary hydroxyl groups in the material.[205] Prim-sec, and sec-sec linkages increases the proportion of primary alcohols, which is expected to impact the reactivity of these sites.[108,109,217] As the degree of polymerisation increases, so does the number of possible structural isomers.

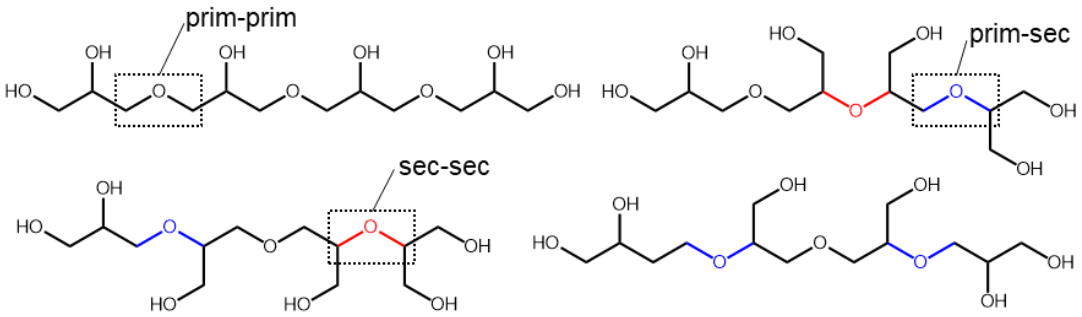

Figure 58 Some examples of the structural isomers of tetraglycerol. Prim-sec, and sec-sec connections are highlighted in blue and red respectively.

The manufacturer, Spiga Nord, has provided analytical data describing the distribution of glycerol oligomers (Table 9). From this data, it is evident that the commercial products are far from a singular species. The commercial sample of PG4 for example, contains 12.5% more triglycerol than tetraglycerol. Average molar mass ranges of the samples are around the theoretical value of the desired PG. ^{1}H-NMR spectroscopy of PG4 supports the average structure, as the ratio of hydroxyl protons and carbon-bound protons is 6:20.9, very close to the expected ratio of 6:20 (Appendix Figure 6). Whereas single-oligomer species of PG would be desirable from a synthetic chemical perspective, the production requirements of such species would detract from the waste-valorisation and green-ness of the raw material.

Glycerol DP	PG4 (%)	PG6 (%)	PG10 (%)
1	0.6	0.6	0.7
2	7.0	6.1	3.6
3	41.3	26.1	6.2
4	28.8	21.5	7.4
5	12.0	13.9	7.2
6	5.0	7.9	7.6
7	2.7	6.0	5.0
8	1.4	4.4	5.0
≥9	1.3	13.7	57.2

Table 9 Manufacturer's specification of oligomer distribution in the PGs utilised.

Aqueous GPC of the starting materials was performed to gain further insight into the distribution of chain lengths (Figure 59). PG4 and PG6 yielded narrow signals in the GPC chromatograms. PG10 however has a significantly broader signal distribution, with a dispersity of 2.7 (Table 10). The broadened dispersity observed can be a result of increased branching present in PG10. Molar masses predicted by aqueous GPC should be interpreted carefully. Since the column calibration is not performed with PG there is expected to be some deviation from the theoretical molar mass obtained. The masses obtained are also close to the lower limit of calibration, possibly resulting in additional error. Especially in the case of PG10, a large discrepancy is observed between theoretical and experimental results. The overestimation of molar mass by GPC could be an effect of increased branching causing unusual elution behaviour.[218,219]

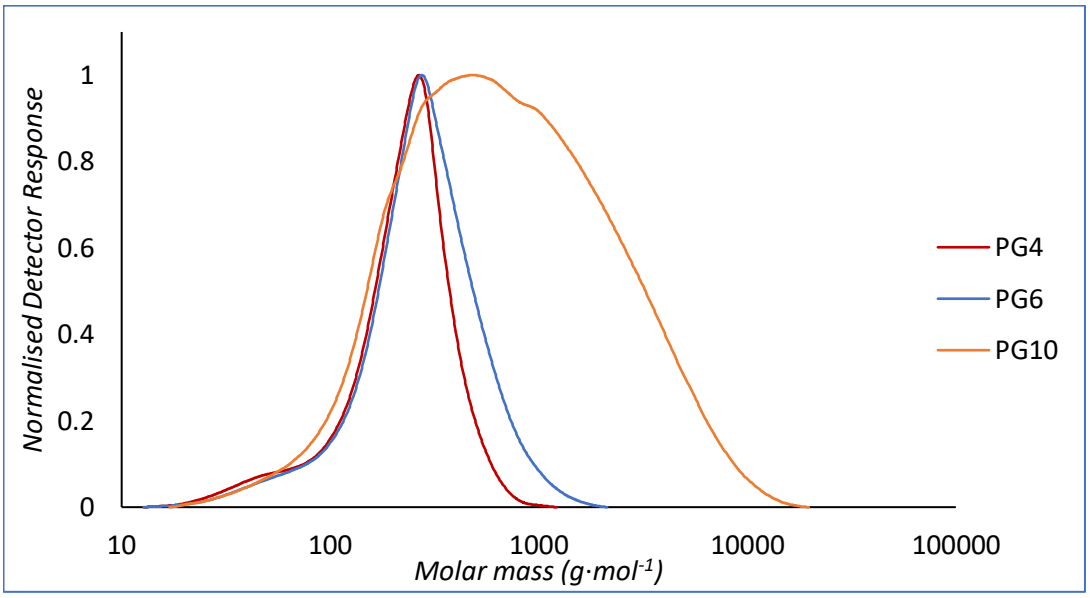

Figure 59 GPC traces of PGs used in this work.

The aqueous GPC results indicate that PG10 features a broader range of oligomeric species in comparison to PG4 and PG6. This difference in structures present in the material could be interesting to explore in terms of final viscosity enhancing performance. For example, a more branched final structure could impact the rheological modification properties of the produced material.[92]

Compound	Theoretical Molar Mass (g·mol^{-1})	M_n (g·mol^{-1})	M_w (g·mol^{-1})	$Đ$
PG-4	314	252	315	1.25
PG-6	462	330	467	1.42
PG-10	745	1234	3269	2.65

Table 10 Tabulated GPC results of commercial PGs.

Branching occurs during glycerol oligomerisation when the secondary hydroxyl group reacts – acting either as nucleophile or leaving group. In base catalysed ether formation, the primary hydroxyl groups are more reactive. Primary hydroxyl groups have a slightly lower pK_a, and are therefore more likely to be deprotonated. Greater steric hindrance surrounding the central carbon of glycerol means nucleophilic attack is more likely to take place at the outer carbons. Both factors result in the preferential formation of prim-prim ether linkages. Whilst the primary hydroxyl groups are more reactive, some background reactivity of the secondary hydroxyl is still expected to occur. The degree of branching is expected to increase with degree of polymerisation. As primary hydroxyl groups are preferentially consumed during oligomerisation, their concentration decreases during the process. Consequently, the

concentration of secondary hydroxyl groups increases, leading to a greater probability of branching prim-sec or sec-sec ether linkages forming.

To gain insight into the degree of branching present in the PG raw materials, quantitative ^{13}C-NMR was employed (Figure 60). ^{1}H-NMR spectroscopy could not be employed to quantify degree of branching due to signal overlap between methine and methylene protons, as seen in the HSQC spectrum of PG4 (Appendix Figure 7). DEPT-135 (Appendix Figure 8) was utilised to distinguish ^{13}C-NMR signals of methine and methylene carbons that are close in chemical shift and challenging to separate using ^{1}H-^{13}C Heteronuclear Single Quantum Coherence (HSQC) NMR spectroscopy. Rollin *et al.* have published detailed ^{13}C-NMR studies of many pure oligoglycerols, which has been extremely useful for signal assignment.[216] From the quantitative ^{13}C-NMR spectrum of PG4, approximately 20% of methine carbons in the sample are connected to a bridging oxygen atom (structural motifs A and B in Figure 60), rather than a secondary hydroxyl group (structural motifs C and D in Figure 60). The presence of these structures implies that there is a greater prevalence of primary hydroxyl groups in the PG4 than in an idealised structure of tetraglycerol. Analysis of PG6 and PG10 by quantitative ^{13}C-NMR spectroscopy revealed that 24% (Appendix Figure 9) and 31% (Appendix Figure 10) of methine carbons are attached to bridging ethers rather than secondary hydroxyls. Showing the increase in prim-sec and sec-sec connections with increasing degree of polymerisation.

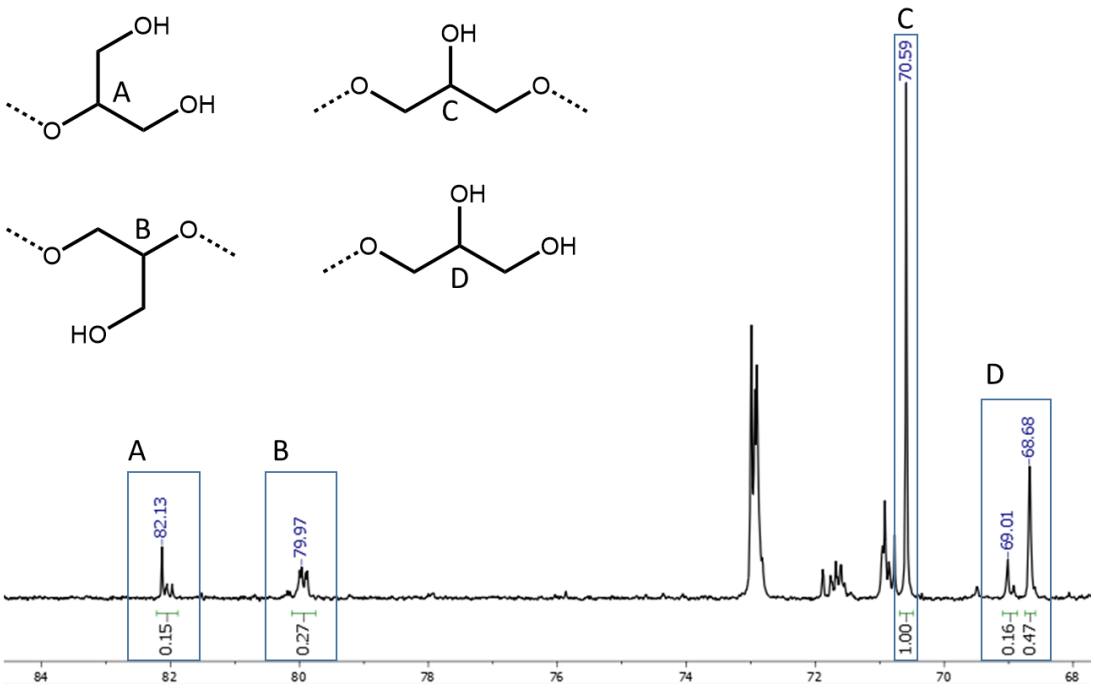

Figure 60 Quantitative ^{13}C-NMR spectrum of PG4 in DMSO-d_6 in the region of 68 to 84 ppm. 2873 scans, relaxation delay of 75 s. Structures shown are representative fragments of oligoglycerols.

The PGs used as starting materials in this chapter are a mixture of various lengths and structural isomers. Aqueous GPC indicates that PG4 and PG6 contain little branching structures, whereas the high dispersity of PG10 implies the presence of more nonlinearity in this material. Analytical data provided by the manufacturer provides greater insight into the chain lengths of PG present in the samples. To assess the proportion of secondary ether linkages present, quantitative ^{13}C-NMR spectroscopy was employed. In PG4, it was found that approximately 20% of methine protons are attached to an ether linkage, whereas this number was 24% and 31% for PG6 and PG10, respectively. The combination of these analytical techniques provides greater insight into the nature of the commercial PG samples.

3.4.2 Polyester Synthesis

Polyglycerol Lengths

A variety of PGs were screened as potential monomers for reaction with DMS (Figure 61). PGs were reacted with DMS to increase the overall molar mass and allow for the formation of structures that could be used as hydrophilic polymers for rheological modification. The dimethyl ester of succinic acid, DMS, was employed in favour of succinic acid itself. Whilst utilising the acid form is beneficial in terms of atom economy, the low volatility of water makes driving the polycondensation more challenging – often requiring high temperatures and vacuum.[220] Instead, performing transesterification with the dimethyl ester eliminates methanol as condensate. Methanol is more volatile than water, and is more readily removed at lower temperatures.[214] DMS has the added benefit of being liquid at room temperature, facilitating material handling and processing.

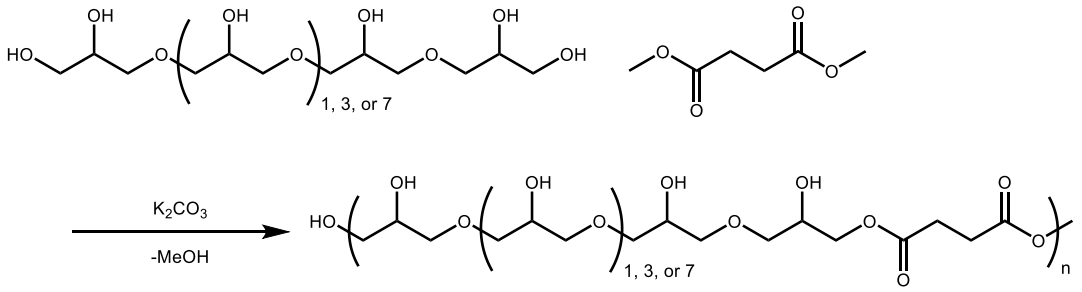

Figure 61 Reaction scheme for the polycondensation of various length PGs and DMS.

The increase in viscosity with PG chain length is rather dramatic, rising orders of magnitude with just a few repeat units (Figure 62). Increases in viscosity are typically perceived as disadvantageous, limiting heat-transfer and mixing.[221] On the other hand, the additional pendant hydroxyl groups are beneficial for water solubility and post-polymerisation functionalisation. In this work, hydrophilicity and pendant functionality are essential.

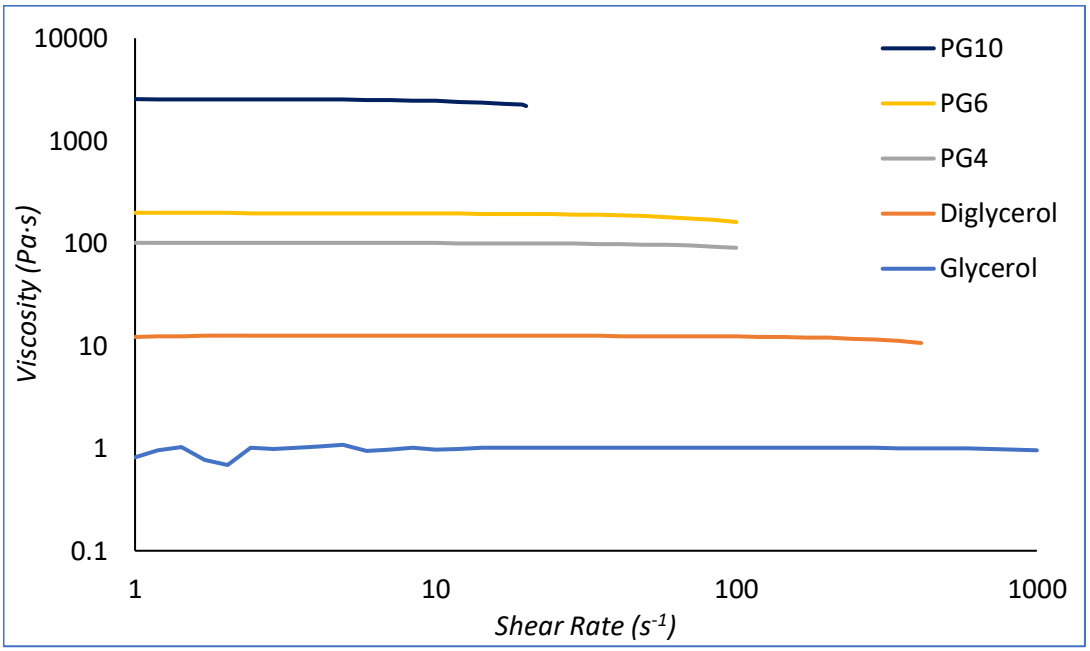

Figure 62 Viscosity against shear rate for a variety of (poly)glycerol samples at 25 °C.

PG4, -6, and -10 were used to investigate which PG would be most suitable as a monomer in the transesterification with DMS. It was found that an increased PG length resulted in greater discolouration during reaction. PG4 remained virtually colourless, whereas PG10 noticeably browned. PG6 did not discolour as strongly as PG-10, although more discolouration was visible in comparison to PG4 (Figure 63). The lower diffusivity of reagents at high viscosity can lead to higher concentrations of byproducts, possibly explaining the increased yellowing of PG6 and PG10.[221] Furthermore, in personal care application, discolouration is highly undesirable due to consumer demand for colourless products. The higher viscosities of PG6, PG10, and their respective polymers also leads to mixing difficulties. On an industrial plant these increases in viscosity are significant, and mass-transfer of products becomes increasingly problematic.[221]

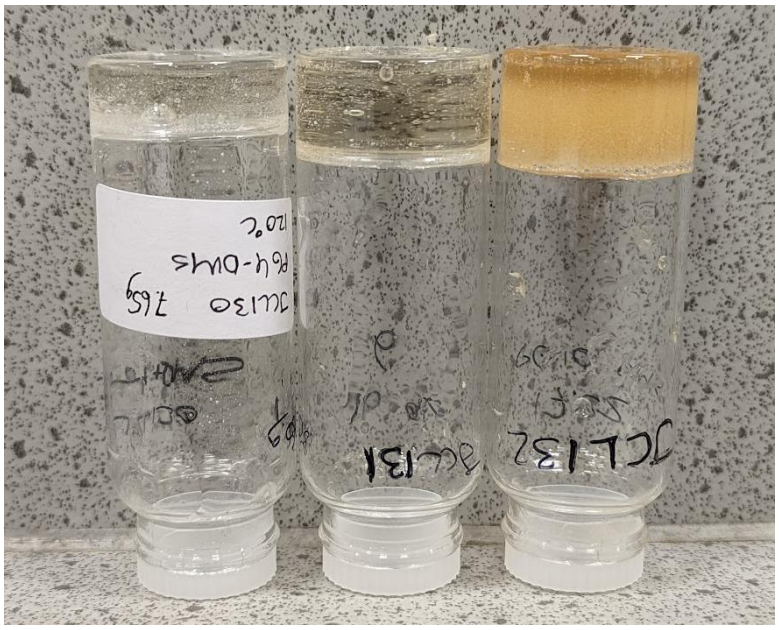

Figure 63 Various lengths of polyglycerol building blocks were polytransesterified with DMS. From left to right: PG4-DMS, PG6-DMS, and PG10-DMS.

Differential Scanning Calorimetry (DSC) was used to analyse the thermal properties of the PG starting materials and PG-succinate polyesters (Table 11). DSC traces revealed that all PGs and polyesters showed amorphous behaviour, exhibiting glass transition temperatures (T_g) but no melting transitions (T_m). Following polycondensation, a significant increase in T_g was observed for all lengths of PG, indicative of polymerisation.[222] With increased chain length, intermolecular forces increase, and more thermal energy is required for the chains to transition from a glassy to a rubbery phase. The most significant increase in T_g was observed for PG-4, increasing by 37.2 °C during polymerisation. This could be a result of the increase in chain length being the most pronounced for PG-4, as PG-4 is the shortest PG tested. Promisingly, no transitions associated with unreacted DMS were observed in the DSC traces. Unreacted DMS would be expected to display a melting transition around 18 °C, and a boiling transition around 196 °C. The absence of these transitions indicates that DMS has successfully incorporated into the polymer.

PG Species	T_g PG (°C)	T_g PG-succinate (°C)	ΔT_g (°C)
PG4	-35.8	1.4	+37.2
PG6	-30.5	-6.4	+24.1
PG10	-17.2	7.0	+24.2

Table 11 Differential scanning calorimetry data for PG starting material and following polyesterification with DMS.

To gain further insight into the polymerisation process ^{1}H-NMR spectroscopic analysis was employed. The ^{1}H-NMR spectrum of DMS features two sharp and distinct signals at 3.64 (C*H*$_3$O-) and 2.58 ppm (-C*H*$_2$-) ideal for monitoring reaction progress. Using the ratio of the integrals between the methoxy and methylene groups the extent of reaction can be determined (Equation 13). Due to the broad nature of PGs in ^{1}H-NMR spectra there is some overlap between the peaks corresponding to PG and DMS, although this is minimal, and conversion can still be estimated.

$$Conversion\ (\%) = \frac{1.5 - (\frac{\int CH_3O}{\int (CH_2)_2})}{1.5} \times 100$$

Equation 13 Conversion of DMS to PG4-DMS using ^{1}H-NMR integrals. Assuming all DMS is converted to PG4-DMS.

The methoxy signal is significantly diminished after 24 hours at reaction conditions (Figure 64, signal B). Assuming DMS is only converted to polymer this is strongly indicative that polymerisation has taken place and that the reaction is forming a polyol polyester. The maintained solubility of these materials is indicative that cross-linking is kept to a minimum and that the species obtained are mostly linear or only slightly branched. The ^{1}H-NMR spectra also show the presence of methanol after 1 and 5 hours of reaction, although none is detected at 24 hours demonstrating the removal of methanol during the reaction. The formation of methanol shows that DMS is undergoing transesterification. In combination with the appearance of new peaks corresponding to PG protons adjacent to ester linkages, labelled A, this provides a convincing picture of the polytransesterification taking place. From the ^{1}H-NMR spectra it can also be seen that the succinate backbone signal, labelled C, and the main PG signal, around 3.4 ppm, maintain a consistent ratio. This demonstrates minimal evaporation of the more volatile DMS monomer is taking place during the reaction, and targeted stoichiometry is maintained.

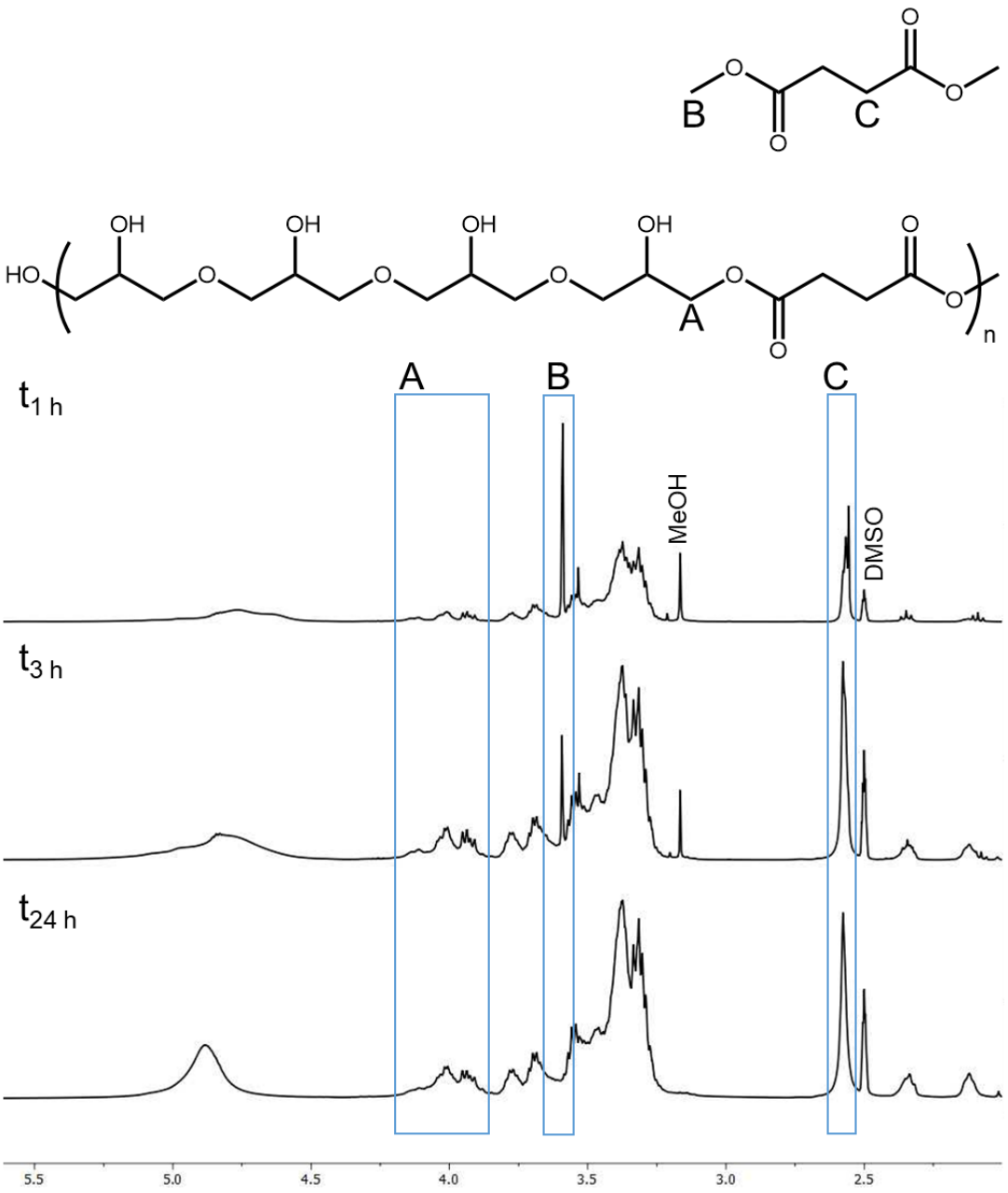

Figure 64 ^{1}H-NMR spectra of the reaction between PG4 and DMS after 1 h (top), 3 h (middle), and 24 h (bottom) in DMSO-d_6.

From the ^{1}H-^{13}C HSQC spectrum of PG4-DMS, it appears that new esters formed consist of methylene protons (Figure 65). No methyl or methine HSQC signals can be observed in relation to the ester-adjacent signals. The HSQC data suggests the primary hydroxyl groups are more likely to esterify during polymerisation. This would be in-line with previous work, which shows that K_2CO_3 has selectivity towards primary hydroxyls.[109] Selectively reacting with primary hydroxyls allows the K_2CO_3 to maintain some control over the polycondensation and minimises cross-linking through the secondary hydroxyls. It is believed that this selectivity originates from the differences in pK_a and sterics of primary and secondary

hydroxyl groups. As primary hydroxyls are slightly more acidic, they are more likely to be deprotonated, heightening nucleophilicity.[223] Primary hydroxyls also feature less steric bulk in comparison to secondary hydroxyl groups, leading to a greater reactivity. Branching cannot be fully controlled however, as the PG4 used is composed of many structural isomers (Figure 58). For oligoglycerols containing prim-sec or sec-sec linkages the number of primary hydroxyl groups is greater than two, and can serve as branching points.

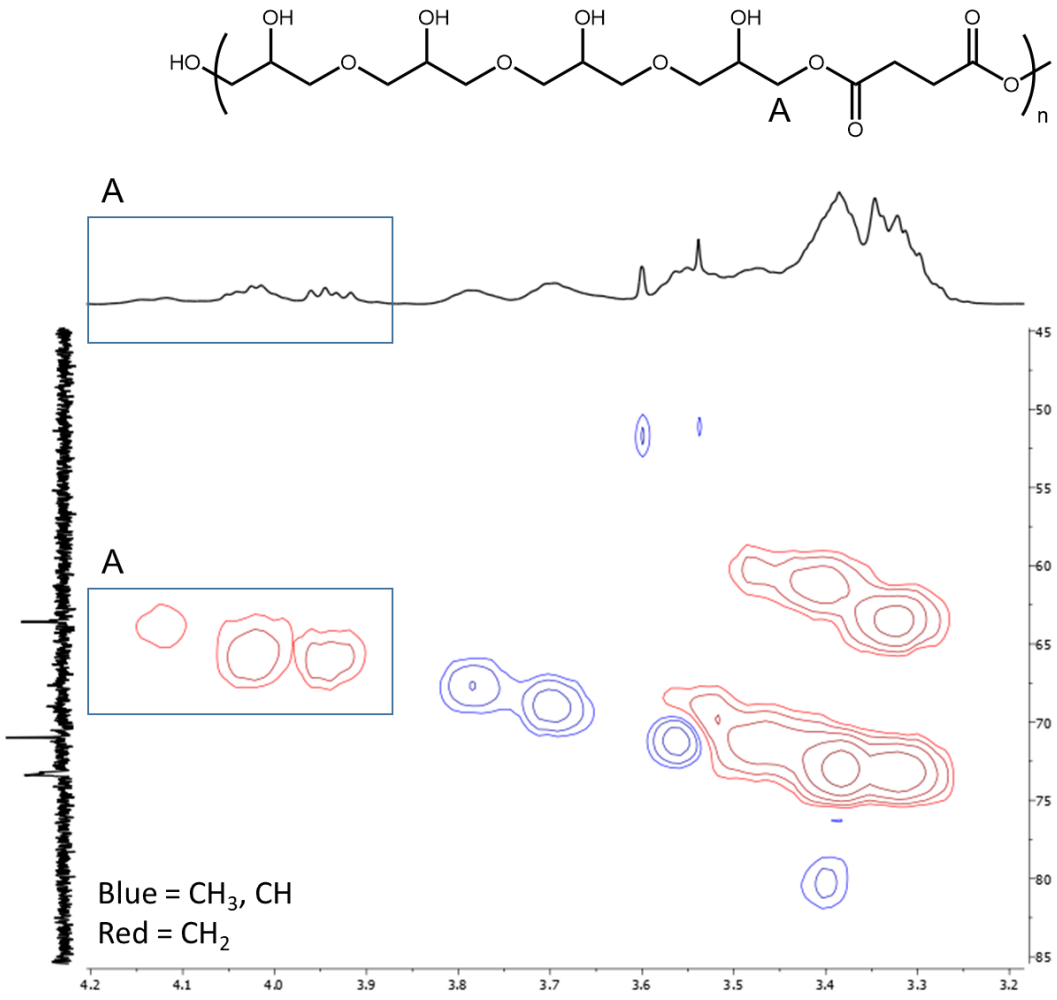

Figure 65 ^{1}H-^{13}C HSQC spectrum of PG4-DMS in DMSO-d_6. Zoomed in on the region between 3.2-4.2 ppm (^{1}H) and 45-85 ppm (^{13}C).

Aqueous gel-permeation chromatography (GPC) was also performed on these materials. GPC further demonstrates polymerisation has taken place, with molar masses increasing significantly compared to the PG monomers employed. GPC indicates that polyesters of PG4 and PG6 obtained are approximately 2214 and 1560 g·mol^{-1}. These numbers would indicate a DP around 7 for PG4-DMS and 3.5 for PG6-DMS. Using the reaction conditions employed these seem to be reasonable estimates, greater DP could potentially be achieved by increasing temperature or using vacuum during polymerisation. Once again, PG-10 proves to

be the outlier. GPC indicates a molar mass of 18 217 g·mol^{-1}, which is almost ten-fold larger than that of PG4-DMS. The large molar mass, in combination with a large dispersity (8.0) indicates that PG-10DMS is significantly branched.

Sample	M_n (g·mol^{-1})	M_w (g·mol^{-1})	$Đ$
PG4-DMS	2214	6829	3.08
PG6-DMS	1560	4080	2.62
PG10-DMS	18217	146338	8.03

Table 12 Aqueous GPC data of PG polyesters synthesised at 120 °C.

From the GPC chromatograms significant portions of unreacted PG can be observed (Figure 66). The unreacted PG suppresses M_n whereas the M_w highlights the presence of higher molar mass species in the products. Whilst DMS goes to high conversions, as seen by ^{1}H-NMR analysis, PGs are unable to go to similar levels of conversion, presumably due to the excess of hydroxyl groups relative to the methyl esters. This would indicate that there is insufficient DMS present for all PG to react, although increased DMS loadings (*vide supra*) lead to reactions solidifying and becoming insoluble, and as a result not suitable for analysis by GPC. The limited conversion of PG can be seen as a fundamental limitation of the methodology employed, as with increased conversion effective mixing becomes increasingly challenging leading to mass- and heat-transfer limitations during the process. Whilst not all PG has reacted, this methodology was carried forward as it was hypothesised that the presence of some unreacted PG would not be detrimental to the performance of the final rheological modifier.

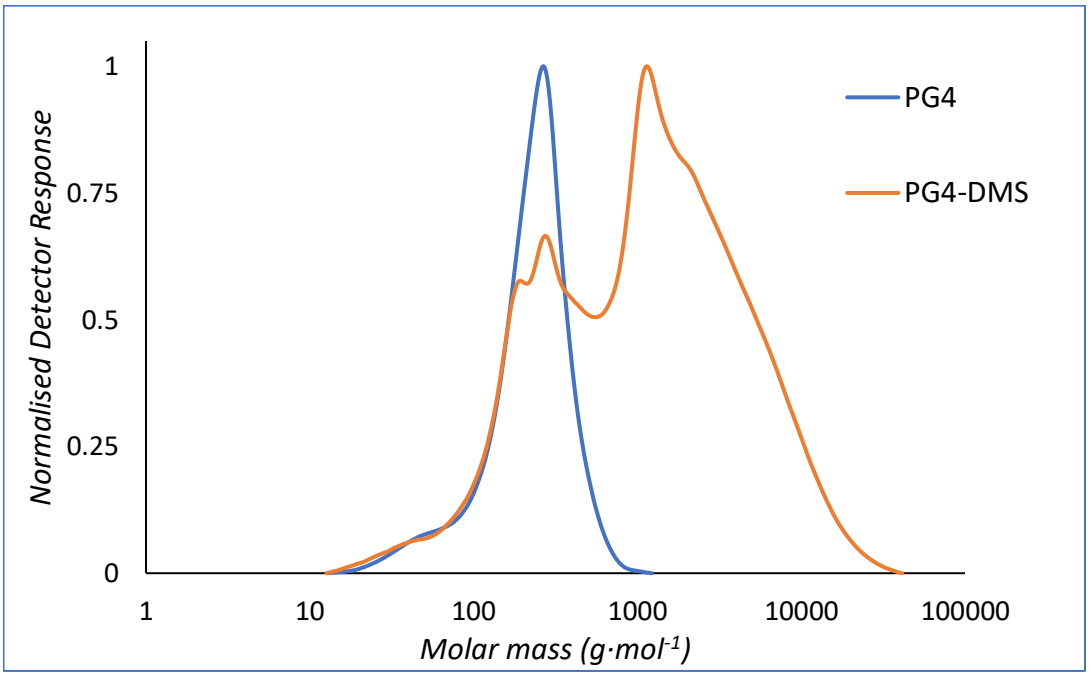

Figure 66 Overlaid GPC traces of PG4 and PG4DMS.

Various length PGs were tested for their behaviour in the polycondensation with DMS. It was found that polymerisation occurred, producing relatively low molar mass polyesters. Analysis by ^{1}H-NMR spectroscopy indicates that DMS goes to very high conversions, whereas GPC shows that there is still unreacted PG present after 24 hours. PG4 was selected as the optimal PG for this reaction, as it did not display any discolouration at reaction conditions and has the lowest viscosity relative to PG-6 and -10. PG4 also possesses multiple hydroxyl groups that imbue hydrophilicity and are suitable for further reactions post-polymerisation.

Temperature Screening

The effect of temperature on the reaction between PG4 and DMS was investigated. This study was performed to ascertain if the polycondensation reaction could be run at decreased temperatures to lessen the energy requirement of the process.

Temperatures between 60 and 180 °C were explored. The driving force of this polycondensation is the removal of methanol by evaporation. As such temperature is a key factor, as a higher reaction temperatures facilitate the volatilisation and removal of the condensate. Increased temperatures also have the additional benefit of lowering the reaction viscosity (Figure 67), improving mass and heat transfer in the process. Decreased viscosity would also improve processability of these highly viscous materials, which is especially important on larger scales. Temperature can therefore be expected to play a fundamental role in the polymerisation process.

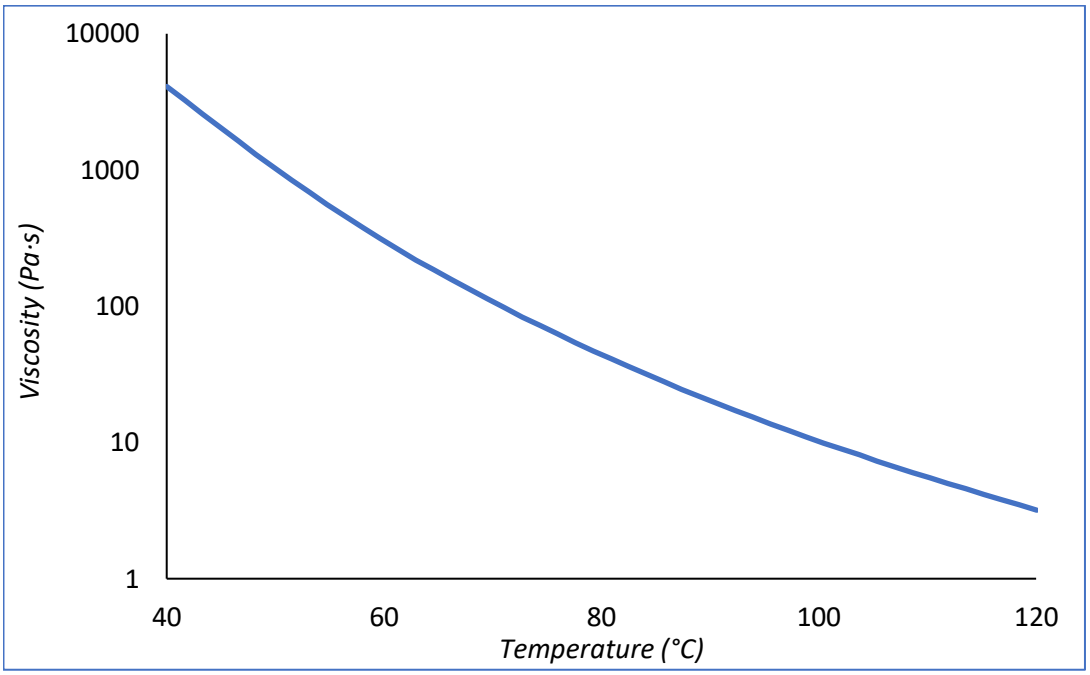

Figure 67 Temperature dependence of PG4-DMS viscosity. Measured at a shear rate of 5 s^{-1}, heating rate of 1 °C·min^{-1}.

These benefits are balanced by the occurrence of discolouration often observed at elevated reaction temperatures.[224] Discolouration was observed during this polytransesterification, with reactions performed above 140 °C displaying significant darkening (Figure 68). Darkening could be a result of thermal oxidation becoming more significant at elevated temperatures. A lower reaction temperature would be highly desirable to avoid darkening during synthesis which would require additional steps downstream to obtain a colourless product.

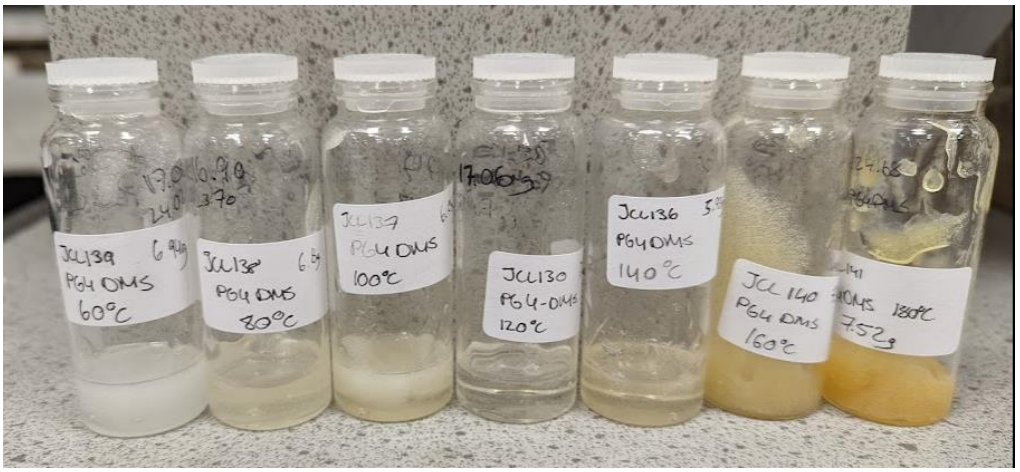

Figure 68 PG4-DMS Synthesised at a variety of temperatures. From left to right: 60, 80, 100, 120, 140, 160, 180 °C.

Conversions of DMS exceeding 95% after 24 h were measured for PG4-DMS synthesised at all temperatures screened (Table 13). These appear to be quantitative, however, due to some signal overlap in the spectra between the methoxy peak of DMS and PG4, this cannot be ascertained definitively by ^{1}H-NMR spectroscopy. The high DMS conversions are indicative that the transesterification proceeds readily under these conditions. Even at a relatively low temperature (60 °C) significant DMS conversion is observed, indicating that under these conditions driving the reaction is straightforward. The ability to utilise lower reaction temperatures is an advantage of performing transesterification using dimethyl esters rather than the equivalent dicarboxylic acid. The ability to use lower reaction temperatures is however offset by the decreased atom economy of using methyl esters, where the condensate accounts for a larger portion of reagent mass. In principle this condensate can be collected and reused, which would alleviate some of the atom economical concerns.

Synth. Temp. (°C)	Conversion (%)	M_n (g·mol^{-1})	M_w (g·mol^{-1})	$Đ$	T_g (°C)	η (kPa·s)	AV (mg KOH·g^{-1})
60	95.3	2637	9733	3.69	-3.2	4.38	1.2
80	96.6	2582	9244	3.58	1.4	7.26	1.2
100	97.3	2418	8416	3.48	2.0	4.97	1.7
120	96.3	2213	6829	3.09	0.4	2.50	2.5
140	97.2	2127	6228	2.93	2.5	4.92	1.2
160	95.7	3297	12275	3.72	2.4	4.00	1.5
180	96.2	4065	18458	4.54	1.3	9.54	1.2

Table 13 Conversion, GPC data, DSC data, and volumetric data of PG4-DMS synthesised at a range of temperatures. T_g reported is the midpoint of the transition. Viscosity measured at a shear rate of 4 s^{-1} and 40 °C.

As seen earlier (Figure 66), PG-4 conversions are not expected to reach similar levels as DMS conversions, as a significant PG peak can be seen in the GPC chromatograms. Since these polymerisations involve a polyol and a bifunctional ester, driving the reaction further increases the occurrence of cross-linking eventually leading to insolubility. Molar mass determination by GPC indicates that similar molar masses were obtained at all temperatures, ranging from 2213 to 4065 g·mol^{-1} (Table 13). The reaction performed at 180 °C showed the highest molar mass. At such an elevated temperature some of this mass increase could reasonably be caused by the etherification of glycerol units with the elimination of water.

Interestingly, molar masses do not increase with reaction temperature. The discrepancy could be a result of batch-to-batch variability of these polycondensations. Final molar mass could vary significantly based on minor variations in reagent stoichiometry. Other sources of inconsistency could include small changes in total scale of the reaction, which would change the ratio of surface area to bulk volume and alter the overall efficiency of condensate removal. Efforts were made to minimise experimental deviation, however the viscous and adhesive-like nature of PGs resulted in these variables not being perfectly controlled. Nevertheless, GPC traces of the produced materials are very consistent across the temperatures screened, featuring unreacted PG4 as well as higher molar mass polyester signals (Figure 69).

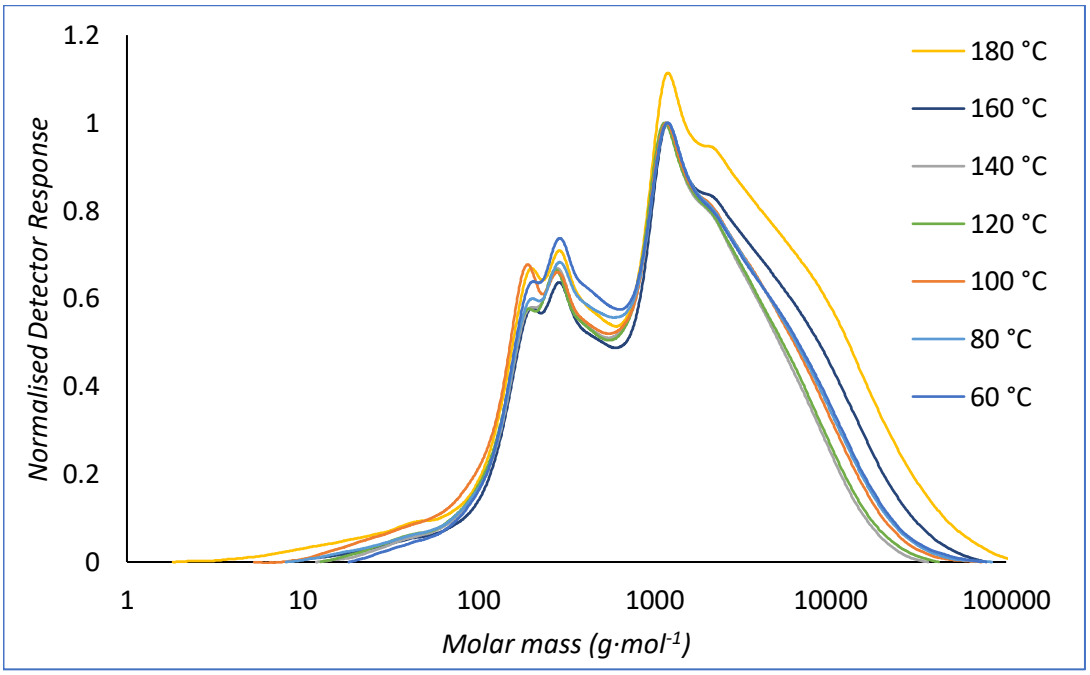

Figure 69 GPC traces of PG4-DMS synthesised at various temperatures.

Thermal analysis using DSC shows glass transition temperatures in the range of -3.2 to 2.5 °C, with the synthesis at 60 °C having a noticeably lower T_g in comparison to the other synthesis temperatures (Table 13). It is thought that the lower T_g of the PG4-DMS synthesised at 60 °C could be indicative of a limited chain length or conversion (Appendix Figure 13). The polyesters synthesised at higher temperatures have T_gs in close proximity, indicating similar conversion and chain length. Since the polyesters synthesised are of relatively low molar mass, it is uncertain whether the T_g obtained for the higher temperature syntheses is the maximum T_g obtainable for these materials.

Viscosities of the polymeric products are in the same order of magnitude, indicating similar molar masses and structures were obtained (Table 13). Relative to PG4 (0.1 kPa·s, 25 °C, Figure 62), a 25-to-95-fold increase in viscosity was observed following polycondensation. The final viscosities of the polyesters provide insight into some of the processing considerations that are encountered during the synthesis of these materials.

Acid values (AV) were measured to assess the extent of hydrolysis during polytransesterification (Table 13). It was found that these materials have very low acid values, as neutralisation was observed immediately upon addition of the smallest volume of titrant. This is indicative that minimal hydrolysis of DMS to succinic acid has taken place during the reaction. Saponification values were also determined (Appendix Table 7), although the theoretical saponification values at zero (244 mg $KOH \cdot g^{-1}$) and full conversion (estimated 279 mg $KOH \cdot g^{-1}$ for DP=5) are close together. As such, no accurate estimation of conversion was made from the saponification values measured. The SAP values demonstrate that the formed polyesters contain hydrolytically sensitive bonds, that can potentially serve as cleavable sites to facilitate degradation.

It was determined that reactions at temperatures exceeding 140 °C should be avoided due to unwanted discolouration becoming significant. From a rheological study, the temperature dependence of PG4-DMS viscosity was measured. It was found that elevated temperatures significantly suppressed the viscosity of these materials, which would aid in reaction processing, material handling, as well as with reaction kinetics. From ^{1}H-NMR spectroscopic analysis it was found that DMS reached high conversions at all reaction temperatures screened. Molar mass determination by GPC found that similar masses were obtained at the conditions explored, except for 180 °C which yielded a much higher molar mass with increased dispersity. Thermal analysis demonstrated that PG4-DMS synthesised at 60 °C had a markedly lower T_g compared to the other products. It is believed this lower T_g is indicative of a lesser extent of polymerisation, although other analytical techniques such as ^{1}H-NMR spectroscopy and GPC did not substantiate this theory. For all temperatures, a significant increase in viscosity was observed during polymerisation compared to PG-4 starting material, indicating that polymerisation has taken place, and highlighting some of the engineering challenges associated with the materials. Acid values showcase that hydrolysis is minimal during transesterification.

For many of the reactions discussed later in this chapter, 80 °C was selected as an appropriate reaction temperature. All analytical techniques in this section indicate reactivity on-par with elevated temperatures. As seen *vide supra*, a reaction temperature below 100 °C is also advantageous for post-polymerisation functionalisation with acid anhydrides, as the lower temperature limits cross-linking whilst facilitating ring-opening during post-polymerisation functionalisation.

Catalyst Screening

This section details experimental work carried out by a master's student (India Gosai) under direct supervision of the author. Experiment design and data analysis was performed by the author.

A selection of catalysts was screened for the polycondensation of PG-4 and DMS. Reactions were analysed by ^{1}H-NMR spectroscopy and GPC after 24 hours to determine DMS conversion and molar mass (Table 14).

Catalyst Species	Conversion (%)	M_n (g·mol^{-1})	M_w (g·mol^{-1})	$Đ$	Observations
DBU	51.9	467	846	1.81	Yellowing
K_2CO_3	93.5	3131	8951	2.86	-
NaOH	87.5	2128	6118	2.88	Limited solubility
$Sc(OTf)_3$	73.3	2698	9179	3.40	-

Table 14 Conversion and molar mass data after 24 h of reaction utilising a variety of catalysts. Experimental observations are also included.

The organic base DBU was investigated as it has been used in the literature to catalyse transesterification.[44,225,226] The polar organic nature was also anticipated to facilitate dissolution into the polymer melt. DBU was found to have the lowest conversion after 24 hours, measuring only 51.9%. GPC consequently yielded a signal corresponding to 467 g·mol^{-1}. Furthermore, yellowing was observed whilst utilising this catalyst. The combination of low reactivity and discolouration shows that DBU is not a suitable catalyst for this reaction under the conditions employed.

K_2CO_3 was found to have the highest final conversion and molar mass. Furthermore, the product obtained was a viscous colourless polymer. K_2CO_3 has the additional advantages of being inexpensive and already established in commercial processes.[109] Previous examples also demonstrate that K_2CO_3 exhibits a preference for esterification at primary alcohols, which is highly advantageous to maintain aqueous solubility thanks to the secondary

hydroxyl groups along the PG backbone.[109] From these reactions it has also been observed that K_2CO_3 is capable of rapidly dissolving in the polymer melt, improving the process kinetics. In addition, K_2CO_3 is also relatively benign and is even used as a food additive (E501). The overall inexpensive and benign nature of K_2CO_3, in combination with good conversions and molar masses make it a highly desirable catalyst for this process.

Sodium hydroxide was also investigated as a potential catalyst. NaOH has also been used as a transesterification catalyst in the literature.[227] NaOH is an interesting alternative to K_2CO_3 in this reaction to assess the effect of increasing basicity and nature of the counterion. It was found that NaOH encountered solubility issues in the reaction mass, and granules of catalyst would persist even upon prolonged heating and agitation. Furthermore, NaOH reached lower conversion and molar mass in comparison to the carbonate, possibly due to these solubility issues. To compound these issues, NaOH is significantly more corrosive than the carbonate, and as such was determined to be an inferior catalyst for this reaction. In addition, handling of solid NaOH with accurate control over stoichiometry is also challenging due to its hygroscopic nature. This hygroscopic nature can introduce water to the reaction system, leading to hydrolytic degradation and suppressed molar masses.

Scandium triflate was explored as a Lewis acidic catalyst that is well known to catalyse polyesterification. It has also been shown that scandium triflate exhibits selectivity towards primary hydroxyl groups and can be used to synthesise polyesters with pendant hydroxyl functionality.[110–112] Interestingly, the triflate yielded higher molar mass polymer than NaOH whilst reaching a lower conversion. This effect is most likely a result of hydrolysis taking place in the NaOH catalysed reaction, meaning DMS is not exclusively converted to polymer. Other acid catalysts, such as sulfuric acid or *p*-toluenesulfonic acid, were not explored as these are known to cause discolouration and cross-linking.[109] The initial results from the triflate are promising, with good molar mass, and yielding a colourless product. Limited conversion and higher cost were the reasons why scandium triflate falls behind potassium carbonate in suitability for this reaction.

All further work was performed using K_2CO_3 which yielded the highest conversion and molar mass, whilst avoiding undesirable discolouration and being a very economically viable catalyst. The literature precedent of K_2CO_3 preferentially catalysing esterification of primary hydroxyl groups is an added benefit, providing a straightforward approach to build molar mass whilst avoiding excessive cross-linking and branching.

Kinetics of PG4 Polycondensation

Polymerisation of PG4 with DMS was sampled at various time points to gain insight into the kinetic profile of this reaction. At predetermined times an aliquot (1 mL) was taken of the melt polycondensation using a syringe. The reaction was monitored using ^{1}H-NMR spectroscopy, aqueous GPC, DSC, and rheometry (Table 15).

Time (h)	Conversion (%)	M_n (g·mol^{-1})	M_w (g·mol^{-1})	$Đ$	T_g (°C)	η (Pa·s)
1	57.6	601	1180	1.96	-3.4	1.66
3	79.0	981	2034	2.07	-2.3	9.37
5	87.2	1716	4343	2.53	0.68	36.20
24	94.4	3687	11433	3.10	3.8	137.17

Table 15 Kinetics data for the polycondensation of PG4 and DMS. Viscosities measured at a temperature of 80 °C and a shear rate of 100 s^{-1}.

Conversion of the polycondensation between PG4 and DMS reaches significant conversions after only 5 h. As is expected for a step-growth polymerisation, molar mass increases significantly with the final percentages of conversion.[223] The difference in GPC molar mass between 5 and 24 h showcases this significant increase with a small increase in conversion (Figure 70). To achieve a molar mass as high as possible it is therefore key to use conditions that drive the reaction forward. As this reaction is in equilibrium, removal of methanol favours polymer formation following Le Chatelier's principle. In this case the reaction was performed at a temperature significantly greater than the boiling point of the methanol condensate formed. Mechanical stirring was employed to thoroughly agitate the polymer melt, exposing trapped methanol to the surface for evaporation. Argon flow was used to further enhance methanol removal by preventing a build-up of methanol vapours in the reaction vessel.[228]

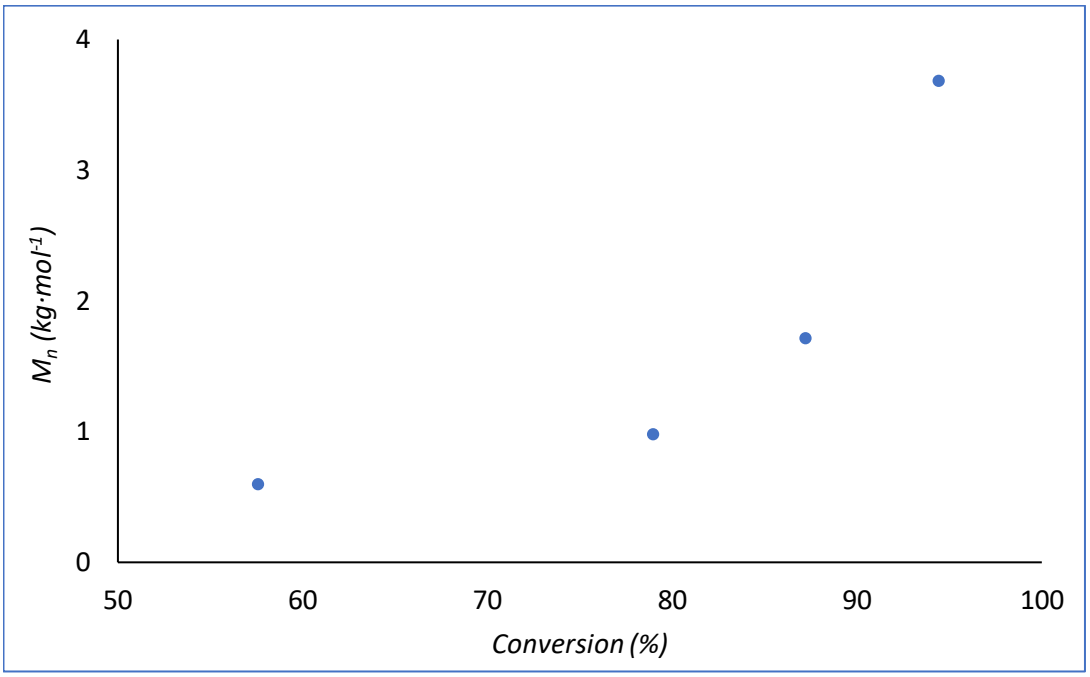

Figure 70 Molar mass (GPC, M_n) plotted against conversion for the polycondensation between PG4 and DMS.

Rheologically, the increase in molar mass is reflected in the viscosity of the material, which undergoes a 4-fold increase between 5 and 24 h (Table 15). Increasing viscosity with molar mass is expected behaviour for polymerisations and can lead to difficulties in manipulating the polymer melt.[228] The increase in viscosity is a result of increased intermolecular attractions as the polymerisation proceeds. As polymers become longer, the likelihood of entanglement also increases, further building viscosity. The weight average molar mass highlights the presence of larger molecules in the reaction mixture. These longer chains will contribute significantly to the overall viscosity due to their ability to entangle and increased resistance to flow. The presence of low-viscosity molecules, such as monomers and unevaporated methanol, are expected to lessen the overall viscosity. Such small molecules can act to solvate and plasticise the reaction mixture. As the reaction proceeds and these low-viscosity molecules are consumed or removed, their viscosity-lowering effects on the polymer melt are eliminated, further compounding the rise in reaction viscosity. Low molar mass materials will also suppress the number average molar mass. The very drastic increase in viscosity observed is caused by a combination of increasing chain entanglement and intermolecular interactions, as well as the removal of low-viscosity molecules. Industrially, measuring the viscosity of the polymer melt could be a rapid way to determine reaction progression and serve as a quality control metric. Viscosity measurements can be performed *in-situ*, which is ideal for industrial environments.[229,230]

T_g measured by DSC increases with conversion. This is expected of a polymerisation, as increasing the chain lengths will result in greater intermolecular interactions and consequently a higher temperature is needed to allow for these chains to transition to a rubbery phase. Furthermore, at higher conversions, T_g decreasing effects caused by unreacted monomer are lessened. The materials display amorphous behaviour throughout the reaction, which is positive as undesirable crystallisations are avoided during processing.

The data obtained during the kinetic experiments show that driving the reaction to high conversion is key to increase molar mass. Commercially available rheological modifiers often have high molar masses (ASTs for example are usually 100 000s g·mol^{-1}),[92] and as such it is hypothesised that large molar masses are required for good performance. Viscosity and T_g also increase along with conversion, as expected for a polymerisation. Dramatic increases in viscosity and T_g were observed especially between 5 and 24 h as molar mass builds significantly. Viscosity measurements can be a promising approach to determine reaction progression rapidly using industrially suitable methodology.

Altering Reagent Stoichiometry

Having gathered insight into the behaviour of the reaction between PG4 and DMS, alternative reactant ratios were explored aiming to introduce slight cross-linking to deliver swelling properties. Cross-linking density of the material impacts the rheological modification performance of the produced polymer. Excessive cross-linking results in the formation of a highly insoluble polymer, unsuitable for rheological modification.[92] Insufficient cross-linking yields a soluble polymer (Figure 71). As such, a variety of stoichiometric ratios were explored to maximise rheological modification in aqueous solution.

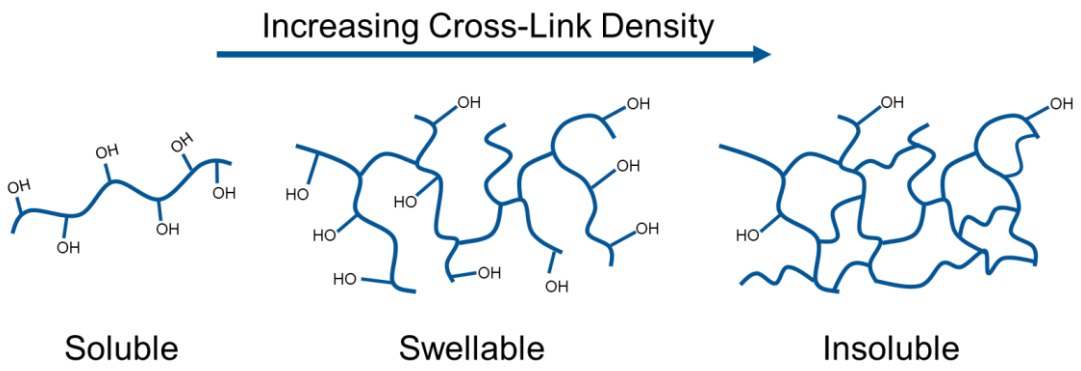

Figure 71 Schematic illustration of cross-linking density and its effect on PG4-DMS behaviour in aqueous medium.

It was found that increasing the loading of DMS resulted in the formation of tough rubber-like materials. Due to the cross-linking taking place, mechanical agitation becomes increasingly challenging. The collected materials did however display very promising water-swelling behaviour (Figure 72). For rheological modification, water absorbing characteristics are essential to form a non-associative viscosity modifier. The ability to entrap water in the polymer matrix restricts the flow of water in the system and increases viscosity. Simply submersing the material in water overnight resulted in the formation of a hydrogel. Promisingly, the swollen gel was completely colourless and appeared capable of absorbing significant quantities of water. It was observed that 1.5 equivalents of DMS appeared to be an optimal loading from initial visual observations (Appendix Table 8). Lower loadings of DMS yielded either less-swellable material (1.25 equiv. DMS) or soluble material (1 equiv. DMS) due to insufficient cross-linking allowing for greater solubility. Higher loadings, 2 and 3 equivalents of DMS, resulted in more rigid, less swellable materials presumably due to their increased cross-linking and subsequent limited flexibility to accommodate water molecules in their structures.

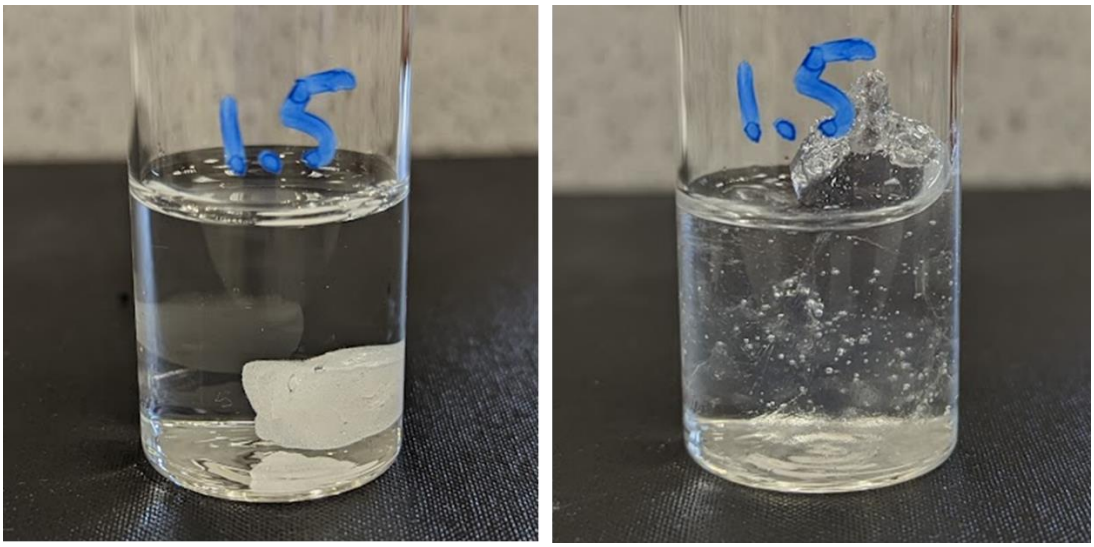

Figure 72 PG4-1.5DMS was found to be capable of swelling in water. Left: PG4-1.5DMS immediately after submersion in water. Right: 24 hours after submersion.

The molecular characterisation of PG4-DMS with greater DMS loadings is complicated by their lack of solubility. To gain some insight into DMS conversion a ^{1}H-NMR spectrum was recorded of the supernatant (Figure 73). Since the gelled fraction was not analysed, the spectrum is not fully representative. Nevertheless, from the spectrum it can be ascertained that there is a soluble fraction present, containing DMS, PG4, and some PG4-DMS esters. A signal corresponding to trace methanol can also be detected. The presence of unreacted DMS indicates conversion does not reach the same quantitative levels as when a single equivalent of DMS used. In the soluble fraction of PG4-1.5DMS analysed the conversion of DMS is 79%. This conversion is most likely to be an underestimate, as in the gel fraction a higher conversion is expected. In addition, ^{1}H-NMR analysis does not provide information regarding the size of the soluble fraction. The presence of unreacted material is probably a result of the increasing rigidity as the polymer develops cross-links, leading to poor reactant diffusion in the latter stages of polymerisation.

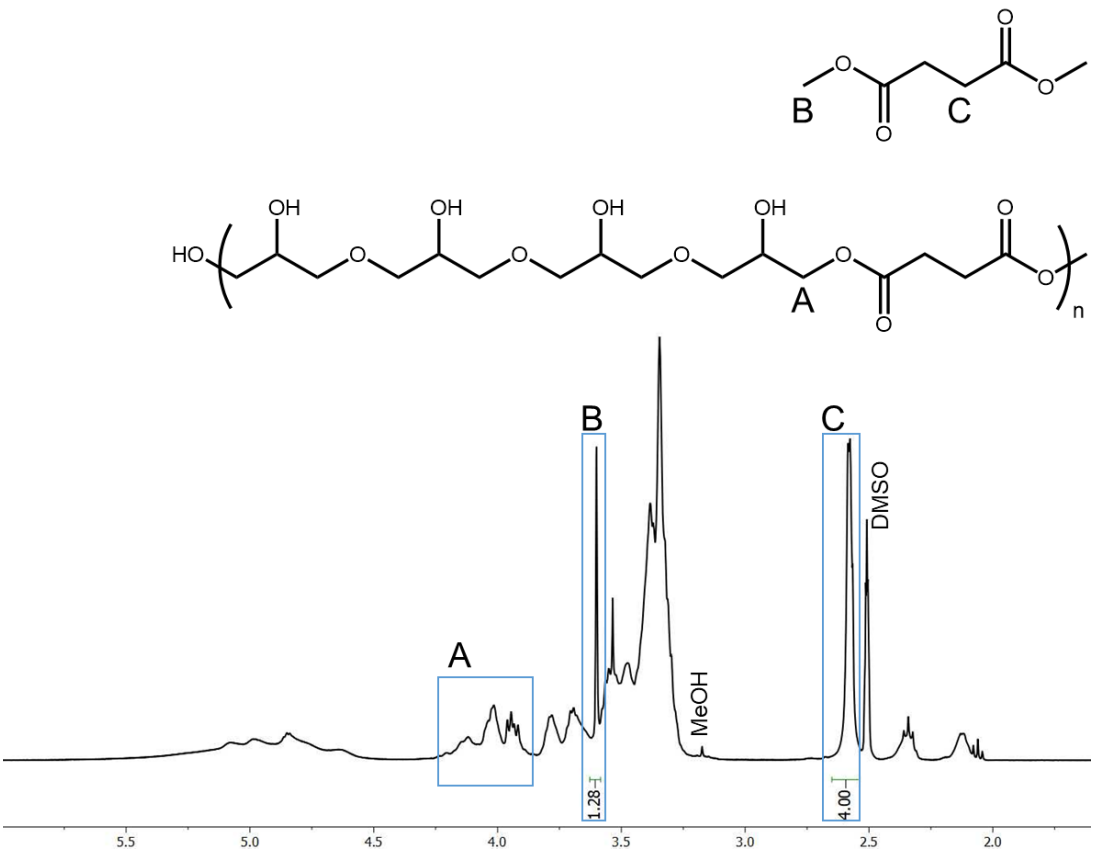

Figure 73 ^{1}H-NMR spectrum of the soluble fraction of PG4-1.5DMS.

Altering reagent stoichiometry provides a facile approach to introduce cross-linking to PG4-DMS. Simply tuning the equivalents of DMS added to the reaction can be used to achieve highly water absorbing materials. This approach is performed in one pot, yielding desirable properties without purification or post-polymerisation processing. Rheological modification and water-absorption characteristics of these materials is explored in more detail in Chapter 4.

3.4.3 Post-Polycondensation Functionalisation

Addition of Succinic Anhydride

To develop polyglycerol-based polyesters mimicking the structure and properties of alkali-swellable non-associative thickeners, introduction of pendant carboxylic acids was investigated. The ring-opening of cyclic acid anhydrides onto the polymer backbone was explored as a method to attach the desired carboxylic functionality (Figure 74). Anhydrides were selected for this purpose, as ring-opening can be performed at mild temperatures whilst avoiding esterification reactions leading to cross-linking.

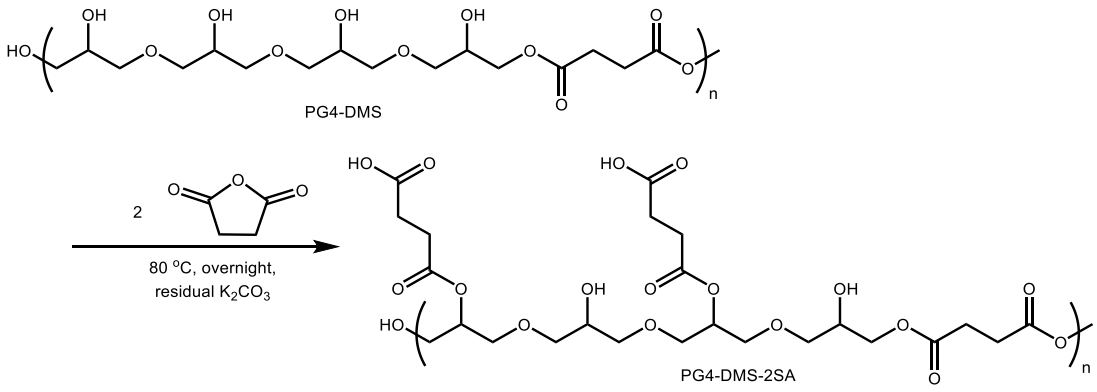

Figure 74 Reaction scheme for the post-functionalisation of PG4-DMS with two equivalents of succinic anhydride. Structure of PG4 shown is idealised.

Addition of Succinic Anhydride to Linear PG4-DMS

The practical considerations for further reaction of linear PG-succinates with cyclic anhydrides are significantly different with respect to further reaction of cross-linked PG-succinates. Linear PG-succinates act as viscous polymer melts with manageable viscosity at reaction temperature (80 °C). This allows for overhead mixing to be effective enough on a lab-scale to distribute the desired anhydride throughout the polymer. This is not the case for the cross-linked material.

A one-pot approach was taken; where polycondensation of PG4 and DMS was performed for 24 hours, after which the anhydride was added, and the reaction allowed to continue. It was found that a one-pot approach significantly eased the synthetic procedure whilst improving yield. Allowing the polymer melt to maintain an elevated temperature removed the need for cooling and subsequent re-heating. Keeping the polymer melt at reaction conditions also facilitated mixing. Minimising transfers between reaction vessels also limited yield loss due to incomplete mass transfer.

Immediately following addition of the solid succinic anhydride, it could be seen visually in the polymer melt as heterogeneous fragments dispersed into the melt. As the reaction proceeded, gradually these fragments dissolved into the reaction mixture, yielding a homogeneous product. It was observed that the ring-opening of succinic anhydride in the reaction mass was quick, and it is believed that the rate-determining step is the initial dissolution of the anhydride into the reaction mass. Performing this post-functionalisation at 80 °C was deemed optimal, as higher temperatures (90 °C) resulted in the formation of an insoluble monolith. Presumably due to condensation reactions occurring between pendant acid and hydroxyl groups, resulting in uncontrolled cross-linking. It was found that monolith

formation was avoided at 80 °C, as the reaction was performed below the boiling point of water and therefore limiting the extent of esterification taking place.

Aliquots of the reaction mixture were taken and analysed using ^{1}H-NMR spectroscopy (Figure 75). The reaction was allowed proceed for 1.5 h, to ensure sufficient mixing of the solid anhydride into the reaction and to facilitate collection of a representative sample. From the ^{1}H-NMR spectrum, 1.5 h was insufficient to fully consume the succinic anhydride. Allowing the reaction to proceed overnight (18 h) resulted in no succinic anhydride being detectable by ^{1}H-NMR spectroscopy. During the reaction new signals appear between 2.25 and 2.50 ppm, corresponding with the methylene protons of the pendant succinate groups. The ^{1}H-NMR spectroscopic analysis matches well with experimental observations, as once the reaction becomes fully homogeneous, no unreacted succinic anhydride can be detected by ^{1}H-NMR analysis.

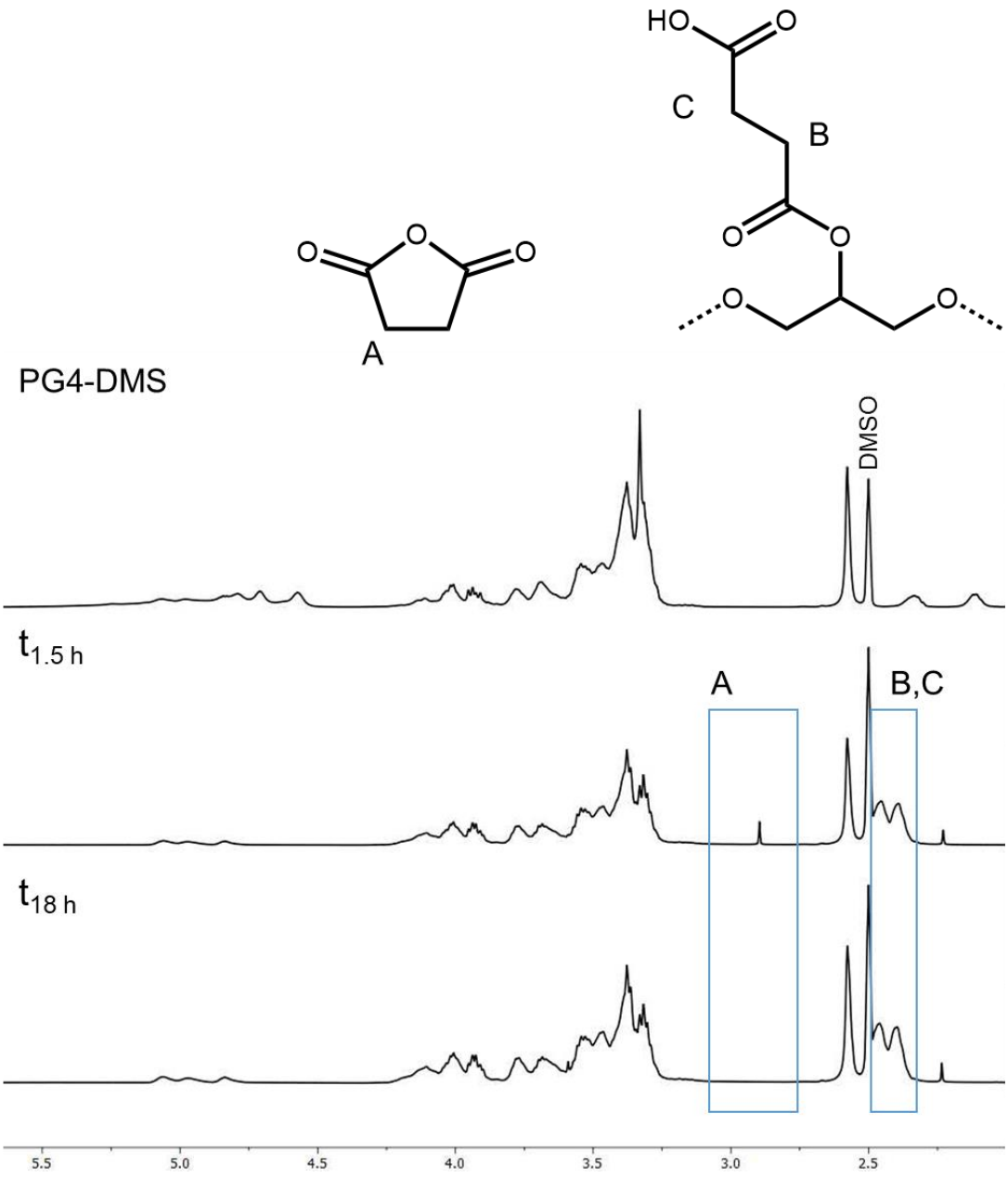

Figure 75 ^{1}H-NMR spectra in DMSO-d_6 of functionalisation of PG4DMS with succinic anhydride. Top: PG4DMS. Middle: 1.5 h after addition of succinic anhydride. Bottom: 18 h after addition of succinic anhydride.

The materials produced exhibit an intriguing increase in T_g following reaction with succinic anhydride. This rise in T_g is believed to stem from additional intermolecular hydrogen bonding taking place, enhancing the stability of the glassy phase. Moreover, the increased molar mass resulting from functionalisation may also contribute to the elevated T_g. The absence of melting or crystallisation transitions in the DSC traces indicates that the amorphous nature of the materials is sustained following post-polymerisation functionalisation.

Equiv. SA	T_g (°C)	η (kPa·s)
0	-2.0	7.3
1	8.5	17.5
2	8.9	79.4
3	13.4	132.6

Table 16 Thermal and rheological analysis of PG4-DMS after addition of SA. Viscosity measurements performed at 40 °C and shear rate of 2 s^{-1}.

Rheologically, a marked increase in viscosity is observed upon functionalisation of the backbone with succinate groups (Table 16). PG4-DMS without pendant succinate groups gave a viscosity of 7.3 kPa·s, compared to 132.6 kPa·s for PG4-DMS-3SA. Viscosities of this order of magnitude are very problematic from a synthetic perspective. This increased resistance to flow could be a result of increased hydrogen bonding between the polymer chains within the sample, and possibly some cross-linking taking place. Greater intermolecular attraction also increases the force required to cause the material to flow. Similarly, T_g also increased as more equivalents of succinic anhydride were added.

To gain deeper analytical insight into the products synthesised titrimetric methods were employed. Acid value (AV), hydroxyl value (OHV), and saponification value (SAP) were all performed on the unfunctionalised and functionalised materials (Table 17). As PG4-DMS is functionalised with succinic anhydride, free hydroxyl groups are consumed to form ester bonds and pendant carboxylic acids are installed. These changes are expected to be reflected in the AV, OHV, and SAP values (Figure 76).

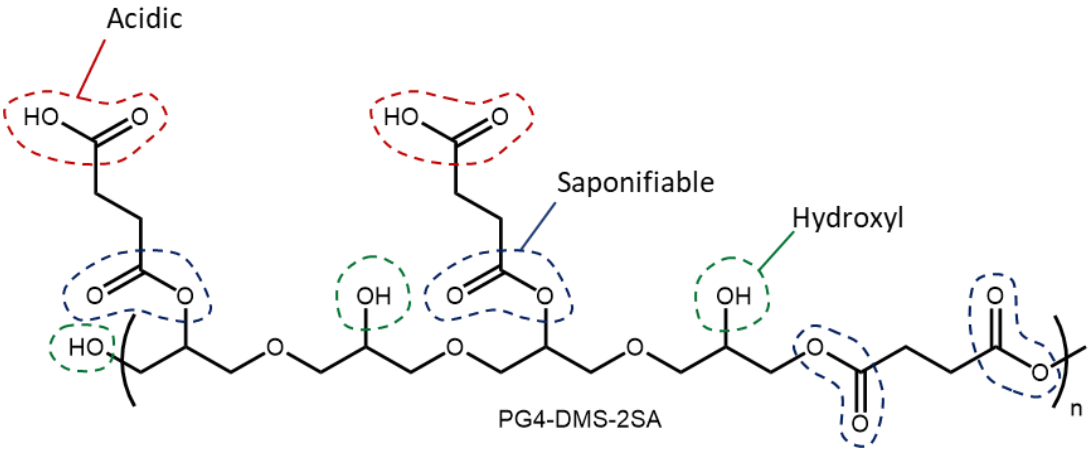

Figure 76 Structure of PG4-DMS-2SA, with functionality contributing to AV, SAP, and OHV highlighted in red, blue, and green, respectively.

Theoretical and measured values are in close agreement for the AVs. The largest deviation from the expected values is 5 mg KOH·g^{-1} sample, observed for PG4-DMS-3SA, which is very minimal. The AV measured for PG4-DMS without any pendant succinate groups is very low, and the solution reached its endpoint instantaneously indicating that hydrolysis of the dimethyl ester is limited during the polymerisation.

Equiv. SA	AV Expected	AV Measured	OHV Expected	OHV Measured	SAP Expected	SAP Measured
0	0	1.2*	566	599	279	222
1	113	105	339	365	335	287
2	179	176	188	251	372	369
3	241	236	81	**	399	449

*Table 17 Volumetric analysis of PG4-DMS functionalised with various succinic anhydride loadings. All values are quoted in mg KOH·g^{-1} sample. *Reached endpoint instantaneously. ** Limited solubility in the acylation reaction mixture.*

Large deviations from expected values were observed in the OHVs. OHV determination of PG4-DMS-3SA was made impossible by the very limited solubility of this sample in the acylation mixture of pyridine and acetic anhydride. Nevertheless, the overall trend of decreasing OHV with increased succinic anhydride functionalisation is still as anticipated for the other samples. This trend shows that hydroxyl groups present on the PG4-DMS are being consumed to attach succinic anhydride. It can be noted that there is some deviation from the expected OHV value in these materials. This could be due to partial hydrolysis of the ester bonds taking place during acylation, which would lead to an overshoot in OHV as is detected here. It should also be noted that the PG4 employed is a mixture, which incorporates another source of deviation from the value calculated assuming only linear PG4 is present. Regardless, OHV values measured are still in good agreement with the theoretical values. The trend of decreasing OHV values supports the occurrence of succinic anhydride attaching to the backbone hydroxyl groups.

The SAP values measured mirror the expected trend. As more equivalents of succinate are attached to the polymer new saponifiable ester bonds are formed. This is clearly shown in the results obtained, where SAP values increase with a greater degree of functionalisation. Some deviations are observed from the expected values due to the uncontrolled nature of the polycondensation and the mixture of polyglycerol species present in the PG4 monomer. Accordingly, a deviation from the theoretical value is expected, and the measured values are still in good agreement. As with the OHV values, the trend of these values supports the hypothesised reaction pathway. The trend demonstrates a significant increase of SAP value, in agreement with the formation of new ester bonds. The experimental SAP for PG4-DMS-3SA is greater than expected, possibly indicating additional esterification has taken place.

During the titrimetric experiments, it was observed that the solubility profile of PG4-DMS polyesters was drastically altered by the addition of pendant carboxylic acids. Attaching pendant succinate groups lowers the aqueous solubility of the PG4-DMS, forming opaque suspensions in aqueous media (Figure 77). This is a result of consuming hydrophilic hydroxyl groups in favour of more hydrophobic succinate groups. Upon deprotonation of the carboxylic acid, an increase in aqueous solubility is observed and the cloudy solution is rapidly clarified as carboxylate salts are formed. Rapid dissolution is promising behaviour, as it is expected that once these materials are cross-linked the electrostatic repulsions between carboxylates will lead to rheological modification of the solution.

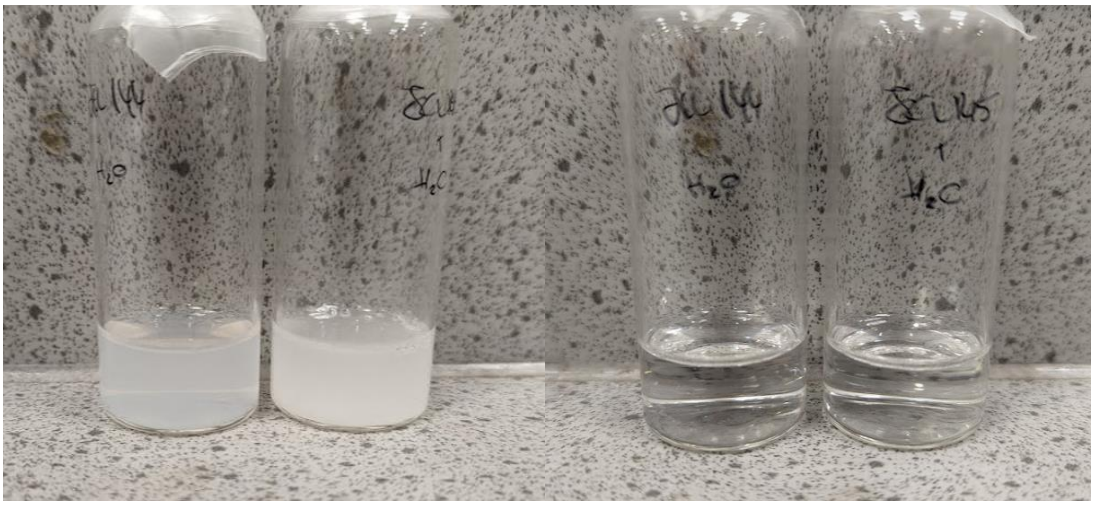

Figure 77 PG4-DMS-2SA (left) and PG4-DMS-3SA (right) undergo rapid dissolution into water as pH is raised.

To summarise, succinic anhydride can be attached to linear PG4-DMS in a straightforward manner. A one-pot synthetic methodology was found to be the simplest approach, minimising mass loss during transfers and time taken to cool and re-heat the reaction. Using a variety of analytical techniques, the successful functionalisation of the polymer backbone has been demonstrated. Disappearance of the signal corresponding to succinic anhydride in the ^{1}H-NMR spectra shows quantitative conversion. Volumetric methods further provide evidence that the succinic anhydride is attached through the pendant hydroxyl groups of PG4-DMS. In terms of material properties, the viscosity increases remarkably after functionalisation, presumed to be a result of additional hydrogen bonding between polymer chains. For the same reason, T_g is also raised with increasing succinate attachment. As a result, handling these polymers in the bulk state is challenging and processing difficulties will hamper large-scale development. The solubility profile of PG4-DMS is significantly altered by the addition of pendant succinate groups. Aqueous solubility is decreased, although upon deprotonation of the carboxylic acids the polymer rapidly dissolves.

No rheological modification was observed at this stage. To achieve aqueous rheological modification, it was attempted to introduce cross-linking of these materials after functionalisation using succinic anhydride. Thermal cross-linking of PG4-DMS-2SA was attempted and found to produce an insoluble resin that did not act as a rheology modifier (See Appendix for Chapter 3).

Addition to Cross-Linked Poly(polyglycerol succinates)

Cross-linked PG polyesters exhibit desirable swelling and rheological modifying behaviour in aqueous solution. Addition of pendant acid functionality was targeted to introduce electrostatic repulsion within and between polymer chains upon deprotonation. In contrast to aqueous soluble PG polyesters, cross-linked PG polyesters cannot be easily stirred using a commonplace overhead stirrer. To overcome the limited ability to agitate these materials alternative methods of finely dispersing succinic anhydride into the polymer matrix were investigated. It was considered critical to achieve a good level of mixing prior to heating to achieve an even distribution of pendant succinate groups throughout the sample.

To achieve close integration of the succinic anhydride and the cross-linked polymer matrix two approaches were tested. The first approach employed cryogenically grinding together PG4-1.5DMS and succinic anhydride. The second approach utilised supercritical CO_2 ($scCO_2$) to plasticise PG4-1.5DMS to enable succinic anhydride to diffuse into the polymer matrix.

Cryo-Grinding

To facilitate grinding, the PG4-1.5DMS was frozen using liquid nitrogen. At room temperature, PG4-1.5DMS is a tough rubber-like material that will not disintegrate when ground – preferring to spread rather than fragment. At cryogenic temperatures however, the rubbery material becomes brittle and grindable. Once the PG4-1.5DMS and succinic anhydride were cooled, they were ground together to form a fine powder before heating in an oven (Figure 78).

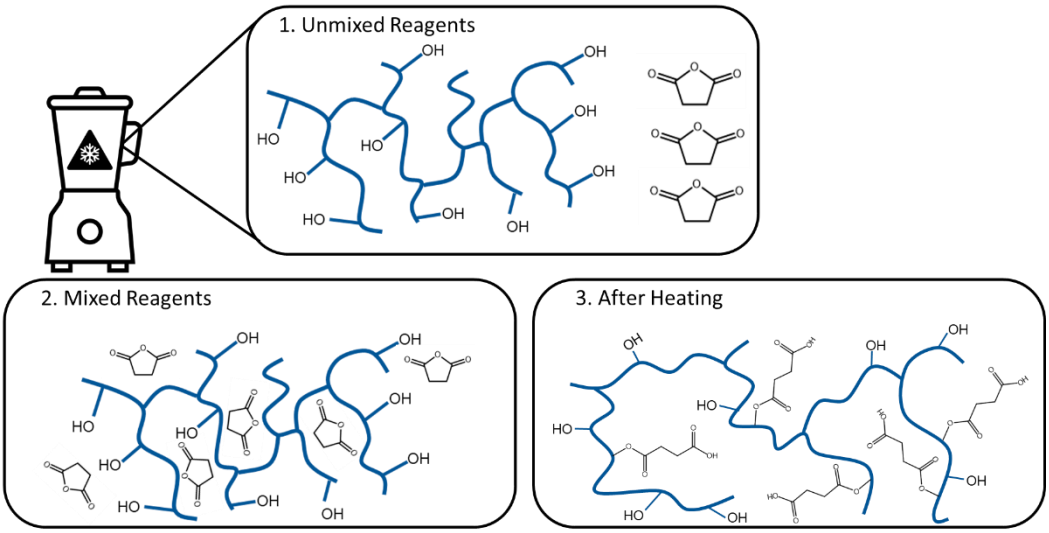

Figure 78 Schematic for functionalisation of cross-linked PG4DMS with succinic anhydride using a cryo-grinding approach. Top: PG4-1.5DMS and succinic anhydride are combined at cold temperatures. Bottom left: after cryo-grinding these reagents are intimately mixed. Bottom right: following heating the polymer matrix is decorated with succinate groups.

Following the reaction procedure, aqueous solutions were prepared for rheological analysis to screen the efficacy of the procedure (Figure 79). Owing to the presence of carboxylic groups it was expected that pH would influence the rheology of the samples, and as such the viscosity at various pHs was measured. It was observed that overall, the viscosity of the functionalised samples was lower than that of an unfunctionalized sample. In addition, viscosity dropped with increasing pH from around pH 5.

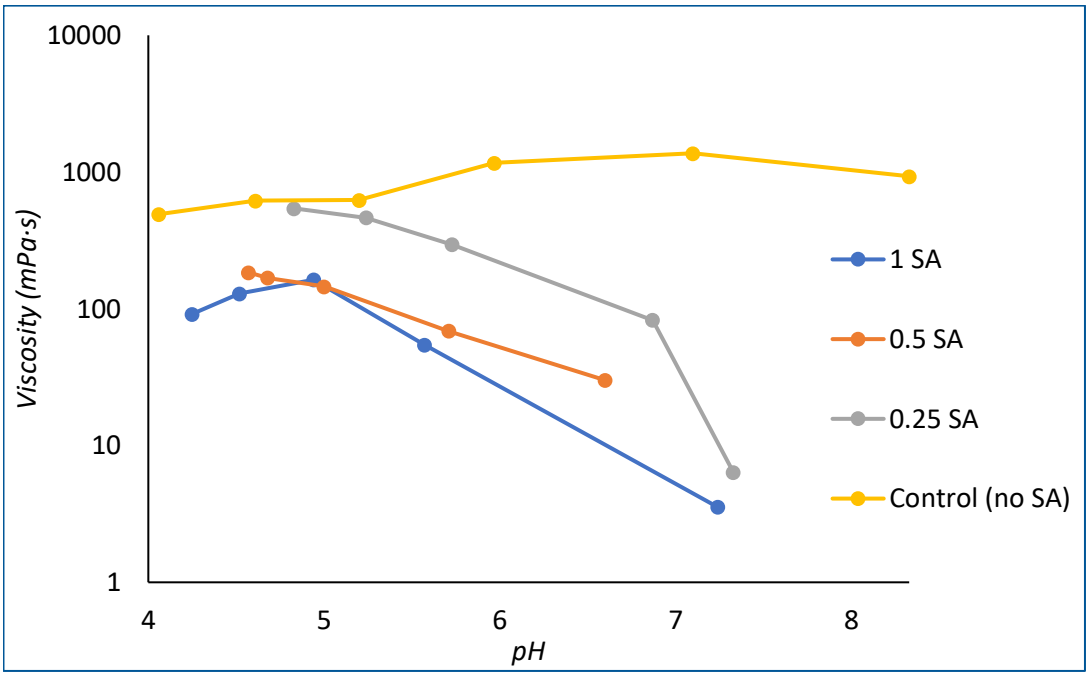

Figure 79 Viscosity at different pH for cross-linked PG4-DMS functionalised with various equivalents of succinic anhydride using the cryo-grinding methodology. 20 wt.% aqueous solution. Viscosity at shear rate 100 s^{-1}, and 25 °C.

As a result of this decreased performance this approach was not further investigated. It is believed that during the cryo-grinding process, condensation accumulated in the sample leading to hydrolysis upon heating and subsequent decrease in performance. Further investigation would require more careful exclusion of atmospheric moisture.

Supercritical CO_2

The use of $scCO_2$ as a reaction medium was explored for the functionalisation of PG4-1.5DMS. It is well established that $scCO_2$ is capable of plasticising polymeric materials.[220] The ability for $scCO_2$ to penetrate polymeric matrices leads to reduced viscosities and softening.[231] These properties make $scCO_2$ a promising candidate to facilitate mixing of succinic anhydride and PG4-1.5DMS. Succinic anhydride was found to be soluble in $scCO_2$ above 13.8 mPa at 60 °C, and from the foaming observed upon depressurisation $scCO_2$ can enter the PG4-1.5DMS matrix. It was hypothesised that the polymer would be impregnated with soluble succinic anhydride carried along with the $scCO_2$ before heating to facilitate reaction between the anhydride and polymer backbone (Figure 80). Through this route undesired hydrolysis, thought to hamper the cryo-grinding method, would also be limited as there is limited opportunity for moisture to accumulate in the $scCO_2$.

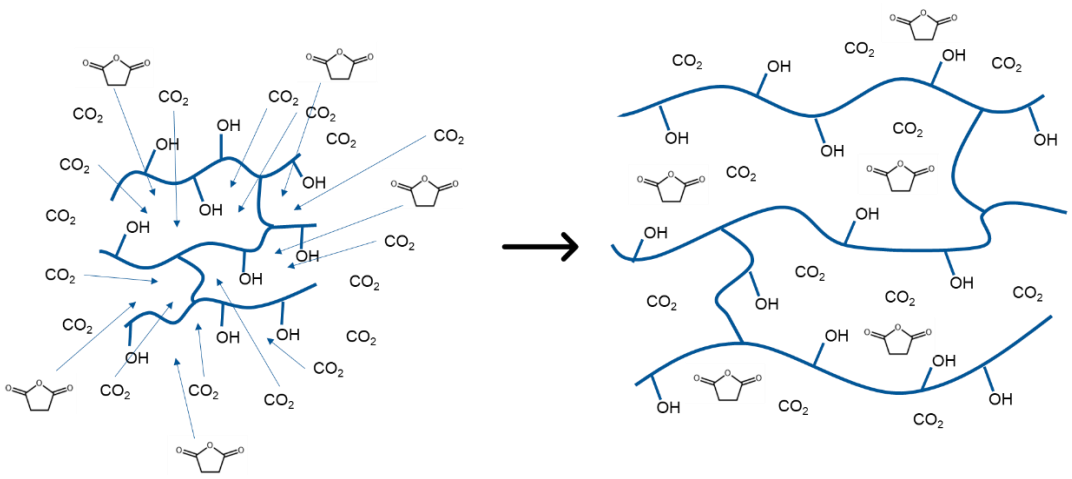

Figure 80 Schematic for the impregnation of cross-linked PG4DMS with succinic anhydride using $scCO_2$ as a processing aid.

Significant foaming was observed during depressurisation following heating to react the succinic anhydride with the polymer (Figure 81). The foaming demonstrates the effectiveness at which $scCO_2$ can penetrate polymeric materials. A benefit of using $scCO_2$ is the ease of solvent removal, as it simply diffuses out from the polymer sample at atmospheric pressure.

Figure 81 Crosslinked PG4DMS before (left), and after (right) functionalisation with succinic anhydride in $scCO_2$. Significant foaming was observed upn depressurisation of the reaction vessel.

Aqueous solutions of the PG4-DMS samples functionalised in $scCO_2$ were tested to assess their behaviour as rheology modifiers. (Figure 82). From these results the pH dependence becomes more pronounced, with PG4-1.5DMS-0.5SA and PG4-1.5DMS-1SA exhibiting their maximum viscosities around a pH of five. The pH dependence of rheological modification demonstrates that the electrostatic repulsion along the pendant groups can be a valuable tool to control rheological properties of formulations. Unfortunately, the attachment of succinic anhydride did result in an overall decrease in viscosity compared to unmodified PG4-1.5DMS. This effect could be an effect of changing the hydrophilic balance in combination with increased hydrogen bonding. The decreased rheological performance meant the route involving addition of succinic anhydride to PG4-1.5DMS was not explored further.

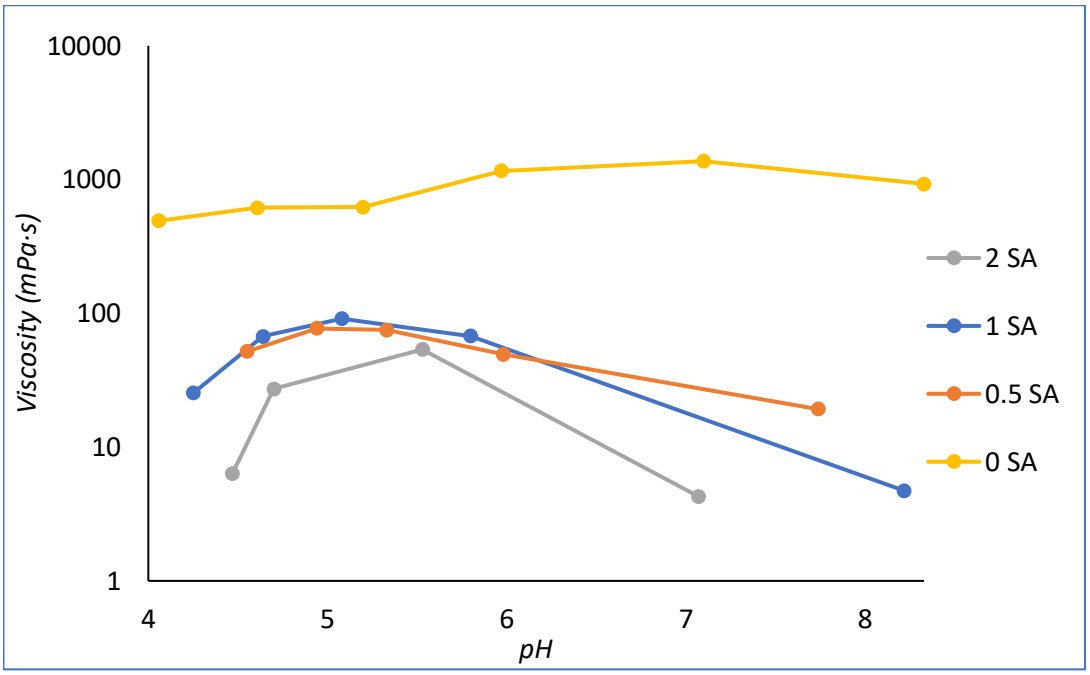

Figure 82 Viscosity at different pH for cross-linked PG4DMS (20 wt.% aqueous solution) functionalised with various equivalents of succinic anhydride. Viscosity measured at a shear rate 100 s^{-1}, and 25 °C.

Addition of Maleic Anhydride

To introduce a double bond to the PG polyesters for further functionalisation the possibility of using maleic instead of succinic anhydride was investigated (Figure 83). The pendant double bond could potentially be suitable for further reactions to introduce cross-linking to the materials.

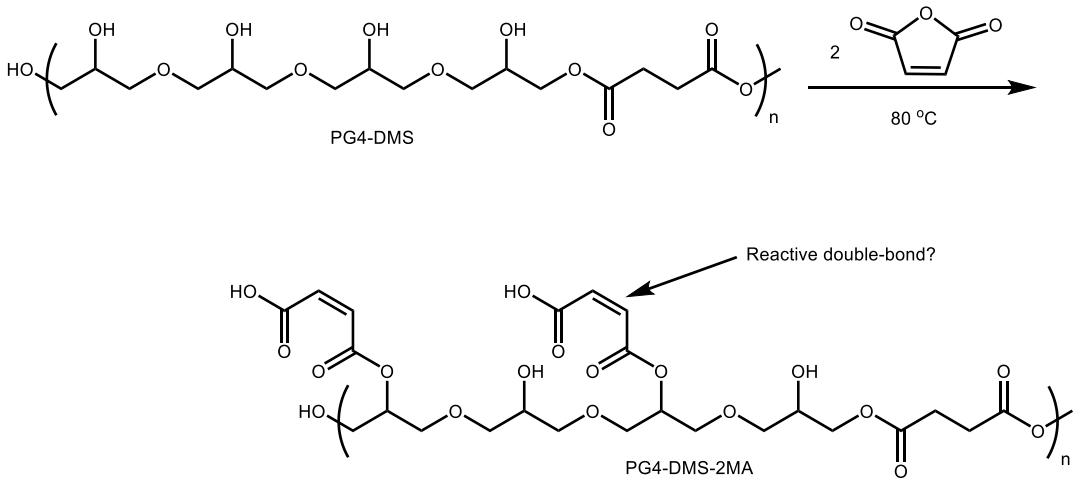

Figure 83 Reaction scheme for the addition of maleic anhydride to PG4-DMS.

Upon addition of maleic anhydride, the viscosity of the polymer melt decreased significantly as the maleic anhydride is liquid at reaction conditions. Following the initial viscosity reduction, the viscosity rapidly increased, until after 15 minutes the stirring had seized completely. The product obtained was a brittle monolith. From the ^{1}H-NMR incomplete consumption of maleic anhydride was observed, in combination with new signals appearing corresponding to pendant maleate groups (Appendix Figure 16).

To gain insight into the process, PG4 and maleic anhydride were combined under reaction conditions as a model. The model reaction was analysed by ^{1}H-NMR spectroscopy (Figure 84). It appeared that maleic anhydride can be attached under the reaction conditions employed, as demonstrated by the disappearance of the maleic anhydride signal, and growth of the signals assigned to pendant maleates. Some hydrolysis can also be detected, showcased by an increase in the signal corresponding to maleic acid (marked with an asterisk, Figure 84). An increase in signals between 4.0 and 4.4 ppm is also observed, corresponding to PG4 protons adjacent to the newly formed ester linkages. From the spectra collected it appears that nearly full maleic anhydride conversion is achieved after only 100 minutes. This rapid conversion is most likely a result of maleic anhydride being molten at reaction conditions, leading to more effective incorporation into the polymer melt relative to succinic anhydride. These ^{1}H-NMR spectra are promising and indicate that maleic anhydride can be a suitable reagent to introduce pendant functional groups.

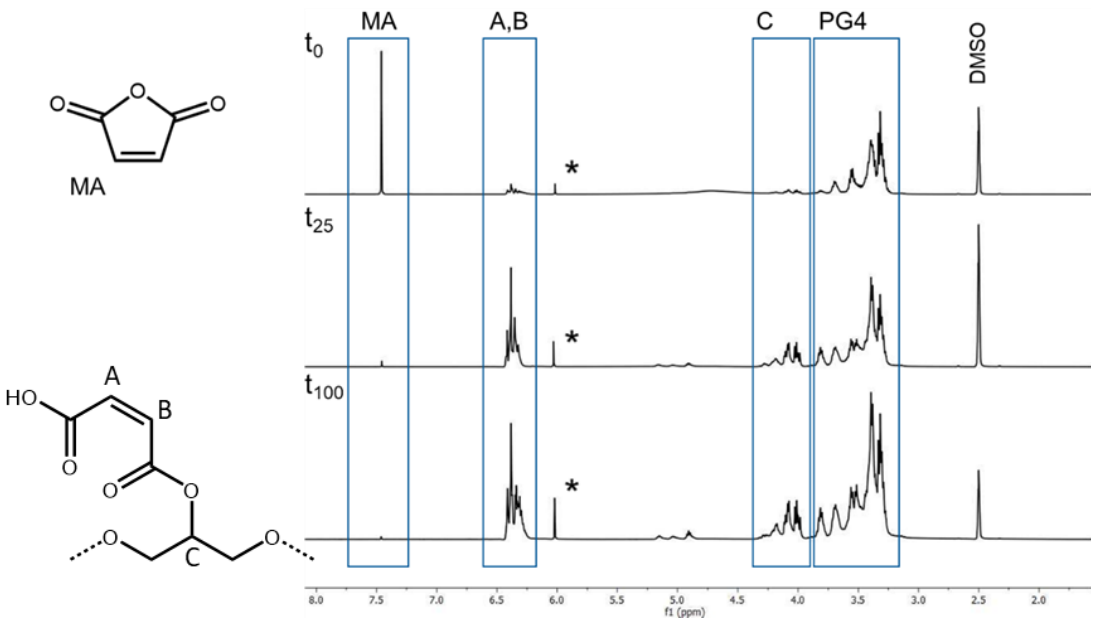

*Figure 84 ^{1}H-NMR spectroscopic analysis of the reaction between PG4 and maleic anhydride. Samples taken immediately following maleic anhydride addition (t_0, top), 25 minutes after addition (t_{25}, middle), and after 100 minutes (t_{100}, bottom). Signal denoted with * corresponds to maleic acid.*

Interestingly, after only 2 hours this reaction also yielded a brittle solid. The solid material was soluble, indicating that no uncontrolled cross-linking or reactivity across the double bond had occurred. In comparison with succinate pendant groups, maleate groups are less flexible due to limited rotational freedom of the double bond. The increased rigidity of these side chains could explain the brittle nature of the products collected.

From the analysis by ^{1}H-NMR spectroscopy, it can be concluded that maleic anhydride can be attached to PG4-DMS using analogous reaction methodology as for succinic anhydride discussed earlier. The prospect of pendant double bonds is intriguing as these could be used for cross-linking using for example thiol-ene click chemistry. Physically however, the maleic anhydride functionalised materials were nearly impossible to manipulate. Their very rigid and brittle nature meant it was challenging to stir and retrieve the product from the reactions. On an industrial scale these materials would be completely unsuitable because of these processing obstacles. It could be that lowering the loading of maleic anhydride would yield more manageable material whilst maintaining the desired functionality. Alternatively, addition of a mixture of maleic and succinic anhydride could be explored. Solvents could also be explored, although this poses additional issues relating to solvent removal and suitability.

3.5 Conclusions

This chapter has discussed the synthesis of renewable hydrophilic polyesters with a targeted end application as rheological modifiers. Polyglycerols were used as biobased, biodegradable building blocks to form these hydrophilic polymers through polytransesterification with DMS.

A variety of commercially available PGs were screened. From the criteria assessed, PG4 was found to be the most appropriate of the PGs. The lower viscosity relative to PG6 and PG10, means that processability and handling are more straightforward. The lack of colouration after being subjected to reaction conditions is another benefit. PG4-DMS was colourless, whereas the PG10 especially discoloured significantly at reaction conditions. It was hypothesised that PG4 would contain sufficient hydroxyl groups to maintain water solubility after polymerisation, as such the ease of use and lack of discolouration meant that PG4 was carried forward as the most viable PG building block for polyester synthesis.

Synthesis temperatures were varied from 60 to 180 °C to determine the which temperature would be most suitable. Upon exceeding 120 °C discolouration became noticeably more intense. Analyses performed on these materials indicated that temperatures exceeding 60 °C yielded polymeric materials with good conversion. This is due to the excess of hydroxyl groups, resulting in full conversion of the DMS during synthesis. In all GPC chromatograms unreacted PG4 was detected. It was found 80 °C was sufficient to drive the reaction to full DMS conversion whilst minimising energy intensity, and therefore further reactions were conducted at this temperature.

Various catalysts were screened to determine the effect on the appearance of the product and rate of reaction. It was determined that K_2CO_3 was the most suitable catalyst. No discolouration, in combination with high conversion made it an ideal catalyst for this reaction. The carbonate has the added benefits of being economical, available on large scale, as well as being non-hazardous. The alternative catalysts that were screened faced various issues relating to discolouration, poor conversions, toxicity, and limited solubility.

A brief kinetic study was conducted to gain further insight into the polymerisation reaction. ^{1}H-NMR spectroscopy and GPC were employed to study conversion and evolution of molar mass during polymerisation. DSC and rheology were used to study thermal and physical characteristics of the materials synthesised. T_g was found to gradually increase over the course of reaction, owing to the greater intermolecular attractions between polymer chains as molar mass increases. The viscosities of the polymers were found to increase drastically

especially between 5 and 24 hours, from 36.2 to 137 Pa·s. This significant increase correlates with the marked jump in molar mass of the polymer between these timepoints, enhancing molecular entanglements and bolstering viscosity.

Post-polymerisation functionalisation of both linear and cross-linked PG4-DMS was performed using succinic anhydride. Functionalisation of PG4-DMS was performed in one pot, simply adding the anhydride to the reaction mixture following polycondensation. Full anhydride conversion was obtained after allowing the reaction to proceed overnight. In the case of cross-linked PG4-1.5DMS, a one pot procedure is not feasible. Cryogenic grinding and $scCO_2$ were explored as methodologies to finely incorporate the polymer and succinic anhydride. Utilising $scCO_2$ was the most promising out of these two approaches, as hydrolysis from atmospheric moisture condensing could be restricted. From rheological testing a pH dependence on rheological modification was observed, indicating that pendant carboxylate groups had been installed. The overall viscosity of the aqueous solution after attaching succinates was however found to decrease relative to unfunctionalized PG4-1.5DMS in both methodologies. The decrease in performance could be attributed to the decrease in hydrophilicity as hydroxyl groups are consumed to attach the succinate functionality. Maleic anhydride was also explored for the post-polymerisation functionalisation of PG4-DMS. It was found that PG4-DMS functionalised with maleic anhydride formed brittle solids, probably a result of the rigidity of the attached maleate moiety.

Altering reagent stoichiometry was found to be an effective method to produce cross-linked hydrophilic polyesters. Using 1.5 equivalents of DMS was found to be optimal in terms of initial swelling performance. Increasing the DMS loading further yielded materials too tightly cross-linked, becoming rigid and unable to effectively absorb water. Lowering the DMS loading yielded materials which did not swell to the same extent, possibly a result of a larger proportion of soluble materials that were insufficiently cross-linked. Initial visual observations showcase the impressive water absorbing capability of PG4-1.5DMS, and it was selected to be explored in greater detail for aqueous rheological modification. The following chapter deals with the application testing of this material.

3.6 Further Work

Alternative processing methods or reaction vessels could be promising for the synthesis of PG based polyesters. The bulk polycondensation of PG4 with DMS is manageable in standard laboratory glassware with an overhead stirrer, however as DMS equivalents are increased viscosity becomes an ever-greater hurdle. A system such as reactive extrusion could avoid mixing limitations encountered in bulk reactions. As the extruders could act to agitate the reaction mixture without seizing as an overhead stirrer does under these conditions. Furthermore, if the polymeric product could be extruded and cut into smaller fragments, material handling for the end consumer would be improved.

To avoid reaction mixtures seizing, addition of solvent can also be considered. Unfortunately, the range of solvents suitable for this reaction are limited. The solvent would have to be polar, aprotic, and of high boiling point to effectively solvate PG4. Examples of such solvents are dimethyl formamide, dimethoxyethane, and dimethyl sulfoxide, none of these are desirable for a variety of reasons – toxicity, and difficulty to remove being just two of them. For a solution polymerisation approach to be viable an alternative greener solvent would have to be found that would not impede the polycondensation.

Another possibility to improve the processability of this reaction would be to utilise a dispersed phase system. In the case of PG4-DMS synthesis, if the PG4 can be emulsified into a hydrophobic solvent using a suitable emulsifier this would be a promising start. Following emulsification of the monomers the reaction could take place in the monomer containing dispersed phase to form cross-linked polymer particles. An emulsion of cross-linked polymer particles would be significantly easier to handle on a large scale in comparison to a cross-linked polymer monolith. Suitable solvent, and emulsifier would have to be determined. PG-fatty acid alcohols are produced commercially as emulsifiers, so these could be a suitable starting point. Alternatively, PEG-based emulsifiers could also be screened.

Introducing a small fraction of a hydrophobic group, such as a fatty acid, or fatty acid methyl ester, into the reaction mixture could allow for associative thickener resembling structures to be formed. Incorporating and aspect of associative thickening could improve the performance of the thickener especially in micellar solutions, providing the opportunity to form micellar networks.

To boost the swelling performance of the PG4-1.5DMS, ionic side groups are an interesting avenue for exploration. In principle, pendant ionically charged groups in proximity will repel each other leading to enhanced water-uptake and rheological modification. The succinate

groups explored in this chapter provide experimental support for this hypothesis, although alternative ionic groups could be explored to improve the performance of the material.

A limitation with the polycondensation methodology employed is the lack of control over final molar mass and high dispersities obtained. A potential method to overcome these issues is to use an alternative polymerisation technique to produce PG. One such technique offering low dispersities and access to greater molar masses is anionic polymerisation. Glycidol, once protected, can be polymerised anionically to form linear PG. This has been explored in Chapter 5.

3.7 Materials and Methods

PG4, PG6, and PG10 were kindly donated by Spiga Nord SpA, Italy. DMS, succinic anhydride, maleic anhydride, glycerol, diglycerol, K_2CO_3, DBU, $Sc(OTf)_3$, glycerol diglycidyl ether, DMSO-d_6, citric acid monohydrate, and PEG diglycidyl ether (average M_n=500 g·mol^{-1}) were purchased from Sigma Aldrich. NaOH was purchased from Fisher Scientific UK. Water was deionised in-house before use. All chemicals were used as received unless otherwise specified.

3.7.1 Instrumentation

Nuclear Magnetic Resonance Spectroscopy (NMR)

Polymer formation and chemical structure assignment was determined using ^{1}H-NMR spectroscopy. Approximately 50 mg of sample was dissolved in 0.7 mL DMSO-d_6 and analysed using a Bruker DPX 400 MHz spectrometer operating at 400 MHz (^{1}H) or 100 MHz (^{13}C), assigning chemical shifts in parts per million (ppm). Spectra were referenced to residual solvent. MestReNova 6.0.2 copyright 2009 (Mestrelab Research S. L.) was used for analysing the spectra.

Rheology

Rheological characterisation was performed using an Anton Paar MCR 102 rheometer. Experiments were performed using 25 mm parallel plate measuring geometry at 25 °C and a 1 mm measurement gap unless otherwise indicated.

Differential Scanning Calorimetry (DSC)

DSC was performed using a TA Instruments Q2000 calibrated using indium and sapphire standards. Samples were analysed in aluminium Tzero pans at a heating rate of 10 °C min^{-1}. TA Instruments Universal Analysis 2000 was used to analyse collected data.

pH Measurements

A Mettler Toledo LE438 sensor connected to a Mettler Toledo FiveEasy FE20 pH meter, calibrated using pH 4 and 7 buffer solutions (VWR Chemicals) was used to measure pH.

Aqueous GPC

Aqueous GPC was performed on an Agilent 1200 system fitted with an dRI detector, two Agilent PL aquagel-OH column and one aquagel guard column eluted with 0.1 M $NaNO_3$ eluent. Molar mass (M_n) and dispersity were calculated according to narrow PEG standards (1 500 kg·mol^{-1} – 105 g·mol^{-1}) using Agilent EasyVial calibrants fitted with a cubic function to

correlate retention time and molar mass. Polymer samples were made by dissolving 3 $mg \cdot mL^{-1}$ pure polymer in 0.1 M $NaNO_3$. 50 µL samples were injected and eluted at 1 $mL \cdot min^{-1}$ for 30 min.

3.7.2 Synthetic Procedures

Poly(polyglycerol succinate) Synthesis General Procedure

Polyglycerol, dimethyl ester, and catalyst were combined. The reaction mixture was heated and mechanically stirred (24 h, 150 RPM) under argon flow. Subsequently the polymeric product was collected in quantitative yield. For kinetics experiments, an aliquot (1 mL) was removed from the reaction mixture at predetermined timepoints for analysis.

Polyglycerol Length Screening

Polyglycerol (10.0 g, see Table 18 for molar quantities), DMS (1 mol equiv. w.r.t. PG), and K_2CO_3 (5 wt.% w.r.t. total monomer mass) were combined in a 50 mL round bottomed flask. The reaction vessel was submerged in an oil bath (120 °C) and mechanically stirred (24 h, 150 RPM) under argon flow. Subsequently the polymeric product was collected in quantitative yield.

Polyglycerol species	Quantity (mmol)
PG4	31.8
PG6	21.6
PG10	13.4

Table 18 Molar quantities of PG used during PG length screening.

Temperature Screening

PG4 (10.0 g, 31.8 mmol), DMS (4.65g, 31.8 mmol), and K_2CO_3 (0.73 g, 5.3 mmol, 5 wt.%) were combined in a 50 mL round bottomed flask. The mixture was submerged in an oil bath (80-140 °C) or an aluminium heating block (160 and 180 °C) and mechanically stirred (24 h, 150 RPM) under argon flow. Subsequently the polymeric product was collected in quantitative yield.

Catalyst Screening

PG4 (10g, 31.8 mmol), DMS (4.65g, 31.8 mmol), and catalyst (Table 19) were combined in a 50 mL round bottomed flask. The reaction vessel was submerged in an oil bath (80 °C) and mechanically stirred (24 h, 150 RPM) under argon flow. Subsequently the polymeric product was collected in quantitative yield.

Catalyst	Mass (g)	Mol (mmol)	Wt.%	Mol.%
K_2CO_3	0.73	5.3	5.0	8.3
NaOH	0.73	18.3	5.0	29
$Sc(OTf)_3$	0.31	0.6	2.1	0.94
DBU	0.49	3.2	3.3	5.0

Table 19 Catalyst loadings for the catalyst screening performed.

Altering Reagent Stoichiometry

PG4 (10.0 g, 31.8 mmol), DMS (1-3 mol equiv., 4.65-13.95 g), and K_2CO_3 (5 wt.% w.r.t. total monomer mass) were combined in a 50 mL round bottomed flask. The reaction vessel was submerged in an oil bath (80 °C) and mechanically stirred (24 h, 150 RPM) under argon flow. Stirring seized overnight. Subsequently the polymeric product was collected in quantitative yield.

Acid Anhydride Addition Post-Polymerisation (Linear PG4-DMS)

PG4 (10.0 g, 31.8 mmol), DMS (4.65 g, 31.8 mmol), and K_2CO_3 (0.73 g, 5.3 mmol, 5 wt.%) were combined in a 50 mL round bottomed flask. The reaction vessel was submerged in an oil bath (80 °C) and mechanically stirred (24 h, 150 RPM) under argon flow. To the heated and stirred reaction vessel, acid anhydride (succinic or maleic, 31.8-95.4 mmol, 1-3 equiv. w.r.t. PG4) was added slowly to maintain stirring. The reaction was allowed to proceed until completion before collecting the polymeric product in quantitative yield. Maleic anhydride caused the reaction mixture to harden, seizing stirring.

Acid Anhydride Addition Post-Polymerisation (Cross-Linked PG4-DMS)

Cryo-Grinding

PG4-1.5DMS (2.00 g) and succinic anhydride (0.15 g, 0.30 g, or 0.60 g) were placed in a mortar and submerged in liquid nitrogen. Once boiling had subsided, the solids were ground together manually using a pestle before being placed in an oven (80 °C, 3 h). Following the initial heating, the materials were collected and re-cooled and re-ground using the same method as above, before being placed in an oven (80 °C, 3 h). Following the second heating the materials were collected.

Supercritical CO_2

Finely divided PG4-1.5DMS (2.00 g) and succinic anhydride (0.30 g, 0.60 g, or 1.20 g) were placed in a 60 ml autoclave and the autoclave was sealed. The reactor was flushed with CO_2 (50 psi, 15 min) before pressurising (800 psi, stirring 300 RPM overhead). Subsequently the

reactor was heated to reaction temperature (80 °C) and additional CO_2 was added to reach reaction pressure (4000 psi). These conditions were maintained (18 h), before the reactor was allowed to cool and slowly vented to atmospheric pressure and product collected in quantitative yield.

Acid Value (AV) Titration

Sample (1.5 g) was allowed to dissolve in MeOH (100 mL). Phenolphthalein (1 mL, 1 wt.% in MeOH) was added, and the solution was titrated under stirring using aqueous NaOH (0.1 mol dm^{-3}) until the solution underwent a colour change from colourless to faint pink. Acid value was calculated using the following equation:

$$\mathrm{AV\ (mg\ KOH \cdot g^{-1})} = \frac{\mathrm{T\ (mL)\ \times\ M\ (mol\ dm^{-3})\ \times\ 56.1}}{\mathrm{m\ (g)}}$$

Where T is volume of titre, M is the concentration of titrant used, 56.1 is the molar mass of KOH, and m is the mass of sample.

Saponification Value (SAP) Titration

Sample (Table 20) was added to aqueous KOH (25 mL, 0.5 mol·dm^{-3}) and heated under reflux (1 h) before being removed from the heat source. Phenolphthalein (1 mL, 1 wt.% in MeOH) was added to the hot solution, yielding a bright pink solution, and the solution was allowed to cool. The solution was titrated under stirring using aqueous HCl (0.5 mol dm^{-3}) until the solution underwent a colour change from bright pink to colourless. A blank (no sample) was also prepared and titrated in parallel following the same procedure. Saponification value was calculated using the following equation:

$$\mathrm{SAP\ (mg\ KOH \cdot g^{-1})} = \frac{\mathrm{(B-T)\ (mL)\ \times\ M\ (mol \cdot dm^{-3})\ \times\ 56.1}}{\mathrm{m\ (g)}} - AV\ \mathrm{(mg\ KOH \cdot g^{-1})}$$

Where B is the volume of the blank titre, T is volume of titre, M is the concentration of titrant used, 56.1 is the molar mass of KOH, and m is the mass of sample.

Sample	Mass Sample (g)
PG4-DMS	1.471
PG4-DMS-1SA	0.354
PG4-DMS-2SA	0.323
PG4-DMS-3SA	0.266

Table 20 Samples and masses used for determination of SAP values.

Hydroxyl Value (OHV) Titration

Finely divided sample (Table 21) was combined with acetic anhydride in pyridine (25% v/v) and gently heated at reflux (1 h), ensuring the mixture did not boil vigorously, a colour change to light brown was observed at this stage. The mixture was allowed to cool, and water (5 mL) was added before gently heating at reflux (10 min). The reaction was cooled to room temperature and ethanol (5 mL) was used to rinse residues in the condenser into the vessel. Phenolphthalein (1 mL, 1 wt.% in MeOH) was added, and the mixture was titrated (0.5 mol dm^{-3} aqueous NaOH) whilst stirring until a persistent light pink colour could be observed. A blank (no sample) was also prepared and titrated in parallel following the same procedure. Hydroxyl value was calculated using the following equation:

$$\mathrm{OHV\ (mg\ KOH \cdot g^{-1})} = \frac{\mathrm{(B-T)\ (mL)\ \times\ M\ (mol \cdot dm^{-3})\ \times\ 56.1}}{\mathrm{m\ (g)}} + AV\ \mathrm{(mg\ KOH \cdot g^{-1})}$$

Where B is the volume of the blank titre, T is volume of titre, M is the concentration of titrant used, 56.1 is the molar mass of KOH, and m is the mass of sample.

Sample	Mass Sample (g)
PG4-DMS	0.736
PG4-DMS-1SA	0.834
PG4-DMS-2SA	0.999

Table 21 Samples and masses used for determination of OHV values.

Chapter 4. Evaluation of Sustainable Aqueous Rheology Modifiers

4.1 Aims & Objectives

Synthetic rheology modifiers for aqueous media are used for a host of applications. Unfortunately, many synthetic products on the market today are petrochemically derived. Regulatory tightening and customer demand are driving research to find biobased and biodegradable alternatives for rheological modification.

This chapter explores the utilisation of the swellable polyglycerol-based polyesters synthesised in Chapter 3 as aqueous rheological modifiers, with a focus on rheological characterisation, water absorption, and degradation.

4.2 Abstract

Rheological characterisation of lightly cross-linked PG4 based polyesters in aqueous solution was performed. Increasing cross-link density decreased the efficacy of the rheological modification. It was found that PG4 polymerised with 1.25 equivalents of DMS yielded the best performing viscosity enhancer, although this material (PG4-1.25DMS) rapidly degraded in aqueous formulation. Further tests were performed on materials prepared by the polycondensation of PG4 with 1.5 equivalents of DMS (PG4-1.5DMS), which demonstrated good rheological modification at loadings above 10 wt.% and had a greater stability in aqueous formulation than PG4-1.25DMS. Formulations prepared using PG4-1.5DMS displayed excellent electrolyte tolerance, only displaying a slight decrease in performance upon addition of NaCl or $MgSO_4$, overcoming an issue typically associated with AST-type rheology modifiers. Formulations were tested at a range of pH values and found to maintain good thickening performance. Oscillatory rheology demonstrated that these formulations display viscoelastic behaviour, with excellent structural recovery following multiple cycles of high shear strain. Swellability in water was investigated, revealing that these materials are capable of absorbing nearly 20 times their own mass of water. Degradability tests revealed that in aqueous solution, hydrolysis takes place, leading to acidification of the solution and a decrease in overall viscosity.

To improve the performance of PG4-1.5DMS, swelling in excess water followed by freeze-drying was explored as a method to remove soluble content from the polymeric material. This procedure significantly increased the performance of the material, and viscosity

enhancements were observed at a loading as low as 2.5 wt.%. Viscoelastic behaviour was maintained, and excellent structural recovery following high shear strain was observed. In addition, swellability increased significantly and freeze dried materials were found capable of absorbing nearly 50 times their own mass of water.

4.3 Introduction

Polyol polyesters synthesised in Chapter 3, specifically PG4 polytransesterified with a slight excess of DMS, are characterized in the context of aqueous rheological modification and water-absorbing capabilities. The envisaged area of application for these materials is in personal care, providing rheological modification to products such as moisturisers, hydrating masks, and similar formulations.

Personal care products are widespread in society. According to Cosmetics Europe, 450 million Europeans use personal care products, such as shampoo, shaving cream, toothpaste, and make-up daily.[232] The large-scale manufacture of personal care products has a significant environmental impact.[232–234] Unsustainable sourcing of ingredients has caught the attention of ever increasingly ecologically conscious consumers, leading to industrial actors incorporating naturally sourced components into their formulations.[235–238] Introducing sustainably sourced components into their products lessens the environmental impact of the industry. Furthermore, increasing the sustainability of their products can also lead to a competitive edge, increased profit margins, and a more positively perceived brand image.[239–241] The PG based polyesters are very promising for personal care applications, as their biobased nature closely aligns with the current market climate.

To be suitable for personal care applications, a rheological modifier needs to fulfil some key parameters. Safety of the material is paramount, and products that cause irritation or display toxicity are unsuitable for application as personal care products.[242] Odours, colours, and other undesirable physical characteristics, such as excessive tackiness or stickiness need to be avoided.[124,243,244] Furthermore, the rheology modifier should provide the desired viscosity enhancement at loadings as low as possible. These criteria are established to formulate personal care products that are agreeable to the consumer. As discussed in Chapter 3, current synthetic aqueous rheology modifiers are not biodegradable or sourced from sustainable feedstocks. Degradability is essential to new personal care formulations. As these products are generally destined for disposal “down the drain”, recycling is highly impractical if not impossible.[245] It follows that it is important that these materials are instead degraded to prevent accumulation in the environment.[245–250]

To summarise, the widespread use of personal care products in society has led to significant environmental impacts, prompting the industry to incorporate sustainably sourced components into their formulations. Growing concern over the environmental persistence of personal care products has driven the development of biodegradable ingredients. Rheological properties play a crucial role in consumer satisfaction, and current synthetic aqueous rheology modifiers are neither sustainably sourced nor biodegradable. Development of degradable and biobased aqueous rheology modifiers is to needed address these issues.

4.4 Results and Discussion

4.4.1 Aqueous Rheological Modification

Prior to rheological characterisation, PG4 polyesters were formulated into aqueous media. The polymers were allowed to absorb a pre-determined quantity of water to form gelled materials, which were subsequently homogenised using a high-speed mixer to yield the tested aqueous solutions (Appendix Figure 18). This facile formulation approach does not require hot processing or pH adjustments allowing for straightforward implementation of the rheology modifier in industrial settings.

Optimising DMS Loading

It was expected that there should exist a maximum viscosity enhancement in relation to cross-linking density, as is the case for AST type systems.[92] Insufficient cross-linking density results in the formation of soluble polymeric materials, whereas excessive cross-linking yields highly insoluble material, neither of which are suitable for rheological modification. During polycondensation of PG4, hydroxyl groups are consumed to form ester bonds, lowering the hydrophilicity of the final material. A lightly cross-linked material is expected to be able to swell and absorb water, without complete dissolution taking place. It is this swelling and absorption that is hypothesised to generate rheological modification by trapping water molecules in the polymer framework and restricting the ability of the water molecules to flow freely.

A screening was performed to determine an optimal loading of DMS during polycondensation with PG4. Synthesised polymers were subsequently formulated at various loadings in water, and the viscosity against shear rate was measured. Flow curves of aqueous solutions of PG4 polyesters (20 wt.%) show the effect of DMS loading in relation to the final viscosity obtained (Figure 85). The formulation containing PG4-1.25DMS has the highest overall viscosity. This demonstrates that only a slight excess of DMS relative to PG4 is

required to achieve the desired rheological modification. It can be observed that increasing DMS loading beyond 1.25 equivalents decreases the viscosity of the aqueous formulation. The lowered viscosity is a result of limiting the freedom of movement with increasing cross-linking density, forming a polymer network that is too tightly held together to facilitate water absorption and rheological modification.

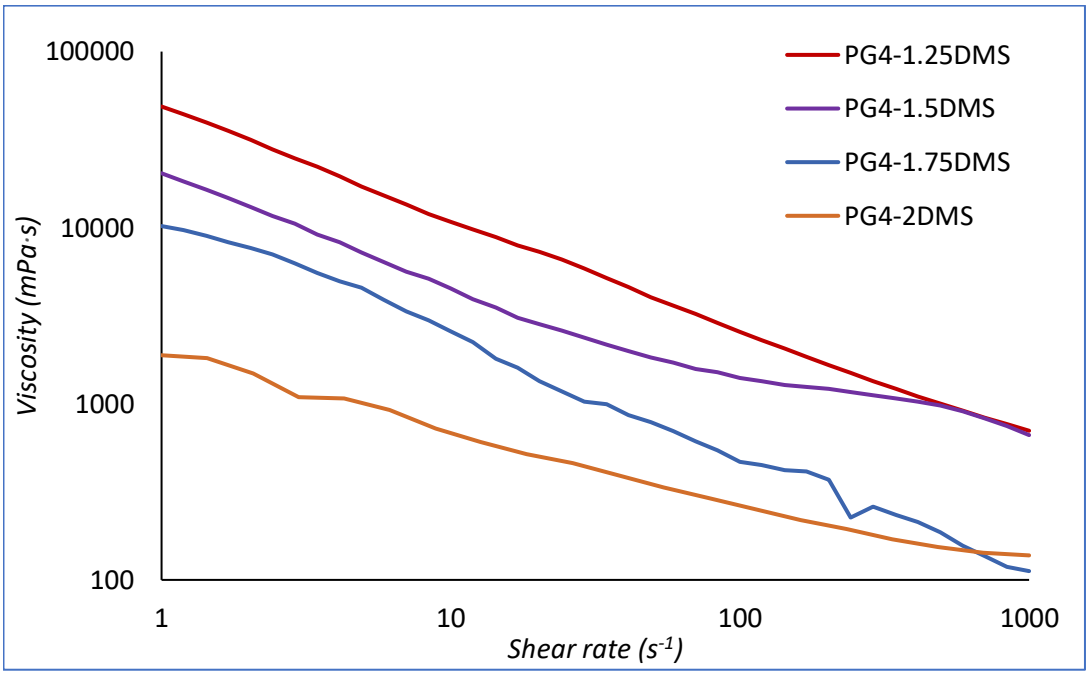

Figure 85 Viscosity over shear rate of PG4-DMS with varying loadings of DMS at 25 °C, 20 wt. % polymer loading in deionised water.

Interestingly, whereas PG4-1.25DMS was found to be the most effective viscosity modifier, it was also observed that rheological performance rapidly deteriorated. To compound the issue, attempts to re-synthesise PG4-1.25DMS proved unsuccessful, yielding only soluble material that did not increase the viscosity of aqueous media. It is hypothesised that PG4-1.25DMS is on a knife-edge between solubility and swellability, where minor experimental variations result in complete loss of performance. On the other hand, PG4-1.5DMS offers performance very close to that of PG4-1.25DMS. Synthesis of PG4-1.5DMS was found to be highly reproducible, yielding consistent performance between batches. As a result of these experimental observations, PG4-1.5DMS was determined to be the most promising material for aqueous rheological modification and was investigated further in greater detail.

The obtained viscosities of aqueous solutions of PG4-1.5DMS at various loadings were compared to those of commercial formulations (Figure 86). CH0107 and C2755a are formulations developed by Croda, marketed as Care & Hydrate and Skin Rejuvenation

creams respectively. CH0107 is an emulsion, stabilised using xanthan gum (0.5 wt.%). It can be noted that the rheological performance of CH0107 originates from the emulsified nature of the formulation, rather than from a rheological modifier. C2755a employs a PAA based AST (1.5 wt.%). It can be observed that loadings of PG4-1.5DMS below 10% in water do not yield adequate rheological modification. The lower shear rates of these loadings are excluded, as due to their low viscosities they are outside the operational window of the rheometer used. At loadings of 10 wt.% and higher, clear rheological modification can be seen. At 20 wt.% PG4-1.5DMS the viscosity profile is approximately a hybrid of CH0107 and C2755a. The close alignment of an aqueous solution of PG4-1.5DMS with a commercial formulation is highly promising and demonstrates that PG4-1.5DMS has strong potential to replicate the viscosity profile desired of personal care formulations.

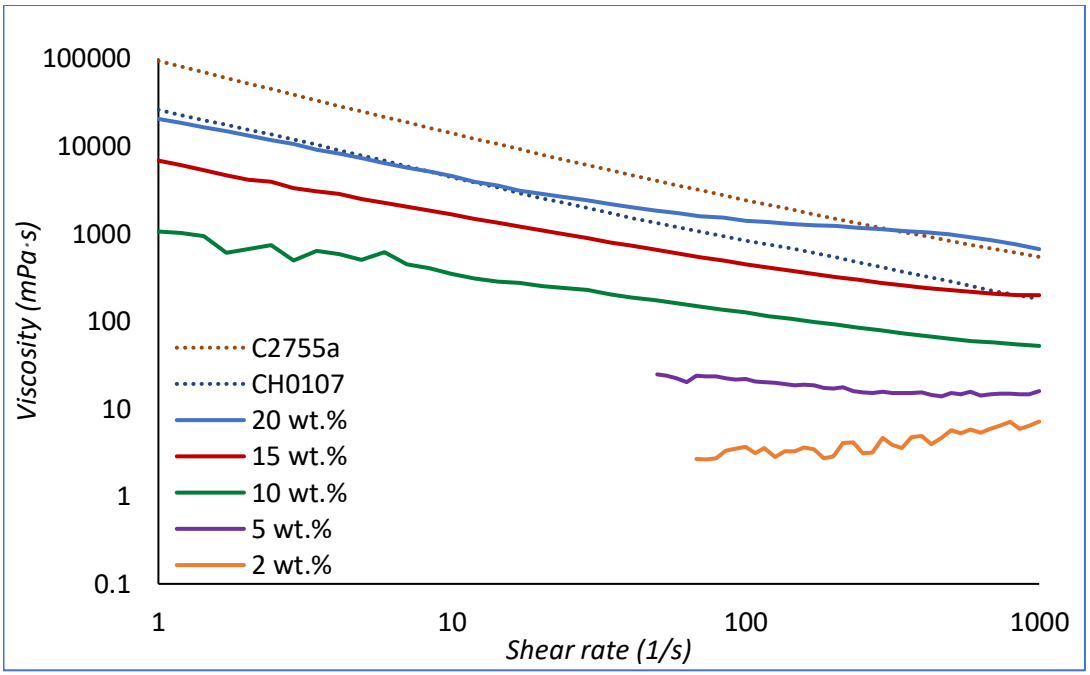

Figure 86 Viscosity over shear rate of PG4-1.5DMS at various loadings in water at 25 °C. CH0107 and C2755a are commercial personal care products.

Electrolyte Tolerance

Electrolytes and salts are commonly found in personal care formulations.[251,252] It is known that ASTs are highly sensitive to additional electrolytes, and addition of salt results in a collapse of the anionic framework critical to rheological modification performance.[253] To assess the electrolyte stability of PG4-1.5DMS, the viscosity profiles were measured at 20 wt.% loadings in two different aqueous solutions containing salts that can be found in personal care formulations (10 wt.% NaCl in water, and 5 wt.% $MgSO_4$ in water, Figure 87). The electrolyte loadings used are high to demonstrate the exceptional electrolyte tolerance of PG4-1.5DMS in aqueous formulation.

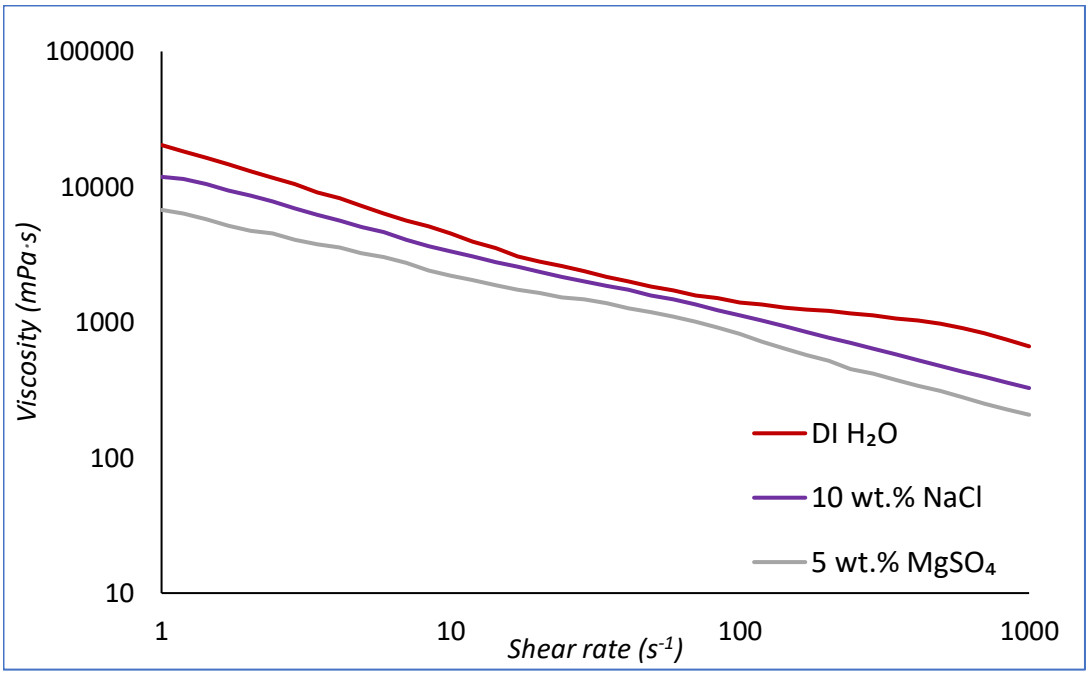

Figure 87 Viscosity over shear rate with changing electrolyte in solution. PG4-1.5DMS, 20 wt.% loading in water, NaCl, and, $MgSO_4$ solutions.

It can be observed that upon introduction of sodium and magnesium salts only a minor loss in viscosity is observed, and that the overall viscosity profile is maintained (Figure 87). It is a well-documented phenomenon that increasing the ionic strength of the medium critically impacts the behaviour of the hydrogel by means of a reduction in osmotic pressure and polymer/salt interactions.[254] Magnesium sulphate was found to be more detrimental to the rheological modification, probably due to greater coordination between pendant hydroxyl groups and the bivalent cation leading to a partial tightening of the polymer network.[254] This might result in a lessened ability to incorporate water molecules present in the system, lowering the overall viscosity (Figure 88).

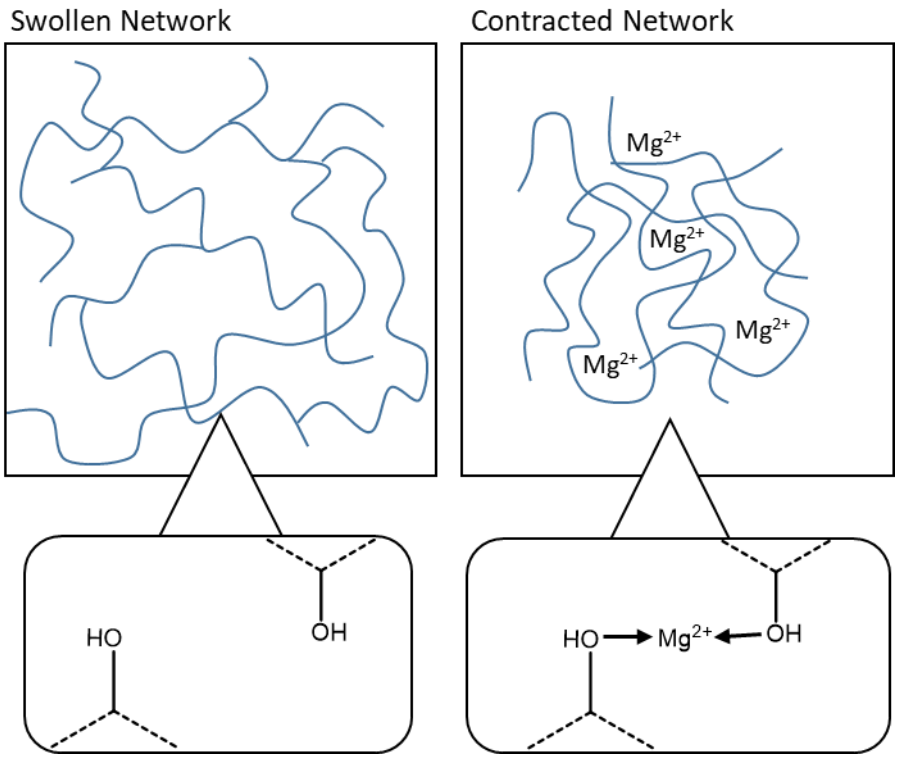

Figure 88 Coordination of pendant hydroxyl groups to Mg^{2+} ions could lead to the polymer network contracting.

The stability of PG4-1.5DMS to electrolytes, in comparison to ASTs, can be explained by the absence of an ionic framework in PG4-1.5DMS. In ASTs the inter- and intramolecular electrostatic repulsions are essential to rheological modification. In PG4-1.5DMS, the swelling is more likely to be caused by the migration of water into the hydrophilic polymer matrix, without electrostatic interactions necessarily required to facilitate water uptake. Overall, these experiments demonstrate the robustness of the thickening achieved in the presence of electrolytes commonly found in personal care formulations.

pH Tolerance

Personal care formulations regularly include pH adjusting components. As skin is generally slightly acidic with a pH around 5, personal care products are often of a similar pH range to prevent irritation.[255] It is therefore important that the rheological modifier is capable of functioning in this pH range.

Aqueous solutions of 20 wt.% PG4-1.5DMS were prepared, and their pH was adjusted to gain insight into the behaviour of the thickener in media of varying acidity. A control measurement was performed using only PG4-1.5DMS in water, which was found to have a pH of 7.10. Both acidification and basification of the solution was found to decrease the viscosity of the formulation, although the overall viscosity profile was generally maintained (Figure 89).

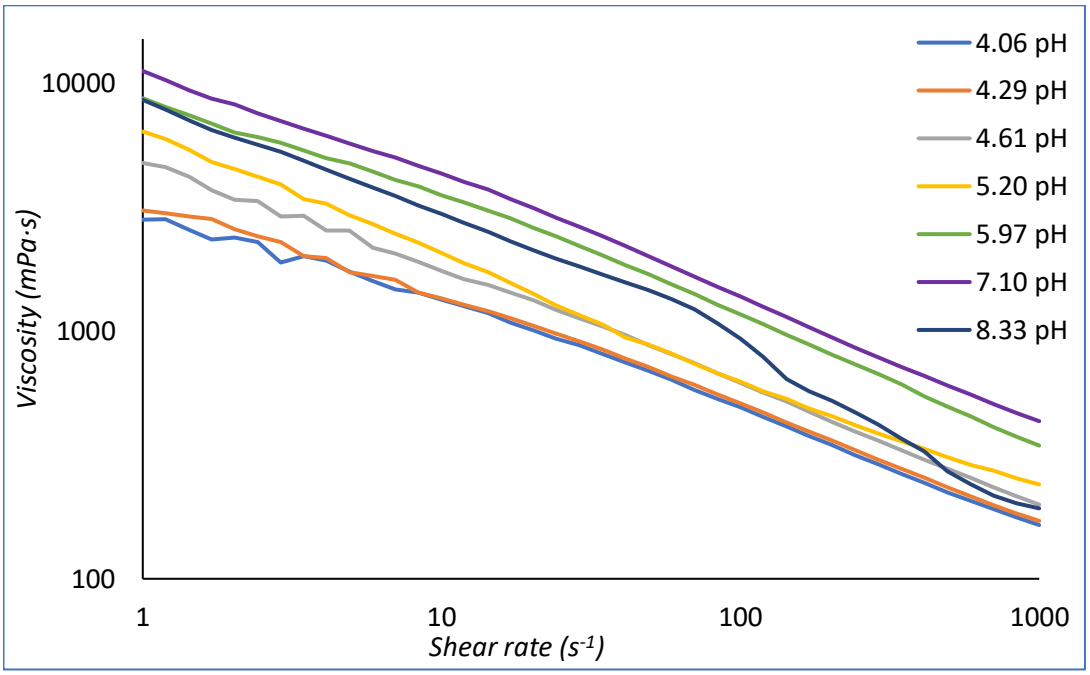

Figure 89 Viscosity over shear rate for a 20 wt.% aqueous solution of PG4-1.5DMS at various pH. The solution was acidified using citric acid and basified using NaOH, pH without adjustment is 7.10.

The adverse effects of altering the pH of the solution can be clearly observed when plotting average viscosity against pH (Figure 90). Average viscosity is the greatest without pH being adjusted. It should also be noted that altering the pH of the formulation can lead to accelerated degradation of the polyester backbone of PG4-1.5DMS through hydrolysis. Further application testing is required to determine the effect on formulation pH and stability.

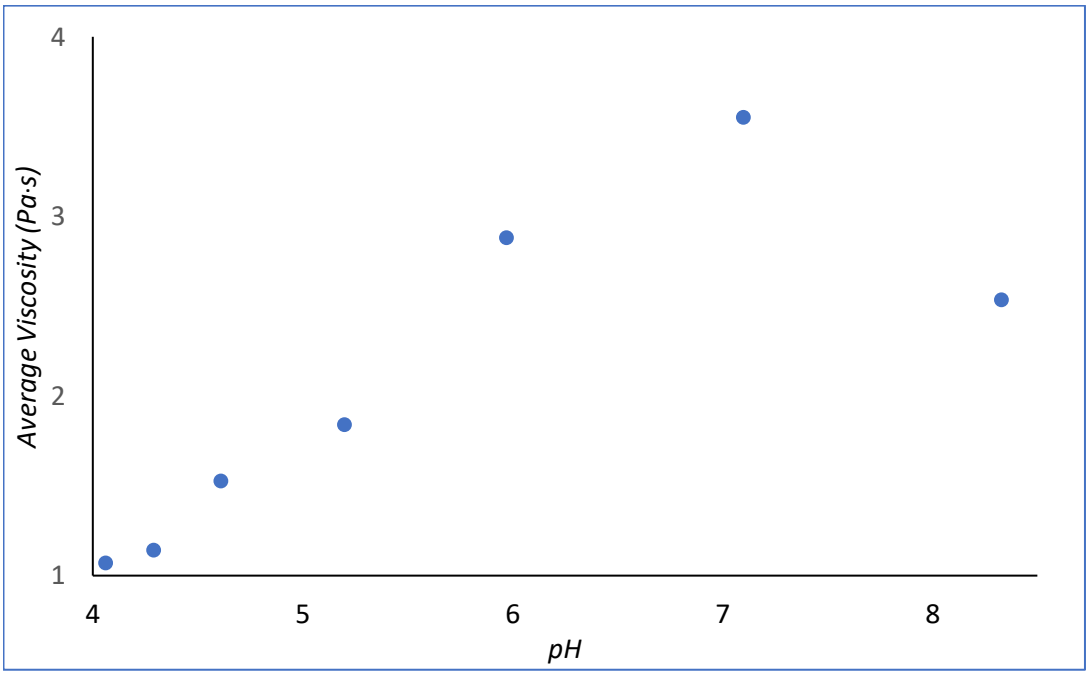

Figure 90 Average viscosity against pH for 20 wt.% aqueous solution of PG4-1.5DMS. The solution was acidified using citric acid and basified using NaOH, pH without adjustment is 7.10.

In summary, adjustment of the pH lowers the viscosity obtained. Around pH 5, a good viscosity was still observed indicating that these rheological modifiers would be suitable for use in skin-care formulations. It should be noted that decreasing pH can lead to an accelerated degradation of the ester bond, lowering the shelf-life of the formulation.

Oscillatory Rheology

Using oscillatory rheology, it is possible to obtain further characterisation of the thickened aqueous media. An amplitude sweep can be used to assess the linear viscoelastic region (LVE) of a material, as well as the flow point (Figure 91).[256] These properties are useful parameters to quantify the physical properties of viscoelastic materials, as they provide insight into the stiffness and the amount of force required to spread the material. In personal care formulations, these properties directly influence the texture and feel of the product.[78] These properties also influence the most suitable method for product delivery, as the rheological requirements for a sprayable product are different than those for a formulation intended to be rubbed into the skin manually.

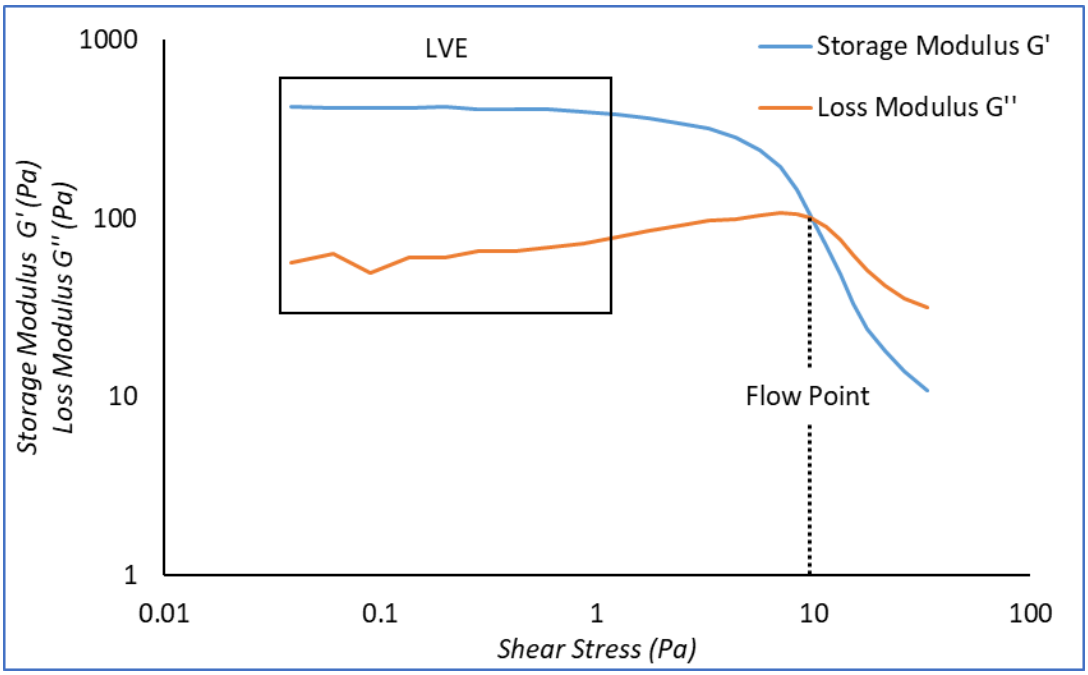

Figure 91 Amplitude sweep of PG4-1.5DMS (20 wt.% aqueous solution). Flow point (τ_f=9.8 Pa) indicated by the dashed line. Linear viscoelastic region indicated by solid outline.

From the oscillatory rheological experiments, the flow points and LVEs of a variety of samples were determined (Table 22). It can be observed that the PG4-1.5DMS samples generally had lower flow points and upper LVE limits compared to the commercial formulations tested. The storage modulus of the materials within the LVE matches with the physical appearance of the formulations, where CH0107 and C2755a are noticeably stiffer creams in comparison to the PG4-1.5DMS thickened solutions. The full oscillatory amplitude sweeps can be found in the Appendix.

Material	G' in LVE (Pa)	LVE Limit (Pa)	Flow point (Pa)
PG4-1.5DMS 20 wt.% H_2O	415	1.2	9.8
PG4-1.5DMS 20 wt.% Aq. NaCl	244	0.9	5.9
CH0107	1095	5.1	29.7
C2755a	1267	37.6	124.3

Table 22 Amplitude sweep data of various formulations.

The viscosity modified solutions exhibit a flow point due to their physical structures. At low shear, the polymeric rheology modifier can entangle and align itself forming a three-dimensional polymeric network. This three-dimensional network exhibits solid-like properties, with a storage modulus greater than the loss modulus (A, Figure 92). As shear stress is increased beyond the flow point, the polymer network collapses and disentangles.

The chains align themselves in the direction of the applied shear stress. At high shear stress the formulation exhibits liquid-like behaviour, with a loss modulus greater than its storage modulus (B, Figure 92). Following a return to low shear stress, the polymer network is reformed, causing a return to predominantly solid-like elastic behaviour (C, Figure 92).[257,258]

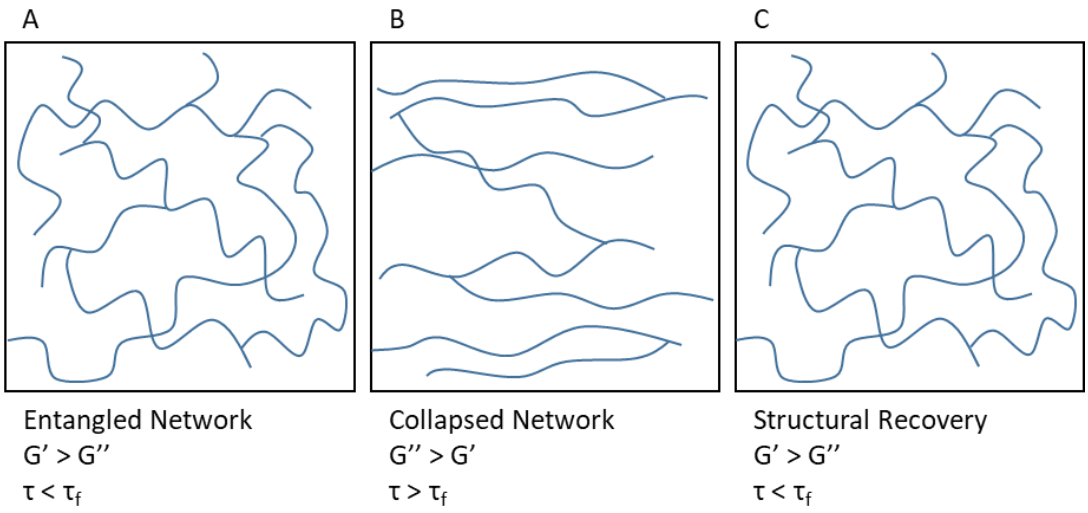

Figure 92 Schematic representation of a swollen polymeric rheology modifier at low shear stress (A), high shear stress (B), and following return to low shear stress (C).

For a formulation to be stable, it needs to return to a structured state after being exposed to shear stress. Shear degradation is unwanted as it would increase the sensitivity of the material and restrict processability. For example, during packaging a cream might be injected through a nozzle into a container. Steps such as injecting are high-shear, and for the product to be commercially feasible it must return to its original state following exposure to high-shear. Application of a cream onto skin is also high-shear and following application, structural recovery is desired to ensure that the applied layer remains.

Cyclic strain rheology can be employed to determine the shear stability of the PG4-1.5DMS formulations (Figure 93). In a cyclic strain experiment, the material is cycled between low and high shear strains. In effect, this transitions the material through its flow point multiple times. In a stable material, the storage modulus will recover to its equilibrium value following periods of high shear. These cyclic strain experiments also give insight into the time required for these materials to recover their structures.[259] Materials exhibiting a delay to attain equilibrium viscosity are considered thixotropic.[260]

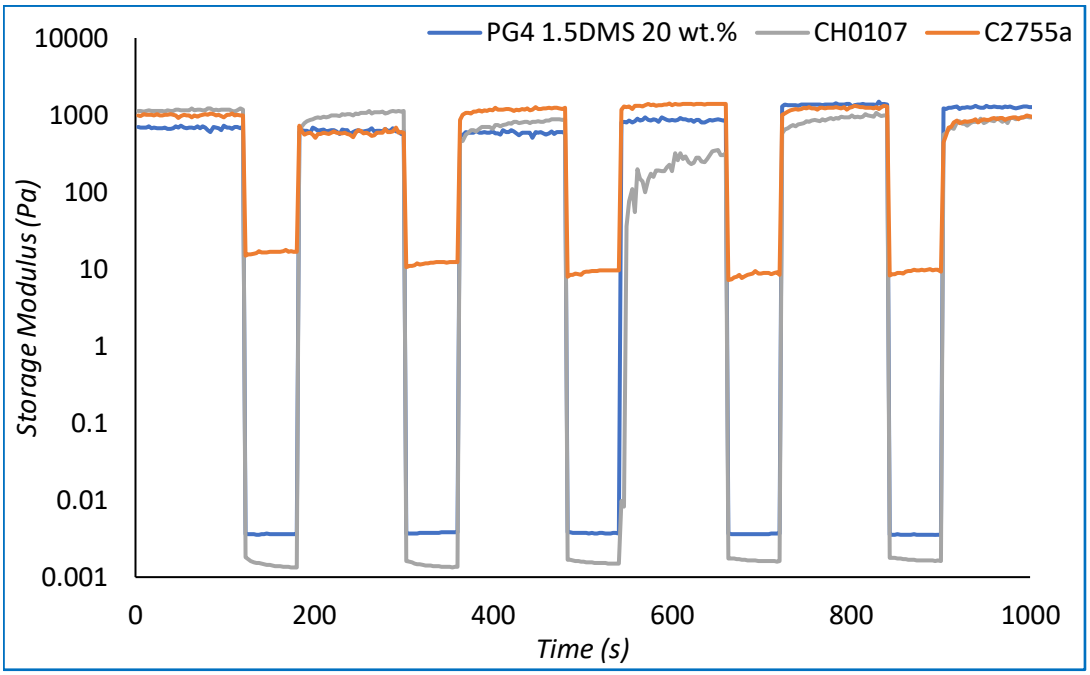

Figure 93 Cyclic strain rheology of 20 wt.% PG4-DMS in deionised water and commercial formulations. Low strain: 2 min, 0.1% shear strain. High strain: 1 min, 200% shear strain.

From the cyclic strain experiments, it is observed that PG4-1.5DMS based formulations exhibit excellent shear stability (Figure 93). PG4-1.5DMS based formulations successfully return to their equilibrium storage modulus following high shear. This was also the case in saline solution (Appendix Figure 27). Overall, these results are highly promising, as PG4-1.5DMS is shown to be competitive with commercial formulations in terms of shear-stability.

Furthermore, the recovery of PG4-1.5DMS appeared to be instantaneous, showcased by the sharp transition between the low shear and high shear regimes. CH0107 exhibits some thixotropic behaviour in all low-shear regimes, demonstrated by the gradual increase in G' following return to a low-shear environment. Interestingly, in the fourth low-shear segment CH0107 displayed a significantly lower storage modulus and significant thixotropic behaviour. This behaviour could be because CH0107 is an emulsion, which could require more time to reform relative to PG4-1.5DMS and the PAA-thickened C2755a. More likely however, is that this effect is a result of the sample "slipping" in the measurement geometry of the rheometer giving misleading results. In the following cycles, this behaviour is not present indicating that it is the result of a measuring anomaly.

4.4.2 Degradability Testing

Due to presence of ester bonds in PG4-1.5DMS, it was expected that in water hydrolytic degradation could occur (Figure 94). As the polymeric rheology modifier degrades, the swollen polymer matrix restricting water flow disintegrates into smaller soluble fragments. The smaller fragments are not expected to contribute to viscosity enhancement, and a decrease in viscosity of the solution should follow. As the ester bonds are cleaved free carboxylic acid groups are released. These free acids will decrease the pH of the solution and act to catalyse further hydrolysis.

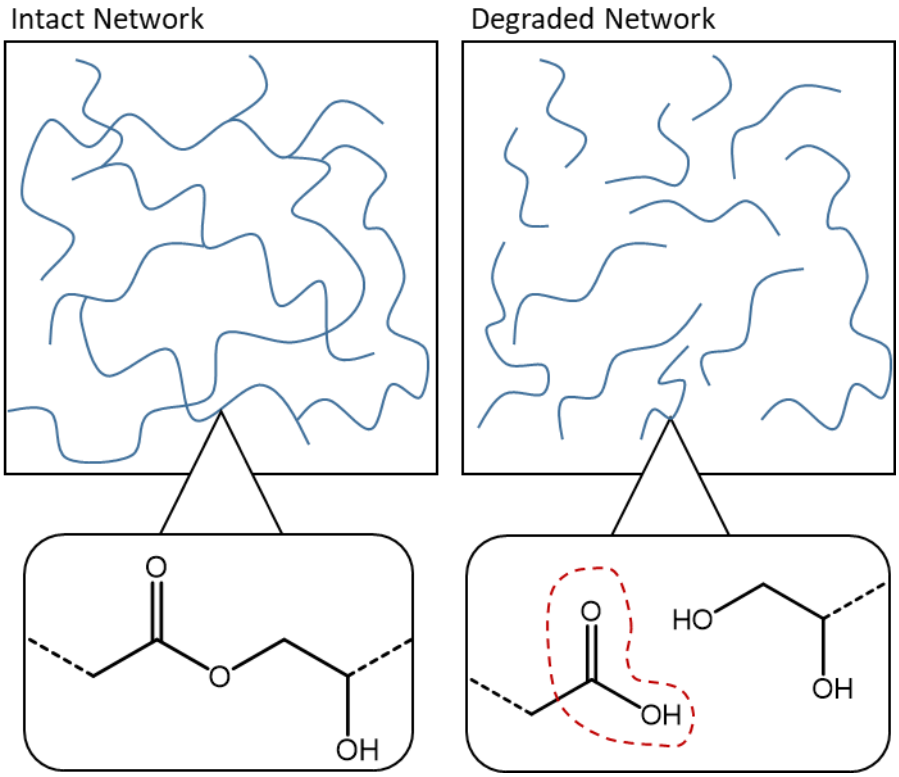

Figure 94 Schematic of an aqueous PG4-1.5DMS network before (left) and after (right) hydrolytic degradation. Free carboxylic acid highlighted by dotted red line.

To track hydrolytic degradation, the pH of a 20 wt.% solution of PG4-1.5DMS was measured over the course of several days. It was found, in both water and NaCl solution, that pH gradually decreased with time at the rate of 0.042 and 0.035 pH units per day on average (Figure 95). This acidification is strongly indicative of ester hydrolysis, as this process liberates carboxylic acids resulting in pH decrease. This reaction is expected to be autocatalytic, as release of free carboxylic acid groups will catalyse further ester hydrolysis. These results demonstrate the degradability of PG4-1.5DMS in aqueous media and is an effective method to prevent environmental accumulation.

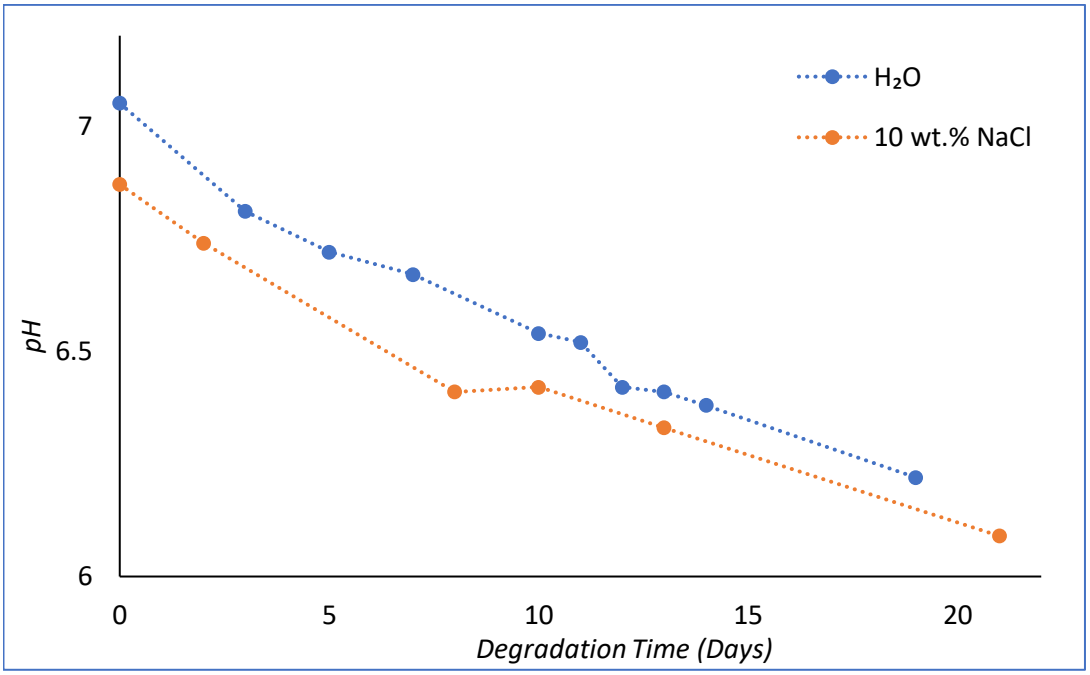

Figure 95 pH drift over time for 20 wt.% PG4-1.5DMS in DI water and an aqueous NaCl solution (10 wt.%).

Rheological measurements were performed over the course of 74 days to gain insight into the viscosity of the solutions as the viscosity modifier degrades (Figure 96). In an ideal scenario, the aqueous rheological modifier would exhibit an extended shelf-life (1-2 years) without decrease in performance, whilst also being readily biodegradable. In reality, a decrease in performance was observed over time for PG4-1.5DMS in aqueous solution. This lessening in viscosity can be explained by ester hydrolysis taking place, gradually shortening the polymer chains in the swollen framework. As the chains decrease in molar mass, they become more soluble and unable to effectively increase formulation viscosity.

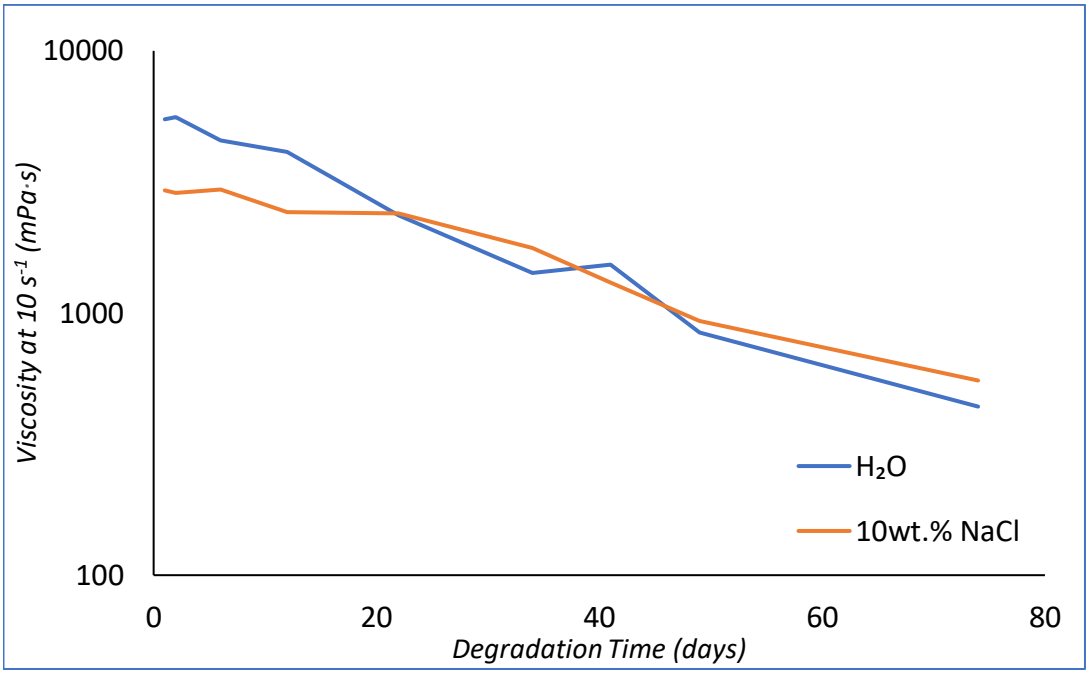

Figure 96 Viscosity at a shear rate of 10 s^{-1} over time for 20 wt.% PG4-1.5DMS in DI water and an aqueous NaCl solution (10 wt.%).

The degradation of the samples is also evident in the collapse of the storage modulus over time (Figure 97). Whilst good stability is observed on day 6, noticeable decreases in storage modulus become evident after day 12. This demonstrates that the formulation loses firmness over time. On day 34, only 10% of the day 1 storage modulus in the LVE remains (420 Pa to 40 Pa). Furthermore, the LVE becomes less well defined with time. Especially on days 22 and 34 the LVE is almost non-existent, as upon application of shear stress the storage modulus rapidly decreases. Flow points were also seen to decrease with time. These data imply that the structure of the polymeric rheology modifier is weakening with time, showing the physical effects of hydrolytic degradation.

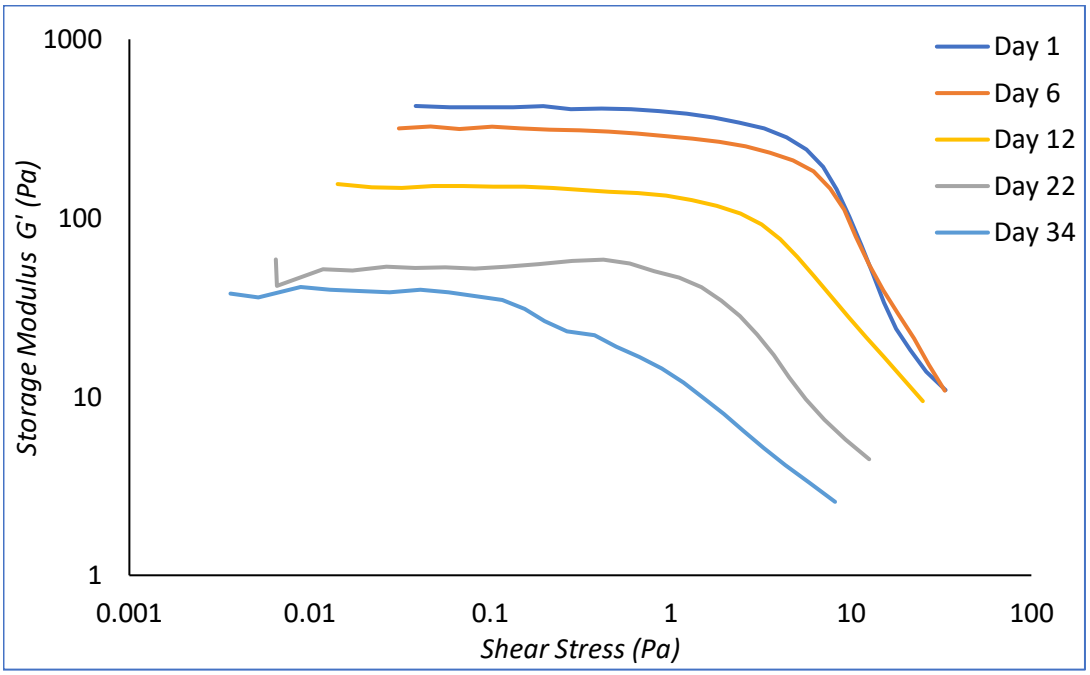

Figure 97 Amplitude sweeps of PG4-1.5DMS (20 wt.% aqueous solution) over the course of 34 days.

The lessening of storage modulus is mirrored in saline solution (Figure 98). This shows the weakening of the swollen polymer matrix caused by hydrolytic degradation of the rheology modifier. Interestingly, in comparison to the aqueous formulation, the LVE is maintained to a greater extent in saline solution. This indicates that the presence of electrolytes can act to stabilise the expanded polymer structure against shear stress. The added stability can be a result of strengthened intermolecular interactions between pendant hydroxyl groups and ionic species present in the solution, leading to improved shear-resistance of the formulation.

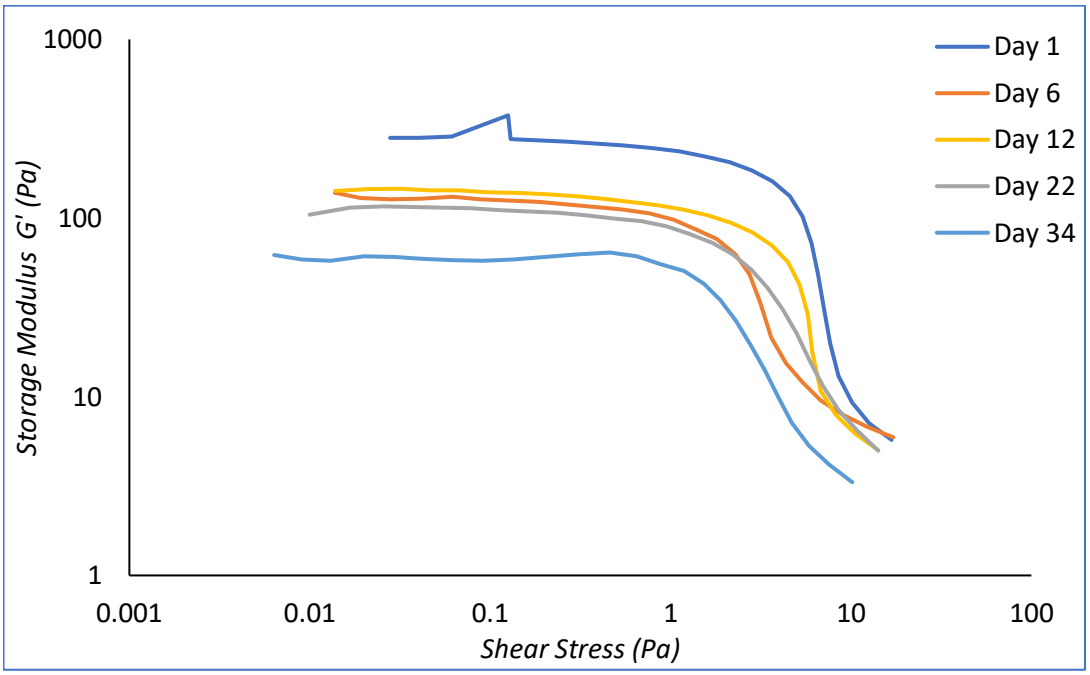

Figure 98 Amplitude sweep of PG4-1.5DMS (20 wt.% polymer in saline solution containing 10 wt.% NaCl) over the course of 34 days.

A drawback of this inherent degradability is the loss of performance over time. The loss of performance limits the shelf-life of the PG4-1.5DMS in aqueous media and can be problematic from the perspective of a consumer. A method to circumvent this issue would be to keep the rheological modifier out of the formulation until the last moment, only unleashing the viscosity enhancement when it is needed.

Overall, the observed behaviour of PG4-1.5DMS in aqueous solution demonstrates the ability of PG4-1.5DMS to act as a degradable aqueous rheology modifier. By utilising a polyester backbone, the inherent hydrolytic degradability can be exploited to produce rheology modifiers with degradability incorporated from the onset. This is a substantial improvement on current synthetic aqueous rheology modifiers that are non-degradable. Further development is required to tune the degradability profile to suit consumer expectations.

4.4.3 Swelling Capability

The water-absorbing capability of PG4-1.5DMS was measured. After 24 h in water, a clear highly swollen gel is formed (Figure 99). From a formulators perspective, the rate of swelling is highly relevant as this determines how long it will take for the prepared formulation to be ready. Ideally, upon addition of the rheological modifier the viscosity increase will be instantaneous. In the case of PG4-1.5DMS however, this process is lengthier as the water must penetrate the gelled polymer matrix.

Figure 99 PG4-1.5DMS before (left) and after (right) 24 h submersion in water.

Monitoring the mass gained over time revealed the rate of water uptake of the dry PG4-1.5DMS (Figure 100). It was found that the polymer samples tested approximately double in mass every hour for the first four hours. Visually, the polymer samples were observed to transition from a dense white material to a colourless gel. This transition occurred gradually, and during the experiments the gelled material formed initially on the outside of the polymer. As the water slowly absorbed into the polymer matrix the colourless swollen phase was seen to gradually expand until eventually none of the unswollen, dry, polymeric material could be seen. To improve on the rate of water uptake, the surface area of the dry PG4-1.5DMS should be increased. As the water enters from the outside, a greater surface area should vastly improve the rate of this process. The samples were not agitated in these experiments, and it is believed that agitation to remove swollen fragments from the surface of un-swollen polymer would drive the reaction to proceed faster by exposing fresh surface for the water to absorb into.

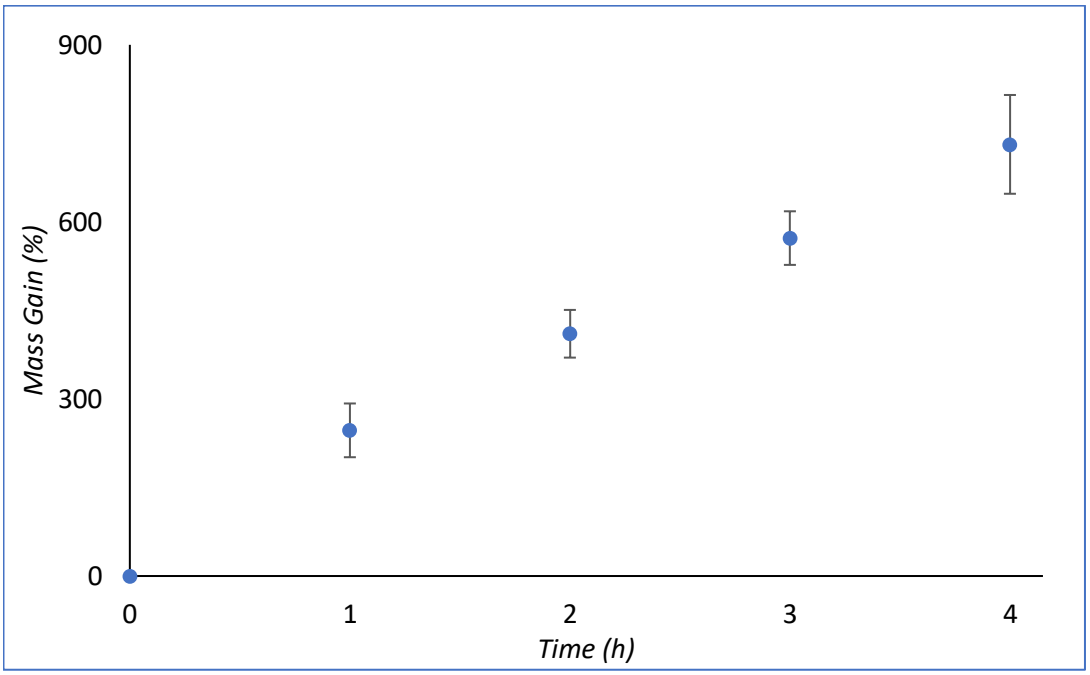

Figure 100 Mass gain against time for PG4-1.5DMS submersed in DI H_2O. Measurements in triplicate, error bars representing ±1 standard deviation.

PG4-1.5DMS demonstrates good water uptake, gaining almost 2000% by mass in water (Table 23). The formation of a colourless and odourless gel is also highly promising for application in personal care. Beneficially, PG4-1.5DMS does not require heat to be activated or any pH adjustments. To further improve the performance of PG4-1.5DMS it should be provided in a more finely divided form to increase the surface area and enhance the rate of swelling. Improving the total capability of PG4-1.5DMS to absorb water would also be highly beneficial, as this in turn would lead to rheological modification at lower loadings.

4.4.4 Freeze-Drying

One avenue explored to improve the performance of PG4-1.5DMS is the use of freeze-drying following swelling in an excess of water. The gel fraction was collected in the metal sieve, and soluble components remained in the aqueous supernatant. The swollen gel fraction was freeze dried, yielding a dry product that is exclusively the swellable fraction of the PG4-1.5DMS (Figure 101). As the soluble fraction has been removed, a performance boost in terms of rheological modification and swelling is expected. The gel fraction of PG4-1.5DMS by mass was measured to be 44±5%.

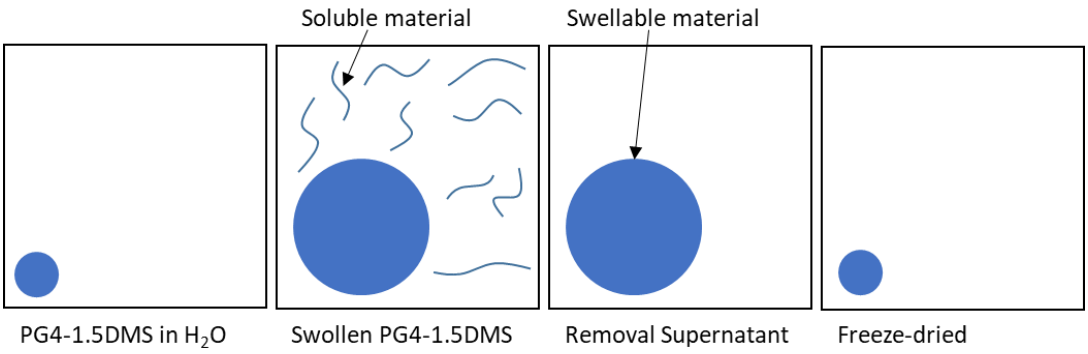

Figure 101 Schematic of swelling-drying process. Initially PG4-1.5DMS is submerged in an excess of water (far left), and allowed to fully swell (centre left). Subsequently, supernatant is removed to yield only the swollen gel (centre right), this gel is then freeze dried to give a dry product (far right).

Following removal of the soluble fraction, the performance of PG4-1.5DMS was significantly improved. In terms of water uptake, an improvement of 2.5-fold increase in mass gain is observed, reaching nearly 5000% mass gain (Table 23). This is accompanied by a rapid increase in rate of swelling, as the freeze dried sample reached 80% of its total mass gain within 1 hour (Figure 102).

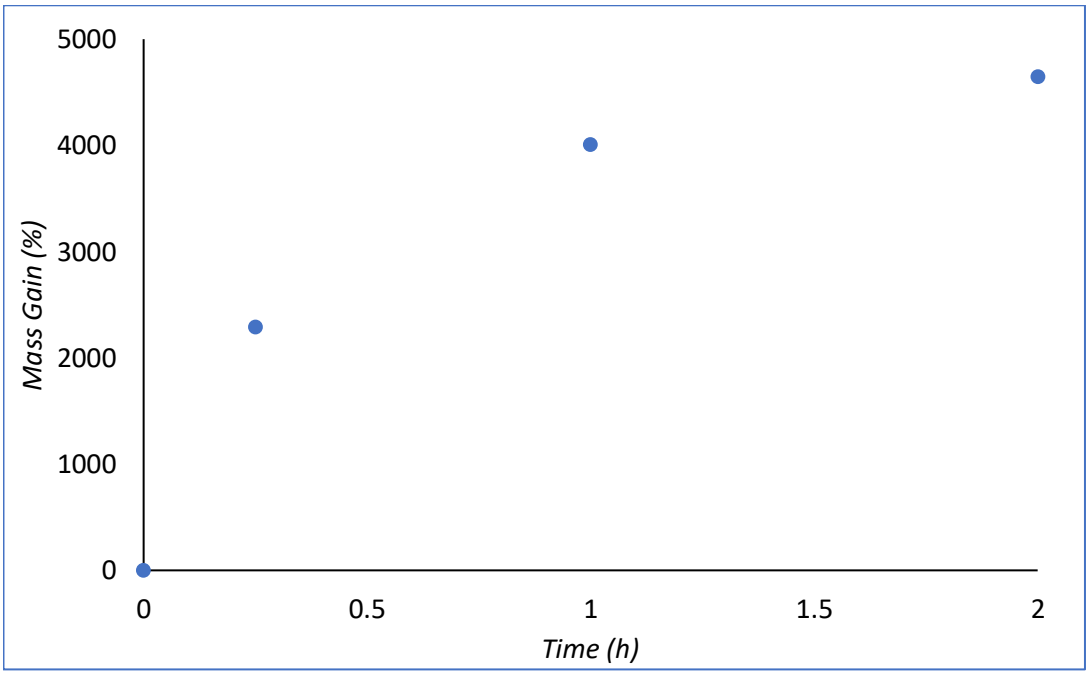

Figure 102 Mass gain against time for freeze dried PG4-1.5DMS submersed in DI H_2O.

The increased rate of swelling can be attributed to the enhanced surface area of the sample, as the freeze-drying process yields a sample that is significantly less dense than PG4-1.5DMS as it is collected from the reaction vessel.

Sample	Total Mass Gain (%)	Initial Mass Gain (%)	Std. Dev.
PG4-1.5DMS*	1993	247	285
Freeze dried	4988	4010	-

*Table 23 Average total mass gain for PG4-1.5DMS after 24 h. Initial mass gain was measured after 1 hour. Freeze dried sample was first soaked in DI water before being dried and re-swollen. *Measurement performed in triplicate.*

The increased performance in water uptake is also mirrored in the ability of freeze dried PG4-1.5DMS to boost the viscosity of aqueous solutions. A benefit of the increased rate of water uptake is that preparing the formulation is significantly faster. A freeze dried sample will achieve almost complete swelling within 1 hour, whereas the non-freeze dried PG4-1.5DMS requires ten times longer to fully swell. This increases throughput and minimises time spent waiting during sample preparation, boosting the suitability of the rheological modifier. Freeze dried PG4-1.5DMS provides similar performance at 5 wt.% as PG4-1.5DMS at 20 wt.% (Figure 103). This drastically improved rheological modification demonstrates the capability of cross-linked PG polyesters to act as efficient viscosity enhancers.

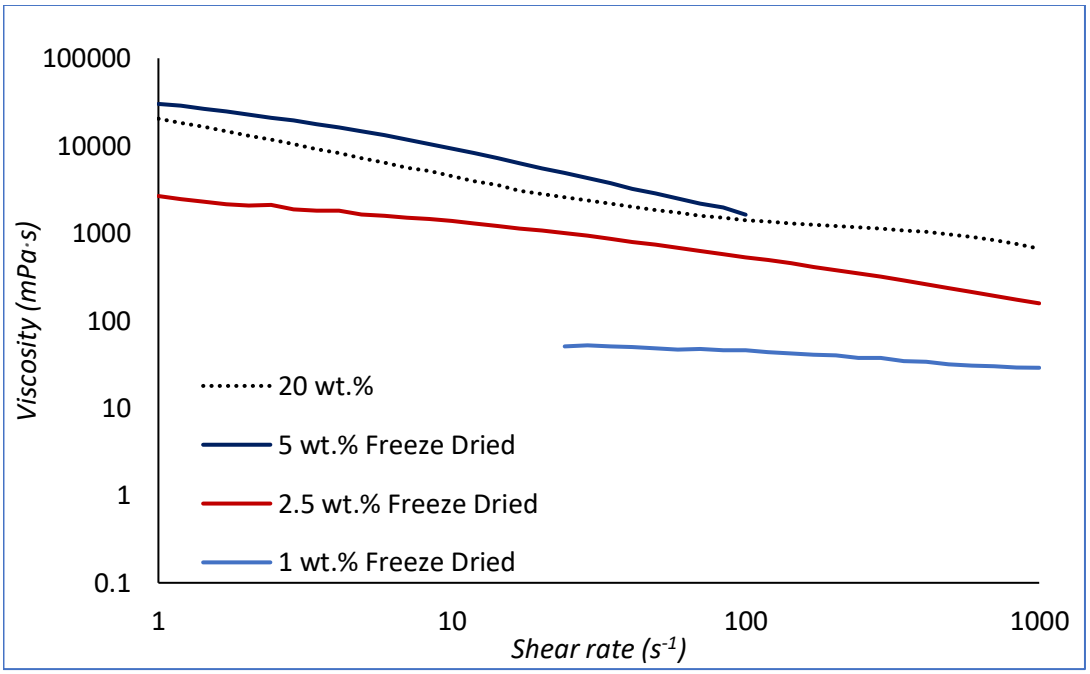

Figure 103 Shear ramp of freeze dried PG4-1.5DMS. Dotted line is PG4-1.5DMS without freeze-drying. For 5 wt.% Freeze Dried, some material escaped the measuring gap at a shear rate of 100 s^{-1}.

The performance enhancement seen after freeze drying is attributed to the removal of unreacted PG and other soluble fractions. As these fractions are soluble, they do not contribute to the viscosity boosting effect of the cross-linked material, and serve to decrease the active content of the thickener. Following the removal of the soluble fraction, the material consists predominantly of the swellable, rheologically active cross-linked species which explains the increased performance observed. The high performance of the swellable fraction shows that cross-linked PG4 based polyesters have great potential for rheological modification at single-digit loadings. Further development of these materials to achieve a greater gel fraction directly from the reaction vessel would be desirable to unlock the improved performance without requiring freeze-drying. Whilst industrial-scale freeze-drying equipment is available, this process results in a mass loss of 56±5% as the soluble fraction is removed. As this loss is significant, improving the synthetic methodology to increase the size of the gel-fraction from the onset would be much more desirable.

From an oscillatory amplitude sweep, it can be observed that the aqueous solutions of freeze dried material behave as viscoelastic solids (Figure 104). The flow point was measured to be 20.4 Pa, which is greater than the values achieved without freeze drying and approaching the values of the commercial formulations (Table 22). An increase in storage modulus in the LVE was also observed, surpassing that of the commercial formulations. This was also confirmed visually, as the 5 wt.% freeze dried formulation was noticeably firmer than other formulations. Whilst the storage modulus in the LVE is greater than that of the commercial formulations, the flow point is lower. This indicates that the thickening caused by PG4-1.5DMS based systems is more sensitive to external forces, demonstrating that the gel structure is more easily disrupted. This could be a result of lower average molar masses and the lack of electrostatic repulsions along the polymer backbone.

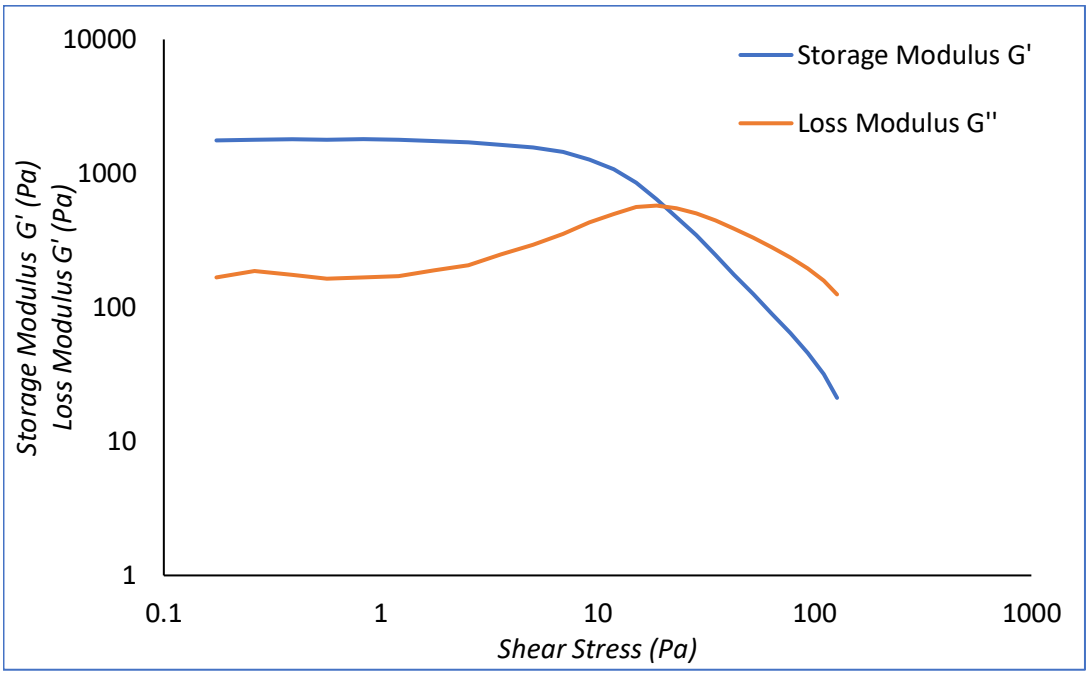

Figure 104 Amplitude sweep of 5 wt.% freeze dried PG4-1.5DMS in DI water. Flow point τ_f=20.4 Pa, LVE limit = 5.1 Pa, G' in LVE = 1738 Pa.

Using cyclic strain experiments it can be observed that freeze dried PG4-1.5DMS shows full structural recovery following exposure to high-strain (Figure 105). The freeze dried material provides similar performance at only one quarter of the loading required before freeze drying. This is an important observation to ensure stability of the thickened formulation during processing and shows that the freeze dried sample maintains the same robustness observed for PG4-1.5DMS at 20 wt.%.

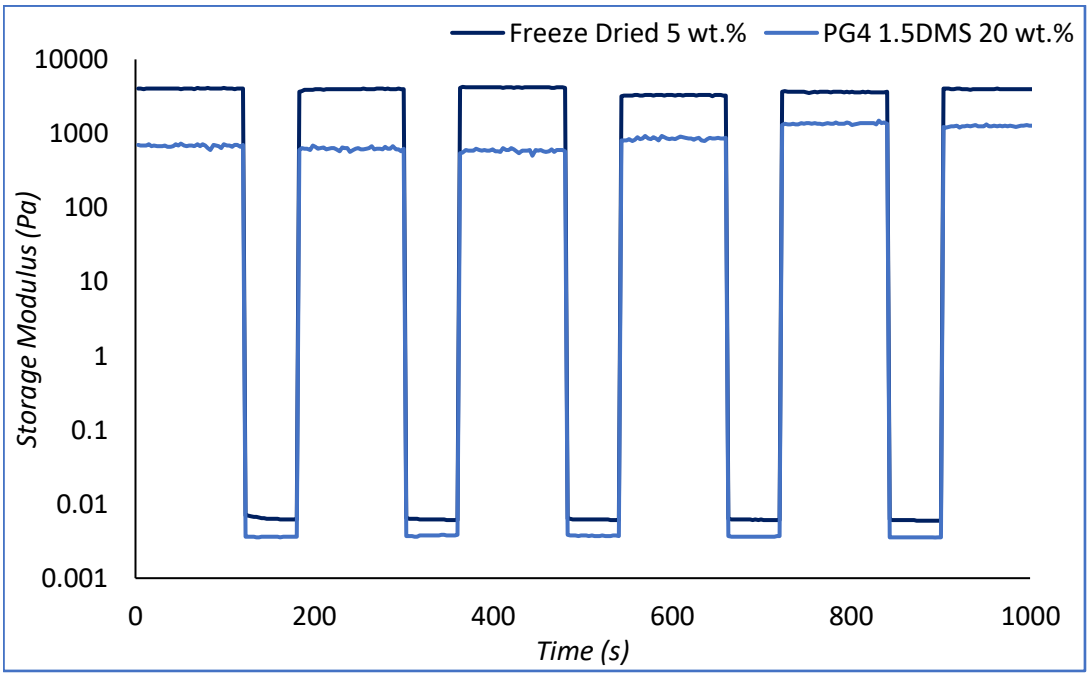

Figure 105 Cyclic strain rheology of 5 wt.% freeze dried PG4-DMS in deionised water. Low strain: 2 min, 0.1% shear strain. High strain: 1 min, 200% shear strain.

Degradability Testing

Degradability testing of freeze dried PG4-1.5DMS in aqueous formulation was conducted. This was done to observe if the freeze-drying procedure influenced the stability of the formulation. Two aqueous formulations were prepared, of 2.5 and 5 wt.% thickener loading. The pH, viscosity, and storage modulus of these samples were measured at intervals up to 43 days of degradation time total.

In terms of pH, a rapid initial decrease in pH is observed in the first 14 days of degradation time (Figure 106). Following this, the pH appears to stabilise. This data indicates that some hydrolysis is occurring, followed by a stabilisation of the system. Promisingly, this indicates a potentially better shelf-life for the freeze-dried material in contrast with the non-freeze-dried material.

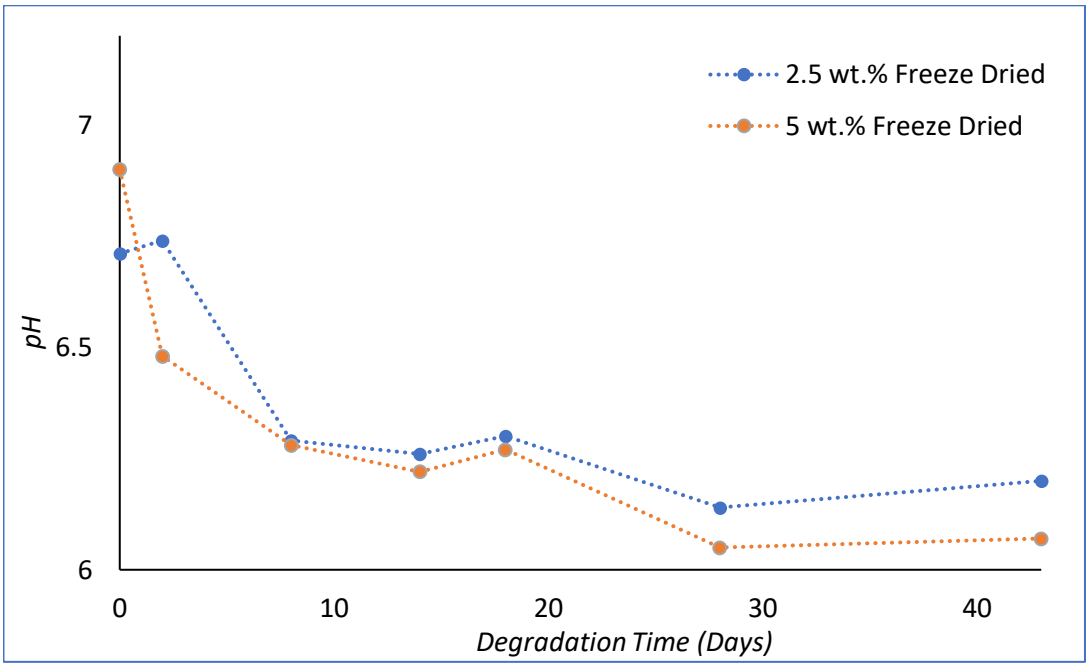

Figure 106 pH drift over time for 2.5 and 5 wt.% freeze-dried PG4-1.5DMS in DI water.

Rheological experiments were also performed on the same samples (Figure 107). It was observed that viscosity of 5 wt.% freeze-dried PG4-1.5DMS decreased from 16 to 5.8 Pa·s over the course of 43 days. A 2.5 wt.% formulation of freeze-dried PG4-1.5DMS decreased from 1.4 to 0.98 Pa·s during the same period. This shows that viscosity of PG4-1.5DMS does decrease over time, indicating that degradation is taking place. In comparison to non-freeze-dried material (5.5 to 1.5 Pa·s over 40 days), the decrease in viscosity is less drastic for the freeze-dried materials, showing that the freeze-drying procedure increases the stability of the formulation. This is thought to be an effect of the increased gel-fraction and lower overall loading of the freeze-dried formulations. The soluble materials could be more accessible for hydrolytic degradation, and the released carboxylic acids can subsequently act to catalyse further ester bond breakage.

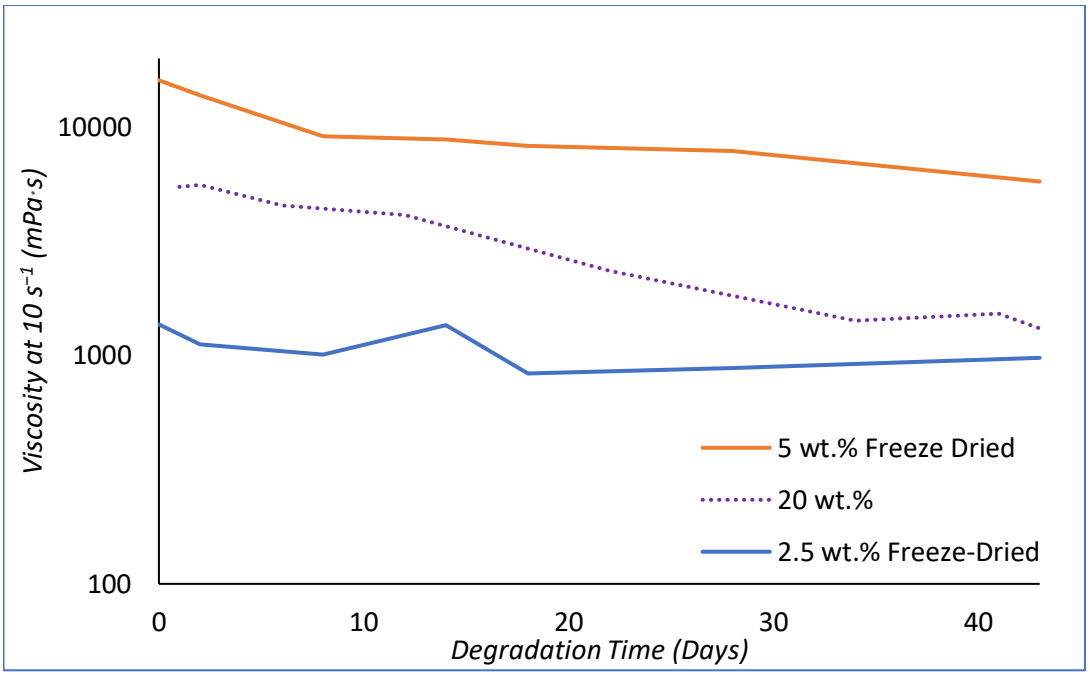

Figure 107 Viscosity at a shear rate of 10 s^{-1} over time for 2.5 and 5 wt.% freeze dried PG4-1.5DMS in DI water.

The degradation of the formulations can also be observed in the storage modulus over time (Figure 108, Appendix Figure 29). The storage modulus in the LVE decreases over time, and LVE collapse is achieved at lower shear stresses over time. This shows a degradation in the structure of the formulation with time. In the case of 5 wt.% freeze-dried PG4-1.5DMS, the LVE storage modulus decreases from 1780 to 420 Pa over the course of 43 days. This is a significant improvement upon the non-freeze-dried material, which decreases from 407 to 40 Pa in 34 days. Analogously to the results from rotational rheology, these values show an increase in stability of the formulation following freeze drying to increase the gel-fraction.

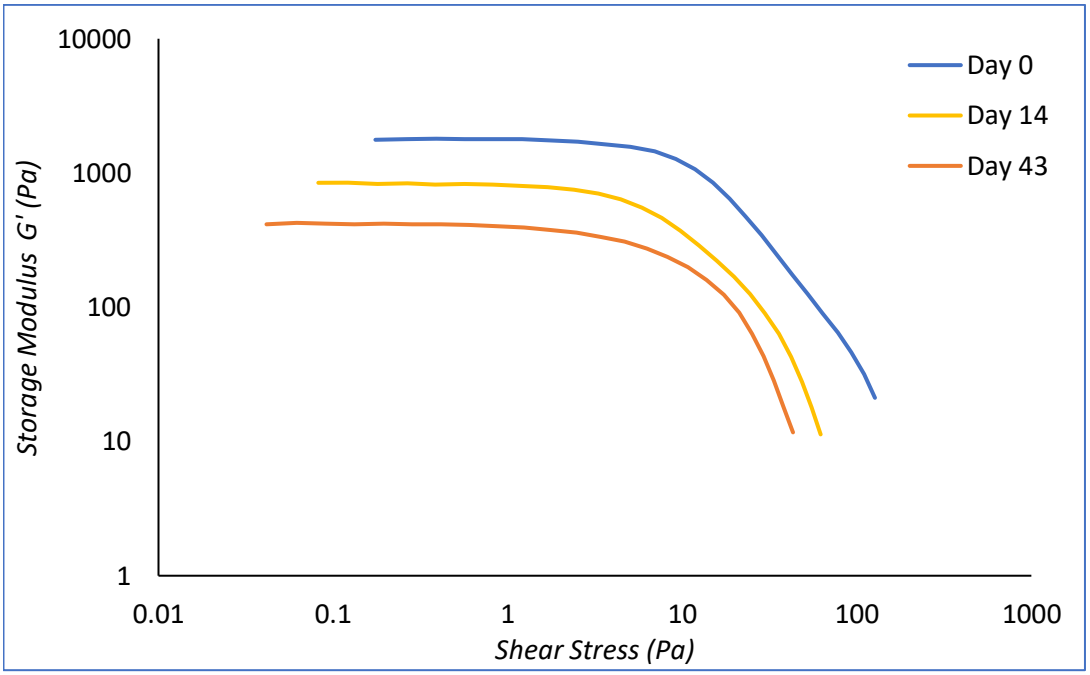

Figure 108 Amplitude sweeps of freeze dried PG4-1.5DMS (5 wt.% aqueous solution) over the course of 43 days.

Freeze-drying PG4-1.5DMS provides a significant boost in performance in water absorption, rheological modification, and formulation stability. A total mass gain of nearly 50 times its own mass was measured, greatly surpassing mass gain of nearly 20 times its own mass observed prior to freeze-drying. Furthermore, the freeze-dried material absorbed water much more rapidly, facilitating the potential for high throughput production of formulations. Decreasing the required loading to achieve rheological modification demonstrates the effectiveness of cross-linked PG polyesters to restrict the flow of water in solution. A loading of 2.5 wt.% already demonstrates good thickening behaviour, which is boosted further when increasing the loading to 5 wt.%. Oscillatory experiments demonstrate the desired viscoelastic behaviour is maintained, and that the formulation undergoes complete structural recovery following high strain. Degradability studies show that freeze drying

increases the stability of the formulation. These results show that a biobased, degradable highly efficient aqueous rheological modifier has been synthesised using mild reaction conditions and benign reagents. The excellent performance of freeze dried PG4-1.5DMS, in combination with its green credentials make it a desirable rheological modifier for personal care applications.

4.4.5 Cytotoxicity Studies

Cytotoxicity experiments were performed in collaboration with Valena Axioti and Robert Cavanagh.

In vitro cytotoxicity studies were used to assess the suitability of the PG4-DMS polyesters for use in on-skin personal care applications. Skin cells were exposed to monomers and polymers in triplicate at three different concentrations (Figure 109). DMS was found to be more toxic than the cell death control at all concentrations tested, giving rise to negative cell viabilities. The toxicity exhibited by DMS highlights the need to ensure full monomer conversion in the final formulation to limit decreases in cell viability. PG4 did not lessen cell viability at 0.125 mg·mL^{-1}, although increasing the concentration of PG4 did lower cell viability to 73±5% at 0.500 mg·mL^{-1}. This shows presence of PG4 can be detrimental to cell proliferation, although the decrease is far less pronounced than what is observed for cells exposed to DMS.

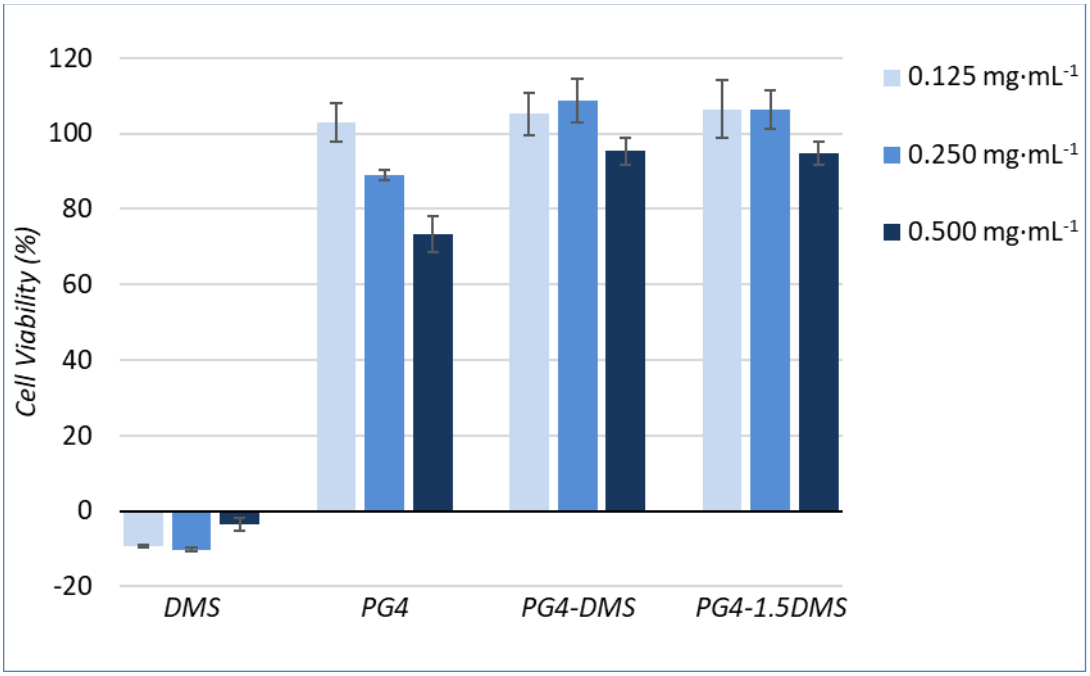

Figure 109 Cell viability following exposure to DMS, PG4, PG4DMS, and PG4-1.5DMS. Error bars represent ± 1 standard deviation.

Promisingly, the polymers tested did not exhibit cytotoxicity, and cell viability was maintained even at 0.500 $mg \cdot mL^{-1}$ for both PG4-DMS and PG4-1.5DMS. This indicates that the presence of unreacted DMS is limited after polymerisation. It was observed previously (Chapter 3) that the soluble fraction of PG4-1.5DMS contains some DMS (Figure 73). These cell viability measurements demonstrate that this fraction does not negatively impact the skin cells at the concentrations tested. The cell viability measurements suggest that PG4 based polyesters can be suitable for application on skin. Further studies *in vivo* would be needed to confirm the suitability of these materials for application on skin.

4.5 Conclusions

Cross-linked PG4 based polyesters were investigated in terms of rheological modification and their water absorption capabilities. Rheological modification was observed at loadings exceeding 10 wt.%. Varying the loading of DMS was found to influence the viscosity modifying behaviour. PG4 reacted with 1.25 equivalents of DMS (PG4-1.25DMS) was observed to provide the best performance, although the synthesis was not reproducible and the formulations rapidly degraded. As a compromise between improved stability, reproducibility of the synthesis, and performance, PG4-1.5DMS was selected as the most promising candidate and explored further. Increasing the DMS loading beyond 1.5 equivalents resulted in decreased performance, as the polymer network becomes too tightly cross-linked for effective swelling and water entrapment to occur.

Loadings of greater than 10 wt.% PG4-1.5DMS were required to achieve notable viscosity enhancement of aqueous solutions. At lower loadings the thickener was unable to absorb all the water in the solution. This unbound water has a detrimental effect on the total viscosity of the system. At a loading of 20 wt.% a viscosity profile similar to those of commercial formulations was achieved, as at this loading no unbound water was present in the system and viscosity could be enhanced. Furthermore, PG4-1.5DMS displayed excellent electrolyte tolerance, losing minimal rheological performance upon addition of high loadings of sodium as well as magnesium salts to the aqueous formulation. This excellent electrolyte tolerance is highly sought after, as electrolytes are widespread in personal care formulations.

It was shown that preparations of PG4-1.5DMS display viscoelastic behaviour using oscillatory rheology. At low shear strain the formulations behave with predominantly elastic, solid-like, characteristics. At high shear strain, beyond the flow point, these materials exhibit viscous, liquid-like behaviour. In the context of personal care formulations this viscoelasticity is desirable to formulate products that can be easily applied, whilst having a desirable thick

consistency when being handled. Using cyclic strain experiments the formulations were cycled between low and high strain. These materials displayed excellent structural recovery, instantaneously recovering their storage modulus following several cycles of high strain. Stability in high strain is essential to withstand operations such as packaging, homogenisation, and application, without premature degradation of the thickening effect.

Degradability studies were performed. It was found that viscosity of the solutions decreased over time alongside a decrease in pH. These two behaviours are thought to be the result of hydrolytic degradation of the polyester bonds of the PG4-1.5DMS. As these bonds are cleaved, the cross-linked polymer matrix disintegrates and its ability to modify the flow of water in solution is hampered. Hydrolytic degradation also releases free carboxylic acid functionality, leading to the decreasing pH observed. The degradability exemplifies the capability of PG4-1.5DMS to be suitable as a thickener without the environmental persistence of commercial synthetic aqueous rheology modifiers. This hydrolytic degradability is highly promising start to enable the development of personal care formulations that address the issue of non-degradable components and microplastic release. For further development, the degradability should be tuned to facilitate shelf-life stability whilst also being readily degraded in waste-water treatment facilities.

Swelling experiments were conducted on PG4-1.5DMS. An average of almost 2000% mass gain was achieved, absorbing nearly 20 g of water per g of PG4-1.5DMS. The capability of PG4-1.5DMS to absorb significant quantities of water expands the applicability of this material beyond aqueous rheology modification, as superabsorbers can be used in various other products. To achieve complete swelling in water extended periods of time were required, usually with samples being left overnight. Improved swelling kinetics can be achieved by increasing the surface area of the polymer, lowering the time taken for water to fully penetrate the polymer matrix.

Following the initial swelling experiments, the formed swollen gel was freeze dried. The gel fraction of PG4-1.5DMS was measured to be 44±5%, highlighting the presence of soluble materials present in the reaction product. It is thought that these soluble materials consist of unreacted PG as well as low molar mass polymer chains. Removal of soluble materials through this process yielded a significant performance boost in terms of both viscosity modification and swellability. Aqueous rheology modification was achieved at loadings as low as 2.5 wt.%, and performance exceeding that of 20 wt.% before freeze-drying was achieved at 5 wt.% following freeze-drying. Increasing the active content of the thickener

decreases the required loadings, which at single digit values are comparable to those required of current commercial rheology modifiers. A significant jump in swellability was also observed, reaching a mass gain of almost 5000% - 50 g of water per g of polymer. In addition, the rate of water uptake was also significantly improved, at 4000% in the first hour compared to only 240% before freeze-drying. Oscillatory rheological experiments demonstrated that the desired viscoelastic behaviour was maintained, and that the formulation underwent full structural recovery following high strain. Furthermore, degradability studies demonstrated an increase in formulation stability following freeze drying, improving the shelf-life of the thickened solutions, and improving commercial viability.

Cytotoxicity measurements were performed to demonstrate the compatibility of the synthesised rheology modifiers with skin cells. It was found that PG4-DMS and PG4-1.5DMS did not decrease cell viability relative to the negative control. These results are very promising, demonstrating that these thickeners could be suitable for on-skin application. Further evaluation *in vivo* would be needed to confirm no negative effects are encountered when applied to skin.

In short, this chapter demonstrates that the PG4-1.5DMS synthesised previously is a highly effective, biobased, and degradable synthetic aqueous rheology modifier. Following freeze-drying, a viscosity boost can be achieved at loadings as low as 2.5 wt.%. Excellent swellability has also been shown, absorbing nearly 50 times its own mass of water. These properties show that PG4-1.5DMS is a highly promising candidate for aqueous rheological modification in personal care products and improves on existing technology in terms of environmental credentials.

4.6 Further Work

To further assess the suitability of these materials in personal care applications they should be incorporated into existing formulations. Stability in the presence of other components, such as oils, fragrances, and surfactants, should be tested further to ensure compatibility of the rheological modifier in the product. Furthermore, sensory perception of the formulations is critical for personal care products. Therefore, testing these thickeners on a sensory panel would provide valuable insight into behaviours such as skin-feel.

Further development of the synthetic approach to produce PG4-1.5DMS would also be valuable. As seen in the freeze-drying section, removing soluble material and increasing the gel content vastly improves performance. Eliminating the freeze-drying step, whilst maintaining the same excellent rheological modification would be highly desirable. Driving

conversion further during synthesis would ideally increase the gel fraction, removing the need for freeze-drying. This has been discussed in Chapter 3.

Improving the hydrolytic stability of these materials could also be a point of interest. As extended shelf-lives are expected of personal care products, the degradation of the thickener can be considered undesirable. Improving the molar mass of the polymers could limit the effects of hydrolytic degradation. Alternatively, adding steric hindrance to the ester group could also improve hydrolytic stability. For example, installation of methyl groups adjacent to the carbonyl carbon could serve to protect the ester bond. Other functionalities, such as carbonates, in the polymer backbone could also be explored to alter the degradability profile. Submitting the produced PG4-1.5DMS for testing using an industrially certified test method, OECD 301F for example, would be highly relevant to assess the biodegradability profile of the material. Increasing stability of the polymer should also be balanced, as eventual degradation is still desired. This presents a fine balancing act between improving stability whilst maintaining (bio-)degradability.

4.7 Materials and Methods

Citric acid monohydrate was purchased from Sigma Aldrich. NaOH was purchased from Fisher Scientific UK. Water was deionised before use. All chemicals were used as received. The PG polyesters tested throughout this chapter were synthesised according to the procedure in Chapter 3, using K_2CO_3 catalysis at 80 °C under argon flow.

4.7.1 Instrumentation

Rheology

Rheological characterisation was performed using an Anton Paar MCR 102 rheometer. Experiments were performed using 25 mm parallel plate measuring geometry at 25 °C and a 1 mm measurement gap.

Amplitude Sweeps: an angular frequency of 10 s^{-1} was used. Shear strain was increased logarithmically from 0.01 to 100%. The sample was allowed to recover for 1 minute after loading before measurements were started.

Shear Ramps: shear rate was increased logarithmically from 1 to 1000 s^{-1}, 40 data points were collected at 6 s per point. The samples were pre-sheared for 1 minute at 10 s^{-1} before measurements were started.

Cyclic Strains: an angular frequency of 10 s^{-1} was used. The material was subjected to low strain (0.01%, 2 minutes) followed by high strain (200%, 1 minute). The material was subjected to 5 intervals of high strain in total. The sample was allowed to recover for 1 minute before measurements were started.

pH Measurements

A Mettler Toledo LE438 sensor connected to a Mettler Toledo FiveEasy FE20 pH meter, calibrated using pH 4 and 7 buffer solutions (VWR Chemicals) was used to measure pH.

Freeze-Drying

Freeze-drying was performed using a GIROVAC freeze drier.

4.7.2 Experimental Procedures

Formulation Preparation

PG polyesters were added to a pre-weighed volume of DI water to achieve a certain wt.% of thickener in the solution (e.g. 2 g polymer was added to 8 g DI H_2O for a 20 wt.% solution). The PG polyesters were allowed to swell at ambient temperature overnight or until complete

solvation of the polymer matrix was achieved. Subsequently, they were mixed using a Silverson high speed mixer (2 min, 7000 RPM) to homogenise the solution.

In the electrolyte stability studies PG polyesters were added to aqueous solutions of 10 wt.% NaCl or 5 wt.% $MgSO_4$.

For the pH tolerance tests, small portions of citric acid or NaOH were added to modify the pH of the solution.

Swelling Experiments

Dry polymer (approx. 2 g, accurately weighed) was placed inside a stainless-steel sieve and submerged into deionised water (750 mL, ambient temperature). Measurements were performed after removing superficial water using paper towel. The swollen gels were subsequently freeze dried.

Cytotoxicity Evaluation

A431 human epidermoid carcinoma cells were obtained from the American Type Culture Collection (ATCC; Manassas, Virginia). Cells were cultured in DMEM (Sigma-Aldrich) supplemented with 10% (v/v) Foetal Bovine Serum (FBS) (Sigma-Aldrich) and 2 mM L-glutamine (Sigma-Aldrich), and at 37°C with 5% CO_2.

The PrestoBlue cell viability assay (Thermo Fisher Scientific) was performed to assess cytotoxicity. Cells were seeded at 1.2×10^5 cells per well in 12 well plates and cultured for 24 hours prior to assaying. Polymeric materials were exposed to cells at 500 $\mu g \cdot mL^{-1}$ for 48 hours and applied in 1 mL phenol red free DMEM containing 10 % (v/v) FBS and 2 mM L-glutamine. TX applied at 1 % (v/v) applied in phenol red free medium was used as a cell death (positive) control and a vehicle control containing no polymeric material used as a negative control. Cells were washed twice with warm phosphate-buffered saline and 10 % (v/v) PrestoBlue reagent diluted in phenol red free medium was applied per well for 60 minutes. The resulting fluorescence was measured at 560/600 nm ($\lambda_{ex}/\lambda_{em}$). Relative cell viability was calculated by setting values from the negative control as 100 % and positive control values as 0 % metabolic activity.

Chapter 5. Anionic Polymerisation for Linear Polyglycerols

5.1 Aims & Objectives

Previous chapters explored aqueous rheology modifiers synthesised using PGs produced by the direct oligomerisation of glycerol. These contain various structural isomers and are of limited molar mass. Producing high molar mass, linear, PG with controlled structures is of interest to potentially enhance the performance of the aqueous rheology modifiers. Anionic polymerisation of protected glycidol is explored in this chapter as a means of producing linear PG of high molar mass.

5.2 Abstract

Anionic polymerisation of ethoxyethyl glycidyl ether (EEGE) (Figure 22) using potassium *tert*-butoxide (*t*-BuOK) was explored as a method to synthesise linear polyglycerol (linPG). Molar masses of up to 20.7 kg·mol^{-1} were obtained, and dispersity of the produced polymers was low ($Đ$<1.2). Conversions obtained were high, and chain transfer side reactions were controlled under the reaction conditions employed. Supercritical extraction using CO_2 was utilised as a green purification protocol to remove unreacted monomer following polymerisation. Following extraction, deprotection using a heterogeneous acidic catalyst, Amberlyst 15, yielded linPG.

5.3 Introduction

Linear polyglycerol (linPG) has become increasingly recognized as a potential alternative to PEG.[136,261] PEG is used in a wide variety of applications, ranging from surfactants to drug delivery systems.[49,262] PEG is biocompatible,[263] nontoxic,[264] and soluble in both organic solvents and aqueous systems.[265] As a result of these and other properties, PEG is often considered a gold standard for aqueous soluble polymers. That is not to say PEG is perfect, and the overuse of PEG has resulted in PEG-antibodies becoming more widespread leading to allergenic responses in humans.[86,88] Furthermore, PEG lacks reactive chemical handles along its backbone rendering mid-chain functionalisation difficult. LinPG is structurally similar to PEG, maintaining aqueous solubility, with the addition of functionisable pendant hydroxyl groups along its backbone (Figure 110). The biocompatibility of linPG is excellent, and no significant effects on cell viability, or coagulation have been observed.[136] As a result, linPG could be an interesting candidate to replace PEG.

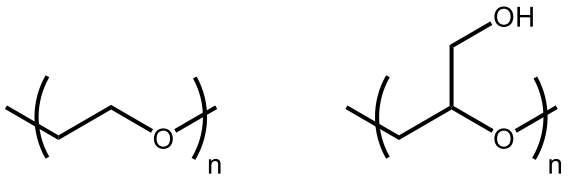

Figure 110 Structure of PEG (left) and linPG (right).

In the context of aqueous rheological modification PEG chains have been extensively used as the hydrophilic component in associative thickeners.[81] As demonstrated in this thesis, cross-linked networks of PG form highly swellable systems that act to boost viscosity in aqueous media. It follows that linPG could be used either as the hydrophilic linking segment in an associative thickener, or as the basis for the formation of a cross-linked network similar to PG4-1.5DMS explored previously. The enhanced linearity and molar masses obtainable through anionic ROP could enhance the performance of the produced rheology modifier upon cross-linking or functionalisation with hydrophobic end-groups.

In this chapter EEGE will be explored as a monomer to synthesise linPG (Figure 111). EEGE was selected as an ideal candidate for polymerisation due to its simple synthesis and deprotection procedures. The synthesis route selected avoids time-consuming and wasteful procedures such as column chromatography.

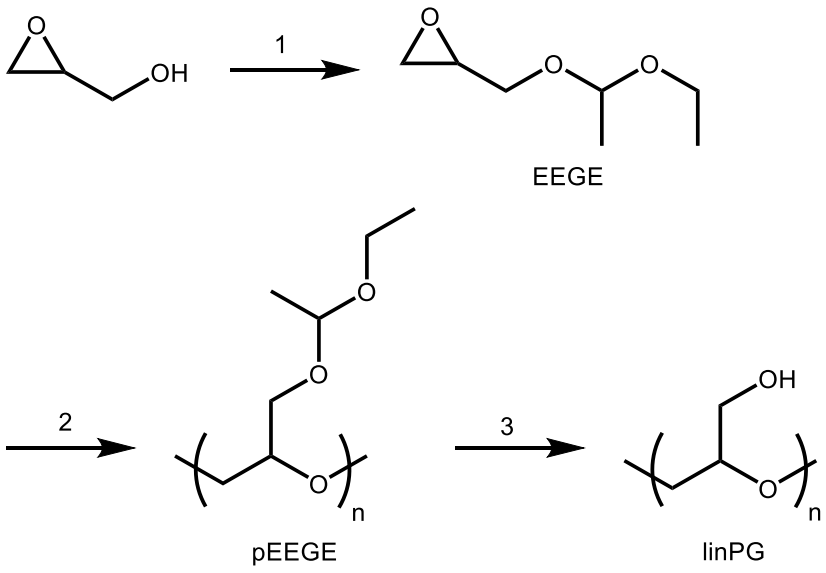

Figure 111 Synthetic strategy for the synthesis of linPG employed in this chapter. 1: Protection of glycidol using ethyl vinyl ether and acid catalysis. 2: Anionic polymerisation using t*-BuOK initiator. 3: Deprotection using Amberlyst 15.*

EEGE has been polymerised in the literature using a selection of catalysts, and molar masses up to 800 000 g·mol^{-1} have been achieved using a partially hydrolysed diethylzinc catalyst.[266]

In this chapter, *t*-BuOK was used as an initiating species to avoid pyrophoric reagents. Work by Hans *et al.* has shown pEEGE with molar masses of up to $M_n \approx 30$ kg·mol^{-1} can readily be synthesised using *t*-BuOK in dry THF at 60 °C.[267] Attempts to synthesise pEEGE of greater molar mass were thwarted by chain transfer reactions resulting from proton abstraction (Figure 112).

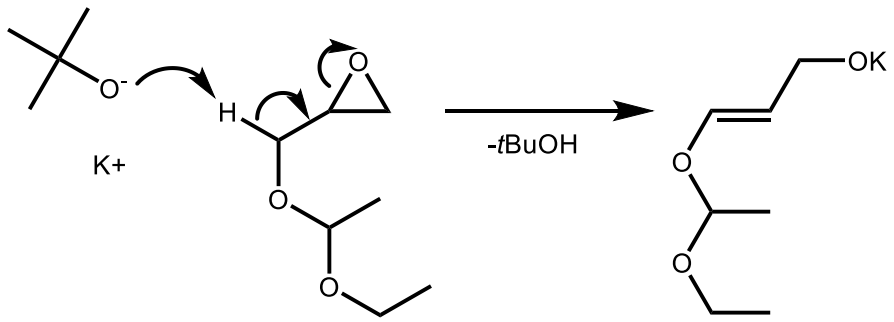

Figure 112 Proton abstraction from EEGE by t-*BuOK.*

The extent of proton abstraction in comparison to propagation is the result of a balance between nucleophilicity and basicity of the propagating chain end. Increased basicity promotes proton abstraction and disfavours polymerisation. Heightening the nucleophilicity of the propagating chain end has the opposite effect.[267] Complexing catalysts have been shown to suppress chain transfer reactions. Alkyl zinc and aluminium based species have been shown to play a dual role; supressing the basicity of the propagating chain end, whilst also increasing the electrophilicity of the epoxide.[134,136,266] Whilst these catalysts can achieve excellent molar masses, alkyl zinc and alkylaluminium species are inherently pyrophoric.[268,269]

This chapter explores the synthesis and polymerisation of EEGE to produce linPG using anionic polymerisation. These linPGs are envisaged for use as alternatives to PEG in synthetic rheology modifiers for aqueous media.

5.4 Results and Discussion

5.4.1 Monomer Synthesis

EEGE Synthesis

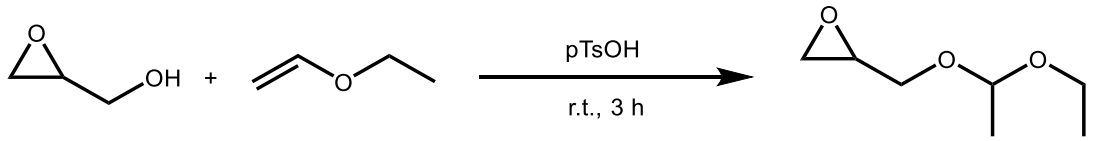

Figure 113 Reaction scheme for the synthesis of EEGE from glycidol and ethyl vinyl ether under acidic conditions.

EEGE was synthesised following an adapted literature procedure (Figure 113).[270] This reaction proceeds rapidly (3 h) at ambient temperature. Pure EEGE can be obtained in high yield (88.9%) following aqueous washing and vacuum distillation, avoiding column chromatography. The simplicity of the reaction and purification make this methodology very applicable to larger scale production. Care should be taken to limit the exotherm that occurs upon addition of the catalyst to the reagents. As ethyl vinyl ether is volatile (b.p. 33 °C), future improvements to the process should focus on controlling this exotherm. Dissolution of the catalyst in an appropriate solvent, followed by slow addition of the catalyst to the reaction mixture would be more suitable method for catalyst addition in an industrial setting. Alternatively, this reaction could be performed in-flow over an acidic reactor bed.[271]

5.4.2 Anionic Polymerisation

EEGE was polymerised using *t*-BuOK as initiator. It was found that molar mass was controlled, and narrow dispersity polymers were obtained.

Entry	M_n Calc. (kg·mol^{-1})	Conv.(%)[a]	Chain Transfer (%)[a]	M_n[b] (kg·mol^{-1})	M_w[b] (kg·mol^{-1})	$Đ$[b]
1	4.57	98	3	4.64	5.1	1.10
2*	10.0	99	4	15.9	16.7	1.05
3	18.0	90	3	11.2	13.1	1.17
4	35.8	72	5	20.7	22.8	1.10

*Table 24 Data of anionic polymerisation of EEGE with varying initiator loading. * Synthesised using a fresh bottle of initiator. [a] Determined by ^{1}H-NMR spectroscopy. [b] Determined by GPC in THF.*

The synthesised polymers are all of low dispersity, remaining below $Đ$=1.2 (Table 24) in accordance with previous literature findings, which typically report dispersities in this range.[261,267] Low dispersity is indicative of a controlled, "living", polymerisation and

showcases the ability to obtain well defined polymer structures. These findings are in stark contrast to PG-polyesters explored in Chapter 3, which feature high dispersities because of the step-growth type polymerisation and the nature of the oligomeric PG monomers used.

The GPC traces obtained are largely unimodal, although some high molar mass "shoulders" can be observed for entries 2, 3, and 4 (Figure 114). This could be a result of some initial rapid polymer growth. The dispersities of the obtained polymers are however low, and this process appears to be very minimal. Work in the literature has suggested that gradual addition of monomer to the initiator can lower the dispersities obtained.[272] The GPC traces also demonstrate the ability to tune molar mass of the polymers by altering the initiator loading. These data demonstrate the ability to synthesise well-defined linear protected polyglycerols using anionic polymerisation as an alternative to polycondensation.

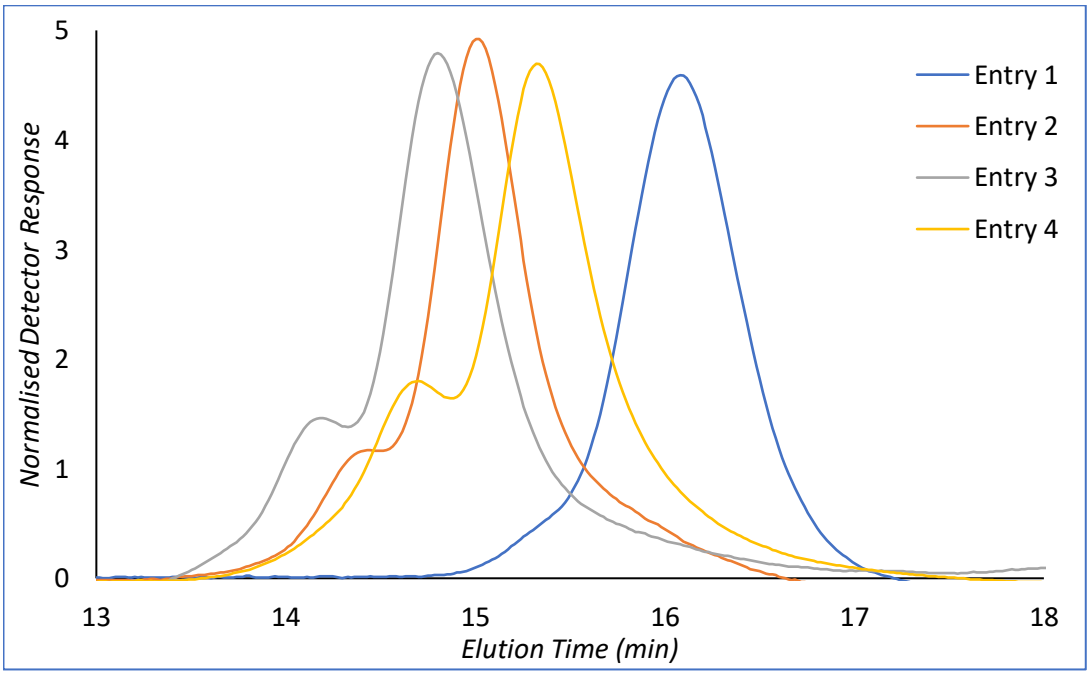

Figure 114 GPC (THF) Elution traces for the samples from Table 24.

Molar masses of up to 20.7 kg·mol^{-1} were achieved, corresponding to approximately 70 monomer units (Table 24). This value is in accordance with what has been observed in the literature, where attempts to synthesise higher molar mass linPG using the same reaction conditions were unsuccessful.[267,272] High conversions were achieved (Table 24). Upon targeting a molar mass of 35.8 kg·mol^{-1} the conversion achieved was lower, 72%. Conversion and extent of chain transfer were readily determined by ^{1}H-NMR spectroscopy (Appendix Figure 32). Chain transfer was minimal for these samples, and close to the lower limit of detection by ^{1}H-NMR analysis.

Polymers obtained were yellow to brown viscous liquids (Appendix Figure 31). Darkening was more intense when targeting lower molar mass, and a greater quantity of initiator was added. This suggests that the discolouration is caused by the *t*-BuOK initiator. From analysis by ^{1}H-NMR spectroscopy no unexpected signals were detected, and as such further investigation would be required to determine the exact species responsible for the colouration. From a personal care perspective any deviation from complete transparency is undesirable, and for these polymers to be suitable for personal care products the colouring would have to be removed. One possible method would be to use activated charcoal as a colour removal agent.[273]

Supercritical Extraction of Residual Monomer

Supercritical extraction was explored as a method to purify the formed pEEGE. Utilising CO_2 as a green method to remove unreacted monomer has many advantages over alternative strategies utilising traditional solvents.[220] Upon depressurisation to ambient conditions, the CO_2 will return to a gaseous phase leaving a clean polymer free of solvent contaminants.[274] In addition, no contaminated solvent waste is produced in this process, and the released CO_2 can be captured and recycled.[274] CO_2 is an excellent supercritical fluid for this process, as it can dissolve a large variety of small organic molecules whilst polymeric materials are generally insoluble.[220] Plasticisation and softening of the polymeric material by the $scCO_2$ can further aid extraction efficiency.[274]

To determine suitable conditions for supercritical extraction, a solubility study of EEGE in $scCO_2$ was performed. It was found that EEGE is soluble in $scCO_2$ above 13.8 mPa at 40 °C (Appendix Figure 33). Following this finding, pEEGE containing unreacted EEGE (72% conversion) was extracted using $scCO_2$ to remove residual monomer content (Figure 115). To aid product retrieval from the autoclave, the pEEGE was placed in a vial which was inserted into the autoclave. Using this method, the whole vial containing the purified polymer could simply be lifted out of the reactor, maximising yield by ensuring complete mass transfer. To improve extraction rate both the glass vial and the headspace of the reactor were stirred vigorously. After removal from the pressurised vessel, significant quantities of gas were released from the polymer, demonstrating that CO_2 can diffuse into the polymer phase and act to enhance extraction efficiency (Figure 115).

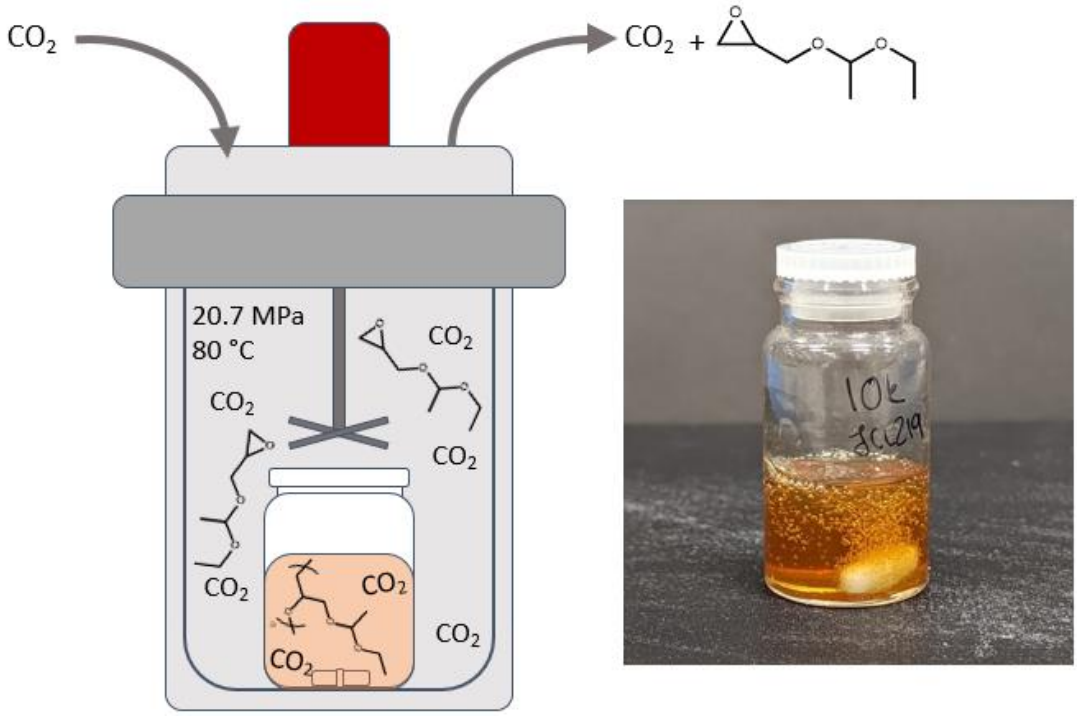

Figure 115 Left: schematic of supercritical extraction of pEEGE in the autoclave set-up, showing residual EEGE being solubilised and extracted, whilst pEEGE remains inside the glass vial. Right: an image of the purified (and carbonated) pEEGE obtained.

From analysis by ^{1}H−NMR spectroscopy it can be observed that signals corresponding to unreacted monomer are no longer visible following supercritical extraction (Figure 116). This shows that pEEGE can be readily purified by supercritical extraction under these conditions. Successful removal of residual monomer is essential considering that these polymers are targeted for personal care applications, and presence of unreacted epoxides in the materials could lead to skin sensitisation.[275]

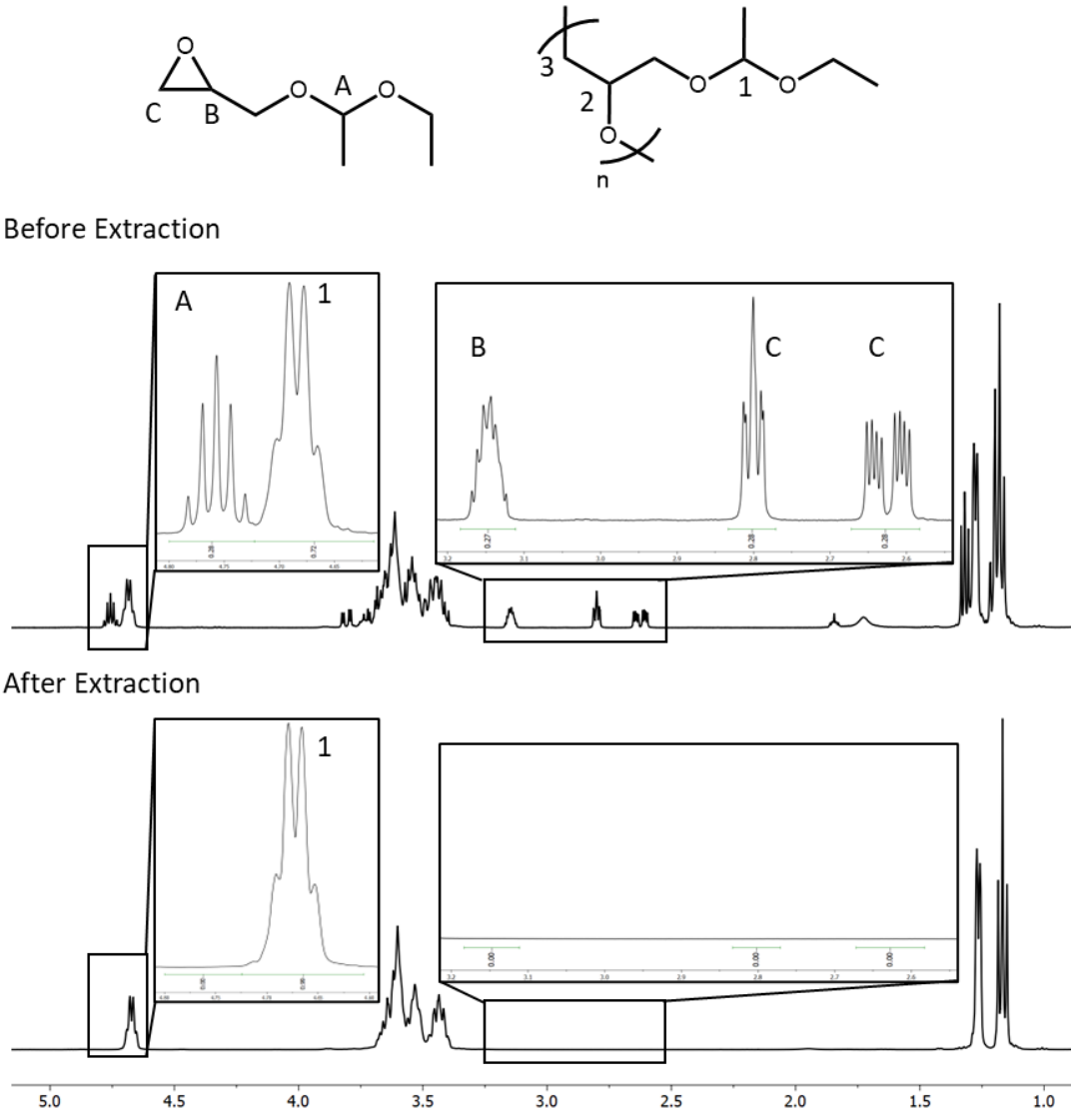

Figure 116 ^{1}H-NMR spectrum of pEEGE in $CDCl_3$ before (top) and after (bottom) purification by $scCO_2$ extraction. Note the presence of monomer signals in the upper spectrum which cannot be detected in the lower spectrum.

Deprotection of pEEGE

A variety of deprotection protocols can be found in the literature.[134,267,276] Many of these protocols feature deprotection using aqueous acid followed by precipitation into large volumes of solvents. To facilitate processability and convenience, an immobilised ion exchange resin, Amberlyst 15, was used in this work. After deprotection, the solid support can simply be removed by filtration, reducing overall solvent-use in the process. The deprotected polymer can subsequently be obtained following drying *in-vacuo*.

During deprotection, the acetal functionality of pEEGE is hydrolytically cleaved to generate ethanol and acetaldehyde (Figure 117). The formation of acetaldehyde can be exploited to drive the reaction equilibrium towards the deprotected linPG. Acetaldehyde is highly volatile (b.p. 20 °C), and it is readily removed by evaporation, preventing the backwards reaction occurring and driving the deprotection. An excess of water is also employed to drive the reaction to completion.

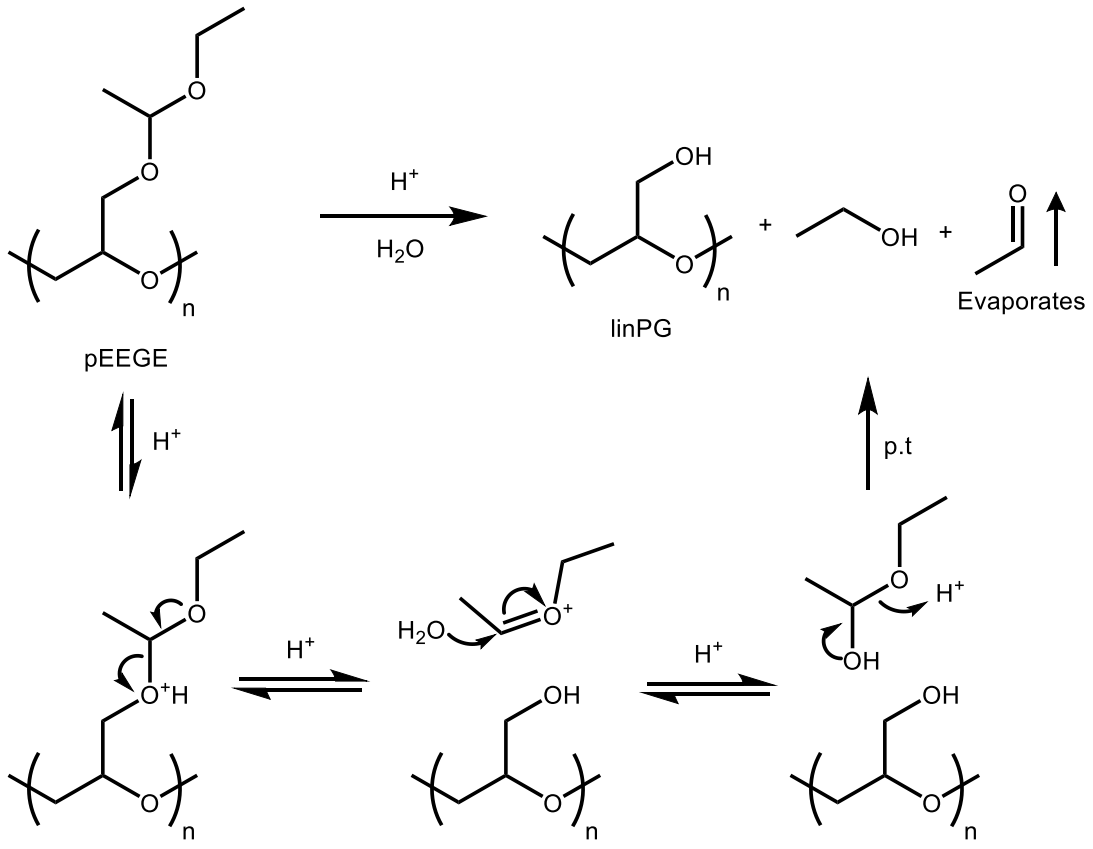

Figure 117 Proposed mechanism for the acid catalysed deprotection of pEEGE in aqueous media. Removal of acetaldehyde by evaporation prevents the reverse reaction taking place.

The synthetic methodology employed in this process has a notable limitation due to the need for protection groups during synthesis. While deprotection can be achieved with relative ease using a straightforward synthetic approach, it introduces an additional step before obtaining the desired polymer. Consequently, the atom economy of the reaction is diminished, with the deprotection process being only 45% atom economic. Ethanol and acetaldehyde account for the remaining 55% of the product mass generated. Furthermore, the ethanol and acetaldehyde generated need to be collected and properly managed, which incurs economic and environmental burden.

Analysis by ^{1}H-NMR spectroscopy shows that signals corresponding to the acetal-fragment are no longer visible after deprotection (Figure 118). In addition, the solubility profile of the polymer is drastically changed: pEEGE is hydrophobic and water insoluble, whereas linPG is hydrophilic and readily water soluble.

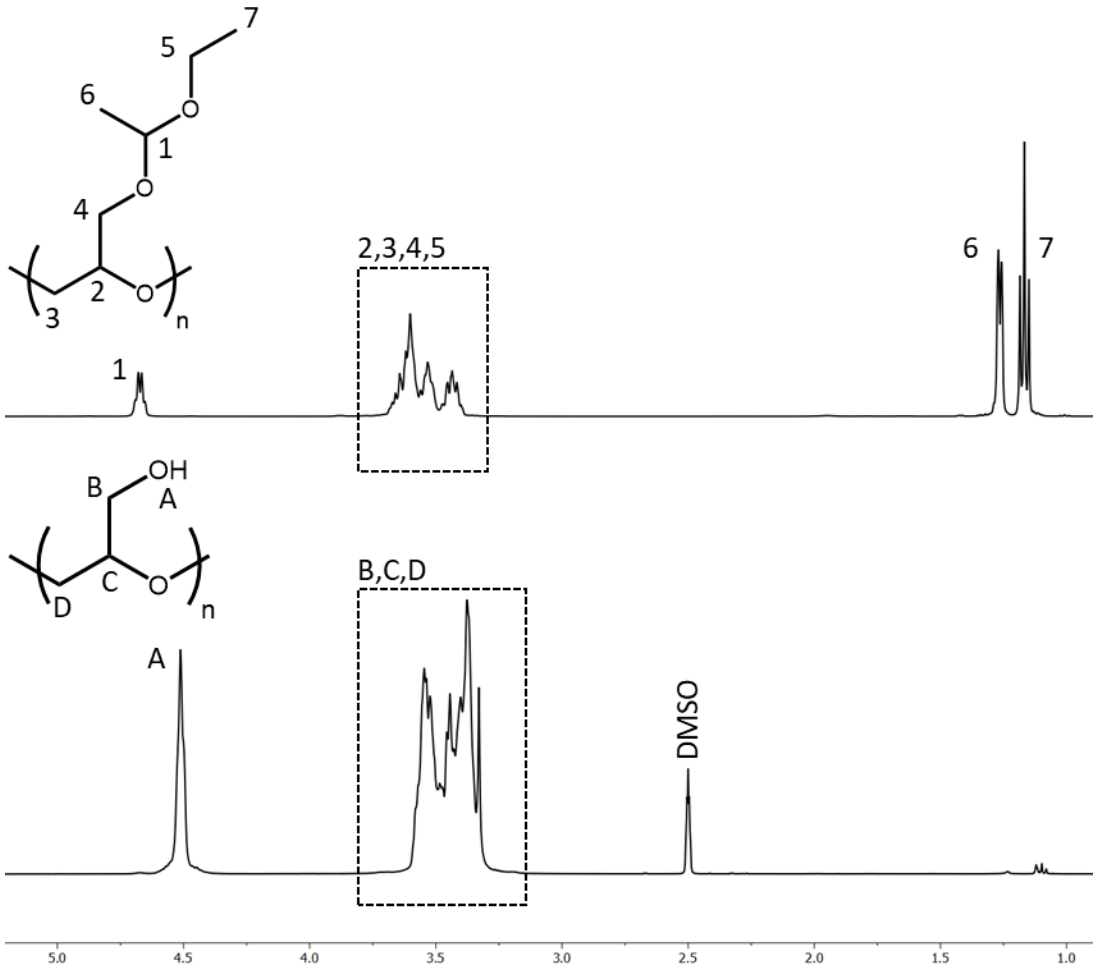

Figure 118 ^{1}H-NMR spectra of pEEGE in $CDCl_3$ (top) and following deprotection in DMSO-d_6 (bottom).

Kinetics in an Industrial Setting

The polymerisation of EEGE was also performed in an industrial research laboratory. This reaction was performed on a 50 g scale, and in solventless conditions. These conditions were selected to demonstrate the ability to increase the scale of reaction and to maximise reactor loading by avoiding the use of volatile organic solvent.

Reaction progression was monitored by gas chromatography (GC) and ^{1}H-NMR spectroscopy (Figure 119). The GC signal corresponding to EEGE was monitored and found to diminish as the reaction progressed. ^{1}H-NMR spectroscopic analysis of the same aliquots shows increasing conversion of EEGE into pEEGE, demonstrating good agreement between the analytical techniques. GC does not require deuterated solvents or cryogenics like NMR spectroscopy and can therefore be considered a more accessible analytical technique. The ability to analyse the anionic polymerisation using GC demonstrates the applicability of commonly used analytical equipment to follow this reaction.

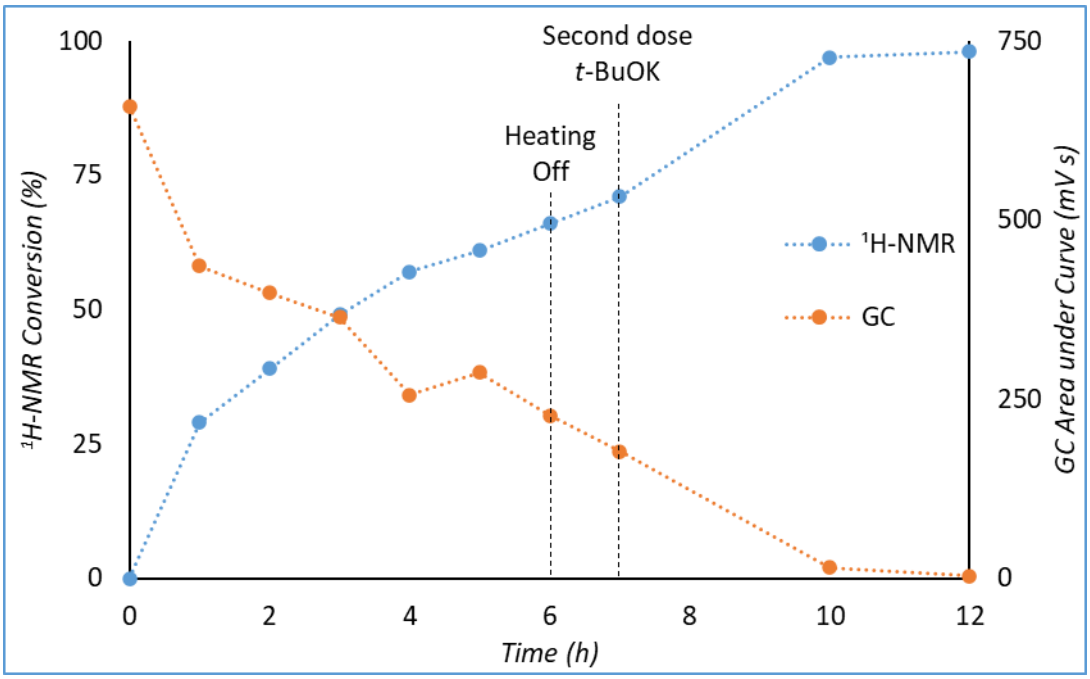

Figure 119 Conversion and area under curve against time during the bulk anionic polymerisation of EEGE. The reaction was cooled after 6 h and brought back up to reaction temperature the following day. Inert atmosphere was maintained overnight. A second dose of t*-BuOK was added at 7 h.*

Due to health and safety regulations in this particular laboratory, reactions were not allowed to proceed overnight. As a result, the heating was switched off at the 6 h mark and the reaction was kept at ambient temperature under a nitrogen atmosphere overnight. The

following day, the reaction was re-heated and allowed to equilibrate for 1 h. A 5% increase in conversion was observed during re-heating, indicating some active chains remained. Following equilibriation, an additional dose of *t*-BuOK was injected to drive the reaction to completion. Conversion rapidly increased from 71 to 97% after the second dose of initiator was added.

Reaching complete conversion during polymerisation limits the requirement to remove residual monomer content, simplifying the purification process. A drawback of a secondary dose of initiator is the potential to deviate from unimodal molar mass distributions in the final polymer. Interestingly, in this reaction deviation from unimodality is observed already prior to the second shot of initiator (Figure 120). This could be a result of uneven heating of the reaction mass due to the relatively high viscosity of the solventless reaction mixture. Between 6 and 12 h the shape of the GPC chromatogram obtained does not change, but it does shift to shorter elution times. This indicates that *t*-BuOK deprotonates the existing polymer chains which can then proceed to extend by addition of more monomer units, rather than forming a second polymer distribution.

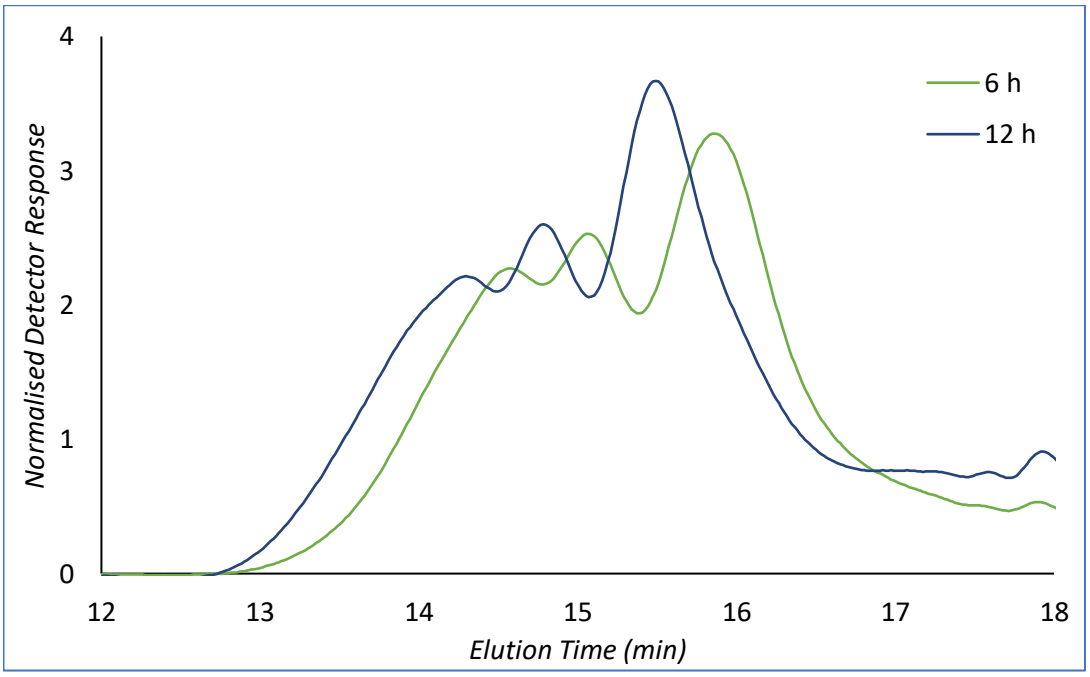

Figure 120 GPC traces at 6 (M_n 10.7 kg·mol^{-1}, Đ 1.57) and 12 h (M_n 14.6 kg·mol^{-1}, Đ 1.38) during solventless anionic polymerisation. of EEGE.

Cross-Linking Attempt

Attempts were made to introduce cross-linking to pEEGE using PEG diglycidyl ether. It was thought that a lightly cross-linked linPG network would exhibit improved rheological modification properties in comparison to the cross-linked poly(glycerol succinate) materials from Chapters 3 and 4. These attempts proved unsuccessful, as no conversion was detected. Whilst the PEG cross-linker was dried using molecular sieves, it is hypothesised that it was not sufficiently dry for the polymerisation reaction. Anionic polymerisation is notoriously moisture sensitive, and introduction of moisture will quench the initiator and propagating species.[133]

5.5 Conclusions

This chapter has demonstrated the synthesis of EEGE, subsequent anionic polymerisation, and deprotection to yield linPG. Glycidol was readily reacted with ethyl vinyl ether to give EEGE in high yield (89%). Anionic polymerisation demonstrated the ability to produce pEEGE with controlled molar masses up to 20.7 $kg \cdot mol^{-1}$ and narrow dispersities. Deprotection was performed using an immobilised anion exchange resin to eliminate extensive purification procedures found in the literature.

Supercritical extraction was demonstrated to be a simple method to remove unreacted EEGE from the polymeric samples. The solubility of EEGE in $scCO_2$, coupled with the insolubility of pEEGE, meant that $scCO_2$ was an ideal solvent for this purpose. Analysis by ^{1}H-NMR spectroscopy following extraction could not detect any signals corresponding to unreacted monomer.

Kinetics were performed in an industrial laboratory to demonstrate the suitability of the process in a commercial setting. GC proved to be a more industrially suitable analytical technique as an alternative to ^{1}H-NMR spectroscopy to monitor reaction progression. Addition of a second dose of initiator was found to be a successful approach to drive the polymerisation to quantitative conversion, limiting the need for purification post-polymerisation.

Cross-linking was attempted using PEG-diglycidyl ether, although no conversion was observed. Presumably this was a result of the cross-linker being insufficiently dried and quenching the polymerisation.

Anionic polymerisation of protected glycidol provides a method to produce high molar mass linPG. In comparison to the polycondensation approach explored in Chapters 3 and 4 this could be beneficial to the eventual performance of rheological modifiers. Unfortunately, these gains in terms of linearity and molar mass are counteracted by the requirement to use less benign feedstocks. Whereas oligomeric PGs, K_2CO_3, and DMS previously employed are all benign, and even approved for use as food additives, the same cannot be said for the chemicals utilised in this chapter. Especially glycidol is a hazardous material, with notable issues regarding toxicity. The advantages of higher molar masses and linearity should therefore be carefully weighed against safety concerns of the monomers required to obtain them.

5.6 Further Work

Further work along the lines of anionic polymerisation would focus on imparting rheological modification behaviour to the materials produced. Many different approaches could be taken to produce rheological modifiers.

To produce an associative thickener, introduction of hydrophobic moieties on either side of the hydrophilic linPG would be required. This could be achieved by using the potassium salt of a fatty-acid alcohol as an initiator, followed by end-capping with a fatty acid. Alternatively, multifunctional initiators could be used to produce star-shaped linPG which could also be end-group functionalised using hydrophobic moieties.

For non-associative thickening behaviour, light cross-linking is desired. Introducing a bifunctional epoxide monomer could achieve this. It is however imperative that the cross-linker used is anhydrous.

Cross-linking linPG post-polymerisation could also be an avenue to obtain the desired swelling properties. Using cross-linking agents such as bifunctional epoxides, diisocyanates, or other bifunctional moieties that are capable of reacting with hydroxyl groups would facilitate the formation of a polymer network. This cross-linking should be performed in a suitable solvent to prevent the formation of a monolithic species.

The biodegradability of the linPG should also be assessed. Whereas oligomeric PGs are biodegradable, it is uncertain whether linPG of significantly greater molar mass will also be. The ability of biological organisms to degrade polymers is known to be molar mass dependent, and so it could be that there exists a threshold above which these materials can no longer be effectively degraded. To circumvent this, hydrolytically cleavable sites could be introduced to the backbone of the polymer by means of co-polymerisation or post-polymerisation chain extension. It is envisaged that cyclic carbonates can be incorporated into the polymer during polymerisation, and that the carbonate linkages could act as hydrolytically sensitive sites to facilitate degradation.[277]

For personal care applications the discolouration observed during polymerisation is unwanted. To increase the applicability of these materials this colour should preferably be avoided altogether or removed post-polymerisation. It is currently uncertain what is the source of the discolouration, and many variables are involved. The simplest avenue to explore for colour removal would be to utilise activated charcoal as a bleaching agent.

5.7 Materials and Methods

Glycidol, *para*-toluenesulfonic acid monohydrate, and anhydrous 2-MeTHF were purchased from Sigma Aldrich. Ethyl vinyl ether, *t*-BuOK (1M in THF), THF, and Amberlyst 15 were purchased from Fisher Scientific UK. Water was deionised before use. THF was dried using aluminium oxide columns in house.

5.7.1 Instrumentation

Nuclear Magnetic Resonance Spectroscopy (NMR)

Polymer formation and chemical structure assignment was determined using ^{1}H-NMR spectroscopy. Approximately 50 mg of sample was dissolved in 0.7 mL deuterated solvent and analysed using a Bruker DPX 400 MHz spectrometer operating at 400 MHz (^{1}H) or 100 MHz (^{13}C), assigning chemical shifts in parts per million (ppm). Spectra were referenced to residual solvent. MestReNova 6.0.2 copyright 2009 (Mestrelab Research S. L.) was used for analysing the spectra.

Gel Permeation Chromatography (GPC)

GPC was performed in THF (HPLC grade, Fisher Scientific) as the eluent at 40 °C using two Agilent PL-gel mixed-D columns in series, an injection loop of 50 µL, with a flow rate of 1 mL·min^{-1}. A differential refractometer (DRI) was used for the detection of samples. Samples were made at a concentration of approximately 2 mg·mL^{-1} in HPLC grade THF, and filtered through a 0.22 µm Teflon filter before injection. The system was calibrated using poly(methyl methacrylate) standards with average molecular weight in the range from 540 to 1.02·10^{6} g·mol^{-1} and low dispersity (*Đ*).

Gas Chromatography

GC was performed using a PerkinElmer Clarus 500 Gas Chromatograph using a flame ionisation detector. Samples were diluted in HPLC grade THF (0.25 g in 25 mL) before injection by an autosampler.

5.7.2 Experimental Procedures

EEGE Synthesis

Glycidol (100 g, 1.35 mol) and ethyl vinyl ether (450 mL) were mixed and cooled (0 °C). To this mixture pTsOH monohydrate (2.00 g, 10.5 mmol) was added slowly (beware of exotherm). The reaction mixture was allowed to reach ambient temperature and stirred (3 h). A slight yellow colour was observed. Subsequently the reaction was washed successively with saturated aqueous $NaHCO_3$, brine, and DI H_2O (approx. 300 mL each). The organic layer

was retained, dried ($MgSO_4$), and concentrated *in vacuo* before vacuum distillation (70-80 °C, 20 mbar) to yield the product as a colourless liquid (175 g, 1.20 mol, 89% yield). See Appendix Figure 30 for ^{1}H-NMR assignment.

Synthesis adapted from Spassky *et al*.[270]

Anionic Polymerisation of EEGE

In a typical procedure, dried EEGE (20.0 g, 137 mmol) was stirred under argon atmosphere in flame-dried glassware. Solvent (dry THF or 2-MeTHF), if used, was added at this stage. The EEGE was heated to reaction conditions and allowed to equilibrate before the rapid injection of initiator (2 mL ^{t}BuOK in THF, 1 mol dm^{-3}, 2 mmol). After 24 h, the reaction was quenched by addition of MeOH (approx. 1 mL), and solvent (if used) was removed *in vacuo*. The reaction was washed (15 mL, water) to give the product as a viscous brown liquid.

Various chain lengths were targeted by altering the quantity of initiator added.

Supercritical Extraction

A glass vial containing pEEGE was placed inside a 60 mL autoclave base. The pEEGE was stirred magnetically (150 RPM). The autoclave headspace was stirred using an impeller (300 RPM). The autoclave was flushed with CO_2 (15 min, 50 psi), before being sealed and pressurised (5.5 mPa). The autoclave was heated (80 °C), and additional CO_2 was added (pressure increased to 20.7 mPa) and allowed to equilibrate (15 min). The outlet tap was opened, and the pressure was maintained by opening the inlet tap in order to establish a flow of $scCO_2$ through the autoclave (approx. 10 mL·min^{-1}, 15 min). Following extraction, the autoclave was allowed to equilibrate (30 min, 20.7 MPa, 80 °C) before repeating the extraction and equilibrating steps two more times.

Deprotection of pEEGE

pEEGE (approx. 20 g) was dissolved into ethanol (15 mL), and water (10 mL) was added. Amberlyst 15 (0.57 g) was added, and the mixture was stirred (5 days, ambient temperature). Amberlyst 15 was removed by filtration, and volatiles were removed *in vacuo* to yield the deprotected polymer.

Kinetics in Solventless Conditions

EEGE (50.0 g, 0.342 mol) was magnetically stirred and heated (60 °C) under a flow N_2 gas. Once the EEGE had equilibrated at reaction temperature, initiator (*t*-BuOK, 1 mol·dm^{-3} in THF, 5 mL, 0.005 mol) was injected rapidly. A colour change from colourless to brown was observed following initiator addition, and temperature rose to 64 °C. After 6 h the reaction

was allowed to cool to ambient temperature and sealed under an N_2 atmosphere. The following day, the flow of N_2 was reinstated and the reaction vessel was heated (60 °C) and allowed to equilibrate (1 h). At this point, additional initiator (*t*-BuOK, 1 mol·dm^{-3} in THF, 2.5 mL, 0.0025 mol) was injected rapidly. A marked increase in viscosity was observed 2 h after the second dose of initiator, and the magnetic stirrer was oscillating rather than rotating freely.

Chapter 6. Project Vole

The experimental work in this chapter was performed in collaboration with Eduards Krumins.

6.1 Aims & Objectives

Volumetric Additive Manufacturing (VAM) is an exciting new technique that enables rapid production of three-dimensional parts on short timescales. Unfortunately, the current selection of resins is limited, and they are usually petrochemically derived.

This chapter investigates commercially available PG6 as a biobased building block to develop a photoactive resin for use in VAM.

6.2 Abstract

Volumetric printing is a ground breaking advancement in Additive Manufacturing, offering a cohesive and efficient approach to create objects, circumventing the traditional layer-by-layer paradigm.[143] This innovative technique provides unparalleled design freedom and significantly reduces printing times.[143] To support this revolutionary technology, PG6 has been used to develop a sustainable resin. PG6 is an easily functionisable, colourless, and bioderived oligomer. The synthetic route used to transform polyglycerol-6 into a photo-printable resin is a scalable, one-pot process. PG6-acrylate meets all the essential criteria for successful volumetric printing and has been effectively used to print various models with intricate geometries and reasonably high resolutions.

An outstanding feature of the resin is its reusability, promoting efficient resin utilisation and minimising waste production. Moreover, through the incorporation of dopants like fluorescein, and 10,12-pentacosadyinoic acid (PCDA), the ability to print objects with diverse functionalities has been demonstrated. This includes temperature sensing probes and builds containing a drug-like molecule, showcasing the vast potential applications of this technology. In this chapter, the successful development of a bio-based, biocompatible, functionisable, and scalable resin for volumetric printing is showcased, signifying a remarkable advancement towards environmentally sustainable resins in the additive manufacturing industry. This resin's versatility and eco-friendly attributes hold great promise for fostering a more sustainable future in AM and opening new avenues for innovative applications across various industries.

6.3 Introduction

In this chapter, the potential of PG (polyglycerol) as a biobased building block for volumetric printing resins was explored. PGs stood out due to their optical clarity, broad range of viscosities, and abundance of accessible hydroxyl groups for functionalisation.

PGs have been previously introduced in this thesis for their viability as green polyol building blocks for the synthesis of polyol polyesters. To enable the curing of PGs, acrylate groups were introduced by esterification. Acrylic acid, being the simplest acrylate source, ensures the highest atom economy during esterification with polyglycerol. Currently, acrylic acid is produced from propene using petrochemical processes in gas phase oxidation.[100] However, with growing consumer demand for responsible and sustainable practices, the development of biobased acrylic acid is gaining traction. Glycerol, lactic acid, and furfural have all shown potential as suitable biobased feedstocks to produce acrylic acid.[22,278,279]

While renewable acrylic acid pathways still face challenges in terms of economies of scale compared to the petrochemical route, ongoing advancements and depletion of petroleum feedstocks can lead to increased commercial competitiveness of bioderived acrylic acid in the future.[278] As a result, volumetric printing resins based on PG hold promise for more environmentally friendly and sustainable 3D printing applications.

Synthesis of a bio-sourced "platform-resin" by utilising PG and acrylic acid as the foundational reagents was targeted. The vision for the platform-resin is to serve as the basis for future formulations, where additional substances can be easily mixed in to impart specific functionalities and behaviours to the resin. From this platform-resin, a wide range of applications can be targeted simply by adjusting the additives in the formulation. This eliminates the need for specialised synthetic expertise in-house, making volumetric printing more accessible to a broader audience.

To develop the platform resin for volumetric printing, PG6 and acrylic acid were employed in a straightforward, one-step, solventless synthesis method. Through this approach, we successfully printed parts with excellent resolution. We also introduced various dopants into the resin to display its ability to incorporate diverse functionalities, further validating its suitability as a platform-resin for volumetric printing applications.

6.4 Results and Discussion

6.4.1 Resin Synthesis

Fischer esterification between PG and acrylic acid in the presence of catalytic sulfuric acid was selected as the synthetic route employed in this work (Figure 121). This synthetic pathway was performed in one step in solvent-free conditions using relatively mild conditions. Utilisation of this straightforward methodology allowed for coupling agents and extensive purification procedures to be avoided, maximising large-scale applicability and atom economy.

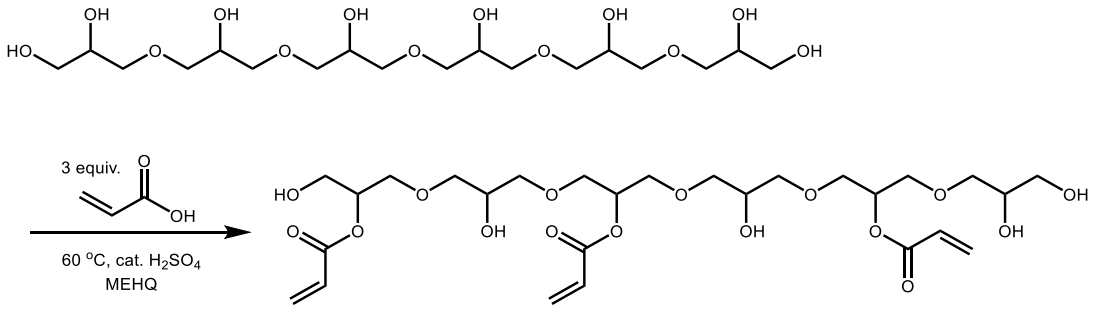

Figure 121 Reaction scheme for the synthesis of PG6-acrylate by Fischer esterification of PG6 and acrylic acid. Structure of PG6 shown is idealised.

Utilising ^{1}H-NMR spectroscopy in combination with acid value titration, conversion of acrylic acid was determined to be 63-75% (Appendix Figure 34,35 and Appendix Table 10). This shows unreacted acrylic acid is present in the produced PG6-acrylate, although for the purposes of VAM this was not deemed to be a cause for concern at this stage. It was expected that residual acrylic acid would simply be co-polymerised during the printing process.

Resins suitable for VAM exist in a “Goldilocks region” with regards to viscosity. Printing using a resin of insufficient viscosity will lead to sedimentation of the building part, which is accompanied by a complete loss of resolution (Figure 122). Excessively high resin viscosity will however make processing impractical during the synthesis and printing stages of the process.

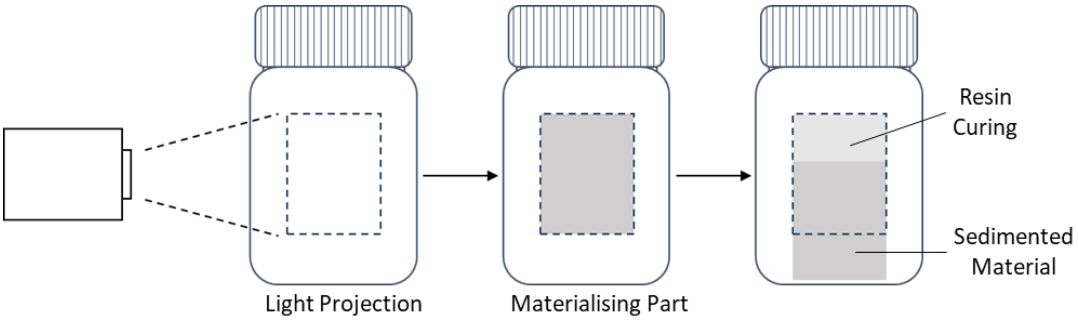

Figure 122 Schematic of a materialising part in a vial containing photoactive resin of insufficient viscosity, resulting in sedimentation of the building part away from the area of light exposure.

The viscosity of PGs is highly dependent on their degree of polymerisation (see Chapter 3). PG4, PG6, and PG10 were all evaluated for their potential as frameworks for a VAM resin. It was found that PG4-acrylate was of insufficient viscosity, and during printing resulted in sedimentation of the printing part. PG10 was found to be excessively viscous, hindering acrylation altogether. PG6-acrylate was found to be a suitable middle ground for VAM, where parts did not visibly sediment during printing, and processing steps were not hindered by excessive viscosity (Figure 123). PG6 was therefore the PG of choice for the production of a VAM resin.

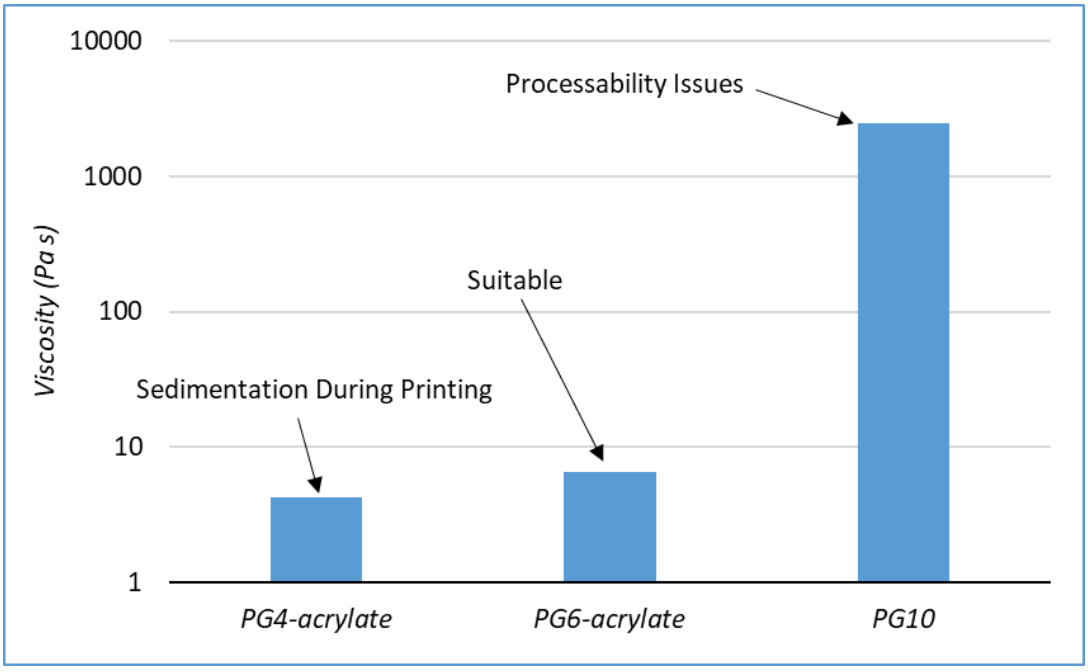

Figure 123 Viscosity of PG4-acrylate, PG6-acrylate, and PG10 at 25 °C, shear rate of 10 s^{-1}.

6.4.2 Printing Optimisation

The investigation into photoinitiator loading was conducted by printing cylindrical pill-like structures. To ensure cytocompatibility and resin solubility, lithium phenyl-2,4,6-trimethylbenzoylphosphinate (LAP) was selected as photoinitiator. A range of loadings, from 1 to 0.005 wt.%, were tested, and it was found that 0.075 wt.% proved to be the most suitable. Higher loadings led to overcuring before the full frame count could be completed, due to excessive absorption of light by the photoinitiator, preventing it from permeating throughout the resin volume. On the other hand, lower loadings (0.05-0.005 wt.%) resulted in unreactive resins, and no curing was observed in the printing parameters investigated. The optimal loading of 0.075 wt.% struck the right balance, enabling successful printing and avoiding overcuring issues. Accordingly, 0.075 wt.% photoinitiator loading has been used throughout this chapter.

The resin's performance with the optimized photoinitiator loading was assessed by printing various objects with diverse geometrical features using the VAM set-up. Initially, the focus was on printing cylindrical pill-like structures using PG6-acrylate (Figure 124A). Three pills were printed simultaneously, increasing the number of pills manufactured per print beyond what is seen in the literature.[146] After successfully printing these basic pill structures, more intricate objects such as a chess piece, a rabbit, a model of Rodin's *The Thinker*, and a sphere encased within a four-pillared cage were printed (Figure 124 B-E). It was essential to fine-tune the printing conditions for each unique structure, considering the voxelization program's varying intensity of projected light, depending on shape thickness and geometry (Appendix Table 11).

For instance, achieving the highest resolution for the sphere trapped in the pillared structure required an 18-second exposure time (Appendix Table 11). Among the printed objects, the chess piece demonstrated the highest resolution, with the smallest feature size measuring between 300 and 500 µm (Figure 124B). While the current maximum resolution achieved in volumetric printing is approximately 80 µm,[149] we managed to achieve a remarkable maximum resolution of around 300 µm.

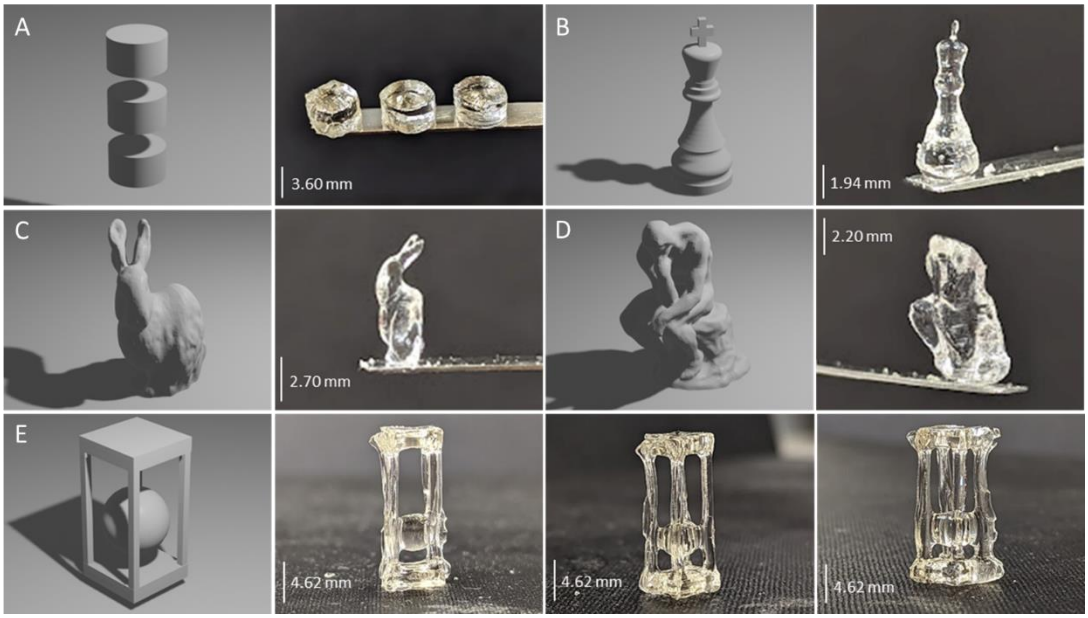

Figure 124 CAD Designs and parts printed with PG6-acrylate.

The ultimate resolution achieved is affected by several factors. Imperfect lateral alignment leads to distortions because the projection is not precisely centred onto the vial. Likewise, imperfect rotational alignment causes precession effects that limit resolution. To address these issues additional optimisation of the experimental set-up is required. For example, recalibrating the projector to the centre before every print could improve the lateral alignment. The cylindrical nature of the vial containing the photoactive resin also results in cylindrical lensing effects, which can lead to warping effects in the build. It is possible computational adjustments to the projection protocol might offer a solution to compensate for this effect and improve print quality.

These builds were produced at exceptional speed. The pills were printed in less than 30 seconds, and more complex shapes were produced in under 60 seconds (Appendix Table 11). Utilising other AM (Additive Manufacturing) techniques, similar builds can take between 20 and 60 minutes.[280] These builds also highlight the ability of VAM to produce parts with overhanging segments without the need for support structures. Owing to the suitable viscosity of the PG6-acrylate resin, the uncured resin present in the vial acts as a built-in support for the building part.

Overall, these builds demonstrate the suitability of PG6-acrylate as a renewably based resin for VAM. Parts with internal cavities, fine features, and various geometries were printed rapidly. Furthermore, the parts obtained exhibit good transparency and smoothness.

6.4.3 Resin Reusability

The reusability of unused resin was examined by collecting uncured resin after a completed build had been removed and utilizing it to volumetrically print an additional structure (Figure 125). The primary focus was to explore the potential of reusing uncured resin, thus significantly reducing waste.

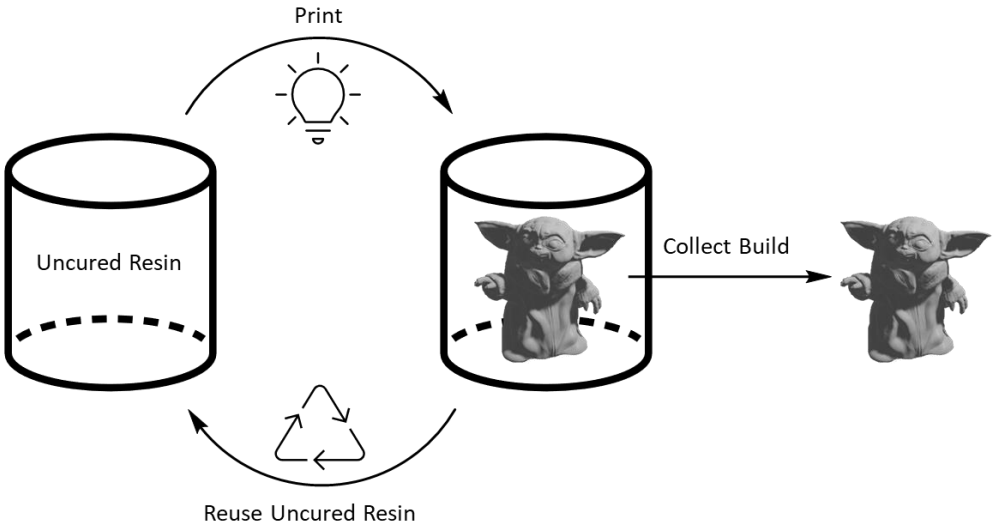

Figure 125 Schematic of the resin reuse strategy employed.

To evaluate the feasibility of using recycled resin, pill structures were chosen as test samples. The results showed that a total exposure time of 14.4 seconds produced a part with resolution comparable to that achieved with virgin material (Figure 126, Appendix Table 12). The slight deviation in printing parameters can be attributed to the light exposure during the initial printing cycle and the interior laboratory lighting during part collection and resin separation. When using the same pill design, it was observed that the pills printed with recycled resin were approximately 90% of the size of those printed with virgin resin (Figure 126). This finding highlights the need to adjust printing parameters based on whether virgin or recycled resin is used, as well as the geometry of the printed part.

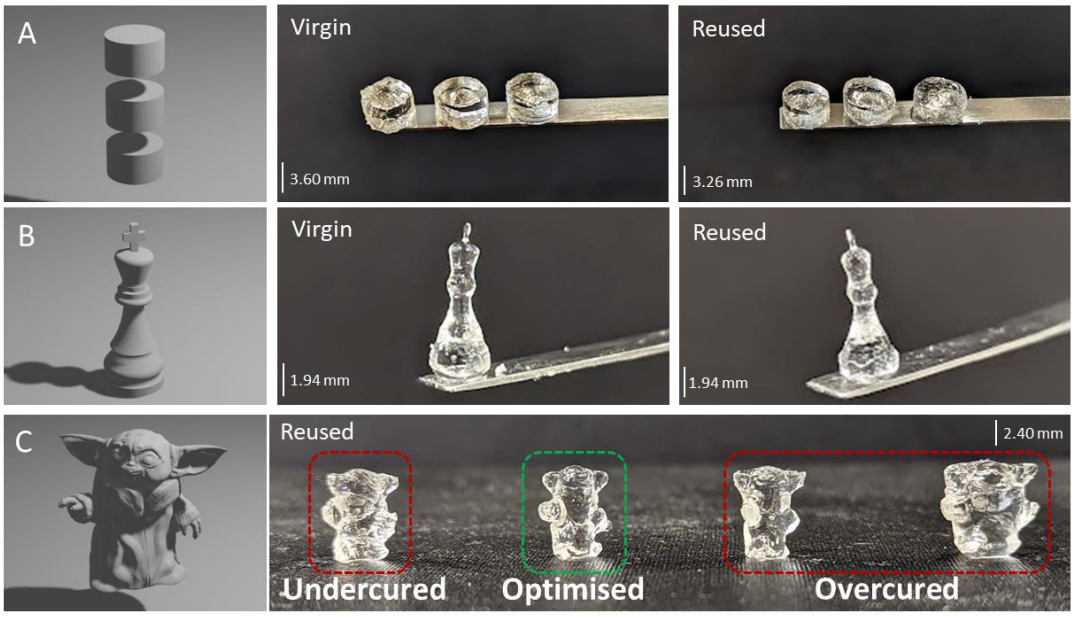

Figure 126 CAD Designs and parts printed with reused and virgin PG6-acrylate.

To assess the performance of the virgin resin compared to the recycled material, we printed alternative designs, including a chess piece (Figure 126B). Both the virgin and recycled chess pieces displayed identical base thickness and remarkably similar minimum feature size. Notably, the recycled chess piece had a top width of 0.5 mm, slightly larger than the virgin material's width of 0.4 mm. This close resemblance between the virgin and recycled parts provides robust evidence supporting the viability of using recycled material for volumetric printing.

To investigate the feasibility of printing more complex geometries using recycled resin, we delved into a more intricate design inspired by a well-known science fiction character. This design featured numerous small features and large overhanging segments (Figure 126D). Through testing different printing parameters, we identified that the optimal resolution for this design was achieved with a total exposure time of 30 seconds. Exposure times outside a narrow temporal window, specifically between 27 and 33 seconds, led to under-curing and over-curing, respectively (Appendix Table 12). To further enhance recyclability, it might be advantageous to blend virgin resin with a fraction of reused resin, an approach commonly adopted in other additive manufacturing techniques.[281] This combination could potentially offer improved printing performance and contribute to a more sustainable VAM process.

6.4.4 Biocompatibility

Biocompatibility experiments were performed in collaboration with Ben Sutcliffe and Robert Owen.

The biocompatibility of pills printed using PG6-acrylate was evaluated both before and after post-processing treatments (Figure 127). Non-processed prints made with PG6-acrylate exhibited the leaching of toxic material into the cell growth medium, resulting in cell death. Moreover, the presence of acidic compounds was indicated by the yellow colour of the phenol red pH indicator in the extraction medium. These findings strongly suggest that unreacted acrylic acid becomes trapped in the print and can elute from the polymer matrix, leading to the observed cytotoxic response. However, the post-processed builds showed no signs of cytotoxicity. This indicates that appropriate post-processing treatments effectively mitigate the release of harmful substances, ensuring the biocompatibility of the printed pills.

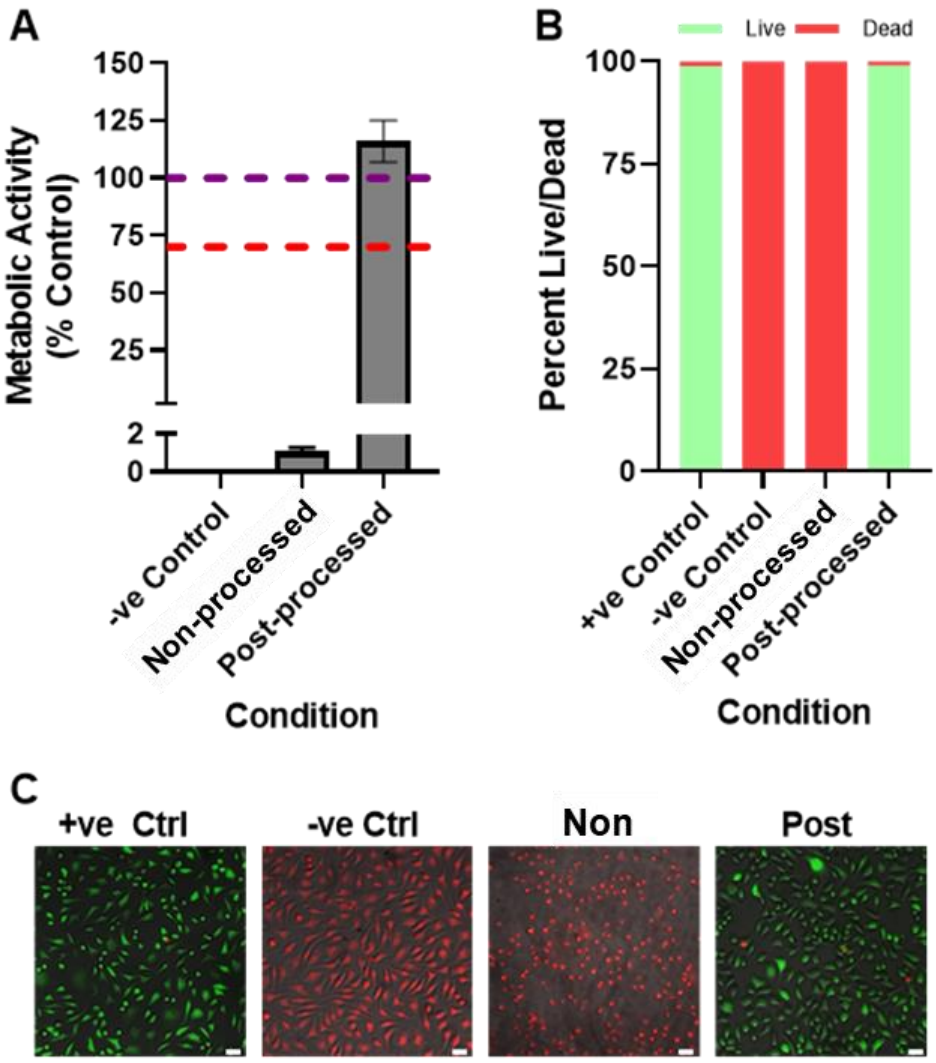

Figure 127 Extract cytotoxicity testing of non-processed and post-processed parts printed using PG6-acrylate. A: Metabolic activity, B: percentage of live/dead cells, C: representative images of overlaid Live (green) and dead (red) images, scale bar 100 µm).

Micro-Raman spectroscopy was employed to evaluate the curing extent of the fabricated samples by quantifying the ratio of signals related to alkene and carbonyl bonds. The analysis revealed a remarkable degree of curing of 99% for the post-processed PG6-acrylate build, whereas the non-processed build exhibited a significantly lower degree of curing at 58% (Appendix Figure 36). These results strongly support the hypothesis that the cytotoxic response observed before post-processing is attributed to the presence of unreacted acrylic compounds. The higher degree of curing achieved through post-processing effectively eliminates these compounds, ensuring enhanced biocompatibility of the printed samples.

6.4.5 Introduction of Guest Species

Fluorescein

To evaluate the potential of the resin to act as a payload carrier, we conducted an initial proof of concept using fluorescein as a model drug to monitor its release from a printed part (Figure 128).[282,283] This exciting prospect could pave the way for custom-made implants with desired shapes and release profiles, enabling targeted and controlled delivery of therapeutic agents in the future. The fluorescein was incorporated by simply mixing it into the PG6-acrylate resin, highlighting the ease of functionalising the resin.

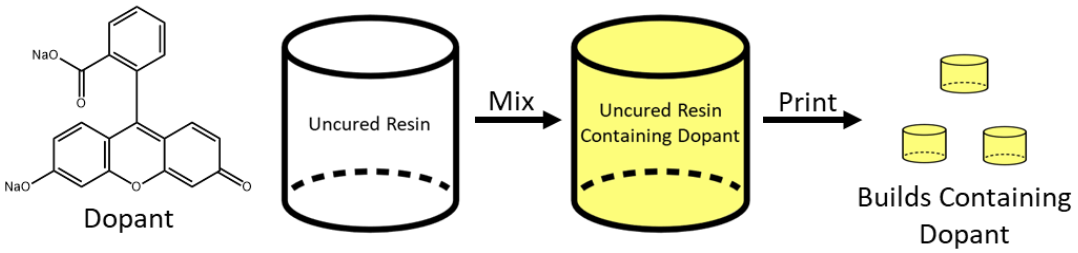

Figure 128 Schematic of incorporation of dopant into PG6-acrylate and subsequent printing.

The resin displayed impressive flexibility, easily accommodating fluorescein while preserving optical purity and homogeneity. This successful integration of fluorescein into the resin further underscores its potential as a versatile and effective payload carrier. The results from this study open new possibilities in the field of drug delivery and personalized medicine, offering the potential for highly tailored treatment approaches utilising VAM and the PG6-acrylate resin.

The introduction of fluorescein into the resin increased the occurrence of partially cured fragments outside the desired build design (Figure 129). As a result, adjustments to the printing conditions were necessary (Appendix Table 13). This change in printing behaviour is due to the dye absorbing incident light and potentially activating the photoinitiator upon re-emission. After optimisation efforts, reasonable resolution was achieved, allowing for the printing of a more complex build with internal voids (Figure 129B).

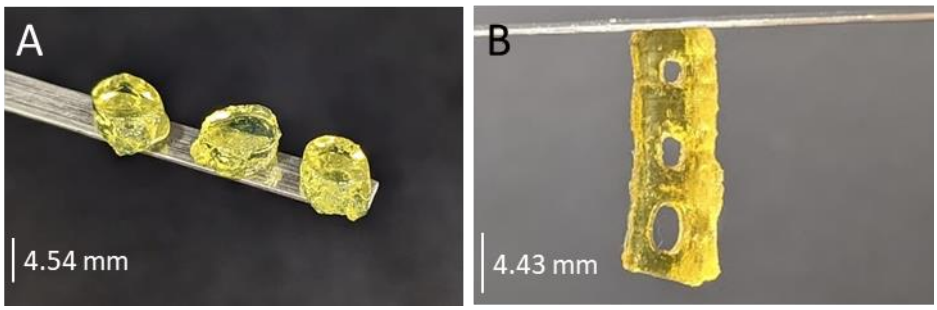

Figure 129 Parts printed with fluorescein-doped PG6-acrylate.

To quantify the release of fluorescein from a pill, UV spectroscopy at 490 nm was employed (Figure 130).[283] The results indicated a remarkably rapid release, with nearly complete release achieved within just one hour. This swift release is attributed to the high-water solubility of the fluorescein sodium salt used in the study. However, to explore different release profiles and fine-tune applications, further investigation involving more hydrophobic compounds is necessary. More hydrophobic compounds are expected to exhibit slower release profiles, allowing for a more prolonged, gradual release.[284] Additionally, modifying the geometry of the printed part can also impact the release characteristics.[285]

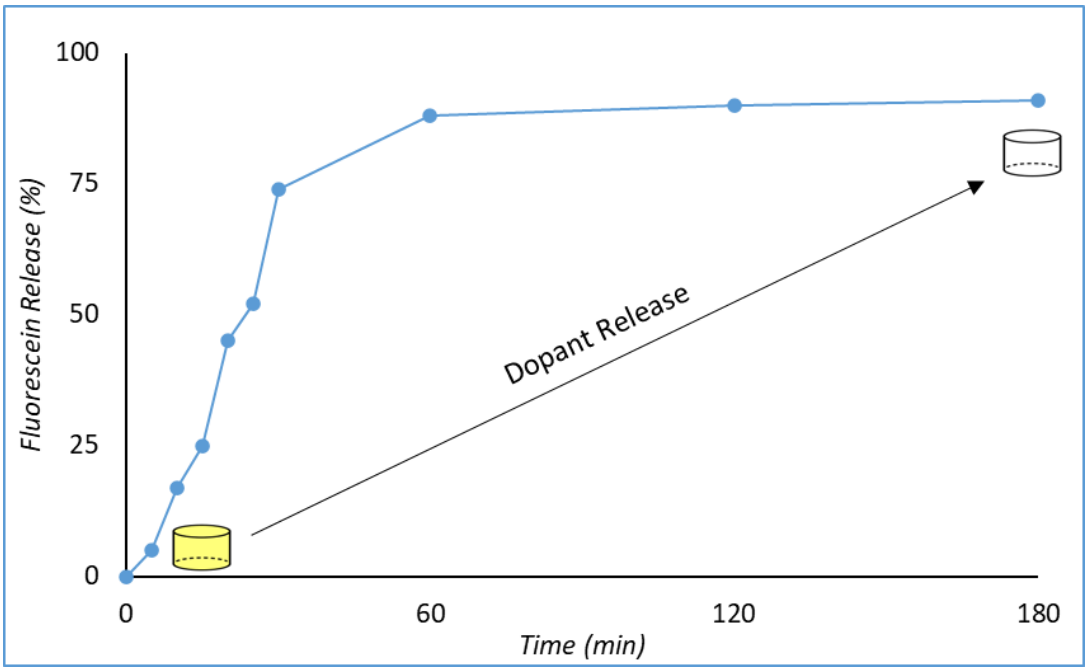

Figure 130 Release of fluorescein into aqueous media from a pill printed with fluorescein-doped PG6-acrylate.

Thermoresponsive PCDA Micelles

Temperature sensing properties were integrated into the formulation by introducing micellar solutions of polydiacetylenes.[286] Diacetylenes polymerise when exposed to UV light, forming a coloured conjugated polymer network. When exposed to heat, polydiacetylenes undergo a conformational transition, resulting in an irreversible colour change.[286]

One example of a thermoresponsive system is based on 10,12-pentacosadiynoic acid (PCDA).[287] PCDA self-assembles into colourless micelles, and the backbone can be polymerised by curing with UV light, imbuing a blue colour to the system. When these blue polymeric micelles are exposed to thermal energy, the conformational change causes the micelles to become red (Figure 131). The suspensions of polydiacetylenes, both before and after thermal stimulation, exhibited a narrow size distribution (Appendix Figure 37). Specifically, the red-phase PCDA displayed larger sizes (Appendix Table 14), due to its conformational change from planar to nonplanar upon stimulation.[287]

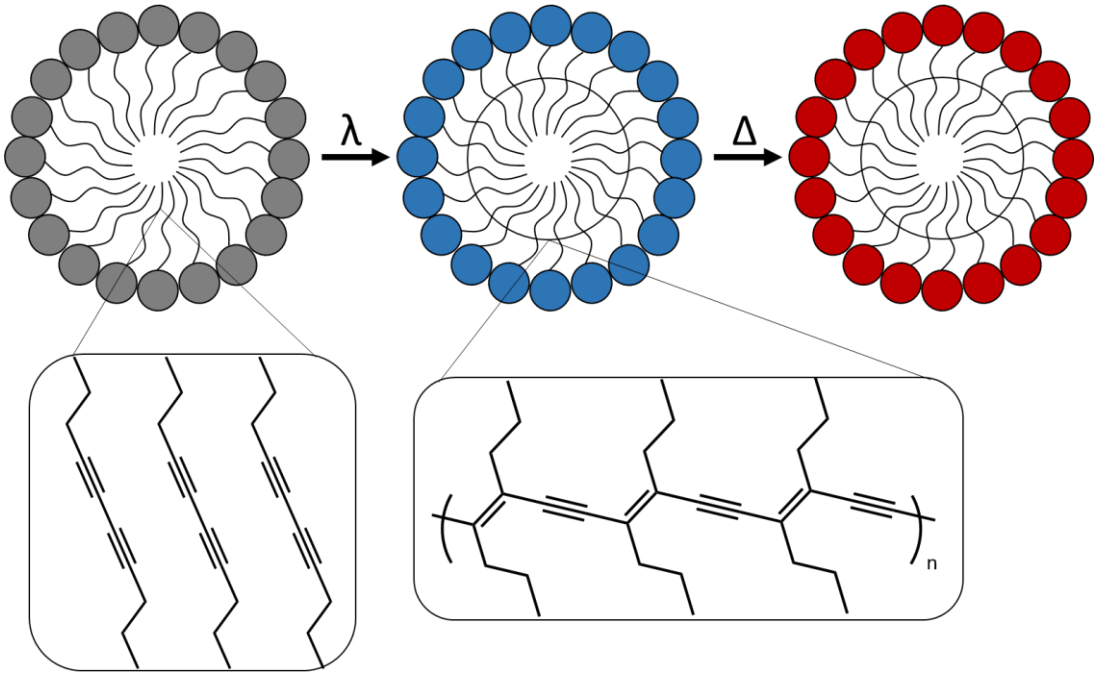

Figure 131 Schematic of a PCDA micelle (left), following photoinduced polymerisation (middle), and following exposure to elevated temperatures (right).

To introduce thermal responsiveness into the PG6-acrylate resin, a suspension of PCDA crosslinked micelles was effortlessly mixed into the resin before printing, highlighting the versatility and simplicity of introducing modifications to the resin. The resulting faintly blue thermoresponsive resin was then used for volumetrically printing cylindrical pills. The printed pills appeared faintly yellow, indicating a partial colour change during the printing process due to localized heating. Subsequently, exposing the printed pills to elevated temperatures triggered a colour change from faint yellow to red (Figure 132). The quality of the printed parts was high following some trial-and-error printing optimisation (Appendix Table 15). This successful demonstration clearly illustrates the resin's capability to incorporate thermoresponsive properties with a straightforward approach. The ability to introduce temperature sensing capabilities expands the potential applications by means of functional modification.

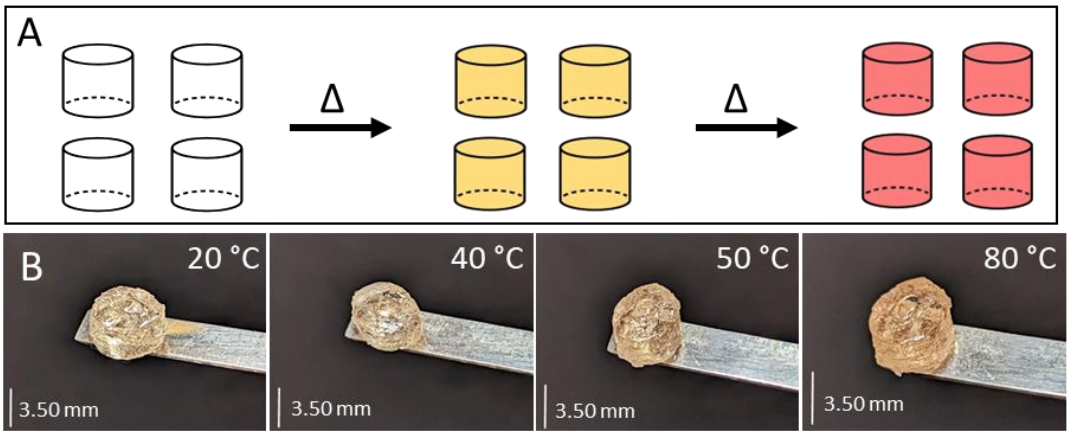

Figure 132 A: Schematic of colour changing parts, B: Images of a printed pill following 30-second exposure to various temperatures.

Fluorescence microscopy clearly captures the temperature-induced change in the build. Prior to heating, the PCDA containing builds exhibited a weak red fluorescent response, whereas after heating, red fluorescence became stronger with increasing temperature (Figure 133). An increase in blue fluorescence is also observed upon heating from 20 to 40 °C. This could be caused by some residual PCDA polymerising, increasing the presence of blue conjugated polymer. A decrease in blue fluorescence is seen between 50 and 80 °C, which would indicate that blue conjugated polymers are undergoing a conformational change to exhibit red fluorescence instead.

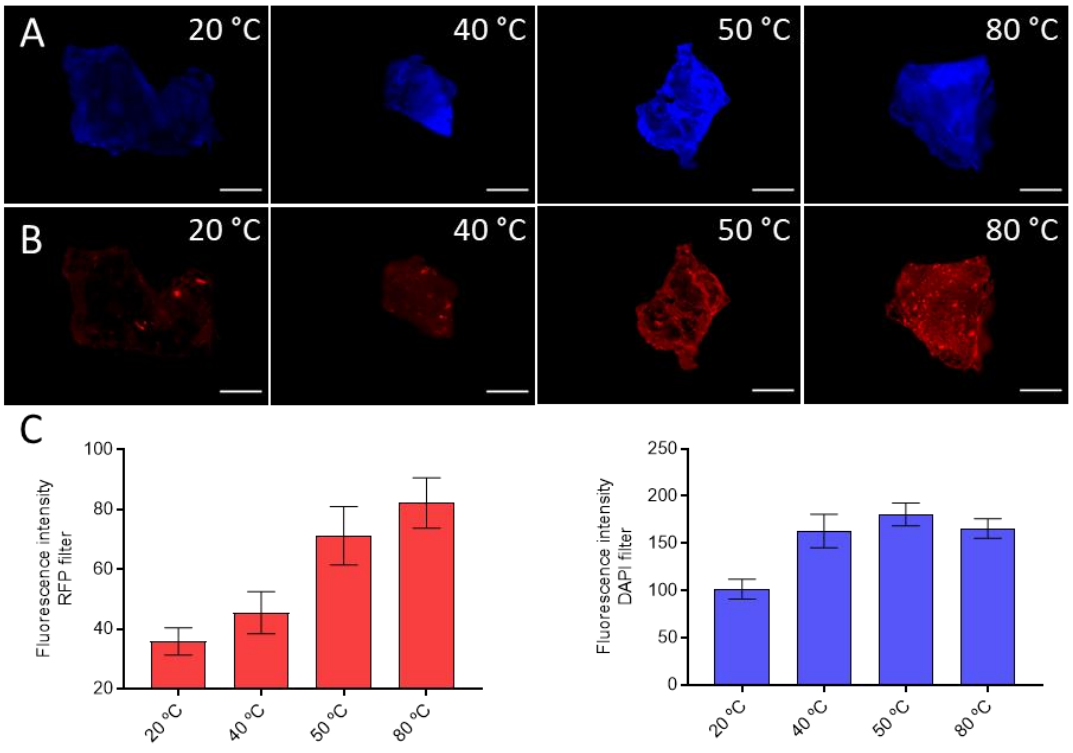

Figure 133 Fluorescence microscopy images using red fluorescent protein (RFP) (A) and 4',6-diamino-2-phenylindole (DAPI) (B) filters. Bar charts represent mean intensity over the RFP and DAPI filtered images (C).

Thermoresponsive polymers find versatile applications in various fields such as biomedicine and the transportation of temperature-sensitive materials like vaccines. In biomedicine, these polymers could be employed to create wearable fever alerts. For temperature-sensitive material transportation, the polymers serve as a clear and visual indicator of adherence to maximum temperature regulations. Moreover, the colour change of the polymers can indicate the temperature in a printing vat, assisting in identifying suitable printing conditions. The incorporation of thermoresponsive properties in the resin broadens its utility and enhances its potential for diverse applications in different industries.

6.5 Conclusions

The primary objective of this experimental work was to expand the range of materials available for VAM. A biobased resin was introduced, with the aim to reduce dependence on petrochemical feedstocks.

PG6 was shown to be a suitable building block for the development of a photoactive material with a suitable viscosity for use in VAM. The resin was produced using a scalable, atom-economical, and robust synthetic process. This PG6-acrylate resin proved versatile, enabling the rapid printing of a variety of objects, from pill-like components to models like *The Thinker* by Rodin. Reusability of uncured resin was also demonstrated, and complex parts with overhanging angles and fine features were printed using recycled resin. Following post-processing, the produced parts were also found to be biocompatible.

To extend the range of functionality present in the resin, active ingredients were incorporated prior to printing. Fluorescein was incorporated to study the effect of introducing a complex organic molecule, and to observe subsequent release behaviour from the printed part. Thermoresponsive PCDA micelles were also added to the PG6-acrylate, enabling the production of parts that changed colour upon heating. This exciting feature could pave the way for applications such as wearable temperature monitors, or temperature sensors for the transportation of sensitive materials such as vaccines.

The transition from petroleum-based resins to bio-resourced, functionisable, and versatile systems like polyglycerol represents a significant advancement toward sustainable manufacturing in volumetric printing. These advancements have the potential to revolutionise not only the Additive Manufacturing field but also interconnected industries, including healthcare and consumer products. Embracing such sustainable practices is crucial for the future of manufacturing and offers a pathway towards a more environmentally friendly and innovative approach to material design and production.

6.6 Further Work

Further developments to the PG6-acrylate synthesis can be made. The current procedure results in 63-75% acrylic acid conversion. Driving this reaction to quantitative conversion would be desirable to prevent acrylic acid being present in the resin. Alternative esterification catalysts (such as titanium butoxide, potassium carbonate, and many others), could be explored. Increasing reaction temperature could aid evaporation of water and increase conversion. In addition, purging the reaction vessel continuously with air would improve the kinetics of condensate evaporation and drive the reaction forward. Decreasing the molar equivalents of acrylic acid present would also increase the conversion due to a shift in the equilibrium between hydroxyl and carboxylic acid groups. Decreasing acrylic acid loading would also influence the cross-linking density of the final printed part, as well as require re-optimisation of printing conditions and photoinitiator loading.

Performing transesterification of methyl acrylate, rather than esterification with acrylic acid, could also be beneficial to improve conversion due to the lowered volatility of the condensate formed.

Incorporating a fraction of water could also be an interesting approach to producing hydrogels with varying geometries. Critical to the success of printing using VAM is the viscosity of the resin, and this would have to be taken into account during resin formulation. A potential method to achieve a suitable viscosity would be to utilise rheological modifiers. Using a rheological modifier, the library of available monomers is expanded, as low-viscosity monomers can be made suitable in an appropriate formulation.

To build on the dopant species aspects of this work, more species should be investigated. More specifically, introducing drug molecules can be a promising avenue to target personalised medicine applications. The sodium salt of fluorescein employed in this work had a very rapid release profile. Increasing hydrophobicity of the drug molecule used could slow down the release rate. Alternatively, binding the drug to the resin backbone with a hydrolytically cleavable bond could allow for more prolonged periods of release. This could also be achieved by incorporating “drug-monomers” into the resin formulation.

6.7 Materials and Methods

Polyglycerols 4,6, and 10 were kindly donated by Spiga Nord. Acrylic acid, lithium phenyl (2,4,6-trimethylbenzoyl) phosphinate (LAP), 10,12-pentacosadyinoic acid (PCDA), and fluorescein (sodium salt) were purchased from Sigma Aldrich UK. 4-Methoxyphenol was purchased from Fluka. Concentrated sulphuric acid, and DMSO were purchased from Fisher Scientific.

6.7.1 Resin Preparations

General Procedure Polyglycerol 6 – Acrylate Resin

Polyglycerol 6 and acrylic acid (3:1 mol:mol ratio of acrylic acid to polyglycerol 6) were combined and mechanically stirred. 4-Methoxyphenol (1 wt.%) was added and dissolved. Subsequently sulphuric acid (2.5 wt.%) was added and the reaction mixture was heated to 60 °C and stirred at 200 RPM for 3 hrs. The reaction mixture was allowed to cool and wrapped in aluminium foil to protect it from light. At this stage, dopants such as PCDA micelles, or fluorescein were added. Photoinitiator (0.075 wt.% LAP) was added and the mixture was stirred until homogeneous. The resin was transferred to aluminium foil wrapped glass scintillation vials (4- or 20-mL vials), the vials were centrifuged (2000 RPM, 10 min) to remove trapped air bubbles.

PCDA Micelles Preparation

PCDA vesicles were made by solubilising PCDA (4 mg) in DMSO (1 mL). The obtained solution was added dropwise to 9 mL of deionised (DI) water under stirring (500 RPM) at room temperature to a final concentration of 0.4 mg·mL^{-1} (1.1 mM). Then, each sample was stored at 4 °C overnight to let the system self-assemble. UV polymerisation was performed at 254 nm for 20 min, by using an UV lamp placed on top of the vial.

6.7.2 Volumetric Printing Procedures

Projection Design from Three-Dimensional Build

A tomographic reconstruction (designed on the basis of CAL Github Repository) was used to generate the dynamically evolving projection image set for the VAM printer. The software is given a three-dimensional model (STL file) and generates a sequence of two-dimensional grayscale images.

Computed Axial Lithography (CAL) Based Volumetric Printer Set-Up

A benchtop version of a CAL system was developed (Figure 134). The system is composed of a digital light processing projector, collimating optics and a rotary stage which carries the vial

containing photocurable resin. The image sequence generated is sequentially projected onto the resin vial in tandem with stepwise rotation of the vial to spatially control the curing of resin within the volume. The projector used has a resolution of 912x1140 pixels arranged in diamond configuration and has a built-in UV LED with a centre wavelength of 405nm and a total output power of 700mW. With 8-bit modulation capability, the projector can vary the intensity of each pixel into 256 levels allowing it to modulate light intensity throughout the projection space. A combination of doublet lenses (50- and 100- mm focal lengths) were used to convert the diverging rays from projector to parallel beams at the vial. These lenses also magnify the projection. This results in a total projection size of 44 x 30 mm and a pixel size of 35 microns at the focus plane.

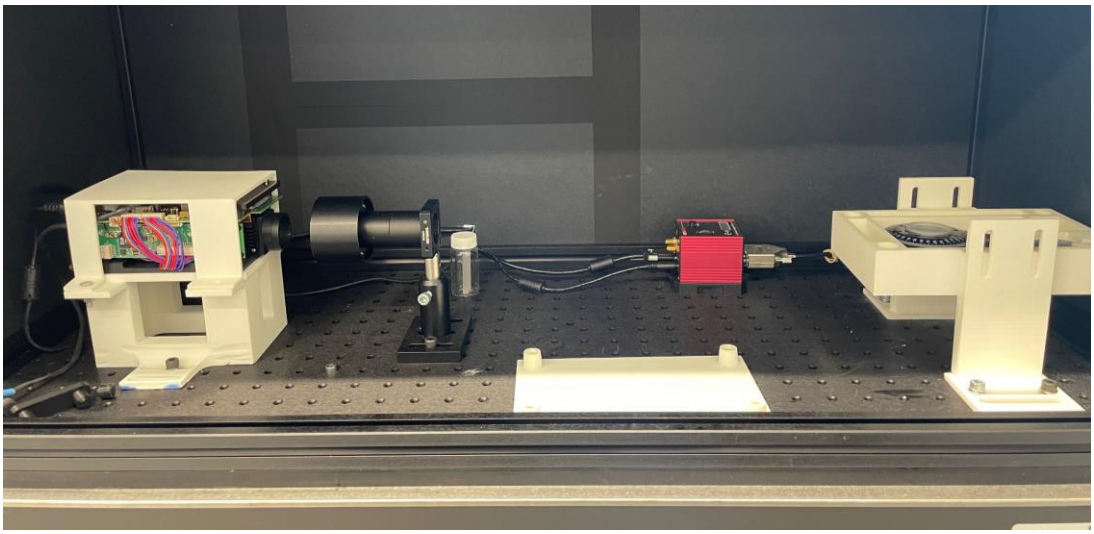

Figure 134 Picture of the volumetric printing set-up used in this work.

Volumetric Printing

A vial containing PG6-acrylate resin (with or without dopants) was mounted onto the rotating stage, and printing conditions specific for each resin and geometry were specified (Appendix Table 11). Upon completion of the printing procedure the vial was removed from the platform, and the sample was collected and rinsed with DI H_2O to remove excess uncured resin. The rinsed samples were placed into a UV chamber (Formlabs) and irradiated to cure unreacted resin (2 min). For cytotoxicity testing purposes the print was post-cured in a UV chamber (Formlabs, 60 min) and washed (500 mL DI water and 500 mL 1M aqueous $NaHCO_3$).

6.7.3 Characterisation

Rheology

Rheological experiments were performed on an Anton Paar MCR102 rheometer, using parallel plate (25 mm) geometry at 25 °C with a measuring gap of 1 mm.

Proton Nuclear Magnetic Resonance Spectroscopy

^{1}H-NMR experiments were performed on a Bruker DPX 400 MHz spectrometer assigning chemical shift in parts per million (ppm). Spectra were analysed using MestreNova 6.0.2 copyright 2009 (MestreLab Research S.L.). Samples were analysed in deuterated DMSO.

Acid Value Determination

Acid value (AV) titrations were performed manually. AV was used to detect the presence of free acidic groups in a certain amount of verging resin and printed scaffold. Desired sample was dissolved in approx. 50 mL of distilled water, and phenolphthalein (0.2 mL, 1 wt.% in MeOH) was added as an indicator. The samples were titrated using aqueous sodium hydroxide (0.5 mol dm^{-3}). The titration was deemed complete when the feintest pink colour persisted for longer than 15 seconds. Acid values in mg KOH per g sample were calculated using the equation below.

$$\mathrm{AV\ (mg\ KOH \cdot g^{-1})} = \frac{\mathrm{T\ (mL)\ \times\ M\ (mol \cdot dm^{-3})\ \times\ 56.1}}{\mathrm{m\ (g)}}$$

Raman Micro-Spectroscopy

Raman spectroscopy was performed using a Horiba Jobin Yvon LabRAM HR Raman microscope. Spectra were acquired using a 785 nm laser, a 50× objective and a 200 µm confocal pinhole. Spectra were detected using a Synapse CCD detector (1,024 pixels) thermoelectrically cooled to −60 °C. Before spectra collection, the instrument was calibrated using the zero-order line and a standard Si(100) reference band at 520.7 cm^{-1}. For single point measurements, spectra were acquired over a minimum range 500–2000 cm^{-1} with an acquisition time of 60 s and 2 accumulations to automatically remove the spikes due to cosmic rays and improve the signal to noise ratio. Spectra were collected from at least three random locations and averaged to give a mean spectrum.

Biocompatibility

Before extract testing, samples were disinfected with 70% ethanol for 15 minutes then rinsed three times in sterile PBS. Extract cytotoxicity testing was performed in accordance with ISO 10993-5. Due to the irregular shape of the printed specimens, extraction was performed at 0.2 g·mL^{-1} for 24 h at 37 °C in basal culture media (BM) composed from Minimum Essential

Medium Eagle (Merck) with 10% FBS. L929 murine fibroblasts (ECACC) were seeded at 20,000 per cm^2 in 24 well plates in 500 µL BM. After 24h, media was exchanged for 500 µL of extract media or control media (BM incubated under the same conditions without extract specimen). After 24 h, negative control wells were killed with exposure to 70% ethanol for 15 minutes then conditions were assayed for viability by PrestoBlue® or Live/Dead staining.

For PrestoBlue® (ThermoFisher) media was replaced with 500 µL of PrestoBlue® working solution (10% PrestoBlue® in BM) and incubated for 1h. The solution was then transferred to a black 96-well plate and read at λex: 560 nm, λem: 590 nm in a plate reader (Tecan Infinite 200, Switzerland), where fluorescence correlates with metabolic activity. In different wells, Live/Dead staining was performed by removing media, rising once with PBS, adding 500 µL staining solution (2 µM Calcein AM, 4 µM Ethidium homodimer-1 in PBS) and incubating for 20 minutes. Cells were rinsed once with PBS, then fluorescently imaged in PBS (Leica DMI3000B). Captured images were analysed using CellProfiler (v2.2.0) by identifying live (green) and dead (red) cells as primary objects (1,000+ cells per condition).

Fluorescent Imaging of Printed Scaffolds

Samples were prepared by slicing into approximately 2 mm cubes, transferred to a glass slide and imaged on an EVOS M5000 fluorescent microscope on DAPI (λex 357/44, λem 447/60) and RFP (λex 542/20, λem 593/40) filters. Subsequent image analysis was performed on ImageJ software (v 1.53) for the quantification of mean fluorescent per gel area.

Chapter 7. Conclusions

7.1 Functional Enzymatic Ring-Opening Polymerisation

In this thesis, the use of HEAA as a functional initiator for eROP using N435 as a green catalyst in a bio-renewable solvent (2-MeTHF) has been demonstrated. The stable HEAA amide bond enables the synthesis of biodegradable aliphatic polyesters with a functional handle, overcoming initiator degradation observed in acrylate-initiated eROP.

Kinetics studies revealed that caprolactone adheres closely to first-order kinetics, while valerolactone deviates slightly from ideal first-order behaviour. The immobilised enzymatic catalyst was found to be highly reusable, retaining catalytic activity for 10 reaction cycles with no detectable support degradation. Incomplete initiator conversion occurred, leading to leftover initiator after all monomer had been consumed. Utilising computational docking techniques, this was revealed to be a result of initiated polymer chains having a greater affinity for the enzyme active site than the initiator itself.

Mono-functional hybrid macromonomers were successfully prepared for the first time *via* eROP. Furthermore, we used HEAA-PCL to produce amphiphilic graft copolymers. Through one-pot eROP and subsequent FRP, we obtained materials capable of self-assembly into nanoparticles, reducing synthetic steps and solvent use. These materials were tested for cytotoxicity against three model cell lines (Caco-2, A549, and A431) and found to be non-toxic at concentrations up to 500 $\mu g \cdot mL^{-1}$, paving the way for future biological applications.

7.2 Synthesis of Sustainable Rheological Modifiers

Hydrophilic polyesters using renewable polyglycerols and DMS were synthesised using K_2CO_3-catalysed polytransesterification. Among the screened polyglycerols, PG4 was the most suitable choice due to its lower viscosity, lack of discolouration upon polymerisation, and processability. The optimal synthesis temperature was found to be 80 °C, resulting in full DMS conversion while minimizing energy intensity and achieving good molar mass (M_w 9244 $g \cdot mol^{-1}$). K_2CO_3 proved to be the ideal catalyst with no discolouration and high conversion. A kinetic study revealed a strong interplay between molar mass, viscosity, conversion, and T_g. Increasing the molar equivalents of DMS in the reaction mixture resulted in the formation of cross-linked material, and when a slight excess (1.25 or 1.5 equivalents) was used the produced material displayed exceptional swelling in aqueous media. The cross-linked species were selected for further evaluation as rheological modifiers for aqueous media.

Post-polymerisation functionalisation with succinic anhydride was successful. Linear PG4-DMS could be readily functionalised in a one-pot procedure. Cross-linked PG4-DMS required alternative methodologies due to the rubber-like consistency of the material. Therefore, functionalisation was attempted using both a cryo-grinding approach as well as a $scCO_2$-based approach. Functionalised cross-linked samples demonstrated a pH dependent viscosity in aqueous solution, although the overall viscosity was decreased relative to cross-linked PG4-1.5DMS without post-polymerisation functionalisation. Maleic anhydride was investigated to incorporate alkene functionality along the polymer backbone, although this yielded brittle solids that were challenging to process.

7.3 Evaluation of Sustainable Rheology Modifiers

Cross-linked PG4-based polyesters were explored for their rheological modification properties and water absorption capabilities. PG4-1.5DMS was selected as the most promising candidate, due to its consistent performance and good viscosity enhancement at loadings exceeding 10 wt.% in water. The thickened solutions exhibited excellent electrolyte tolerance, desirable viscoelasticity, and structural recovery following subjection to high shear. Degradability studies showed hydrolytic degradation, which is highly promising to prevent environmental accumulation following use. Swelling experiments demonstrated significant water absorption capabilities, absorbing as much as 20 times its own mass in water.

Freeze drying gels swollen in an excess of water improved performance. After freeze drying, viscosity enhancements of aqueous solutions were observed already at 2.5 wt.% thickener loading. Viscoelasticity and excellent structural recovery following high shear were also retained. The freeze-dried material was capable of absorbing 50 times its own mass of water, more than doubling the performance relative to the non-freeze-dried material. In addition, the rate of water uptake was greatly increased, as 80% of the total swelling was achieved within one hour instead of the several hours required prior to freeze drying. Furthermore, degradability tests indicate that the freeze-dried material has an improved shelf life, maintaining viscosity of the thickened aqueous solutions for longer periods.

Cytotoxicity of polymers and monomers was tested against skin cells. It was found that DMS was more toxic than the cell death control, and increasing PG4 concentration decreased cell viability to 73% at 0.500 $mg \cdot mL^{-1}$. Thankfully, neither PG4-DMS or PG4-1.5DMS exhibited cytotoxicity towards skin cells at any concentration tested. These data pave the way for *in vivo* testing of these thickeners on skin and are highly promising.

Overall, PG4-1.5DMS is a highly effective, biobased, biocompatible, and degradable aqueous rheology modifier with superior environmental credentials in comparison to commercially available viscosity enhancers.

7.4 Anionic Polymerisation for Linear Polyglycerol

To explore alternatives to the branched oligomeric PGs employed for polyol polyester synthesis, anionic polymerisation of EEGE was performed targeting linear polyglycerol of low dispersity and high molar mass. Utilising *t*-BuOK as an initiator, pEEGE of up to 20.7 $kg \cdot mol^{-1}$ was synthesised with low dispersity ($Đ < 1.2$). Deprotection to linPG was achieved using an immobilised anion exchange resin, simplifying the purification process by eliminating the need for extensive precipitation steps seen in the literature. Supercritical fluid extraction of crude pEEGE was used to efficiently remove unreacted EEGE monomer from the polymer whilst avoid organic solvents. Kinetics in an industrial setting showed successful polymerisation that can be monitored using GC. The viability of a second initiator dose to drive monomer conversion was also demonstrated. Attempts at cross-linking using PEG-diglycidyl ether were unsuccessful, presumably due to contamination of the PEG with water. Anionic polymerization of protected glycidol offers advantages in molar mass and linearity, but involves less benign feedstocks of petrochemical origin, raising safety and environmental concerns. Furthermore, protecting groups are essential to the synthesis, lowering the atom economy of the process.

7.5 Project Vole

A biobased resin for VAM was introduced utilising PG6 as the primary building block. Acrylation of PG6 using Fischer esterification yielded a clear resin, which was suitable for volumetric printing after addition of 0.075 wt.% photoinitiator. This resin was used to print various geometries with overhanging feature and fine details. Uncured resin was reused, and was used to manufacture a selection of objects, including a well-known science fiction character with complex features and protruding segments. Following additional UV curing and washing the produced parts exhibited biocompatibility.

Fluorescein and thermoresponsive PCDA micelles were incorporated into the resin to enhance its functionality. Fluorescein was incorporated into the resin as a drug-like molecule and released from the printed part within one hour. Embedding PCDA micelles into the resin allowed for the volumetric printing of thermoresponsive parts, which undergo a permanent colour change upon heating. The transition from petroleum-based to biobased resins represents a significant step towards sustainable manufacturing in volumetric printing, with

potential applications in various industries, including healthcare and consumer products. Embracing such sustainable practices is essential for a more environmentally friendly and innovative approach to material design and production.

Appendix

Appendix for Chapter 2

$$Conversion\ of\ CL\ to\ PCL\ (\%) = \frac{\int 2.36\ to\ 2.26\ ppm}{\int 2.61\ ppm + \int 2.36\ to\ 2.26\ ppm} \times 100$$

$$Conversion\ of\ VL\ to\ PVL\ (\%) = \frac{\int 2.39\ to\ 2.28\ ppm}{\int 2.55\ ppm + \int 2.39\ to\ 2.28\ ppm} \times 100$$

Appendix Equation 1 Conversion of CL and VL can be calculated using ^{1}H-NMR

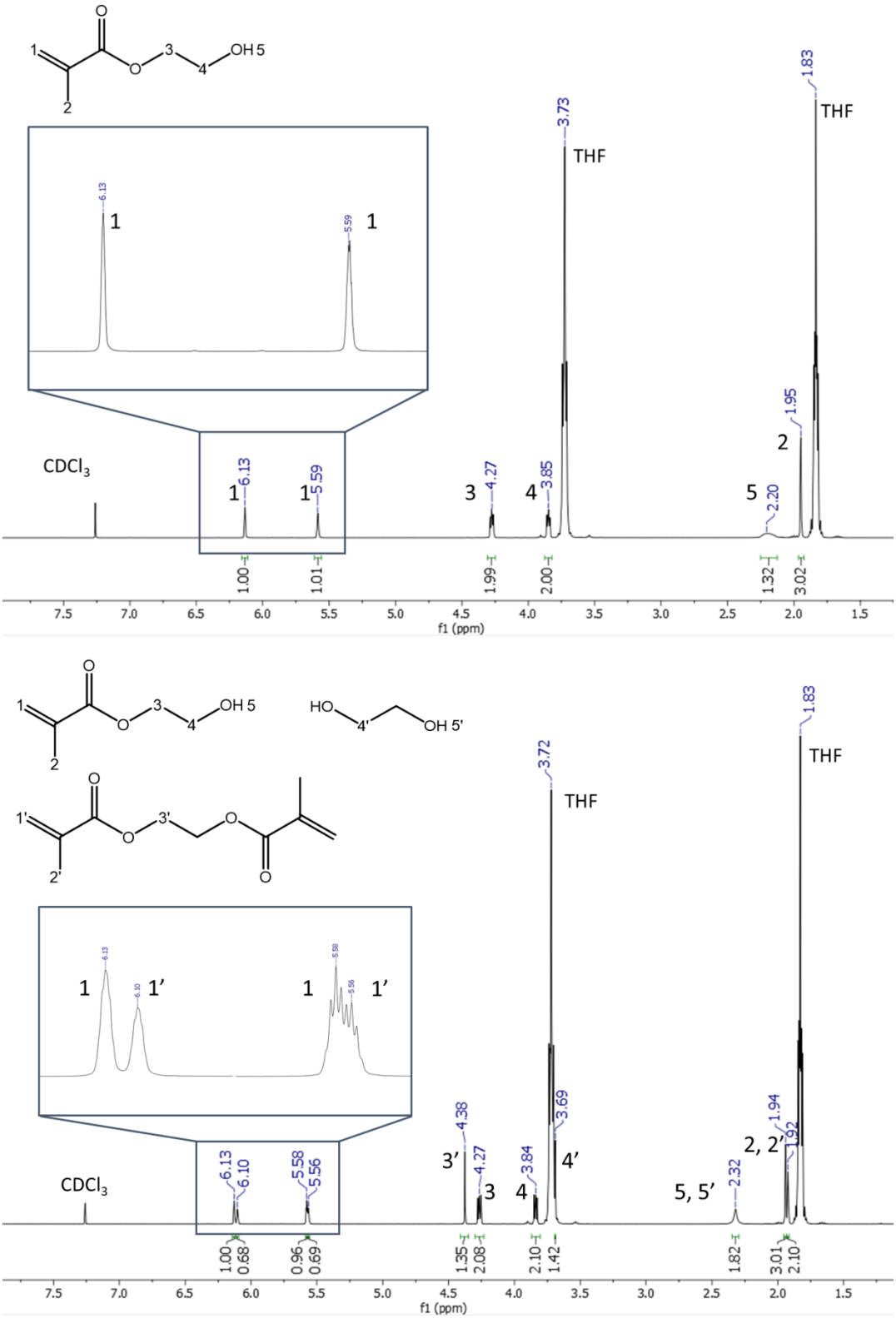

Appendix Figure 1 ^{1}H-NMR spectra of HEMA in $CDCl_3$ before (top) and after 20 h at 65 °C with 20 wt. % N435 (bottom) with an indent to focus on the vinyl region. Note the appearance of new peaks corresponding to ethylene glycol dimethacrylate and ethylene glycol in the lower spectrum.

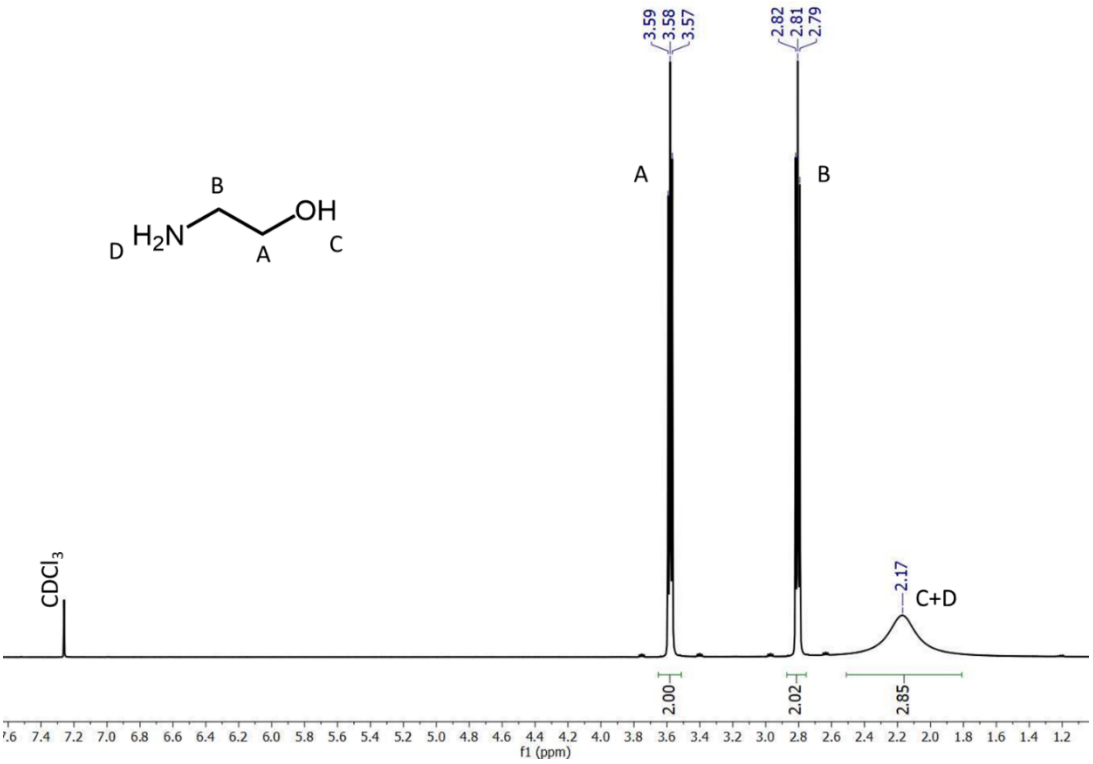

Appendix Figure 2 ^{1}H-NMR spectrum of ethanolamine in $CDCl_3$.

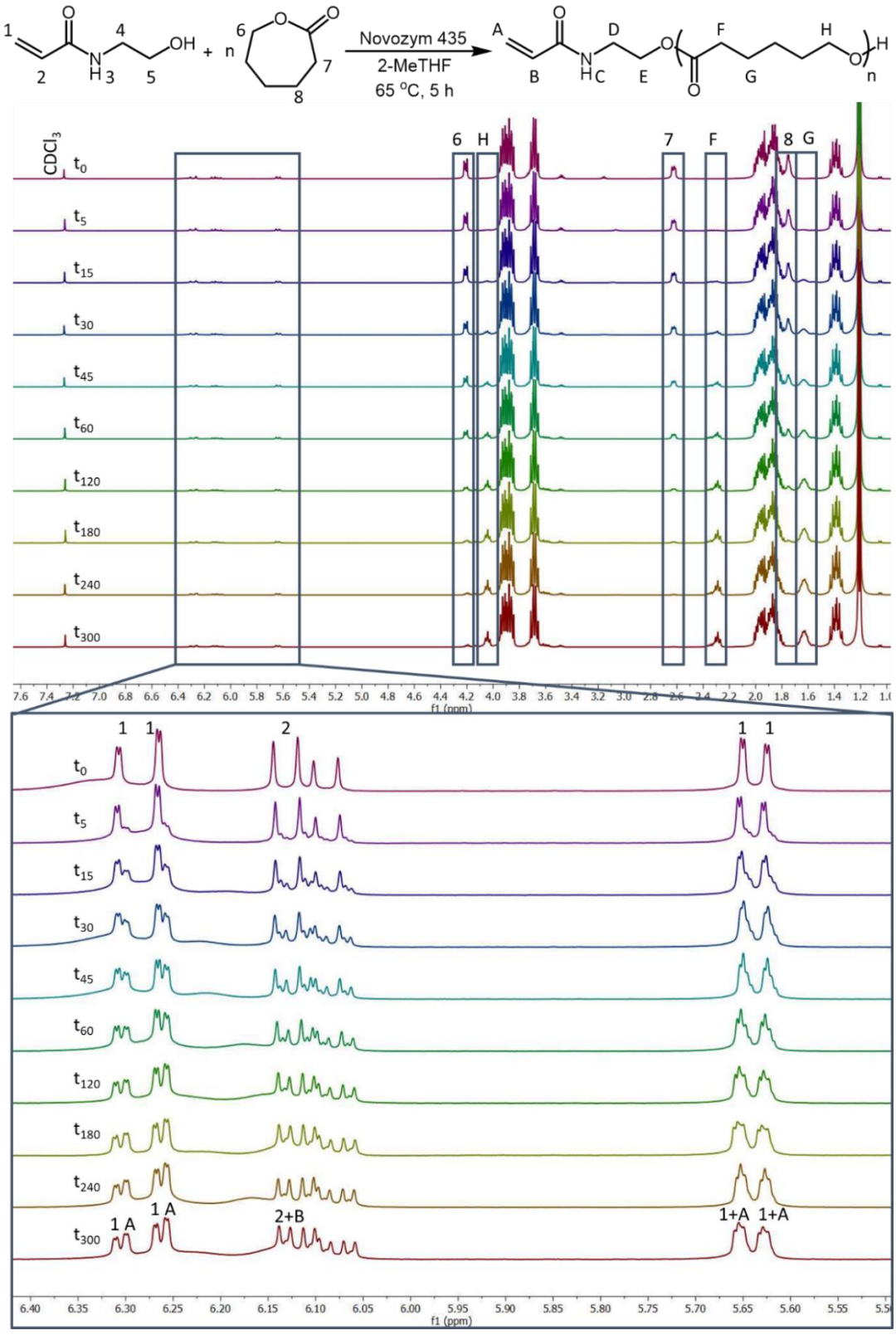

Appendix Figure 3 Full stack of ^{1}H-NMR spectra used to monitor the kinetics of HEAA initiated eROP of CL (M:I = 5:1). Zoomed in region highlights the formation of two distinct acrylamide species. Monomer concentration of 0.143 g·mL^{-1}.

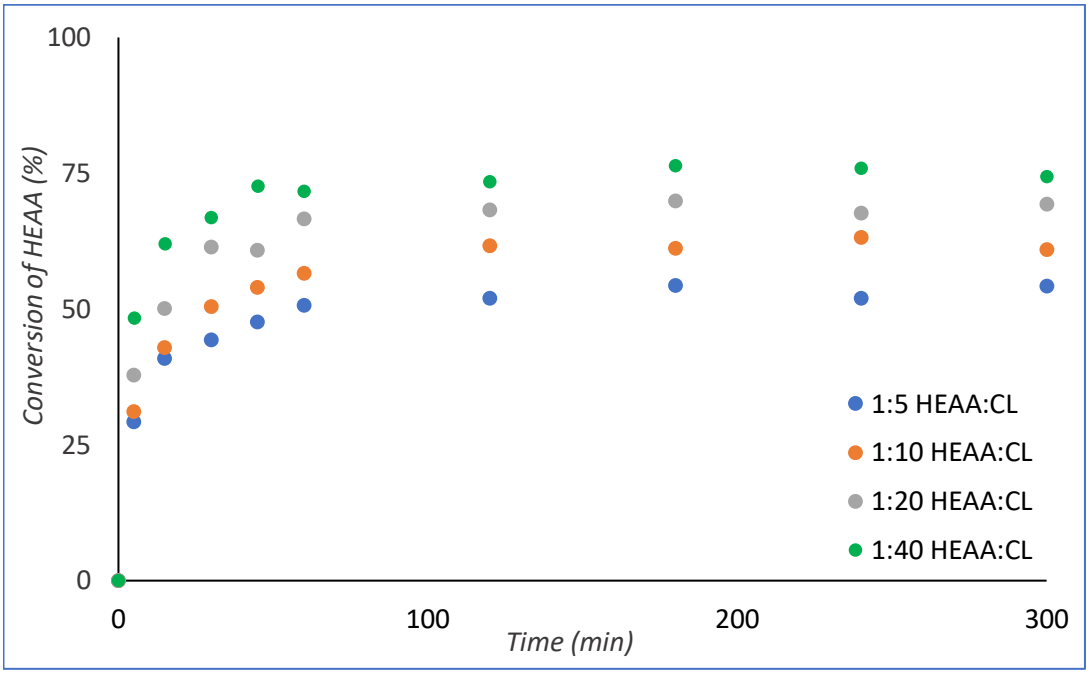

Appendix Figure 4 HEAA conversions obtained during eROP of CL in 2-MeTHF with 10 wt.% N435.

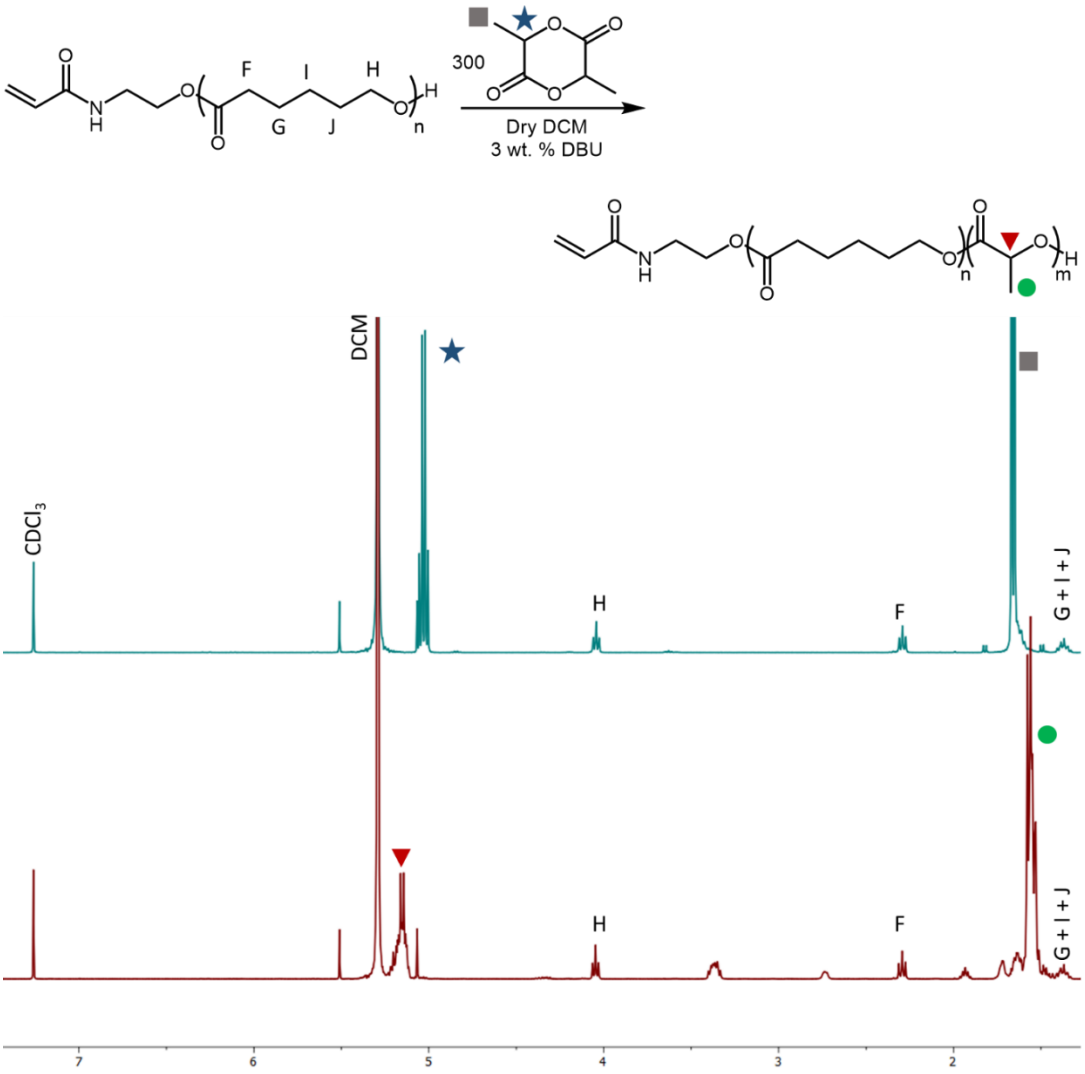

Appendix Figure 5 [1]H-NMR spectra of lactide extension of HEAA-PCL. Top: reaction scheme. Middle: reaction at time zero. Bottom: reaction after 30 minutes.

Time (min)	CL Conversion (%)[a]				HEAA Conversion (%)[a]			
	1:5 HEAA:CL	1:10 HEAA:CL	1:20 HEAA:CL	1:40 HEAA:CL	1:5 HEAA:CL	1:10 HEAA:CL	1:20 HEAA:CL	1:40 HEAA:CL
0	0	0	0	0	0	0	0	0
5	8.48	9.00	7.18	12.2	29.2	31.1	30.1	48.4
15	22.2	22.8	23.5	27.5	40.9	42.9	53.9	62.0
30	40.1	39.5	38.4	46.8	44.3	50.5	60.8	66.8
45	52.0	53.0	50.1	58.4	47.6	54.0	64.9	72.6
60	61.7	62.7	62.6	67.4	50.6	56.5	69.1	72.7
120	83.6	85.8	82.8	89.1	52.0	61.6	72.5	73.5
180	92.8	94.4	93.0	95.8	54.3	61.1	74.2	76.4
240	96.7	97.7	96.6	98.5	52.0	63.1	71.8	76.0
300	98.5	98.9	98.5	99.3	54.1	61.0	73.0	74.4

Appendix Table 1 Time and conversion of CL and HEAA in 2-MeTHF with 10 wt. % N435, varying the targeted molecular weight by changing the ratio of initiator to monomer. [a] Determined by H-NMR analysis. Monomer concentration of 0.143 g·mL^{-1}.

Time (min)	VL Conversion (%)[a]				HEAA Conversion (%)[a]			
	1:5 HEAA:VL	1:10 HEAA:VL	1:20 HEAA:VL	1:40 HEAA:VL	1:5 HEAA:VL	1:10 HEAA:VL	1:20 HEAA:VL	1:40 HEAA:VL
0	0.0	0.0	0.0	0.0	0.0	0.0	0.0	0.0
5	11.7	11.1	12.6	10.7	19.6	22.8	33.6	32.9
15	20.4	21.9	24.2	21.3	28.6	38.9	50.6	46.7
30	32.1	36.8	38.7	33.4	31.4	51.6	57.8	52.3
45	40.3	46.9	49.7	43.0	35.3	55.0	60.4	56.0
60	49.7	56.1	57.8	51.0	34.9	57.6	62.7	62.0
120	63.8	77.2	79.0	73.6	41.3	63.1	65.6	69.0
180	75.3	84.6	85.4	83.7	47.8	61.7	71.5	71.7
240	81.2	88.0	87.7	87.9	49.1	63.3	68.1	72.0
300	85.2	89.3	88.8	89.5	50.5	65.6	70.7	73.6

Appendix Table 2 Time and conversion of VL and HEAA in 2-MeTHF with 10 wt. % N435, varying the targeted molecular weight by changing the ratio of initiator to monomer. [a] Determined by H-NMR analysis. Monomer concentration of 0.143 g·mL^{-1}.

Time	1:5 HEAA:CL		1:10 HEAA:CL		1:20 HEAA:CL		1:40 HEAA:CL	
(min)	M	$\ln(M_0/M)$	M	$\ln(M_0/M)$	M	$\ln(M_0/M)$	M	$\ln(M_0/M)$
0	6.07	0.00	11.81	0.00	23.38	0.00	39.12	0.00
5	4.61	0.27	9.37	0.23	17.77	0.27	33.94	0.14
15	3.69	0.50	7.14	0.50	15.97	0.38	28.91	0.30
30	3.20	0.64	6.38	0.62	13.03	0.59	26.28	0.40
45	2.53	0.88	4.94	0.87	10.02	0.85	20.58	0.64
60	2.07	1.08	3.90	1.11	7.54	1.13	14.51	0.99
120	0.88	1.93	1.79	1.89	3.48	1.91	5.13	2.03
180	0.49	2.52	0.64	2.91	1.29	2.90	2.21	2.88
240	0.17	3.57	0.31	3.64	0.53	3.79	0.83	3.85
300	0.09	4.21	0.12	4.61	0.23	4.62	0.37	4.66

Appendix Table 3 Tabulated data used to plot first-order kinetics for HEAA initiated eROP of CL (2-MeTHF, 65 °C, 10 wt.% N435, monomer concentration of 0.143 g·mL^{-1}). M_0 designates the value of M at time zero.

Time (min)	1:5 HEAA:VL		1:10 HEAA:VL		1:20 HEAA:VL		1:40 HEAA:VL	
	M	$\ln(M_0/M)$	M	$\ln(M_0/M)$	M	$\ln(M_0/M)$	M	$\ln(M_0/M)$
0	5.34	0.00	10.78	0.00	22.85	0.00	49.74	0.00
5	4.37	0.20	9.89	0.09	18.82	0.19	44.94	0.10
15	4.15	0.25	8.24	0.27	15.33	0.40	39.53	0.23
30	3.22	0.51	7.14	0.41	13.31	0.54	35.46	0.34
45	3.36	0.46	5.18	0.73	12.50	0.60	28.88	0.54
60	2.70	0.68	5.18	0.73	9.28	0.90	29.84	0.51
120	2.15	0.91	2.51	1.46	4.55	1.61	15.39	1.17
180	1.30	1.42	1.79	1.79	3.38	1.91	9.98	1.61
240	0.92	1.75	1.21	2.18	2.85	2.08	7.10	1.95
300	0.81	1.89	1.19	2.20	2.66	2.15	6.70	2.00

Appendix Table 4 Tabulated data used to plot first-order kinetics for HEAA initiated eROP of VL (2-MeTHF, 65 °C, 10 wt.% N435, monomer concentration of 0.143 g·mL^{-1}). M_0 designates the value of M at time zero.

Enzyme Cycle	HEAA Conversion (%)[ab]	Std. dev. HEAA Conversion (%)[c]	CL Conversion (%)[ab]	Std. dev. CL Conversion (%)[c]
0	55.6	0.56	94.8	1.60
1	56.1	0.16	95.7	1.44
2	56.5	0.76	95.9	1.40
3	57.2	0.90	93.2	2.67
4	61.3	0.08	96.8	1.36
5	61.1	1.21	95.4	2.43
6	59.1	1.24	96.2	1.40
7	59.0	0.32	95.5	1.97
8	61.2	0.92	95.7	0.36
9	55.1	2.67	93.5	1.99
10	56.7	2.79	93.2	0.97

Appendix Table 5 Tabulated results of the N435 recyclability study. [a] Determined by H-NMR spectroscopy. [b] Calculated using a simple mean of three reactions run in parallel to ensure reproducibility. [c] Calculated using the STDEV.P function in Microsoft Excel 2016.

Time (min)	CL Conversion (%)[a]	M_n (g·mol^{-1}) [b]	M_w (g·mol^{-1}) [b]	$Đ$[b]
0	0.8	-	-	-
5	2.6	-	-	-
15	7.3	-	-	-
30	20.0	-	-	-
45	24.5	-	-	-
60	35.5	-	-	-
120	51.2	4954	8685	1.75
180	67.1	4389	8475	1.93
240	79.0	5054	9538	1.89
300	85.5	5147	9686	1.88

Appendix Table 6 Tabulated data of N435 catalysed eROP without explicit addition of initiating species. [a] Determined by ^{1}H-NMR spectroscopy, [b] determined by GPC. Monomer concentration of 0.143 g·mL^{-1}.

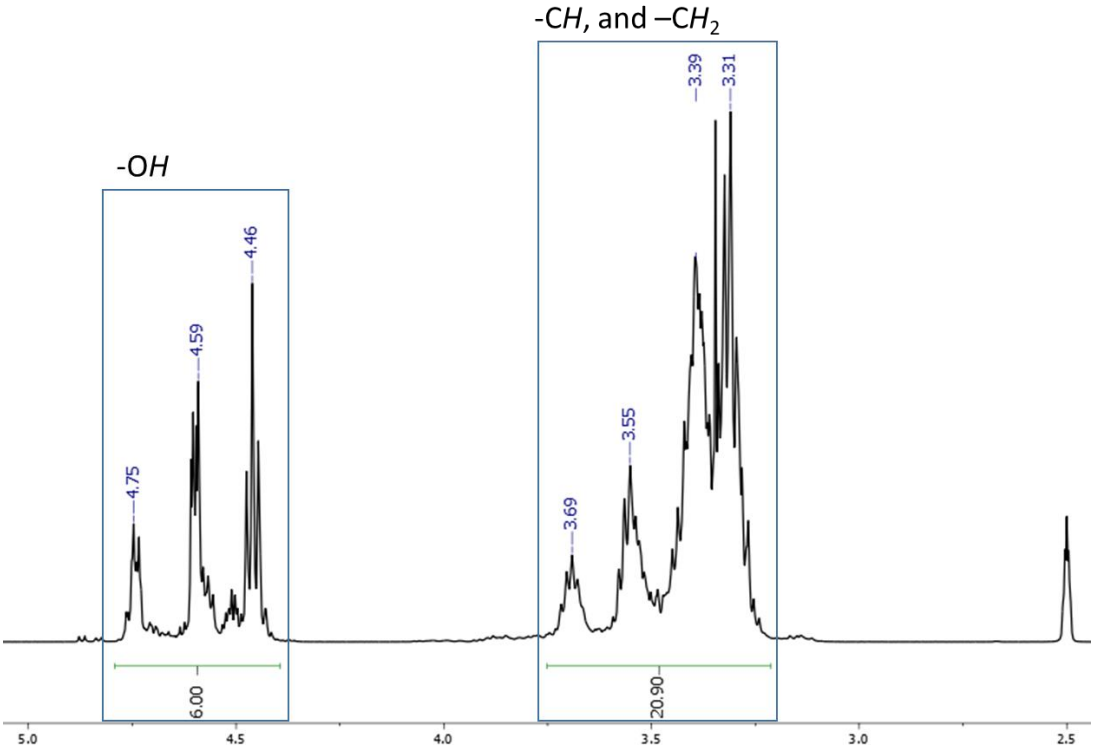

Appendix Figure 6 ^{1}H-NMR spectrum of PG4 in DMSO-d6.

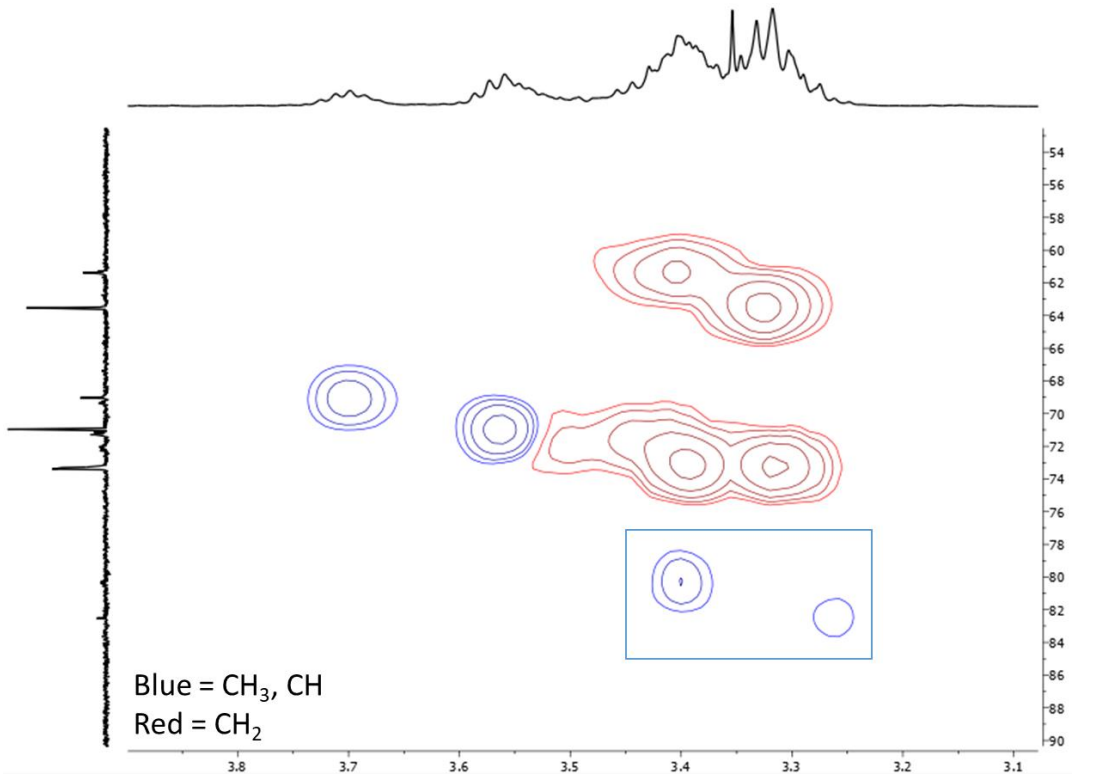

Appendix Figure 7 HSQC Spectrum of PG4 in DMSO-d_6, cropped to show the regions between 3.1 and 3.9 ppm (^{1}H) and 54 to 90 ppm (^{13}C). The blue box highlights the overlap between bridging methine and methylene protons in PG4.

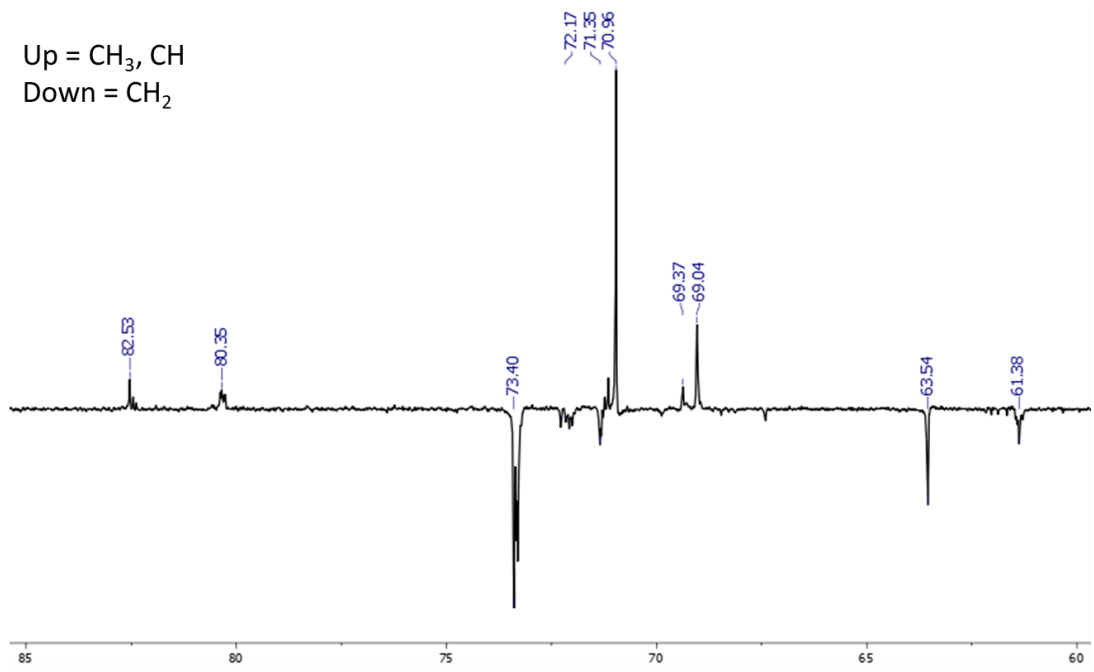

Appendix Figure 8 ^{13}C DEPT-135 Spectrum of PG4 in DMSO-d_6, zoomed to show the region between 60 and 85 ppm. 2500 scans.

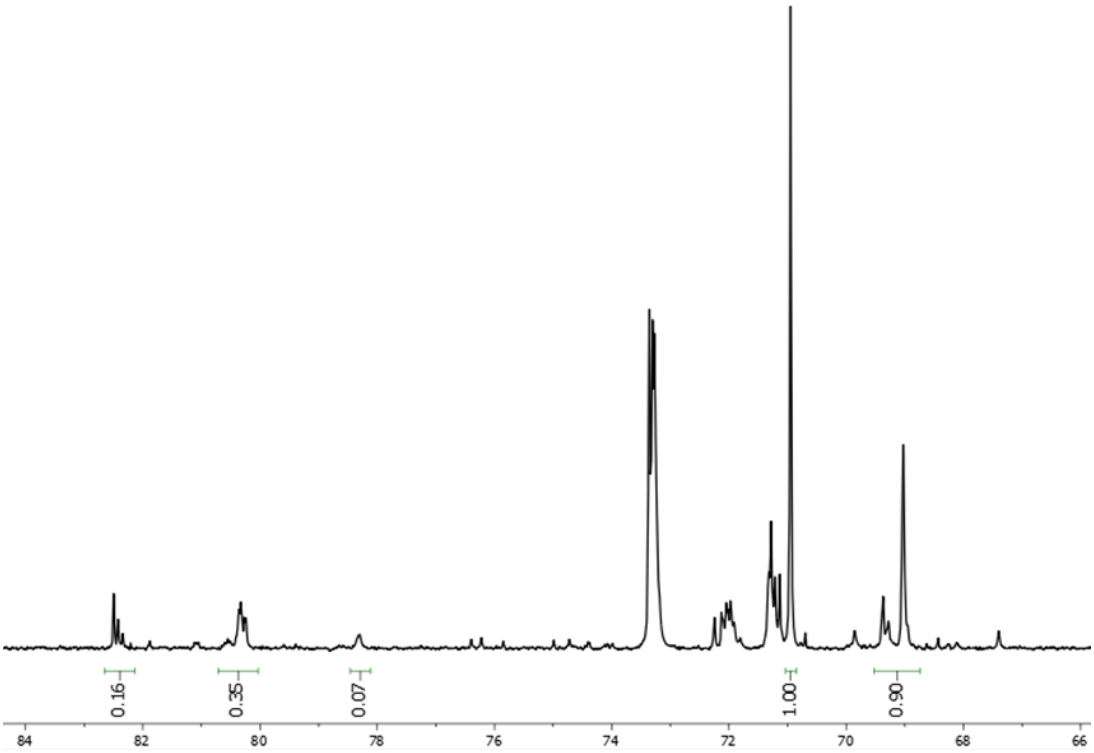

Appendix Figure 9 Quantitative ^{13}C Spectrum of PG6 in DMSO-d_6, zoomed to show the region between 60 and 85 ppm. 4096 scans, relaxation delay 5 s.

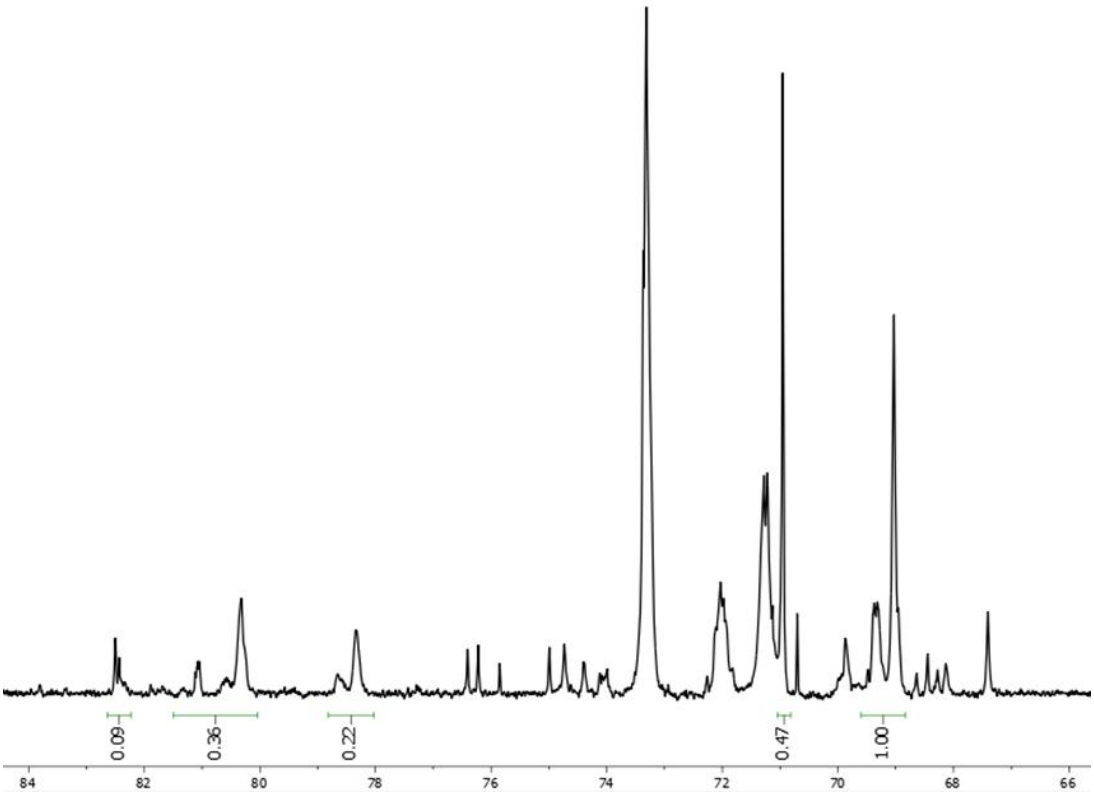

Appendix Figure 10 Quantitative ^{13}C Spectrum of PG10 in DMSO-d_6, zoomed to show the region between 60 and 85 ppm. 4096 scans, relaxation delay 5 s.

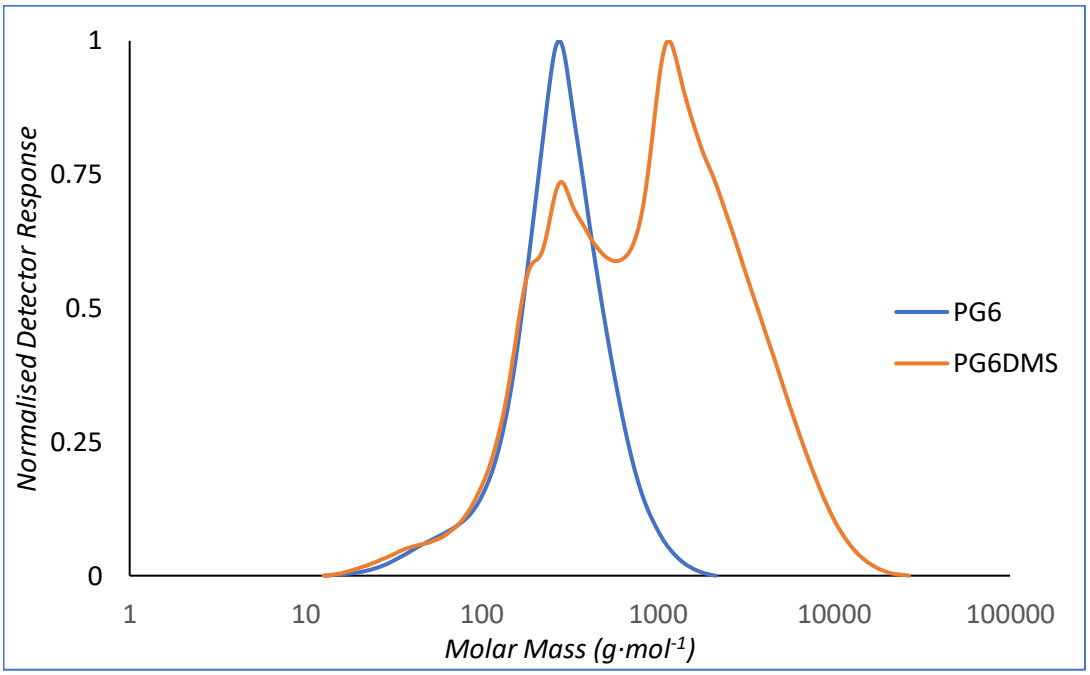

Appendix Figure 11 Aqueous GPC of PG6 and PG6DMS, showing the increase in molar mass following polytransesterification.

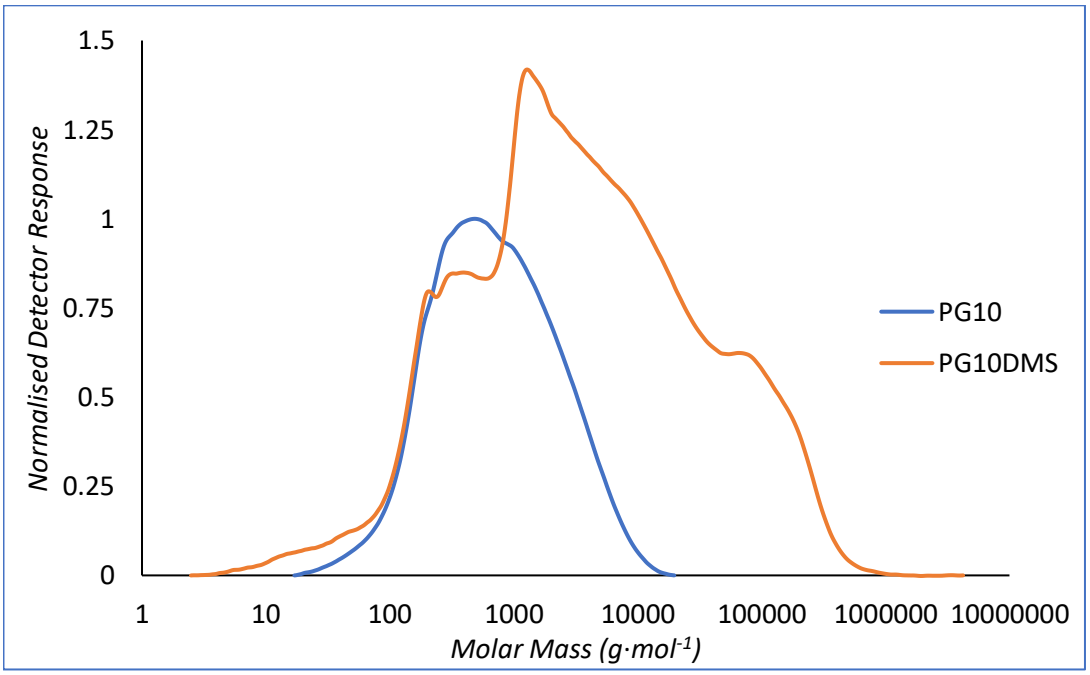

Appendix Figure 12 Aqueous GPC of PG10 and PG10DMS, showing the increase in molar mass following polytransesterification.

Synthesis temp (°C)	Saponification Value (mg KOH·g^{-1})
60	232
80	222
100	216
120	219
140	217
160	228
180	229

Appendix Table 7 Acid and saponification values of PG4DMS synthesised at various temperatures.

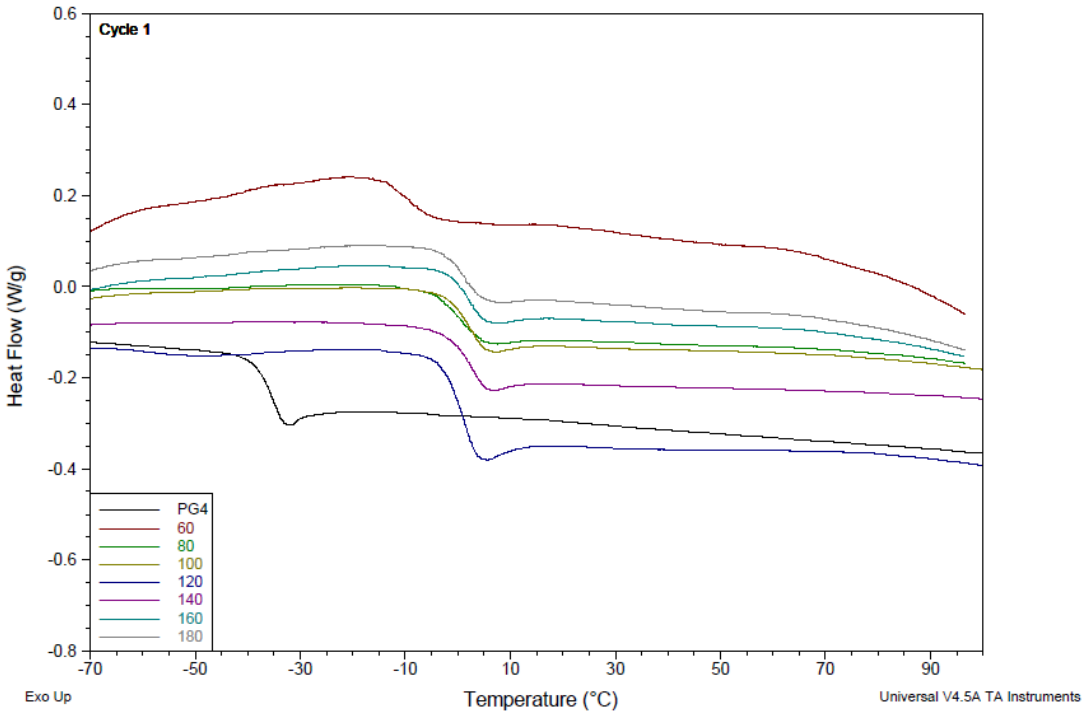

Appendix Figure 13 DSC traces of PG4 and PG4-DMS synthesised at different temperatures.

DMS loading (equiv. w.r.t. PG4)	Behaviour in H_2O	Product Appearance
1.00	Dissolves	Highly viscous
1.25	Swells	Flexible
1.50	Swells	Semi-flexible
2.00	Swells	Rigid
3.00	Minimal Interaction	Brittle material

Appendix Table 8 PG4-DMS behaviour in water and appearance with various loadings of DMS. Molar mass of PG4 was assumed to be 314 g·mol^{-1}.

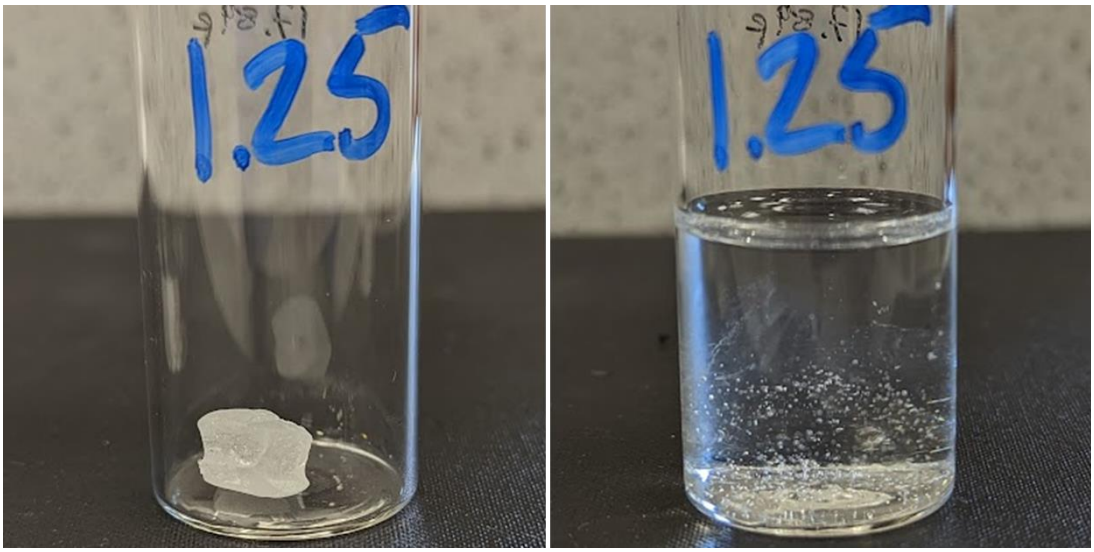

Appendix Figure 14 PG4-1.25DMS before (left) and 24 hours after (right) submersion in water.

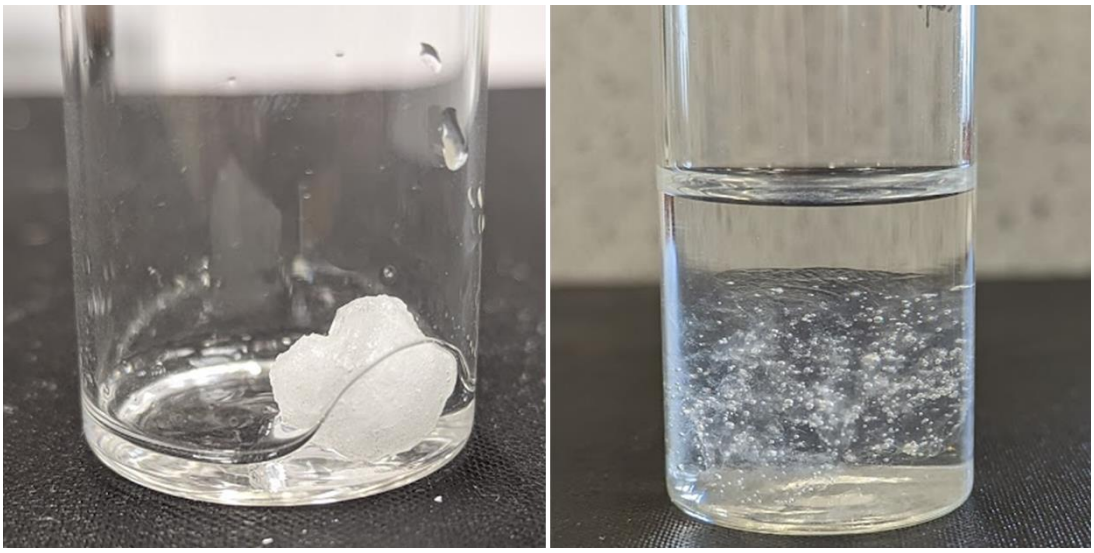

Appendix Figure 15 PG4-2DMS before (left) and 24 hours after (right) submersion in water.

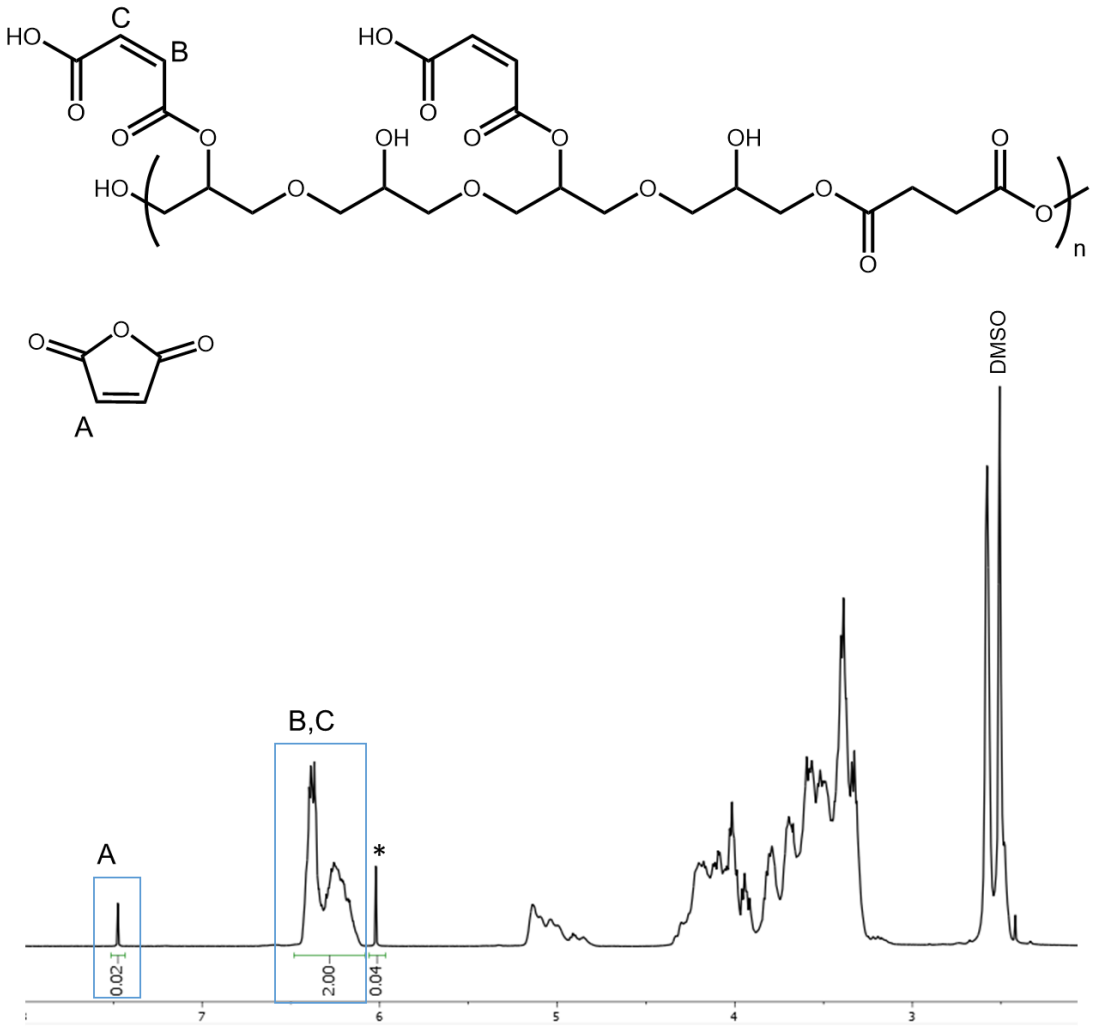

*Appendix Figure 16 ^{1}H-NMR spectrum of PG4-DMS-2MA. Signal denoted with * corresponds to maleic acid, a hydrolysis by-product.*

Post-Polymerisation Thermal Cross-Linking

It was observed during functionalisation of PG4-DMS with succinic anhydride that elevated temperatures resulted in the formation of an insoluble resin. This methodology was explored as a potential method to introduce a degree of cross-linking that could be suitable for rheological modification.

Using oscillatory rheology at reaction temperature provided insight into the rate of curing (Appendix Figure 17). As the chains cross-link the storage modulus increases gradually, eventually resulting in the storage modulus exceeding the loss modulus. It was found that under the conditions employed this crossover point was at approximately five hours.

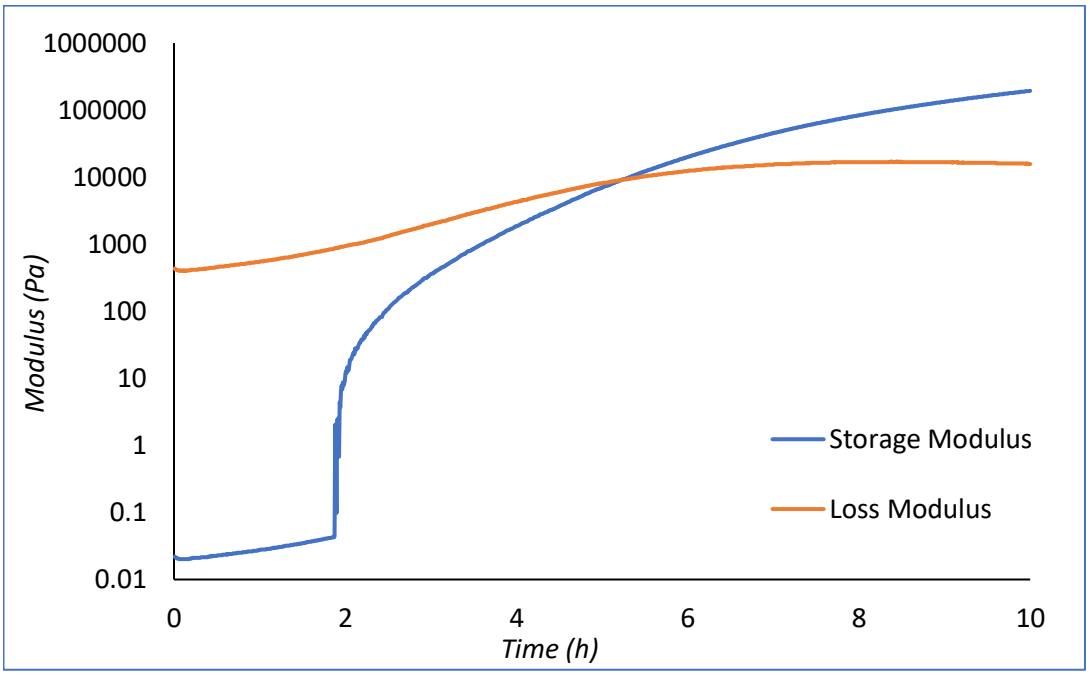

Appendix Figure 17 Monitoring storage and loss moduli of PG4DMS-2SA over time using oscillatory rheology at 120 °C.

To confirm that the curing taking place was the result of pendant carboxylic acids reacting with backbone hydroxyl groups AVs were measured of the samples allowed to cure for various lengths of time (Appendix Table 9). It was found that AV decreases with time, indicating that carboxylic acid groups are being consumed and indicative of esterification taking place.

Time (h)	AV (mg KOH·g^{-1})
0	189
3	177
5	76
6	25
24	5

Appendix Table 9 Acid values of PG4DMS-2SA over time during thermal curing at 120 °C.

Upon the preparation of aqueous solutions of thermally cross-linked samples only minimal swelling was observed. These materials were unable to provide any noteworthy rheological modification. The lack of rheological modification could be caused by polymer chains reacting with themselves rather than with other chains, resulting in lessened hydrophilicity without the formation of a water-swellable network. The thermal curing could be interesting

for the development of a biobased resin, although it was deemed unsuitable for rheological modification and not explored further.

Appendix for Chapter 4

Appendix Figure 18 Formulation of PG4-1.5DMS into aqueous solution. Vials from left to right: 5, 10, 15, 20 wt.% polymer loading. Top: immediately after submersion in water. Middle: 3 hours after submersion. Bottom: Following homogenisation using a high-speed mixer.

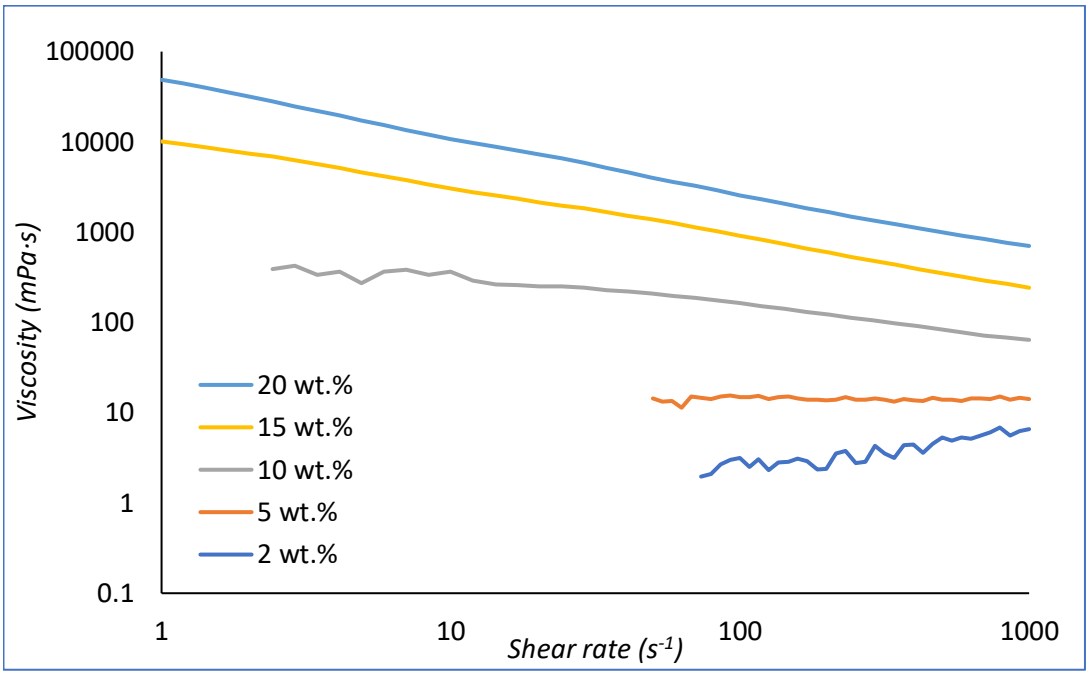

Appendix Figure 19 Viscosity over shear rate of PG4-1.25DMS at various loadings in aqueous solution.

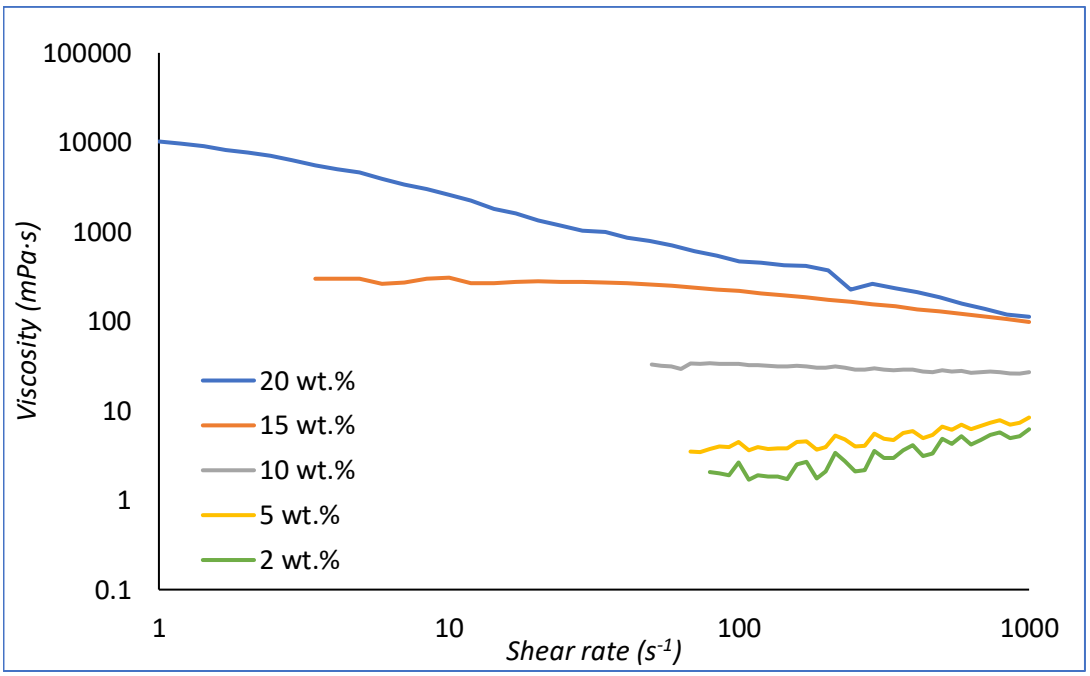

Appendix Figure 20 Viscosity over shear rate of PG4-1.75DMS at various loadings in aqueous solution.

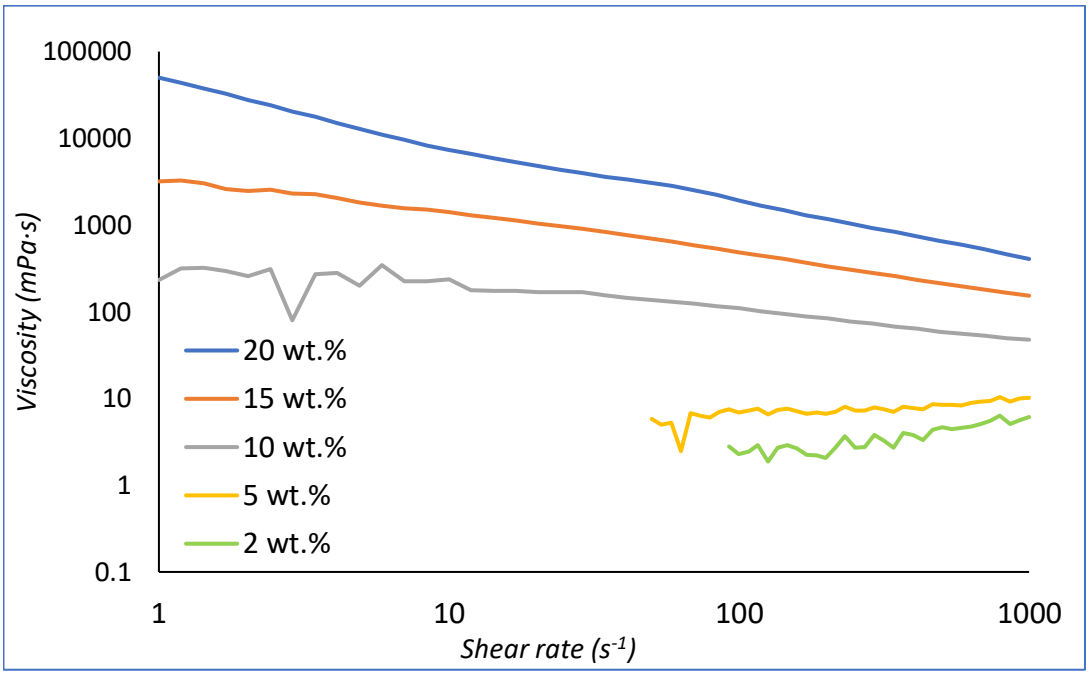

Appendix Figure 21 Viscosity over shear rate of PG4-1.25DMS at various loadings in aqueous NaCl (10wt.%) solution.

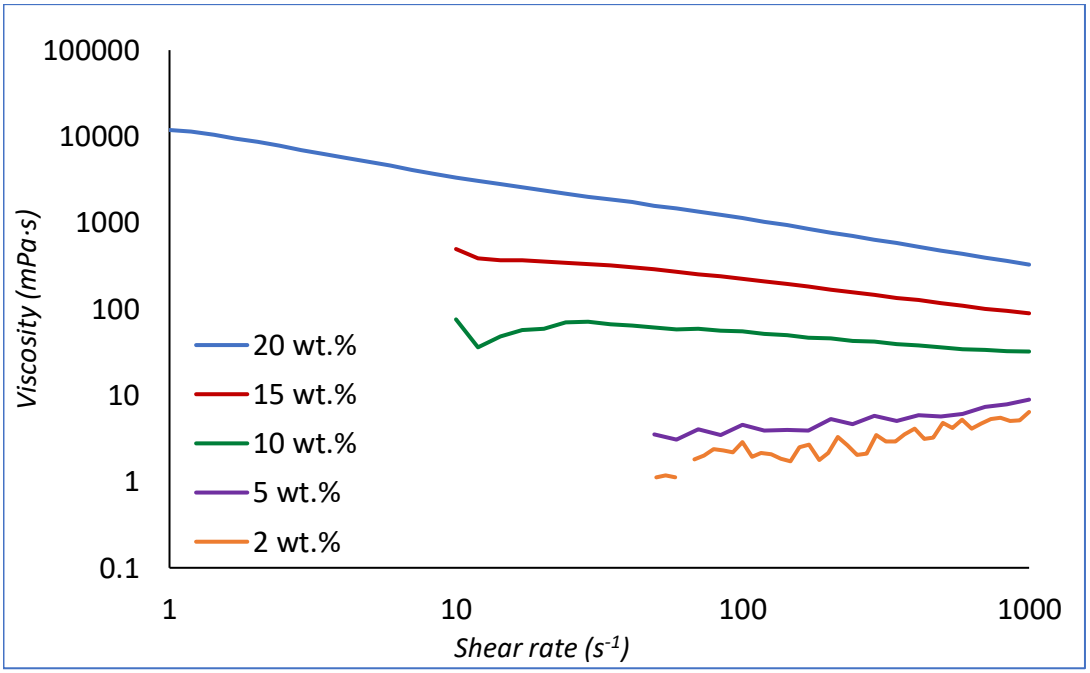

Appendix Figure 22 Viscosity over shear rate of PG4-1.5DMS at various loadings in aqueous NaCl (10wt.%) solution.

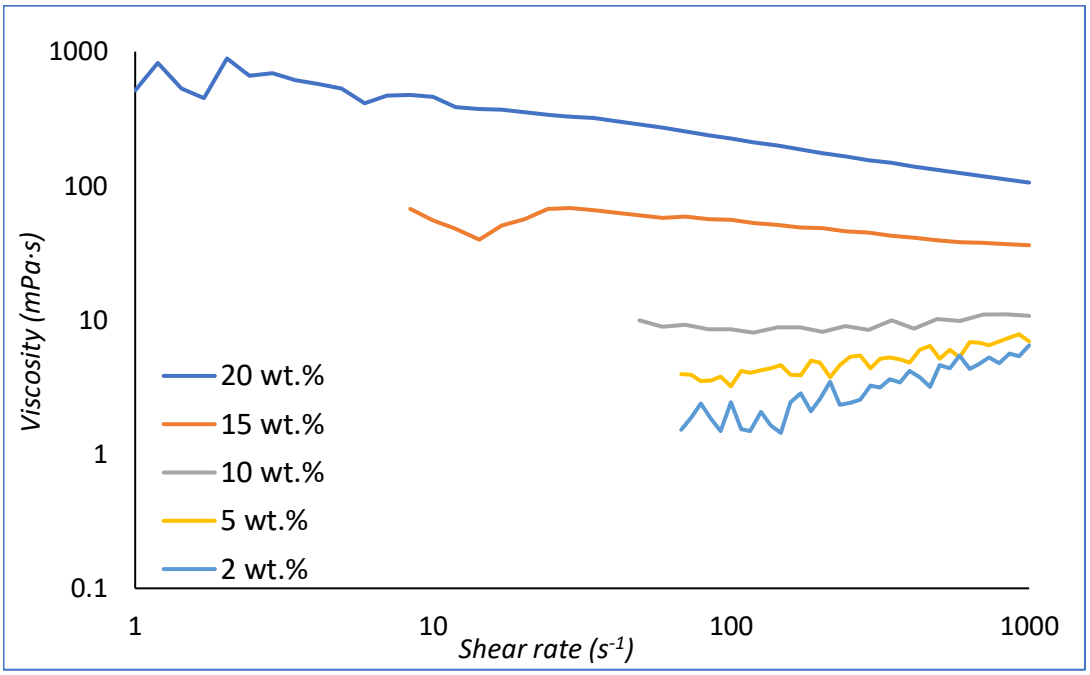

Appendix Figure 23 Viscosity over shear rate of PG4-1.75DMS at various loadings in aqueous NaCl (10wt.%) solution.

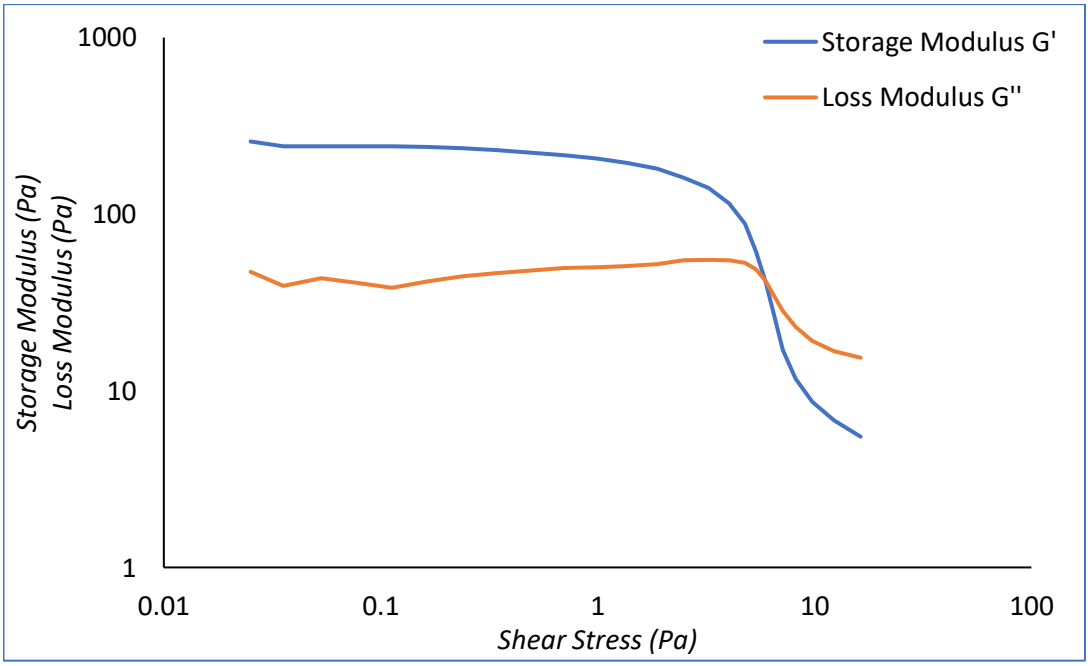

Appendix Figure 24 Amplitude sweep of PG4-1.5DMS (20 wt.% in 10 wt.% NaCl solution). Flow point τ_f=5.9 Pa.

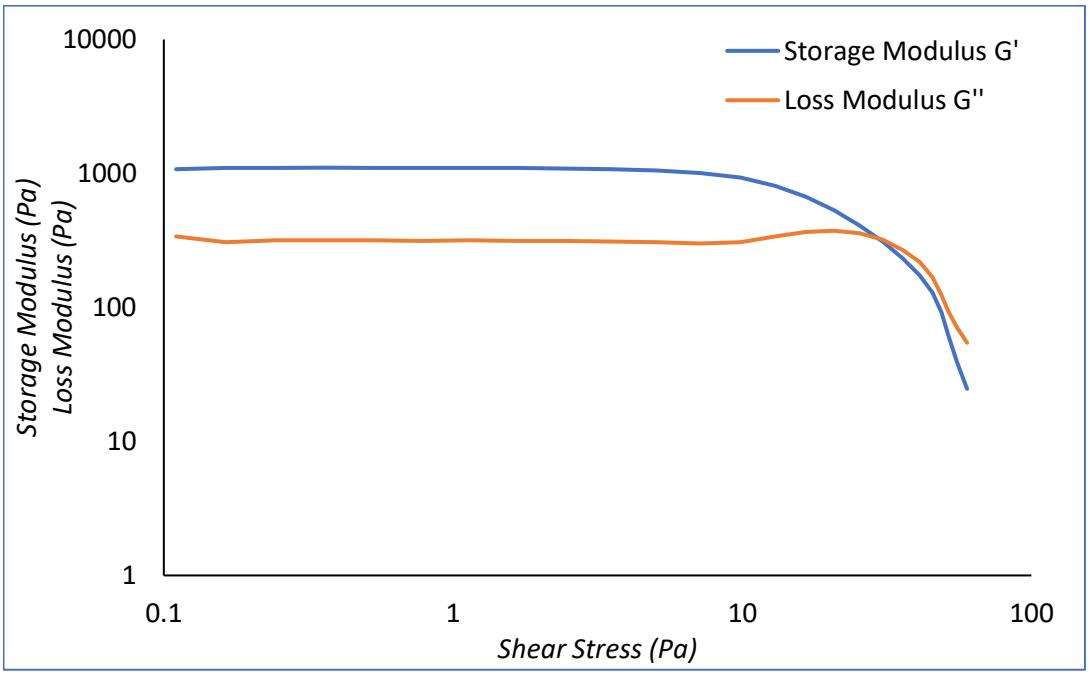

Appendix Figure 25 Amplitude sweep of personal care formulation CH0107. Flow point τ_f=29.7 Pa.

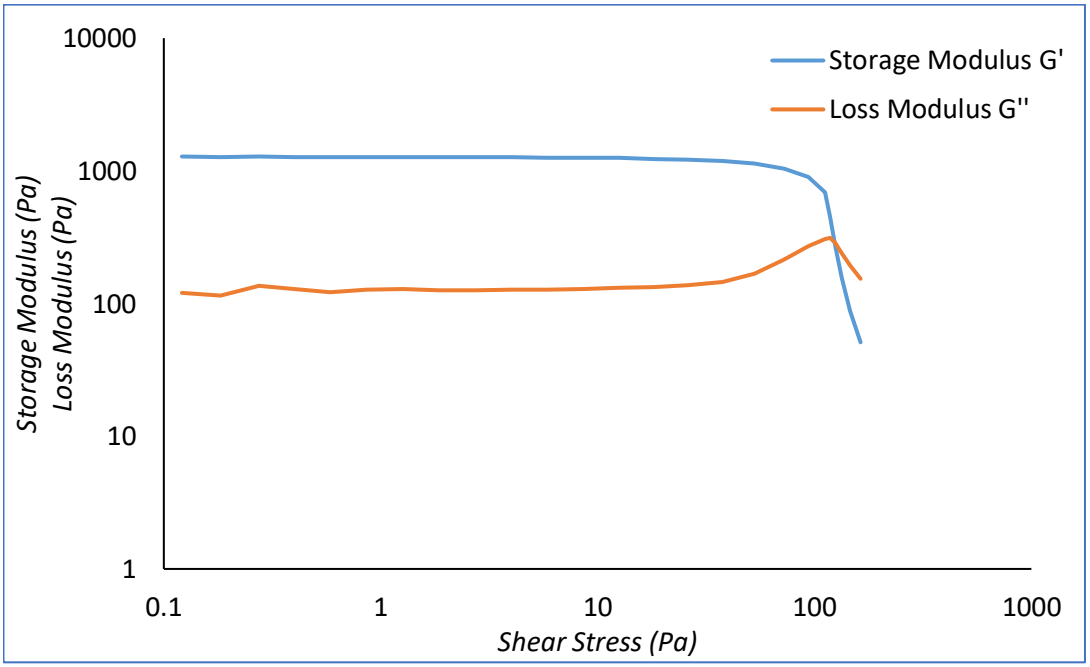

Appendix Figure 26 Amplitude sweep of personal care formulation C2755a. Flow point τ_f=124.3 Pa.

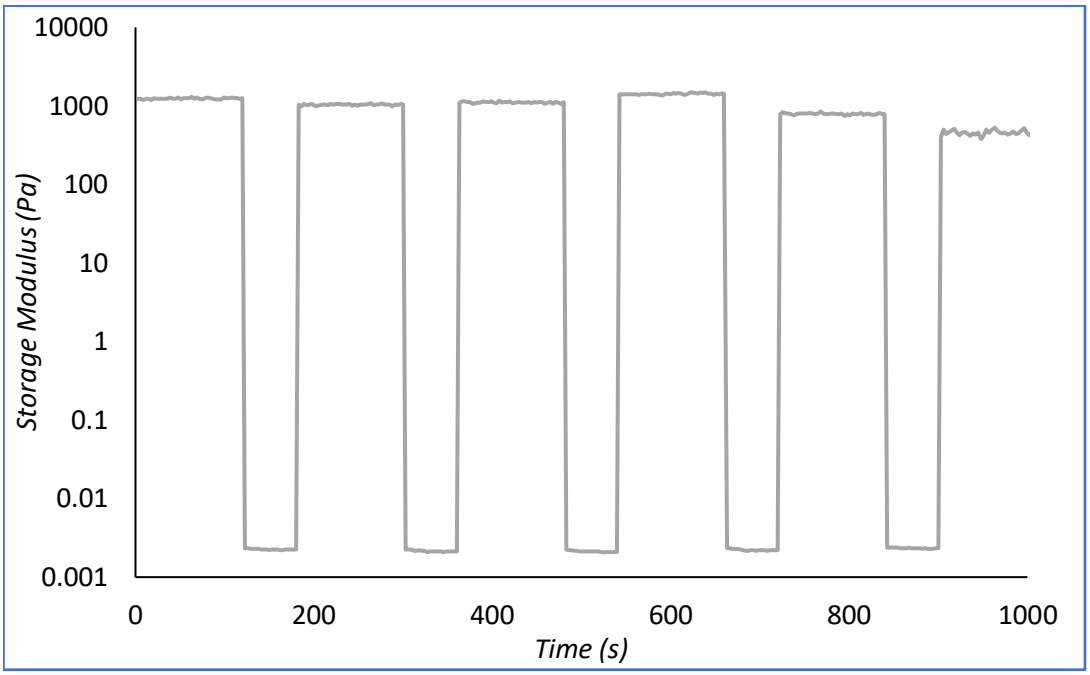

Appendix Figure 27 Cyclic strain rheology of 20 wt.% PG4-DMS in NaCl solution (10 wt.% NaCl). Low strain: 2 min, 0.1% shear strain. High strain: 1 min, 200% shear strain.

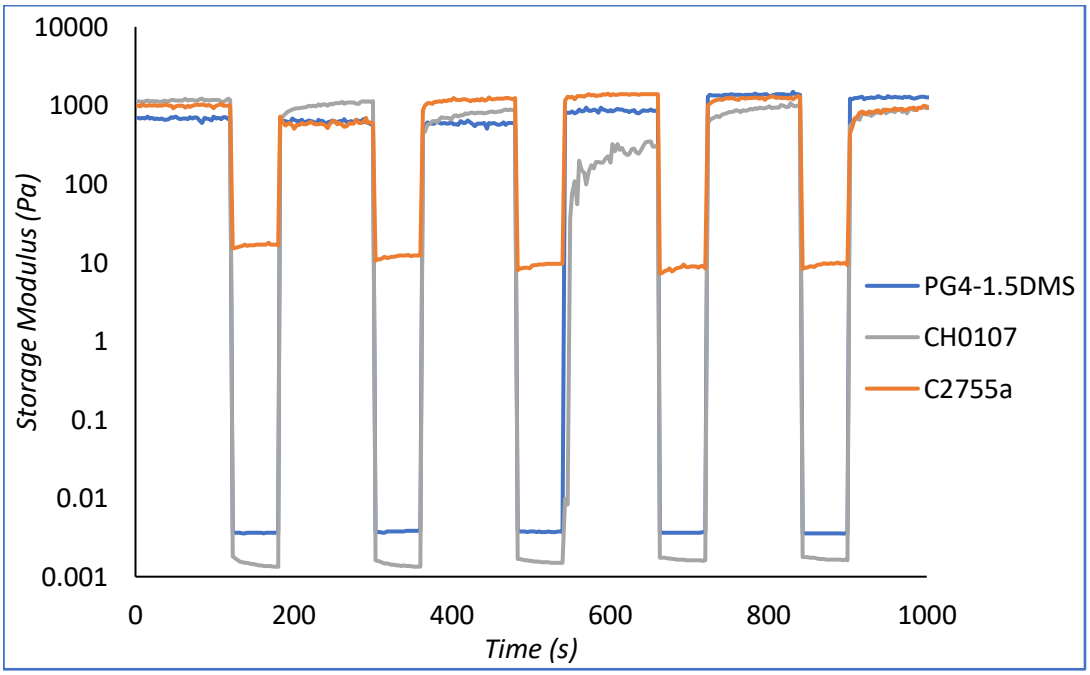

Appendix Figure 28 Cyclic strain rheology of 20 wt.% PG4-1.5DMS in DI H_2O, and two commercial personal care formulations (CH0107, and C2755a). Low strain: 2 min, 0.1% shear strain. High strain: 1 min, 200% shear strain.

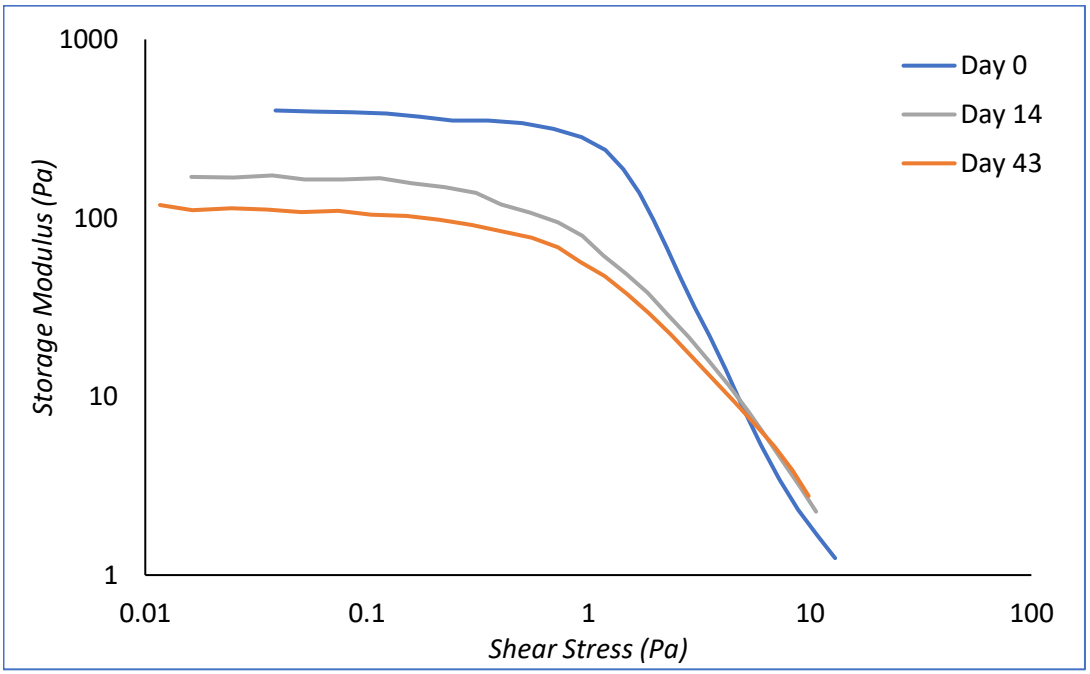

Appendix Figure 29 Amplitude sweeps of freeze dried PG4-1.5DMS (2.5 wt.% aqueous solution) over the course of 43 days.

Appendix for Chapter 5

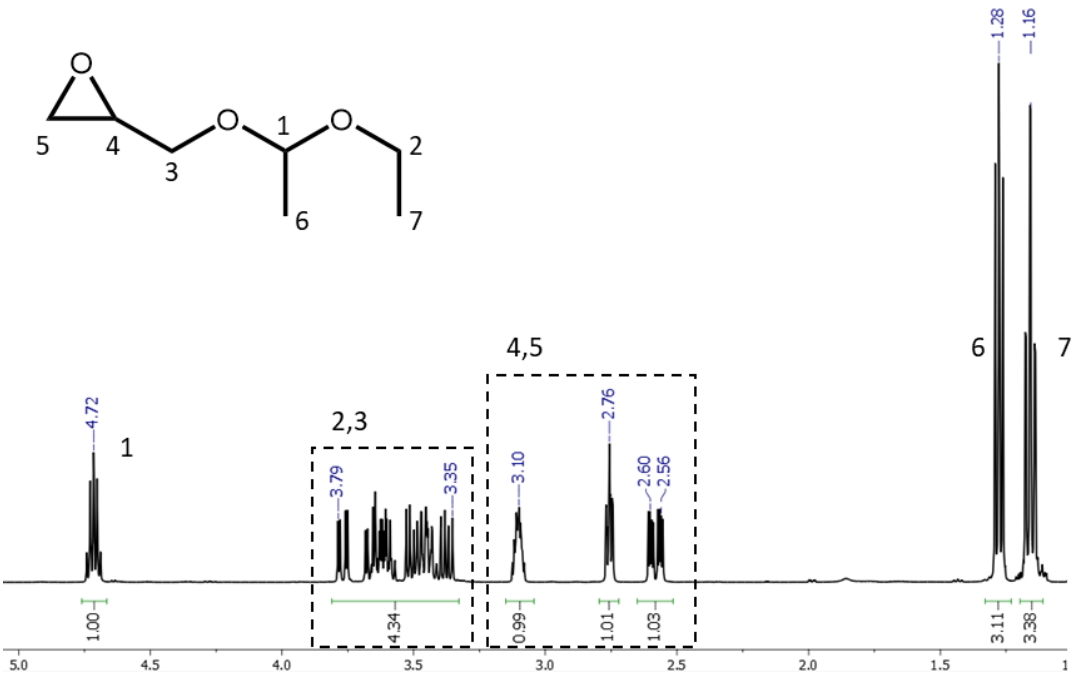

Appendix Figure 30 ^{1}H-NMR spectrum of EEGE in $CDCl_3$.

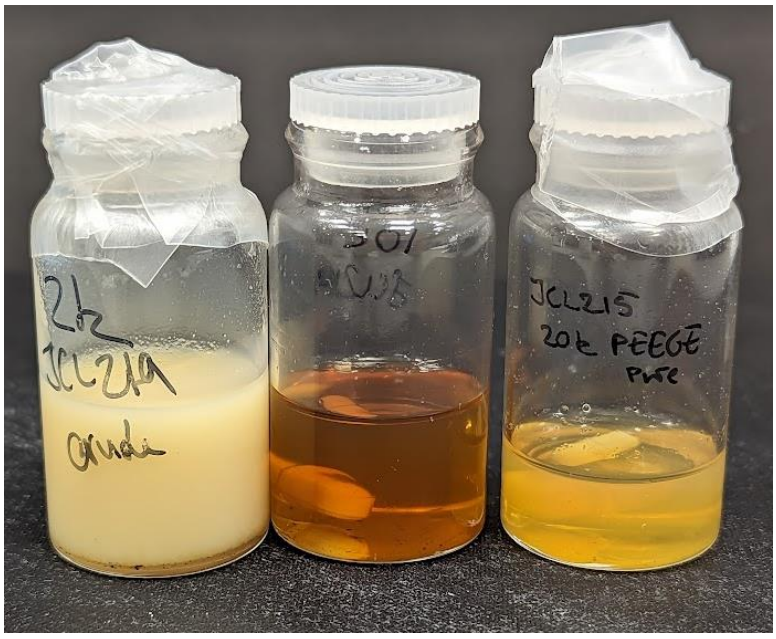

Appendix Figure 31 Samples of pEEGE synthesised using anionic ROP. Left to right: entries 1,2,4 from Table 24. Left sample appears opaque due to precipitated KOH.

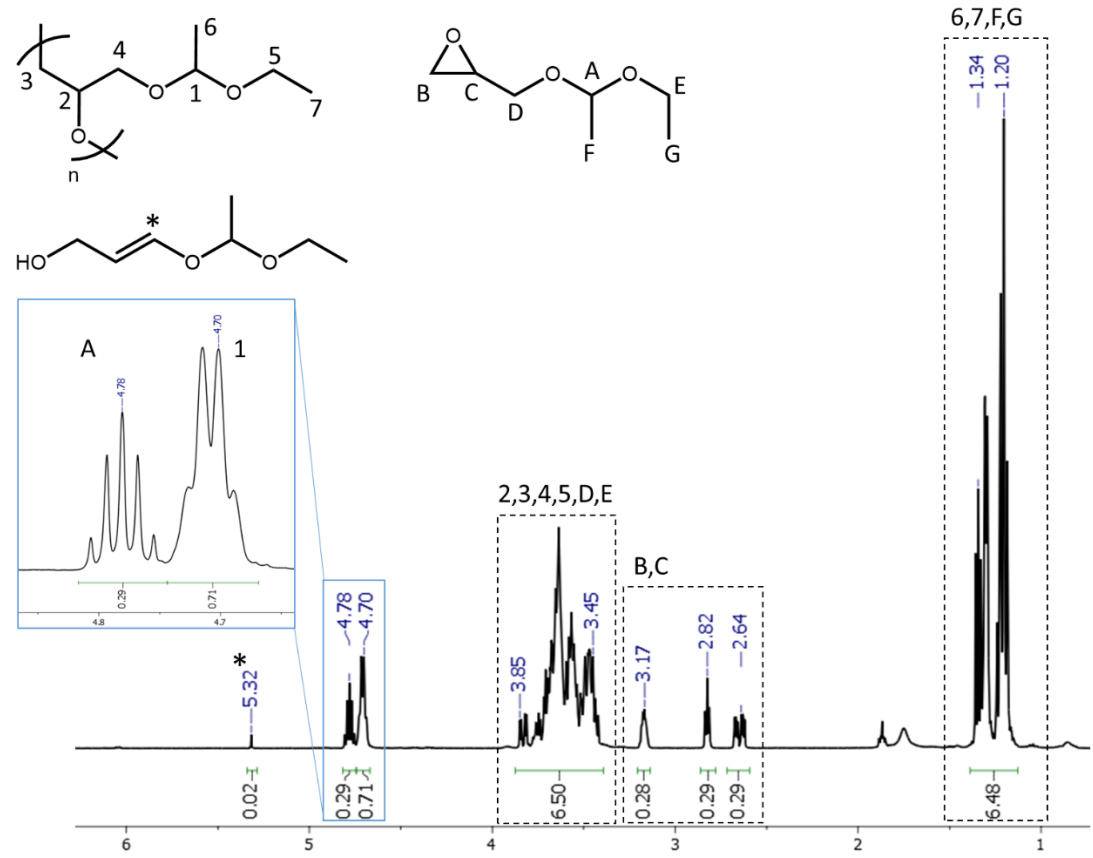

Appendix Figure 32 ^{1}H-NMR spectrum of crude pEEGE in $CDCl_3$. Inset shows the peaks used to determine conversion.

Appendix Figure 33 Solubility study of EEGE in CO_2. Left: at ambient pressure EEGE remains liquid in the glass vial. Right: at 13.8 mPa and 40 °C EEGE is solubilised in the $scCO_2$ and no longer present as a liquid in the vial.

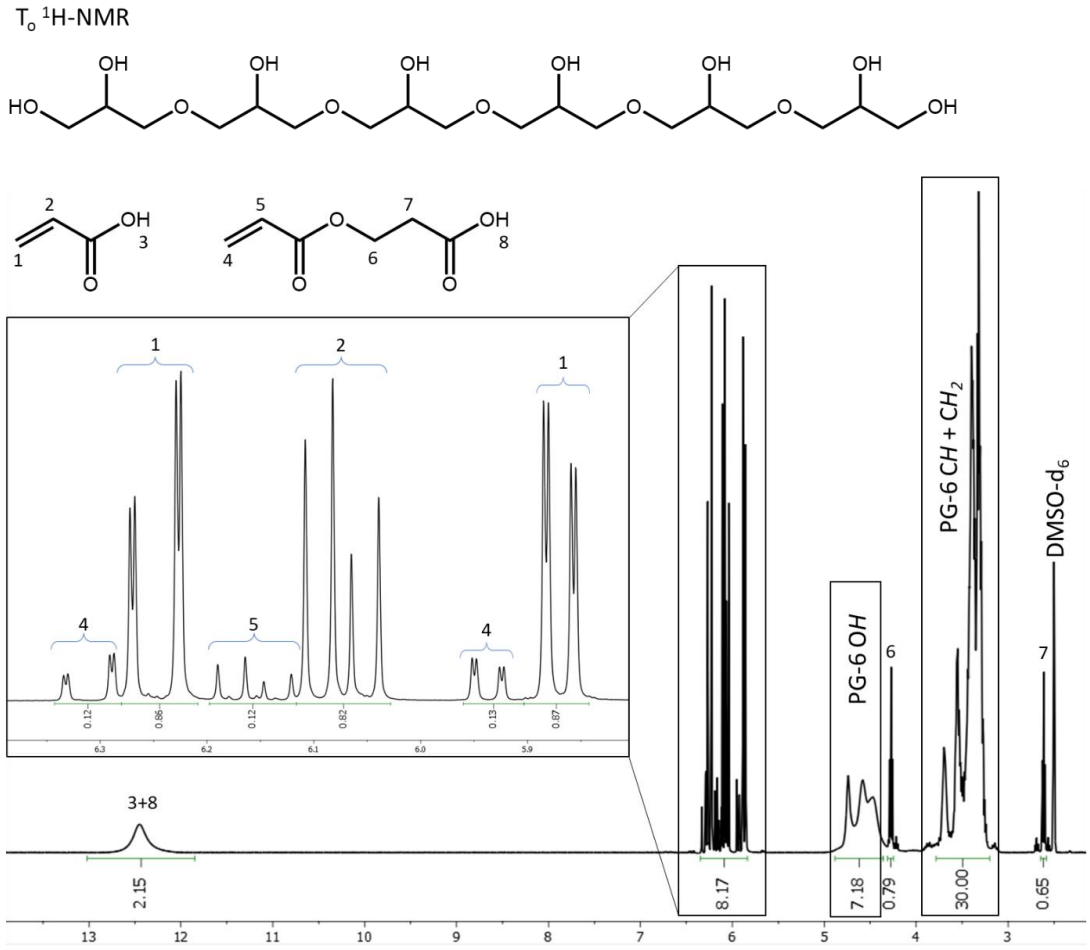

Appendix Figure 34 ^{1}H-NMR at Time Zero of resin synthesis. Note the presence of a -COOH signal around 12.5 ppm, and the presence of Michael addition product in the acrylic acid starting material.

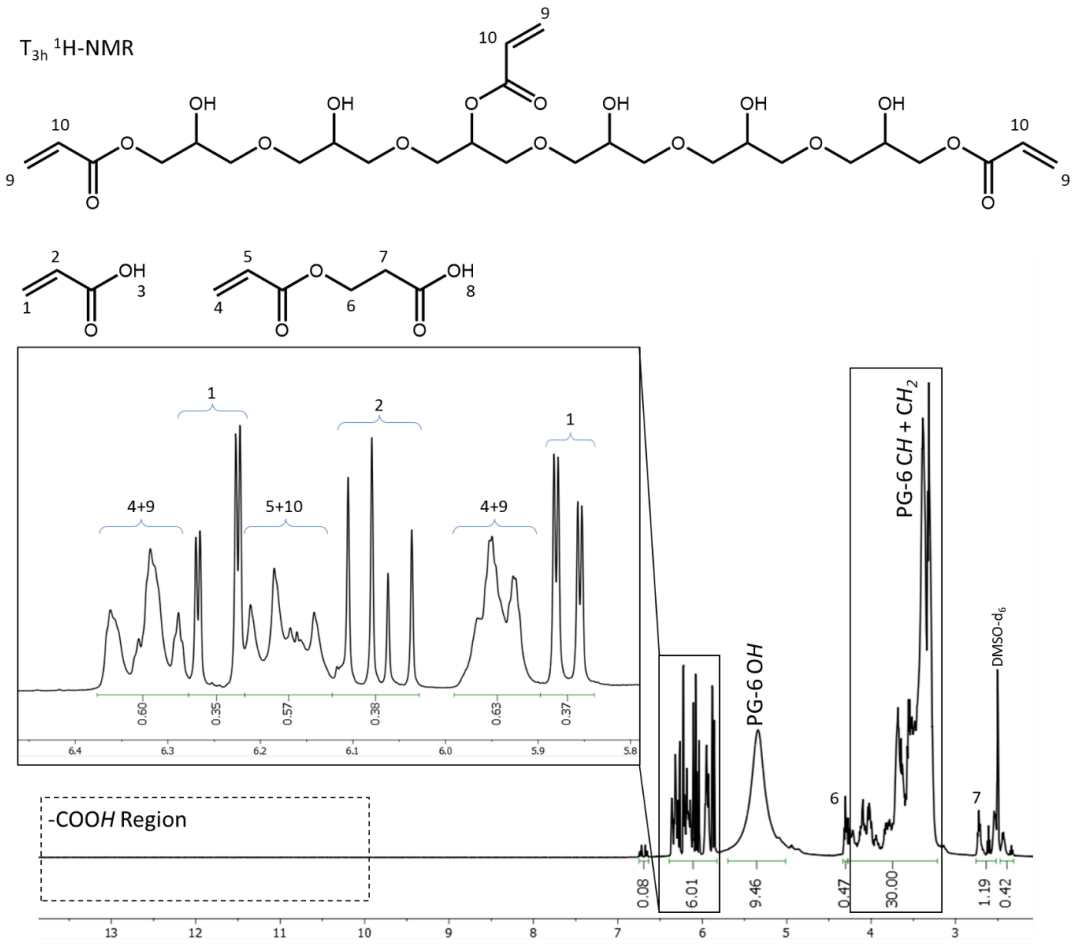

Appendix Figure 35 [1]H-NMR spectrum at Time=3 h of resin synthesis. Indent showing the acrylate region of the spectrum. New signals corresponding to acrylate esters have formed. Conversion of acrylic acid is calculated to be approximately 63%, using the integrals of signals assigned 4+9 and 1. Some error in this estimation is a result of signal overlap between acrylic esters with the Michael addition product.

Time (h)	AV (mg KOH·g^{-1})	Conversion of Acrylic Acid (%)
0	220.4	0
3	55.0	75

Appendix Table 10 Acid Values of the reaction mixture at time zero and time = 3 h. A correction has been applied to account for the presence of catalytic sulphuric acid (AV of batch used= 1112 mg KOH·g^{-1}). Conversion was calculated following Appendix Equation 2

$$Conversion\ (\%) = 100 \times (1 - \frac{AV\ Time\ zero}{AV\ Time\ X})$$

Appendix Equation 2 Conversion of acrylic acid (%) from acid value obtained at time zero and at measured timepoint during PG6-acrylate synthesis.

Design	Vial size (mL)	Exposure per frame (s)	Frames	Total Exposure Time (s)	Rotation per Frame (°)	Result
Pill	4	0.1	120	12	3	1
Pill	4	0.1	40	4	9	2
Pill	4	0.1	60	6	6	10
Chess piece	4	0.1	60	6	6	10
Ball in cage	20	0.1	60	6	6	1
Ball in cage	20	0.12	60	7.2	6	2
Ball in cage	20	0.12	120	14.4	3	3
Ball in cage	20	0.12	210	25.2	3	4
Ball in cage	20	0.12	160	19.2	3	6
Ball in cage	20	0.12	150	18	3	9
Rectangle	20	0.1	60	6	3	10
Thinker*	20	0.11 + 0.11	120 + 120	26.4	3	9
Rabbit*	20	0.12 + 0.15	120 + 30	18.9	3	9
Tensile bar	20	0.12	60	7.2	6	6
Tensile bar	20	0.12	120	14.4	3	9

Appendix Table 11 Volumetric Printing Optimisation of Base Resin. Print result was assessed visually based on physical appearance of the print on a scale from 1 to 10, where 1 denotes a poor print and 10 an excellent print. Parts marked with an asterisk (*) were produced using two consecutive printing cycles.

Design	Vial size (mL)	Exposure per frame (s)	Frames	Total Exposure Time (s)	Rotation per Frame (°)	Result
Pills	20	0.12	120	12	3	10
Pills	20	0.12	140	16.8	3	7
Pills	20	0.12	120	12	3	10
Yoda	20	0.225	120	27	3	5
Yoda	20	0.25	120	30	3	10
Yoda	20	0.3	120	33	3	7
Yoda	20	0.3	120	36	3	4

Appendix Table 12 Volumetric Printing Optimisation of Recycled Resin. Print result was assessed visually based on physical appearance of the print on a scale from 1 to 10, where 1 denotes a poor print and 10 an excellent print.

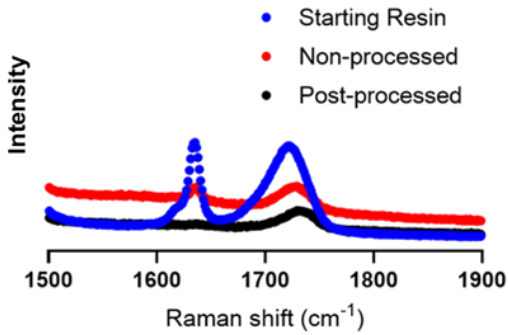

$$DC = \left[1 - \frac{(A_{c=c}/A_{C=O})\text{monomer}}{(A_{c=c}/A_{C=O})\text{polymer}}\right] \times 100$$

Sample	DC (%)
Non-processed	58±4.0
Post-processed	99±0.4

Appendix Figure 36 Raman Spectroscopy to assess degree of curing (DC). Left, Stacked Raman spectra of an example of starting resin, printed resin (non-processed) and resin post curing (post-processed) in the Raman shift range between 1500-1900 cm^{-1}. Right, DC was determined by measuring the change in the ratio of peak areas associated with the C=C (≈1634 cm^{-1}) and C=O (≈1720 cm^{-1}) bonds before and after polymerisation.

Design	Vial size (mL)	Exposure per Frame (s)	Frames	Total Exposure Time (s)	Rotation per Frame (°)	Result
Pill	20	0.25	240	60	3	7
Pill*	20	0.12 + 0.15 + 0.2	120 + 120 + 70	46.4	3	8
Rectangle	20	0.75	120	90	3	8

Appendix Table 13 Volumetric Printing Optimisation of Fluorescein Doped Resin. Print result was assessed visually based on physical appearance of the print on a scale from 1 to 10, where 1 denotes a poor print and 10 an excellent print. Parts marked with an asterisk (*) were produced using three consecutive printing cycles.

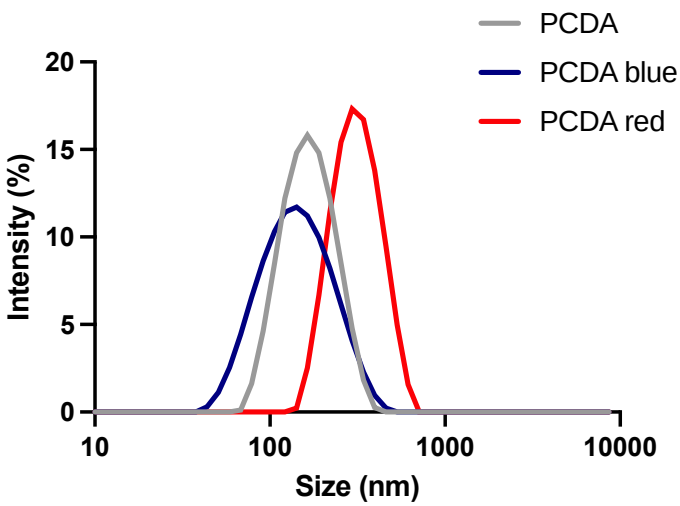

Appendix Figure 37 DLS traces of PCDA micelles in water. Non-polymerised (grey), polymerised (blue) and after thermal stimulus (red).

Sample	Hydrodynamic diameter (nm)	PDI
PCDA	152.1 ± 0.1	0.12 ± 0.10
PCDA blue	120.3 ± 0.5	0.21 ± 0.01
PCDA red	293.2 ± 0.8	0.10 ± 0.01

Appendix Table 14 Size of PCDA micelles in water non-polymerised, polymerised (blue) and after thermal stimulus (red).

Design	PCDA Content (wt.%)	Exposure per frame (s)	Frames	Total Exposure Time (s)	Rotation per Frame (°)	Result
Pills	10	0.12	60	7.2	6	5
Pills	10	0.12	80	9.6	3	5
Pills	10	0.12	40	4.8	6	8
Pills	20	0.12	40	4.8	6	8
Pills	30	0.12	40	4.8	6	3

Appendix Table 15 Volumetric Printing Optimisation of 10,12-Pentacosadyinoic Acid (PCDA) Doped Resin. Print result was assessed visually based on physical appearance of the print on a scale from 1 to 10, where 1 denotes a poor print and 10 an excellent print. All prints were performed in 4 mL vials.

References

1 W. B. Jensen, *J. Chem. Educ.*, 2008, **85**, 624.

2 M. Vert, Y. Doi, K.-H. Hellwich, M. Hess, P. Hodge, P. Kubisa, M. Rinaudo and F. Schué, *Pure Appl. Chem.*, 2012, **84**, 377–410.

3 G. Patterson, *Carbohydr. Polym.*, 2021, **252**, 117182.

4 H. Staudinger, *Berichte der Dtsch. Chem. Gesellschaft (A B Ser.*, 1920, **53**, 1073–1085.

5 H. Frey and T. Johann, *Polym. Chem.*, 2020, **11**, 8–14.

6 C. Williams and M. Hillmyer, *Polym. Rev.*, 2008, **48**, 1–10.

7 S. Kubowicz and A. M. Booth, *Environ. Sci. Technol.*, 2017, **51**, 12058–12060.

8 M. A. Hillmyer, *Science*, 2017, **358**, 868–870.

9 S. Chiba, H. Saito, R. Fletcher, T. Yogi, M. Kayo, S. Miyagi, M. Ogido and K. Fujikura, *Mar. Policy*, 2018, **96**, 204–212.

10 M. Bergmann, F. Collard, J. Fabres, G. W. Gabrielsen, J. F. Provencher, C. M. Rochman, E. van Sebille and M. B. Tekman, *Nat. Rev. Earth Environ.*, 2022, **3**, 323–337.

11 Y. Wang, H. Okochi, Y. Tani, H. Hayami, Y. Minami, N. Katsumi, M. Takeuchi, A. Sorimachi, Y. Fujii, M. Kajino, K. Adachi, Y. Ishihara, Y. Iwamoto and Y. Niida, *Environ. Chem. Lett.*, 2023, **21**, 3055–3062.

12 A. D. Vethaak and J. Legler, *Science*, 2021, **371**, 672–674.

13 A. Sinhamahapatra, A. Sinha, S. K. Pahari, N. Sutradhar, H. C. Bajaj and A. B. Panda, *Catal. Sci. Technol.*, 2012, **2**, 2375.

14 M. L. Granados, A. C. Alba-Rubio, I. Sádaba, R. Mariscal, I. Mateos-Aparicio and Á. Heras, *Green Chem.*, 2011, **13**, 3203.

15 R. Mariscal, P. Maireles-Torres, M. Ojeda, I. Sádaba and M. López Granados, *Energy Environ. Sci.*, 2016, **9**, 1144–1189.

16 H. Wang, G. Ding, X. Li, H. She, Y. Zhu and Y. Li, *Sustain. Energy Fuels*, 2021, **5**, 930–934.

17 M. T. Musser, in *Ullmann's Encyclopedia of Industrial Chemistry*, Wiley-VCH Verlag

GmbH & Co. KGaA, Weinheim, Germany, 2011.

18 Lanxess, bp and LANXESS join forces on renewable raw materials for plastics production, https://lanxess.com/en/Media/Press-Releases/2021/10/bp-and-LANXESS-join-forces-on-renewable-raw-materials-for-plastics-production, (accessed 3 February 2023).

19 World Intellectual Property Organization, WO 2010/132845 A1, 2010.

20 World Intellectual Property Organization, WO2017155441A1, 2017.

21 State Intellectual Property Office of the People's Republic of China, CN102367246A, 2010.

22 N. Hernández, R. C. Williams and E. W. Cochran, *Org. Biomol. Chem.*, 2014, 12, 2834–2849.

23 S. H. Pyo, J. H. Park, V. Srebny and R. Hatti-Kaul, *Green Chem.*, 2020, **22**, 4450–4455.

24 V. Thaore, D. Chadwick and N. Shah, *Chem. Eng. Res. Des.*, 2018, **135**, 140–152.

25 L. A. Ruiz-Cantu, A. K. Pearce, L. Burroughs, T. M. Bennett, C. E. Vasey, R. Wildman, D. J. Irvine, C. Alexander and V. Taresco, *Macromol. Chem. Phys.*, 2019, **220**, 1–11.

26 G. Englezou, K. Kortsen, A. A. C. Pacheco, R. Cavanagh, J. C. Lentz, E. Krumins, C. Sanders-Velez, S. M. Howdle, A. J. Nedoma and V. Taresco, *J. Polym. Sci.*, 2020, **58**, 1571–1581.

27 M. Inam, G. Cambridge, A. Pitto-Barry, Z. P. L. Laker, N. R. Wilson, R. T. Mathers, A. P. Dove and R. K. O'Reilly, *Chem. Sci.*, 2017, **8**, 4223–4230.

28 M. A. Al-Natour, M. D. Yousif, R. Cavanagh, A. Abouselo, E. A. Apebende, A. Ghaemmaghami, D. H. Kim, J. W. Aylott, V. Taresco, V. M. Chauhan and C. Alexander, *ACS Macro Lett.*, 2020, **9**, 431–437.

29 R. F. Storey and J. W. Sherman, *Macromolecules*, 2002, **35**, 1504–1512.

30 N. E. Kamber, W. Jeong, R. M. Waymouth, R. C. Pratt, B. G. G. Lohmeijer and J. L. Hedrick, *Chem. Rev.*, 2007, **107**, 5813–5840.

31 S. Kobayashi, *Proc. Japan Acad. Ser. B*, 2010, **86**, 338–365.

32 O. Dechy-Cabaret, B. Martin-Vaca and D. Bourissou, *Chem. Rev.*, 2004, **104**, 6147–6176.

33 M. C. Tanzi, P. Verderio, M. G. Lampugnani, M. Resnati, E. Dejana and E. Sturani, *J. Mater. Sci. Mater. Med.*, 1994, **5**, 393–396.

34 N. Mase, Moniruzzaman, S. Mori, J. Ishizuka, F. Kumazawa, S. Yamamoto, K. Sato and T. Narumi, *Tetrahedron Lett.*, 2018, **59**, 4392–4396.

35 B. Kost, M. Basko, M. Bednarek, M. Socka, B. Kopka, G. Łapienis, T. Biela, P. Kubisa and M. Brzeziński, *Prog. Polym. Sci.*, 2022, **130**, 101556.

36 F. Nederberg, E. F. Connor, M. Möller, T. Glauser and J. L. Hedrick, *Angew. Chemie Int. Ed.*, 2001, **40**, 2712–2715.

37 B. G. G. Lohmeijer, R. C. Pratt, F. Leibfarth, J. W. Logan, D. A. Long, A. P. Dove, F. Nederberg, J. Choi, C. Wade, R. M. Waymouth and J. L. Hedrick, *Macromolecules*, 2006, **39**, 8574–8583.

38 H. A. Brown, A. G. De Crisci, J. L. Hedrick and R. M. Waymouth, *ACS Macro Lett.*, 2012, **1**, 1113–1115.

39 I. Kaljurand, A. Kütt, L. Sooväli, T. Rodima, V. Mäemets, I. Leito and I. A. Koppel, *J. Org. Chem.*, 2005, **70**, 1019–1028.

40 A. Dzienia, P. Maksym, B. Hachuła, M. Tarnacka, T. Biela, S. Golba, A. Zięba, M. Chorążewski, K. Kaminski and M. Paluch, *Polym. Chem.*, 2019, **10**, 6047–6061.

41 P. Bana, Á. Szigetvári, J. Kóti, J. Éles and I. Greiner, *React. Chem. Eng.*, 2019, **4**, 652–657.

42 Y. Shen, C. Yuan, X. Zhu, Q. Chen, S. Lu and H. Xie, *Green Chem.*, 2021, **23**, 9922–9934.

43 K. Fukushima, O. Coulembier, J. M. Lecuyer, H. A. Almegren, A. M. Alabdulrahman, F. D. Alsewailem, M. A. Mcneil, P. Dubois, R. M. Waymouth, H. W. Horn, J. E. Rice and J. L. Hedrick, *J. Polym. Sci. Part A Polym. Chem.*, 2011, **49**, 1273–1281.

44 D. Xue, Y. Mu, Y. Mao, T. Yang and Z. Xiu, *Green Chem.*, 2014, **16**, 3218–3223.

45 N. Zanda, A. Sobolewska, E. Alza, A. W. Kleij and M. A. Pericàs, *ACS Sustain. Chem. Eng.*, 2021, **9**, 4391–4397.

46 S. Kobayashi, *Polym. Adv. Technol.*, 2015, **26**, 677–686.

47 S. Kobayashi, *Macromol. Rapid Commun.*, 2009, **30**, 237–266.

48 L. Gustini, B. A. J. Noordover, C. Gehrels, C. Dietz and C. E. Koning, *Eur. Polym. J.*, 2015,

67, 459–475.

49 S. Kobayashi and A. Makino, *Chem. Rev.*, 2009, **109**, 5288–5353.

50 Y. Lu, Q. Lv, B. Liu and J. Liu, *Biomater. Sci.*, 2019, **7**, 4963–4983.

51 C. S. Craik, S. Roczniak, C. Largman and W. J. Rutter, *Science*, 1987, **237**, 909–913.

52 F. Hofer, J. Kraml, U. Kahler, A. S. Kamenik and K. R. Liedl, *J. Chem. Inf. Model.*, 2020, **60**, 3030–3042.

53 F. Hollmann, P. Grzebyk, V. Heinrichs, K. Doderer and O. Thum, *J. Mol. Catal. B Enzym.*, 2009, **57**, 257–261.

54 D. J. Ericsson, A. Kasrayan, P. Johansson, T. Bergfors, A. G. Sandström, J. E. Bäckvall and S. L. Mowbray, *J. Mol. Biol.*, 2008, **376**, 109–119.

55 A. Magnusson, K. Hult and M. Holmquist, *J. Am. Chem. Soc.*, 2001, **123**, 4354–4355.

56 C. Ortiz, M. L. Ferreira, O. Barbosa, J. C. S. dos Santos, R. C. Rodrigues, Á. Berenguer-Murcia, L. E. Briand and R. Fernandez-Lafuente, *Catal. Sci. Technol.*, 2019, **9**, 2380–2420.

57 H. Uyama, S. Suda and S. Kobayashi, *Acta Polym.*, 1998, **49**, 700–703.

58 U. Meyer, A. R. A. Palmans, T. Loontjens and A. Heise, *Macromolecules*, 2002, **35**, 2873–2875.

59 R. K. Srivastava and A.-C. Albertsson, *Macromolecules*, 2006, **39**, 46–54.

60 A. A. Homaei, R. Sariri, F. Vianello and R. Stevanato, *J. Chem. Biol.*, 2013, **6**, 185–205.

61 R. A. Sheldon, *Adv. Synth. Catal.*, 2007, 349, 1289–1307.

62 C. Garcia-Galan, Á. Berenguer-Murcia, R. Fernandez-Lafuente and R. C. Rodrigues, *Adv. Synth. Catal.*, 2011, 353, 2885–2904.

63 T. Jesionowski, J. Zdarta and B. Krajewska, *Adsorption*, 2014, **20**, 801–821.

64 A. Iemhoff, J. Sherwood, C. R. McElroy and A. J. Hunt, *Green Chem.*, 2018, **20**, 136–140.

65 D. Remonatto, R. H. Miotti Jr., R. Monti, J. C. Bassan and A. V. de Paula, *Process Biochem.*, 2022, **114**, 1–20.

66 D. Brady and J. Jordaan, *Biotechnol. Lett.*, 2009, 31, 1639–1650.

67 D. Feder and R. A. Gross, *Biomacromolecules*, 2010, **11**, 690–697.

68 R. C. Rodrigues, C. Ortiz, Á. Berenguer-Murcia, R. Torres and R. Fernández-Lafuente, *Chem. Soc. Rev.*, 2013, **42**, 6290–6307.

69 M. Hajar, S. Shokrollahzadeh, F. Vahabzadeh and A. Monazzami, *Enzyme Microb. Technol.*, 2009, **45**, 188–194.

70 J. Wang, S.-S. Gu, H.-S. Cui, X.-Y. Wu and F.-A. Wu, *Bioresour. Technol.*, 2014, **158**, 39–47.

71 F. C. Loeker, C. J. Duxbury, R. Kumar, W. Gao, R. A. Gross and S. M. Howdle, *Macromolecules*, 2004, **37**, 2450–2453.

72 S. Spinella, M. Ganesh, G. Lo Re, S. Zhang, J.-M. Raquez, P. Dubois and R. A. Gross, *Green Chem.*, 2015, **17**, 4146–4150.

73 J. C. Lentz, R. Cavanagh, C. Moloney, B. Falcone Pin, K. Kortsen, H. R. Fowler, P. L. Jacob, E. Krumins, C. Clark, F. Machado, N. Breitkreuz, B. Cale, A. R. Goddard, J. D. Hirst, V. Taresco and S. M. Howdle, *Polym. Chem.*, 2022, **13**, 6032–6045.

74 B. Dobraszczyk and M. Morgenstern, *J. Cereal Sci.*, 2003, **38**, 229–245.

75 J. Aho, S. Hvidt and S. Baldursdottir, Springer, New York, NY, 2016, pp. 719–750.

76 S. Sun, M. Li and A. Liu, *Int. J. Adhes. Adhes.*, 2013, **41**, 98–106.

77 C. Gallegos and J. M. Franco, *Curr. Opin. Colloid Interface Sci.*, 1999, **4**, 288–293.

78 Y. J. Zheng and X. J. Loh, *Polym. Adv. Technol.*, 2016, **27**, 1664–1679.

79 J. R. Stokes, L. Macakova, A. Chojnicka-Paszun, C. G. de Kruif and H. H. J. de Jongh, *Langmuir*, 2011, **27**, 3474–3484.

80 A. Mohamed, S. Salehi and R. Ahmed, *Geothermics*, 2021, **93**, 102066.

81 R. G. Larson, A. K. Van Dyk, T. Chatterjee and V. V. Ginzburg, *Prog. Polym. Sci.*, 2022, **129**, 101546.

82 T. Kealy, A. Abram, B. Hunt and R. Buchta, *Int. J. Pharm.*, 2008, **355**, 67–80.

83 J. E. Glass, D. N. Schulz and C. F. Zukoski, 1991, pp. 2–17.

84 D. D. Braun and M. R. Rosen, *Rheology Modifiers Handbook: Practical Use and Application*, Elsevier Science, 2013.

85 G. Fadat, *Nord. Pulp Pap. Res. J.*, 1993, **8**, 191–194.

86 P. Zhang, F. Sun, S. Liu and S. Jiang, *J. Control. Release*, 2016, **244**, 184–193.

87 M. J. Mitchell, M. M. Billingsley, R. M. Haley, M. E. Wechsler, N. A. Peppas and R. Langer, *Nat. Rev. Drug Discov.*, 2021, **20**, 101–124.

88 M. A. Bruusgaard-Mouritsen, J. D. Johansen and L. H. Garvey, *Clin. Exp. Allergy*, 2021, **51**, 463–470.

89 F. Kawai, in *Biopolymers Online*, eds. S. Matsumura and A. Steinbüchel, Wiley, 2001.

90 G. Pio and E. Salzano, *Chem. Eng. Sci.*, 2020, **212**, 115331.

91 U. Kästner, *Colloids Surfaces A Physicochem. Eng. Asp.*, 2001, **183**–**185**, 805–821.

92 G. D. Shay, in *Alkali-Swellable and Alkali-Soluble Thickener Technology*, 1989, pp. 457–494.

93 C. J. Verbrugge, *J. Appl. Polym. Sci.*, 1970, **14**, 897–909.

94 C. M. Miller, K. R. Olesen and G. D. Shay, in *ACS Symposium Series*, 2000, vol. 765, pp. 338–350.

95 M. Paderes, D. Ahirwal and S. Fernández Prieto, *Phys. Sci. Rev.*, 2017, **2**, 0021.

96 P. Bajaj, M. Goyal and R. B. Chavan, *J. Macromol. Sci. Part C*, 1993, **33**, 321–348.

97 A. W. Jackson, S. R. Mothe, P. Ang, L. R. Chennamaneni, A. M. V. Herk and P. Thoniyot, *Chemosphere*, 2022, **293**, 133487.

98 S. M. Barbon, M. C. D. Carter, L. Yin, C. M. Whaley, V. C. Albright, R. E. Tecklenburg, S. M. Barbon, C. M. Whaley, R. E. Tecklenburg, M. C. D. Carter, L. Yin and V. C. Albright, *Macromol. Rapid Commun.*, 2022, **43**, 2100773.

99 A. J. J. Straathof, S. Sie, T. T. Franco and L. A. M. van der Wielen, *Appl. Microbiol. Biotechnol.*, 2005, **67**, 727–734.

100 X. Suo, H. Zhang, Q. Ye, X. Dai, H. Yu and R. Li, *Chem. Eng. Res. Des.*, 2015, **104**, 346–356.

101 M. Fujita, Y. Izato, Y. Iizuka and A. Miyake, *Process Saf. Environ. Prot.*, 2019, **129**, 339–

347.

102 P. T. Anastas and J. C. Warner, *Green Chemistry: Theory and Practice*, Oxford University Press, 1998.

103 H. C. Erythropel, J. B. Zimmerman, T. M. de Winter, L. Petitjean, F. Melnikov, C. H. Lam, A. W. Lounsbury, K. E. Mellor, N. Z. Janković, Q. Tu, L. N. Pincus, M. M. Falinski, W. Shi, P. Coish, D. L. Plata and P. T. Anastas, *Green Chem.*, 2018, **20**, 1929–1961.

104 K. Sevim and J. Pan, *Acta Biomater.*, 2018, **66**, 192–199.

105 S. Tian, Q. Yue, C. Liu, M. Li, M. Yin, Y. Gao, F. Meng, B. Z. Tang and L. Luo, *J. Am. Chem. Soc.*, 2021, **143**, 10054–10058.

106 L. S. Nair and C. T. Laurencin, *Prog. Polym. Sci.*, 2007, **32**, 762–798.

107 K. R. Kunduru, R. Hogerat, K. Ghosal, M. Shaheen-Mualim and S. Farah, *Chem. Eng. J.*, 2023, **459**, 141211.

108 M. d'Almeida Gameiro, A. Goddard, V. Taresco and S. M. Howdle, *Green Chem.*, 2020, **22**, 1308–1318.

109 A. R. Goddard, E. A. Apebende, J. C. Lentz, K. Carmichael, V. Taresco, D. J. Irvine and S. M. Howdle, *Polym. Chem.*, 2021, **12**, 2992–3003.

110 C. Hahn, S. Wesselbaum, H. Keul and M. Möller, *Eur. Polym. J.*, 2013, **49**, 217–227.

111 Y. Shibata and A. Takasu, *J. Polym. Sci. Part A Polym. Chem.*, 2009, **47**, 5747–5759.

112 L. Gustini, C. Lavilla, W. W. T. J. Janssen, A. Martínez De Ilarduya, S. Muñoz-Guerra and C. E. Koning, *ChemSusChem*, 2016, **9**, 2250–2260.

113 M. Ayoub and A. Z. Abdullah, *Renew. Sustain. Energy Rev.*, 2012, **16**, 2671–2686.

114 H. W. Tan, A. R. Abdul Aziz and M. K. Aroua, *Renew. Sustain. Energy Rev.*, 2013, **27**, 118–127.

115 J. Li, X.-Y. Zheng, X.-J. Fang, S.-W. Liu, K.-Q. Chen, M. Jiang, P. Wei and P.-K. Ouyang, *Bioresour. Technol.*, 2011, **102**, 6147–6152.

116 V. R. Dhongde, B. S. De and K. L. Wasewar, *J. Chem. Eng. Data*, 2019, **64**, 1072–1084.

117 Y. Deng, L. Ma and Y. Mao, *Biochem. Eng. J.*, 2016, **105**, 16–26.

118 A. Köckritz and A. Martin, *Eur. J. Lipid Sci. Technol.*, 2011, **113**, 83–91.

119 Z. Dai, F. Guo, S. Zhang, W. Zhang, Q. Yang, W. Dong, M. Jiang, J. Ma and F. Xin, *Biofuels, Bioprod. Biorefining*, 2020, **14**, 965–985.

120 V. R. Thalladi, M. Nüsse and R. Boese, *J. Am. Chem. Soc.*, 2000, **122**, 9227–9236.

121 A. Douka, S. Vouyiouka, L. M. Papaspyridi and C. D. Papaspyrides, *Prog. Polym. Sci.*, 2018, 79, 1–25.

122 S. Y. Chan, W. S. Choo, D. J. Young and X. J. Loh, *Carbohydr. Polym.*, 2017, **161**, 118–139.

123 P. Sterchele, in *Encyclopedia of Toxicology*, Elsevier, 2005, pp. 671–672.

124 S. Ozkan, C. Alonso and R. L. McMullen, *Int. J. Cosmet. Sci.*, 2020, **42**, 536–547.

125 D. Balzer, S. Varwig and M. Weihrauch, *Colloids Surfaces A Physicochem. Eng. Asp.*, 1995, **99**, 233–246.

126 T. G. Mezger, *The Rheology Handbook*, Vincentz Network, Hannover, 2nd edn., 2006.

127 A. Hirao, R. Goseki and T. Ishizone, *Macromolecules*, 2014, **47**, 1883–1905.

128 J. Herzberger, K. Niederer, H. Pohlit, J. Seiwert, M. Worm, F. R. Wurm and H. Frey, *Chem. Rev.*, 2016, **116**, 2170–2243.

129 O. Wichterle, J. Šebenda and J. Králíček, in *Fortschritte Der Hochpolymeren-Forschung*, Springer-Verlag, Berlin/Heidelberg, 1961, pp. 578–595.

130 A. F. Johnson and D. J. Worsfold, *J. Polym. Sci. Part A Gen. Pap.*, 1965, **3**, 449–455.

131 A. Duda and S. Penczek, *Makromol. Chemie. Macromol. Symp.*, 1991, **42**–**43**, 135–143.

132 K. Hong, D. Uhrig and J. W. Mays, *Curr. Opin. Solid State Mater. Sci.*, 1999, **4**, 531–538.

133 C. Guerrero-Sanchez, C. Abeln and U. S. Schubert, *J. Polym. Sci. Part A Polym. Chem.*, 2005, **43**, 4151–4160.

134 M. Gervais, A.-L. Brocas, G. Cendejas, A. Deffieux and S. Carlotti, *Macromolecules*, 2010, **43**, 1778–1784.

135 A. Sunder, R. Hanselmann, H. Frey and R. Mülhaupt, *Macromolecules*, 1999, **32**, 4240–4246.

136 A. Thomas, S. S. Müller and H. Frey, *Biomacromolecules*, 2014, **15**, 1935–1954.

137 E. MacDonald and R. Wicker, *Science*, 2016, **353**, aaf2093.

138 S. C. Ligon, R. Liska, J. Stampfl, M. Gurr and R. Mülhaupt, *Chem. Rev.*, 2017, **117**, 10212–10290.

139 R. D. Sochol, E. Sweet, C. C. Glick, S. Venkatesh, A. Avetisyan, K. F. Ekman, A. Raulinaitis, A. Tsai, A. Wienkers, K. Korner, K. Hanson, A. Long, B. J. Hightower, G. Slatton, D. C. Burnett, T. L. Massey, K. Iwai, L. P. Lee, K. S. J. Pister and L. Lin, *Lab Chip*, 2016, **16**, 668–678.

140 A. Zolfaghari, T. Chen and A. Y. Yi, *Int. J. Extrem. Manuf.*, 2019, **1**, 012005.

141 B. Blakey-Milner, P. Gradl, G. Snedden, M. Brooks, J. Pitot, E. Lopez, M. Leary, F. Berto and A. du Plessis, *Mater. Des.*, 2021, **209**, 110008.

142 J. Jiang, *J. Clean. Prod.*, 2020, **272**, 122916.

143 B. E. Kelly, I. Bhattacharya, H. Heidari, M. Shusteff, C. M. Spadaccini and H. K. Taylor, *Science*, 2019, **363**, 1075–1079.

144 M. Regehly, Y. Garmshausen, M. Reuter, N. F. König, E. Israel, D. P. Kelly, C.-Y. Chou, K. Koch, B. Asfari and S. Hecht, *Nature*, 2020, **588**, 620–624.

145 C. C. Cook, E. J. Fong, J. J. Schwartz, D. H. Porcincula, A. C. Kaczmarek, J. S. Oakdale, B. D. Moran, K. M. Champley, C. M. Rackson, A. Muralidharan, R. R. McLeod, M. Shusteff, C. C. Cook, E. J. Fong, J. J. Schwartz, D. H. Porcincula, A. C. Kaczmarek, J. S. Oakdale, B. D. Moran, K. M. Champley, M. Shusteff, C. M. Rackson, R. R. McLeod and A. Muralidharan, *Adv. Mater.*, 2020, **32**, 2003376.

146 L. Rodríguez-Pombo, L. Martínez-Castro, X. Xu, J. J. Ong, C. Rial, D. N. García, A. González-Santos, J. Flores-González, C. Alvarez-Lorenzo, A. W. Basit and A. Goyanes, *Int. J. Pharm. X*, 2023, **5**, 100166.

147 B. Wang, E. Engay, P. R. Stubbe, S. Z. Moghaddam, E. Thormann, K. Almdal, A. Islam and Y. Yang, *Nat. Commun.*, 2022, **13**, 367.

148 J. Huang, Z. Chen, C. Wen, T. Ling and Z. Chen, *Addit. Manuf.*, 2022, **59**, 103088.

149 D. Loterie, P. Delrot and C. Moser, *Nat. Commun.*, 2020, **11**, 852.

150 P. N. Bernal, P. Delrot, D. Loterie, Y. Li, J. Malda, C. Moser and R. Levato, *Adv. Mater.*, 2019, **31**, 1904209.

151 Q. Thijssen, A. Quaak, J. Toombs, E. De Vlieghere, L. Parmentier, H. Taylor and S. Van Vlierberghe, *Adv. Mater.*, 2023, **35**, 1–16.

152 M. Xie, L. Lian, X. Mu, Z. Luo, C. E. Garciamendez-Mijares, Z. Zhang, A. López, J. Manríquez, X. Kuang, J. Wu, J. K. Sahoo, F. Z. González, G. Li, G. Tang, S. Maharjan, J. Guo, D. L. Kaplan and Y. S. Zhang, *Nat. Commun.*, 2023, **14**, 210.

153 R. Ferrari, Y. Yu, M. Morbidelli, R. A. Hutchinson and D. Moscatelli, *Macromolecules*, 2011, **44**, 9205–9212.

154 M. Takwa, Y. Xiao, N. Simpson, E. Malmström, K. Hult, C. E. Koning, A. Heise and M. Martinelle, *Biomacromolecules*, 2008, **9**, 704–710.

155 Y. Xiao, M. Takwa, K. Hult, C. E. Koning, A. Heise and M. Martinelle, *Macromol. Biosci.*, 2009, **9**, 713–720.

156 M. Sponchioni, L. Morosi, M. Lupi and U. Capasso Palmiero, *RSC Adv.*, 2017, **7**, 50981–50992.

157 A. K. Pearce, C. E. Vasey, A. B. Anane-Adjei, F. Sodano, V. C. Crucitti, D. J. Irvine, S. M. Howdle, C. Alexander and V. Taresco, *Macromol. Chem. Phys.*, 2019, **220**, 1900270.

158 J. Xu, J. Song, S. Pispas and G. Zhang, *Polym. Chem.*, 2014, **5**, 4726–4733.

159 C. Li, S. Pan, W. Xu, Y. Lu, P. Wang, F. Zhang and R. A. Gross, *Green Chem.*, 2020, **22**, 662–668.

160 A. E. Polloni, V. Chiaradia, E. M. Figura, J. P. De Paoli, D. de Oliveira, J. V. de Oliveira, P. H. H. de Araujo and C. Sayer, *Appl. Biochem. Biotechnol.*, 2018, **184**, 659–672.

161 Á. Cruz-Izquierdo, L. A. M. van den Broek, J. L. Serra, M. J. Llama and C. G. Boeriu, *Pure Appl. Chem.*, 2015, **87**, 59–69.

162 A. Pellis, F. P. Byrne, J. Sherwood, M. Vastano, J. W. Comerford and T. J. Farmer, *Green Chem.*, 2019, **21**, 1686–1694.

163 H. Zhao, C. Zhang and T. D. Crittle, *J. Mol. Catal. B Enzym.*, 2013, **85**–**86**, 243–247.

164 A. Narumi, Y. Chen, M. Soné, K. Fuchise, R. Sakai, T. Satoh, Q. Duan, S. Kawaguchi and T. Kakuchi, *Macromol. Chem. Phys.*, 2009, **210**, 349–358.

165 Y. Sun, L. Fu, M. Olszewski and K. Matyjaszewski, *Macromol. Rapid Commun.*, 2019, **40**, 1800877.

166 M. N. Albarghouthi, T. M. Stein and A. E. Barron, *Electrophoresis*, 2003, **24**, 1166–1175.

167 A. Bal, B. Özkahraman and Z. Özbaş, *J. Appl. Polym. Sci.*, 2016, **133**, 43226.

168 C. Zhao, Q. Chen, K. Patel, L. Li, X. Li, Q. Wang, G. Zhang and J. Zheng, *Soft Matter*, 2012, **8**, 7848–7857.

169 C. Y. Gong, S. Shi, P. W. Dong, B. Kan, M. L. Gou, X. H. Wang, X. Y. Li, F. Luo, X. Zhao, Y. Q. Wei and Z. Y. Qian, *Int. J. Pharm.*, 2009, **365**, 89–99.

170 D. F. Aycock, *Org. Process Res. Dev.*, 2007, **11**, 156–159.

171 V. Pace, P. Hoyos, L. Castoldi, P. Domínguez de María and A. R. Alcántara, *ChemSusChem*, 2012, **5**, 1369–1379.

172 D. M. O'Brien, C. Vallieres, C. Alexander, S. M. Howdle, R. A. Stockman and S. V. Avery, *J. Mater. Chem. B*, 2019, **7**, 5222–5229.

173 V. Pace, W. Holzer and B. Olofsson, *Adv. Synth. Catal.*, 2014, **356**, 3697–3736.

174 D. Kaiser, A. Bauer, M. Lemmerer and N. Maulide, *Chem. Soc. Rev.*, 2018, **47**, 7899–7925.

175 United States Patent Office, US 8,466,299 B2, 2013.

176 A. Kumari, S. K. Yadav and S. C. Yadav, *Colloids Surfaces B Biointerfaces*, 2010, **75**, 1–18.

177 W. Saiyasombat, R. Molloy, T. . Nicholson, A. . Johnson, I. . Ward and S. Poshyachinda, *Polymer (Guildf).*, 1998, **39**, 5581–5585.

178 S. Shoda, H. Uyama, J. Kadokawa, S. Kimura and S. Kobayashi, *Chem. Rev.*, 2016, **116**, 2307–2413.

179 P. Atkins and J. De Paula, *Physical Chemistry*, W.H. Freeman and Company, New York, Ninth., 2010.

180 C. Luna, C. Verdugo, E. D. Sancho, D. Luna, J. Calero, A. Posadillo, F. M. Bautista and A. A. Romero, *Bioresour. Bioprocess.*, 2014, **1**, 11.

181 M. M. R. Talukder, J. C. Wu, S. K. Lau, L. C. Cui, G. Shimin and A. Lim, *Energy and Fuels*, 2009, **23**, 1–4.

182 F. Deng and R. A. Gross, *Int. J. Biol. Macromol.*, 1999, **25**, 153–159.

183 L. Corici, A. Pellis, V. Ferrario, C. Ebert, S. Cantone and L. Gardossi, *Adv. Synth. Catal.*, 2015, **357**, 1763–1774.

184 J. Liu, R. S. Loewe and R. D. McCullough, *Macromolecules*, 1999, **32**, 5777–5785.

185 V. H. Dao, N. R. Cameron and K. Saito, *Polym. Chem.*, 2017, **8**, 6834–6843.

186 U. Capasso Palmiero, M. Sponchioni, N. Manfredini, M. Maraldi and D. Moscatelli, *Polym. Chem.*, 2018, **9**, 4084–4099.

187 N. J. Sherck, H. C. Kim and Y. Y. Won, *Macromolecules*, 2016, **49**, 4699–4713.

188 X. Shi, J. Wu, Z. Wang, F. Song, W. Gao and S. Liu, *RSC Adv.*, 2020, **10**, 19759–19769.

189 L. Liu, S. Li, H. Garreau and M. Vert, *Biomacromolecules*, 2000, **1**, 350–359.

190 N. Kamaly, B. Yameen, J. Wu and O. C. Farokhzad, *Chem. Rev.*, 2016, **116**, 2602–2663.

191 L. Shi, J. Zhang, M. Zhao, S. Tang, X. Cheng, W. Zhang, W. Li, X. Liu, H. Peng and Q. Wang, *Nanoscale*, 2021, **13**, 10748–10764.

192 G. M. Morris, H. Ruth, W. Lindstrom, M. F. Sanner, R. K. Belew, D. S. Goodsell and A. J. Olson, *J. Comput. Chem.*, 2009, **30**, 2785–2791.

193 D. A. Case, H. M. Aktulga, K. Belfon, I. Y. Ben-Shalom, S. R. Brozell, D. S. Cerutti, T. E. Cheatham, III, G. A. Cisneros, V. W. D. Cruzeiro, T. A. Darden, R. E. Duke, G. Giambasu, M. K. Gilson, H. Gohlke, A. W. Goetz, R. Harris, S. Izadi, S. A. Izmailov, C. Jin, K. Kasavajhala, M. C. Kaymak, E. King, A. Kovalenko, T. Kurtzman, T. S. Lee, S. LeGrand, P. Li, C. Lin, J. Liu, T. Luchko, R. Luo, M. Machado, V. Man, M. Manathunga, K. M. Merz, Y. Miao, O. Mikhailovskij, G. Monard, H. Nguyen, K. A. O'Hearn, A. Onufriey, F. Pan, S. Pantano, R. Qi, A. Rahnamoun, D. R. Roe, A. Roitberg, C. Sagui, S. Schott-Verdugo, J. Shen, C. L. Simmerling, N. R. Skrynnikov, J. Smith, J. Swails, R. C. Walker, J. Wang, H. Wei, R. M. Wolf, X. Wu, Y. Xue, D. M. York, S. Zhao and P. A. Kollman, *Amber 2021, Univ. California, San Fr.*

194 C. Tian, K. Kasavajhala, K. A. A. Belfon, L. Raguette, H. Huang, A. N. Migues, J. Bickel, Y. Wang, J. Pincay, Q. Wu and C. Simmerling, *J. Chem. Theory Comput.*, 2020, **16**, 528–552.

195 J. Wang, W. Wang, P. A. Kollman and D. A. Case, *J. Mol. Graph. Model.*, 2006, **25**, 247–

260.

196 J. Wang, R. M. Wolf, J. W. Caldwell, P. A. Kollman and D. A. Case, *J. Comput. Chem.*, 2004, **25**, 1157–1174.

197 W. L. Jorgensen, J. Chandrasekhar, J. D. Madura, R. W. Impey and M. L. Klein, *J. Chem. Phys.*, 1983, **79**, 926–935.

198 J. P. Ryckaert, G. Ciccotti and H. J. C. Berendsen, *J. Comput. Phys.*, 1977, **23**, 327–341.

199 A. Onufriev, D. Bashford and D. A. Case, *Proteins Struct. Funct. Genet.*, 2004, **55**, 383–394.

200 D. Cespi, R. Cucciniello, M. Ricciardi, C. Capacchione, I. Vassura, F. Passarini and A. Proto, *Green Chem.*, 2016, **18**, 4559–4570.

201 C. C. Chong, A. Aqsha, M. Ayoub, M. Sajid, A. Z. Abdullah, S. Yusup and B. Abdullah, *Environ. Technol. Innov.*, 2020, **19**, 100859.

202 K. Hill, in *Biorefineries-Industrial Processes and Products*, Wiley-VCH Verlag GmbH, Weinheim, Germany, 2007, vol. 79, pp. 291–314.

203 R. Wilson, B. J. van Schie and D. Howes, *Food Chem. Toxicol.*, 1998, **36**, 711–718.

204 Reaction mass of oxybispropanediol, triglycerol and tetraglycerol, https://echa.europa.eu/registration-dossier/-/registered-dossier/13319, (accessed 8 June 2023).

205 A. Martin and M. Richter, *Eur. J. Lipid Sci. Technol.*, 2011, **113**, 100–117.

206 N. Galy, R. Nguyen, P. Blach, S. Sambou, D. Luart and C. Len, *J. Ind. Eng. Chem.*, 2017, **51**, 312–318.

207 F. J. S. Barros, R. Moreno-Tost, J. A. Cecilia, A. L. Ledesma-Muñoz, L. C. C. de Oliveira, F. M. T. Luna and R. S. Vieira, *Mol. Catal.*, 2017, **433**, 282–290.

208 J. Hu, W. Gao, A. Kulshrestha and R. A. Gross, *Macromolecules*, 2006, **39**, 6789–6792.

209 A. Kumar, A. S. Kulshrestha, W. Gao and R. A. Gross, *Macromolecules*, 2003, **36**, 8219–8221.

210 H.-Y. Wang, W.-W. Zhang, N. Wang, C. Li, K. Li and X.-Q. Yu, *Biomacromolecules*, 2010, **11**, 3290–3293.

211 C. Pang, X. Jiang, Y. Yu, L. Chen, J. Ma and H. Gao, *ACS Macro Lett.*, 2019, 1442–1448.

212 Y. Jiang, G. O. R. A. van Ekenstein, A. J. J. Woortman and K. Loos, *Macromol. Chem. Phys.*, 2014, **215**, 2185–2197.

213 Succinic Acid, https://echa.europa.eu/registration-dossier/-/registered-dossier/15265/5/3/1, (accessed 8 June 2023).

214 A. Llevot, E. Grau, S. Carlotti, S. Grelier and H. Cramail, *Polym. Chem.*, 2015, **6**, 6058–6066.

215 Dimethyl succinate, https://echa.europa.eu/registration-dossier/-/registered-dossier/15043, (accessed 8 June 2023).

216 S. Cassel, C. Debaig, T. Benvegnu, P. Chaimbault, M. Lafosse, D. Plusquellec and P. Rollin, *European J. Org. Chem.*, 2001, **2001**, 875–896.

217 Y. Yang, W. Lu, J. Cai, Y. Hou, S. Ouyang, W. Xie and R. A. Gross, *Macromolecules*, 2011, **44**, 1977–1985.

218 S. Podzimek, T. Vlcek and C. Johann, *J. Appl. Polym. Sci.*, 2001, **81**, 1588–1594.

219 P. Castignolles, R. Graf, M. Parkinson, M. Wilhelm and M. Gaborieau, *Polymer (Guildf).*, 2009, **50**, 2373–2383.

220 A. I. Cooper, *J. Mater. Chem.*, 2000, 10, 207–234.

221 M. Amon and C. D. Denson, *Ind. Eng. Chem. Fundam.*, 1980, **19**, 415–420.

222 V. N. Novikov and E. A. Rössler, *Polymer (Guildf).*, 2013, **54**, 6987–6991.

223 R. S. Karinen, J. A. Linnekoski and A. O. I. Krause, *Catal. Letters*, 2001, **76**, 81–87.

224 D. S. Marques, M. H. Gil and C. M. S. G. Baptista, *J. Appl. Polym. Sci.*, 2013, **128**, 2145–2151.

225 K. N. Onwukamike, S. Grelier, E. Grau, H. Cramail and M. A. R. Meier, *ACS Sustain. Chem. Eng.*, 2018, **6**, 8826–8835.

226 K. Ratzenböck, D. Pahovnik and C. Slugovc, *Polym. Chem.*, 2020, **11**, 7476–7480.

227 G. Arzamendi, I. Campo, E. Arguiñarena, M. Sánchez, M. Montes and L. M. Gandía, *Chem. Eng. J.*, 2007, **134**, 123–130.

228 B.-G. Woo, K. Y. Choi and K. H. Song, *Ind. Eng. Chem. Res.*, 2001, **40**, 3459–3466.

229 O. Brand, J. M. English, S. A. Bidstrup and M. G. Allen, *Int. Conf. Solid-State Sensors Actuators, Proc.*, 1997, **1**, 121–124.

230 E. Frauendorfer, A. Wolf and W. D. Hergeth, *Chem. Eng. Technol.*, 2010, **33**, 1767–1778.

231 S. Curia, D. S. A. De Focatiis and S. M. Howdle, *Polymer (Guildf).*, 2015, **69**, 17–24.

232 F. Mellou, A. Varvaresou and S. Papageorgiou, *Int. J. Cosmet. Sci.*, 2019, **41**, 517–525.

233 R. R. Zepon Tarpani and A. Azapagic, *J. Environ. Manage.*, 2018, **215**, 258–272.

234 B. C. McDonald, J. A. de Gouw, J. B. Gilman, S. H. Jathar, A. Akherati, C. D. Cappa, J. L. Jimenez, J. Lee-Taylor, P. L. Hayes, S. A. McKeen, Y. Y. Cui, S.-W. Kim, D. R. Gentner, G. Isaacman-VanWertz, A. H. Goldstein, R. A. Harley, G. J. Frost, J. M. Roberts, T. B. Ryerson and M. Trainer, *Science*, 2018, **359**, 760–764.

235 T. Suphasomboon and S. Vassanadumrongdee, *Sustain. Prod. Consum.*, 2022, **33**, 230–243.

236 D. P. de Carvalho Neto, X. P. Gonot-Schoupinsky and F. N. Gonot-Schoupinsky, *Front. Sustain.*, 2021, **2**, 697092.

237 J. Hartmann and S. Moeller, *J. Oper. Manag.*, 2014, **32**, 281–294.

238 L. K. Aguiar, D. C. Martinez and S. M. Q. Caleman, *J. Food Prod. Mark.*, 2018, **24**, 297–310.

239 P. F. Ng, M. M. Butt, K. W. Khong and F. S. Ong, *J. Bus. Ethics*, 2014, **121**, 203–215.

240 S. Fankhauser, A. Bowen, R. Calel, A. Dechezleprêtre, D. Grover, J. Rydge and M. Sato, *Glob. Environ. Chang.*, 2013, **23**, 902–913.

241 M. I. Seelig, R. Sun, H. Deng and S. Pal, *J. Mark. Commun.*, 2021, **27**, 436–456.

242 G. J. Nohynek, E. Antignac, T. Re and H. Toutain, *Toxicol. Appl. Pharmacol.*, 2010, **243**, 239–259.

243 V. A. L. Wortel and J. W. Wiechers, *Food Qual. Prefer.*, 2000, **11**, 121–127.

244 M. Abendrot and U. Kalinowska-Lis, *Int. J. Cosmet. Sci.*, 2018, **40**, 319–327.

245 R. A. Gross and B. Kalra, *Science*, 2002, **297**, 803–807.

246 D. R. Lapen, E. Topp, C. D. Metcalfe, H. Li, M. Edwards, N. Gottschall, P. Bolton, W.

Curnoe, M. Payne and A. Beck, *Sci. Total Environ.*, 2008, **399**, 50–65.

247 N. Gottschall, E. Topp, C. Metcalfe, M. Edwards, M. Payne, S. Kleywegt, P. Russell and D. R. Lapen, *Chemosphere*, 2012, **87**, 194–203.

248 L. Deng, H. Xi, C. Wan, L. Fu, Y. Wang and C. Wu, *J. Hazard. Mater.*, 2023, **451**, 131199.

249 D. Capela, A. Alves, V. Homem and L. Santos, *Environ. Int.*, 2016, **92**–**93**, 50–62.

250 R. Dong, G. Yu, Y. Guan, B. Wang, J. Huang, S. Deng and Y. Wang, *Emerg. Contam.*, 2016, **2**, 1–6.

251 A. A. S. Alves, F. J. P. M. Sousa, M. Sebastião and F. E. Antunes, *J. Surfactants Deterg.*, 2022, **25**, 775–787.

252 D. H. Ochoa, J. W. B. Braga and F. Machado, *J. Surfactants Deterg.*, 2017, **20**, 467–481.

253 D. Benderly and Y. Zolotarsky, in *ACS Symposium Series*, American Chemical Society, 2013, vol. 1148, pp. 205–218.

254 K. Kabiri, H. Omidian, M. J. Zohuriaan-Mehr and S. Doroudiani, *Polym. Compos.*, 2011, **32**, 277–289.

255 Z. D. Draelos, *Clin. Dermatol.*, 2014, **32**, 809–812.

256 A. R. Yousefi and S. M. A. Razavi, *Starch - Stärke*, 2015, **67**, 567–576.

257 J. M. Townsend, E. C. Beck, S. H. Gehrke, C. J. Berkland and M. S. Detamore, *Prog. Polym. Sci.*, 2019, **91**, 126–140.

258 M. Guvendiren, H. D. Lu and J. A. Burdick, *Soft Matter*, 2012, **8**, 260–272.

259 M. H. Chen, L. L. Wang, J. J. Chung, Y.-H. Kim, P. Atluri and J. A. Burdick, *ACS Biomater. Sci. Eng.*, 2017, **3**, 3146–3160.

260 J. Mewis and N. J. Wagner, *Adv. Colloid Interface Sci.*, 2009, **147**–**148**, 214–227.

261 K. Shin, H. W. Suh, J. Grundler, A. Y. Lynn, J. U. Pothupitiya, Z. M. Moscato, M. Reschke, L. G. Bracaglia, A. S. Piotrowski-Daspit and W. M. Saltzman, *Biomaterials*, 2022, **287**, 121676.

262 S. Grinberg, V. Kolot and D. Mills, *Ind. Crops Prod.*, 1994, **3**, 113–119.

263 C. Caddeo, L. Pucci, M. Gabriele, C. Carbone, X. Fernàndez-Busquets, D. Valenti, R. Pons, A. Vassallo, A. M. Fadda and M. Manconi, *Int. J. Pharm.*, 2018, **538**, 40–47.

264 V. V. Namboodiri and R. S. Varma, in *Green Chemistry*, Royal Society of Chemistry, 2001, vol. 3, pp. 146–148.

265 J. Chen, S. K. Spear, J. G. Huddleston and R. D. Rogers, *Green Chem.*, 2005, 7, 64–82.

266 A. Dworak, B. Trzebicka, W. Wałach, A. Utrata and C. Tsvetanov, *Macromol. Symp.*, 2004, **210**, 419–426.

267 M. Hans, H. Keul and M. Moeller, *Polymer (Guildf).*, 2009, **50**, 1103–1108.

268 W. E. Rhine, D. P. Eyman and S. J. Schauer, *Polyhedron*, 1999, **18**, 905–908.

269 H. Bunzen, M. Grzywa, A. Kalytta-Mewes and D. Volkmer, *Dalt. Trans.*, 2017, **46**, 2618–2625.

270 D. Taton, A. Le Borgne, M. Sepulchre and N. Spassky, *Macromol. Chem. Phys.*, 1994, **195**, 139–148.

271 K. Masuda, T. Ichitsuka, N. Koumura, K. Sato and S. Kobayashi, *Tetrahedron*, 2018, **74**, 1705–1730.

272 M. Kuhlmann and J. Groll, *RSC Adv.*, 2015, **5**, 67323–67326.

273 S. V. Mohan and J. Karthikeyan, *Environ. Pollut.*, 1997, **97**, 183–187.

274 J. L. Kendall, D. A. Canelas, J. L. Young and J. M. DeSimone, *Chem. Rev.*, 1999, **99**, 543–563.

275 D. W. Roberts, A. Aptula and A. M. Api, *Chem. Res. Toxicol.*, 2017, **30**, 524–531.

276 A.-L. Brocas, C. Mantzaridis, D. Tunc and S. Carlotti, *Prog. Polym. Sci.*, 2013, **38**, 845–873.

277 K. Tezuka, K. Komatsu and O. Haba, *Polym. J.*, 2013, **45**, 1183–1187.

278 J. G. H. Hermens, A. Jensma and B. L. Feringa, *Angew. Chemie - Int. Ed.*, 2022, **61**, 1–6.

279 J. Kim, J. Bang, J. S. Choi, D. H. Lim, D. G. Guk and J. Jae, *J. Catal.*, 2023, **421**, 271–284.

280 G. Hu, Z. Cao, M. Hopkins, C. Hayes, M. Daly, H. Zhou and D. M. Devine, *Procedia Manuf.*, 2019, **38**, 117–124.

281 P. C. Gomes, O. G. Piñeiro, A. C. Alves and O. S. Carneiro, *Materials (Basel).*, 2022, **15**, 5486.

282 C. E. Vasey, A. K. Pearce, F. Sodano, R. Cavanagh, T. Abelha, V. Cuzzucoli Crucitti, A. B. Anane-Adjei, M. Ashford, P. Gellert, V. Taresco and C. Alexander, *Biomater. Sci.*, 2019, **7**, 3832–3845.

283 K. A. Fisher, K. D. Huddersman and M. J. Taylor, *Chem. - A Eur. J.*, 2003, **9**, 5873–5878.

284 Y.-D. Tang, S. S. Venkatraman, F. Y. C. Boey and L.-W. Wang, *Int. J. Pharm.*, 2007, **336**, 159–165.

285 S. Borandeh, B. van Bochove, A. Teotia and J. Seppälä, *Adv. Drug Deliv. Rev.*, 2021, **173**, 349–373.

286 X. Chen, G. Zhou, X. Peng and J. Yoon, *Chem. Soc. Rev.*, 2012, **41**, 4610–4630.

287 X. Qian and B. Städler, *Chem. Mater.*, 2019, **31**, 1196–1222.